Biobased Aerogels: From Lab to Technical Scale

Inaugural-Dissertation
zur Erlangung des Doktorgrades
der Mathematisch-Naturwissenschaftlichen Fakultät
der Universität zu Köln

vorgelegt von
M.Sc. Diogo Manuel Amaral Santos Costa
aus Oeiras, Portugal

Köln, 2024

Die vorliegende Arbeit wurde von der Mathematisch-Naturwissenschaftlichen

Fakultät der Universität zu Köln als Dissertation angenommen.

If it is well written and to the point, that is what I wanted; if it is poorly done and mediocre, that is the best I could do.

Holy Bible - 2 Maccabees, 15:38

Que prova o conclui? Que há aí proveitoso como elemento que reorganize o individuo ou a espécie ? Respondo: Nada (...) O meu romance não pretende reorganizar coisa nenhuma. E o autor desta obra estéril assevera, em nome do patriarca Voltaire, que deixaremos este mundo tolo e mau, tal e qual era quando cá entrámos.

A Brasileira de Prazins, Camilo Castelo Branco

Pai, foste cavaleiro.
Hoje a vigília é nossa.
Dá-nos o exemplo inteiro
E a tua inteira força!
Dá, contra a hora em que, errada,
Novos infiéis vençam,
A bênção como espada,
A espada como bênção!

Dom Afonso Henriques, Fernando Pessoa

Acknowledgment

The data presented here was collected and analyzed for three years, from April 2021 to April 2024, in Germany and France. These years were characterized globally by the end of the COVID pandemic, by geopolitical turbulence in Europe and the Middle East, and by economic and logistic crises that have affected my personal life as well as my work. I would like here to acknowledge all the people who have contributed to the success of this journey.

From DLR, I would like to thank the very helpful support of my supervisor, Prof. Dr. Barbara Milow, who always encouraged me when I needed it and gave me space to develop my ideas, succeed, and learn from my mistakes. I would like to thank Dr. Kathirvel Ganesan for his technical supervision, especially in the first months of the PhD. With him, I learned the importance of rigor in the scientific method. A special thanks to Mr. Alexander Francke for his support in the XRD analysis, to Ms. Rebekka Probst for helping record SEM pictures, and to Lana Möltgen for supporting the TG analysis. I give special thanks to my colleagues and friends, Bruno Serrador Gonçalves, Philipp Niemeyer, and Thomas Anklam, for their insightful discussions, shared moments, and occasional analysis they did for me while living abroad. I owe a lot of my scientific and personal growth to all remaining members of this big DLR family.

From KEEY Aerogels, I thank the invaluable support and scientific guidance of Dr. Kanda Philippe, whose insight helped me to improve my experiment design and how to handle scientific challenges from an industry-oriented perspective, and Dr. Francisco Ruiz, who provided support on thinking the upscaling process. I thank other members of the KEEY Aerogel team, namely Michael O'Connor for our discussions on the state of the aerogel industry, Alex, for her technical support in the lab, and Allan and Sebastian, for their support with the technical equipment used.

For providing me with financial support during these years, I am extremely grateful to the Biobased Value Circle consortium. I am thankful to all the other ESRs, for sharing their insights about their and my work and for our good moments. I owe a special thanks to my "fellow sailors" Simon Schick, with whom I collaborated closely in our strand, and to Zhou Fang, whose expertise in polymers and rigorous scientific approach, inspired me to further improve my methods. I am thankful as well to Prof. Dr. Annette Schmidt and her team for their support in the determination of the molecular weight of cellulose samples.

Abstract

This work is focused on the synthesis of cellulose aerogels from biomass wastes, at laboratory and technical scales. These aerogels were produced in different shapes (beads, sheets, monoliths, and fibers), and they were studied as potential thermal insulators. Unretted hemp and flax bast waste fibers were used as sources of cellulose for the synthesis of the aerogels. Commercial cellulose was used for the creation of standard aerogel samples. Laboratory scale recipes were developed to determine the influence on the aerogel's properties of different cellulose dissolution and regeneration conditions. For dissolution, the role of time and temperature were investigated. Additionally, the influence of different acidic regeneration baths and the addition of salts to the cellulose solutions on the regeneration of cellulose were evaluated. The best synthesis recipes were chosen for upscaling and were applied using the technical scale equipment JetCutter® (beads) and the CAProLi (**C**ellulose **A**erogel **Pro**duction **Li**ne, for sheets). Different routes to coat the cellulose aerogels with lignin were tested to protect them from moisture and water absorption. The aerogel samples were characterized in their chemical composition, morphology, structure, and further properties to evaluate the influence of the synthesis parameters.

Pure cellulose was extracted from bast waste fibers at a laboratory scale. This standard extraction process was shortened and it was successfully upscaled to a two-liter scale. This thesis explains how the properties of cellulose aerogels can be modified by selectively changing their synthesis. It was found that smoother cellulose gelation was achieved when weaker organic acids were used as regeneration baths. These contributed to the formation of a filigree porous structure in the aerogels which maximized their specific surface area. The pore size distribution of the aerogels could be tailored depending on the acid used. Regarding the use of salts, the addition of sodium chloride ($NaCl$) and sodium sulfate (Na_2SO_4) to cellulose solutions accelerated their gelation but did not significantly modify the internal structure of the aerogel samples formed. This was due to competition between the induced faster gelation of cellulose, which produced bigger pores during the formation of the wet gel network, and the scaffold effect that occurred when the salt was removed during the washing of the wet gel. This latter trend induced the creation of smaller pores. The addition of three-sodium citrate (Na_3Cit) to the cellulose solution extended its gelation time due to the organic and weak base character of the anion citrate. Concerning the dissolution of cellulose, it was achieved at -10°C under continuous stirring for 30 minutes. This faster process contributes to the scalability of the process and its industrial application.

Abstract

Cellulose aerogels, from commercial and biomass waste sources, were synthesized in the shape of beads, sheets, and fibers. These materials presented high porosities (over 80%), high specific surface areas (over 200 m^2 g^{-1}) and low densities (< 0.21 g cm^{-3}), depending on the source of cellulose and the recipe followed. The aerogels created from hemp-based cellulose and commercial cellulose had similar properties for the same synthesis route. It indicated that biomass wastes were a suitable source of cellulose for the synthesis of aerogels. This was due to the close degree of polymerization (DP) between the two celluloses, which contributed to the creation of cellulose solutions of similar viscoelastic properties. The samples obtained from flax-extracted cellulose had lower specific surface areas and bigger pores due to its higher DP and therefore used less-concentrated cellulose solutions.

The upscaling of the synthesis of aerogels using the CAProLi and the JetCutter® technologies was effective with little differences between samples obtained at both scales. These materials had a thermal conductivity between 37 mW m^{-1} K^{-1} and 40 mW m^{-1} K^{-1}, providing space for further improvement. Lower values of thermal conductivity were obtained when less concentrated cellulose solutions were used. The use of different acidic coagulation baths or the addition of salts to the cellulose solutions had a negligible influence on this property. Lastly, it was found that soda lignin was a promising coating agent for cellulose wet gels. A maximum of 40 wt.-% reduction in water absorption for the coated aerogels was observed when a weight ratio of 1:5 lignin:cellulose wet gel (L:C) was applied, while the internal structure of the coated samples was preserved.

Overall, the protocols developed in this study were integrated into a continuous technical scale industrial scheme. This approach has environmental and economic advantages compared to laboratory batch-wise synthetic routes, which can contribute to the development of the industrial aerogel market and a circular biobased value economy.

Key-words: aerogels; hemp; flax; biobased; cellulose; lignin; JetCutter® ; wet-spinning; thermal insulation

Abstract

Zusammenfassung

Diese Arbeit konzentriert sich auf die Synthese von Cellulose-Aerogele aus Biomasseabfällen im Labor- und technischen Maßstab. Diese Aerogele wurden in verschiedenen Formen (Perlen, Platten, Monolithen und Fasern) hergestellt und als potenzielle Wärmedämmstoffe untersucht. Ungereinigte Hanf- und Flachsbastabfälle wurden als Zellulosequellen für die Synthese der Aerogele verwendet. Für die Herstellung von Standard-Aerogel-Proben wurde handelsübliche Zellulose verwendet. Es wurden Rezepte im Labormaßstab entwickelt, um die Auswirkungen verschiedener Bedingungen für die Auflösung und Regeneration von Cellulose auf die Eigenschaften des Aerogels zu bestimmen. Für die Auflösung wurde die Rolle von Zeit und Temperatur untersucht. Außerdem wurde der Einfluss verschiedener saurer Regenerationsbäder und der Zusatz von Salzen zu den Celluloselösungen auf die Regeneration der Cellulose bewertet. Die besten Syntheserezepte wurden für das Upscaling ausgewählt und mit der technischen Anlage JetCutter® (Perlen) und der CAProLi (Cellulose-Aerogel-Produktionsanlage, für Platten) angewendet. Es wurden verschiedene Verfahren zur Beschichtung der Cellulose-Aerogele mit Lignin getestet, um sie vor Feuchtigkeit und Wasseraufnahme zu schützen. Die Aerogelproben wurden hinsichtlich ihrer chemischen Zusammensetzung, Morphologie, Struktur und weiterer Eigenschaften charakterisiert, um die Auswirkungen der Syntheseparameter zu bewerten.

Reine Cellulose wurde im Labormaßstab aus Bastabfallfasern extrahiert. Dieser Standardextraktionsprozess wurde verkürzt und erfolgreich auf einen Zwei-Liter-Maßstab hochskaliert. In dieser Arbeit wird erläutert, wie die Eigenschaften von Cellulose-Aerogelen durch eine gezielte Änderung ihrer Synthese modifiziert werden können. Es wurde festgestellt, dass eine sanftere Cellulosegelierung erreicht wurde, wenn schwächere organische Säuren als Regenerationsbäder verwendet wurden. Diese trugen zur Bildung einer filigranen porösen Struktur in den Aerogelen bei, die deren spezifische Oberfläche maximierte. Die Porengrößenverteilung der Aerogele konnte in Abhängigkeit von der verwendeten Säure maßgeschneidert werden. Was die Verwendung von Salzen betrifft, so beschleunigte die Zugabe von Natriumchlorid (NaCl) und Natriumsulfat (Na2SO4) zu Zelluloselösungen deren Gelierung, veränderte aber die innere Struktur der gebildeten Aerogelproben nicht wesentlich. Dies war auf die Konkurrenz zwischen der induzierten schnelleren Gelierung der Zellulose, die während der Bildung des nassen Gel-Netzwerks größere Poren erzeugte, und dem Gerüsteffekt zurückzuführen, der auftrat, wenn das Salz während des Waschens des nassen Gels entfernt wurde. Der letztgenannte Trend führte zur Bildung kleinerer Poren. Die Zugabe von

Abstract

Dreinatriumcitrat (Na3Cit) zu der Celluloselösung verlängerte die Gelierzeit aufgrund des organischen und schwach basischen Charakters des Anions Citrat. Die Auflösung der Cellulose wurde bei -10°C unter kontinuierlichem Rühren für 30 Minuten erreicht. Dieses schnellere Verfahren trägt zur Skalierbarkeit des Prozesses und seiner industriellen Anwendung bei.

Cellulose-Aerogele aus kommerziellen Quellen und Biomasseabfällen wurden in Form von Kügelchen, Filmen/Bahnen und Fasern synthetisiert. Diese Materialien wiesen eine hohe Porosität (über 80%), eine hohe spezifische Oberfläche (über 200 m2 g-1) und eine niedrige Dichte (< 0,21 g cm-3) auf, abhängig von der Zellulosequelle und dem verwendeten Rezept. Die aus hanfbasierter Cellulose und kommerzieller Cellulose hergestellten Aerogele wiesen bei gleichem Syntheseweg ähnliche Eigenschaften auf. Dies deutet darauf hin, dass Biomasseabfälle eine geeignete Cellulosequelle für die Synthese von Aerogelen sind. Dies ist auf den ähnlichen Polymerisationsgrad (DP) der beiden Cellulosen zurückzuführen, der zur Herstellung von Celluloselösungen mit ähnlichen viskoelastischen Eigenschaften beiträgt. Die aus der aus Flachs gewonnenen Cellulose hergestellten Proben hatten aufgrund des höheren DP eine geringere spezifische Oberfläche und größere Poren, weshalb weniger konzentrierte Celluloselösungen verwendet wurden.

Das Upscaling der Synthese von Aerogele mit der CAProLi- und der JetCutter®-Technologie war effektiv und die Unterschiede zwischen den in beiden Maßstäben erhaltenen Proben gering. Diese Materialien hatten eine Wärmeleitfähigkeit zwischen 37 mW m-1 K-1 und 40 mW m-1 K-1, was Raum für weitere Verbesserungen bietet. Niedrigere Werte der Wärmeleitfähigkeit wurden erzielt, wenn weniger konzentrierte Zelluloselösungen verwendet wurden. Die Verwendung verschiedener saurer Koagulationsbäder oder die Zugabe von Salzen zu den Zelluloselösungen hatte einen vernachlässigbaren Einfluss auf diese Eigenschaft. Schließlich wurde festgestellt, dass Lignin aus Soda ein vielversprechendes Beschichtungsmittel für Cellulose-Nassgele ist. Bei einem Gewichtsverhältnis von 1:5 Lignin:Cellulose-Nassgel (L:C) wurde eine maximale Verringerung der Wasseraufnahme der beschichteten Aerogele um 40 Gew.-% beobachtet, während die innere Struktur der beschichteten Proben erhalten blieb.

Insgesamt wurden die in dieser Studie entwickelten Protokolle in ein kontinuierliches industrielles System im technischen Maßstab integriert. Dieser Ansatz hat ökologische und wirtschaftliche Vorteile im Vergleich zu synthetischen Verfahren im Labormaßstab und kann zur Entwicklung des industriellen Aerogelmarktes und einer zirkulären biobasierten Wertschöpfung beitragen.

Abstract

Schlüsselwörter: Aerogele; Hanf; Flachs; biobasiert; Zellulose; Lignin; JetCutter®; Nassspinnen; Wärmedämmung

Abstract

Index

List of Abbreviations

3D	**Three-dimensional**
a.u.	**Arbitrary unit**
Al$_2$O$_3$	**Alumina**
AMIBM	**Aachen-Maastricht Institute for Biobased Materials**
AMIMCl	**1-allyl-3-methylimidazolium chloride**
APD	**Ambient pressure drying**
AWG	**American wire auge**
BC	**Bacteria cellulose**
BET	**Brunauer-Emmett-Teller method**
BF	**Bright field**
BJH	**Barett-Joyner-Halenda method**
BSO	**Building Stock Observatory**
c*	**Critical overlap concentration**
CAProLi	**Cellulose Aerogel Production Line**
CBD	**Cannabidiol**
CN	**Coordination number**
CNC	**Cellulose nanocrystals**
CNF	**Cellulose nanofibers**
CuKα	**Copper Kα; type of radiation used for X-Ray diffraction**
DIM	**Dynamic insulation material**
DLR	**German Aerospace Center**
DP	**Degree of polymerization**
EED	**Energy Efficiency Directive**
EPBD	**Energy Performance of Buildings Directive**
EPS	**Expanded polystyrene**
EtOH	**Ethanol**
EU	**European Union**
FC	**Flax cellulose**
FD	**Freeze drying**
FF	**Flax fibers**
FTIR	**Fourier-transform infrared spectroscopy**
G´	**Storage Modulus**
G´´	**Loss Modulus**
GBRS	**Green Building Rating Systems**
GFP	**Gas-filled panel**
GHG	**Greenhouse gas**
GPC	**Gel permeation chromatography**
GWP	**Global warming potential**
h	**hours**
HC	**Hemp cellulose**
HF	**Hemp fibers**
IC$_S$	**Index of crystallinity (Segal method)**
IL	**Ionic liquid**
Ind	**Indulin AT**
IUPAC	**International Union of Pure And Applied Chemistry**
L:C	**Lignin:cellulose wet gel ratio (wt.-%)**

LCA	**Life-cycle assessment**
LiCl/DMAc	**LiCl/N,N-dimethylacetamide**
LS	**Laboratory scale**
LTSCD	**Low-temperature supercritical drying**
MC	**Commercial cellulose**
MCC	**Microcrystalline cellulose**
MF	**Melamine/formaldehyde**
MFC	**Microfibrillated cellulose**
min	**Minutes**
MM	**Molecular weight**
N_2	**Nitrogen**
Na_2SO_4	**Sodium sulfate**
Na_3Cit	**Three-sodium citrate**
NaCl	**Sodium chloride**
NIM	**Nano insulation materials**
NMMO	**N-methylmorpholine-N-oxide**
Oh	**Ohnesorge number**
p/p°	**Partial pressure**
P1	**Protobind^{TM} 1000 lignin**
PCM	**Phase change materials**
PDMS	**Poly-(dimethylsiloxane)**
PEB	**Positive energy buildings**
PEG	**Polyethylenogicol**
PGM	**Phase change material**
PUR	**Polyurethane**
Re	**Reynolds number**
RF	**Resorcinol/formaldehyde**
RSCE	**Rapid supercritical extraction**
s	**Seconds**
SCD	**Supercritical drying**
SEM	**Scanning electron microscopy**
STP	**Standard temperature and pressure**
T	**Temperature**
TEOS	**Tetraethoxysilane**
THC	**Tetrahydrocannabinol**
TiO_2	**Titania**
TMOS	**Tetramethoxysilane**
TS	**Technical scale**
VIP	**Vacuum insulation panel**
vol.-%	**Volume percentage**
w/v	**Weight per volume**
wt.-%	**Weight percentage**
XPS	**Extruded polystyrene**
XRD	**X-Ray diffraction**
ZEB	**Zero-energy buildings**
ZrO_2	**Zirconia**

1. Introduction

The world´s current demographic and carbon emissions trends are driving changes in how buildings are designed and built. By 2050, the world´s population is expected to increase from 7.7 billion to 9.7 billion. At the same time, it is estimated that over the next decades the populations in large areas of Europe, Asia, and North America, will shrink and overage.[1] Most of these new human beings will increasingly live in cities, ascending to 68% of the urban population in 2050.[2]

As a result, the European Union (EU) is investing in the energetic efficiency and resilience of its buildings to combat extreme climate phenomena.[3] It is urgent to promote the remodeling and construction of buildings that use more efficient materials and smart management energy technologies.[4-8] Better thermal insulation materials are needed to save energy in the construction, transportation, and space exploration sectors, among others. Traditional materials comprise inorganic and organic alternatives. Common alternatives include mineral wool (40 mW m^{-1} K^{-1} to 50 mW m^{-1} K^{-1}), high porous ceramic foams (50 mW m^{-1} K^{-1} to 70 mW m^{-1} K^{-1}), cellulose (40 mW m^{-1} K^{-1} to 50 mW m^{-1} K^{-1}), extruded/expanded polystyrene (XPS/EPS, 30 mW m^{-1} K^{-1} to 40 mW m^{-1} K^{-1}) and polyurethane (PUR, 20 mW m^{-1} K^{-1} to 30 mW m^{-1} K^{-1}).[9-11] These last two, plus mineral wool, dominate the European market due to their low cost and low thermal conductivity. Nonetheless, scientists are researching safer alternatives with improved thermal and mechanical performance.[12] A new generation of insulating systems includes vacuum insulation panels (VIPs), gas-filled panels (GFPs), and nano insulation materials (NIMs), which are known for their extremely low thermal conductivities (3 mW m^{-1} K^{-1} to 4 mW m^{-1} K^{-1}). However, VIPs and GFPs can be breached and NIMs are still in an early stage of development.[10, 12, 13]

A good thermal insulator is a material that minimizes the conduction of heat by having high thermal resistance (m^2 K W^{-1}) and low thermal transmittance (W m^{-2} K^{-1}). If so, it can be applied in thin layers, saving costs and space. The low density, high specific surface area, and porosity of aerogels make them suitable candidates for super thermal insulation (< 20 mW m^{-1} K^{-1}).[14] Furthermore, it is essential to produce these materials from sustainable biobased feedstocks, following the tenets of a circular biobased economy. In a circular economy, materials are used as long as possible and the products are incorporated at their end of life back into the economic system. This maximizes their value and minimizes waste production. In a bio-economy, this system still applies but the resources used are renewable and environmentally friendly biological feedstocks.[15-17] By following these perspectives, biobased aerogels are particularly interesting. They share the same properties as their organic or silica counterparts

Introduction

(low density, low thermal conductivity, high surface area) while being produced from sustainable sources such as polysaccharides. These are dissolved and, through the triggering of their association, a gel is created. After neutralization, occasional solvent exchange, and supercritical drying, a 3D nanostructured porous aerogel is obtained.[18] Some of the most frequently used polysaccharides for the synthesis of aerogels are cellulose, alginate, carrageenan[19-21], chitosan[22], starch, and pectin, among others. These can be combined with inorganic components to create aerogel hybrids.[18, 23, 24] This work focuses on the development of cellulose aerogels from agriculture wastes (unretted hemp and flax bast waste fibers), their characterization in different shapes (beads, sheets, monoliths, fibers), and the upscaling of their production from laboratory to technical scale. These materials were investigated as potential sustainable thermal insulators. The cellulose dissolution and regeneration conditions were investigated to understand their influence on the specific surface area, porosity, density, pore size distribution, and thermal conductivity of the produced aerogels. All of them influence their efficiency as thermal insulators. The work had as main objectives:

- Development of an efficient and scalable method to extract pure cellulose from hemp and flax bast waste fibers.
- Study of the influence of different cellulose dissolution (temperature and time) and regeneration conditions (addition of salts to cellulose solutions, use of different acidic regeneration baths) on the cellulose aerogel properties. Maximization of specific surface area and minimization of average pore size and thermal conductivity were desired.
- Synthesis of cellulose aerogels from extracted and commercial cellulose at optimized conditions, in different shapes (beads, sheets, monoliths, and fibers), and their characterization.
- Upscale of optimized recipes using the JetCutter® (beads) and the CAProLi (sheets) technology.
- Research of an effective method to coat cellulose aerogels with lignin to protect them from moisture and water absorption.
- Optimum desirable aerogel properties including thermal conductivity < 30 mW m^{-1} K^{-1}, resistance to moisture, mechanical strength, acoustic insulation, flame retardancy, antimildew, and antimicrobial activity.

Introduction

The development of recipes at the laboratory scale for the extraction of cellulose from bio-wastes, synthesis of cellulose aerogel beads, monoliths, and sheets, and the experiments with the CAProLi technology were performed at the German Aerospace Center (DLR), in Cologne, Germany. Part of the data used in **Chapter 4.3.1** and the data used in **Chapter 4.5** was collected in collaboration with a master student, Bruno Serrador Gonçalves.[25] Characterization of all samples in their composition, structure, and morphology was also performed at DLR. Upscaling of the extraction of cellulose, production of cellulose aerogel beads using the JetCutter® technology as well as the study of the coating of cellulose aerogels with lignin were performed within the industrial partner KEEY Aerogels, Habsheim, France. Thermal conductivity analysis of the aerogels was also performed at KEEY Aerogels. The work developed on cellulose aerogel fibers was performed in collaboration with Simon Schick at AMIBM, Maastricht University, Netherlands, under the European Biobased Value Circle consortium.

Introduction

2. State of the Art

2.1 Aerogels

The International Union of Pure and Applied Chemistry (IUPAC) defines an aerogel as a gel composed of a microporous solid in which the dispersed phase is a gas.[26] However, this simple definition does not fully capture the wide variety of materials that are considered aerogels in academic and industrial circles, and there is an ongoing debate regarding a more comprehensive definition. These materials share a nanostructured solid backbone and open porous structure, but their properties and structures differ based on the synthesis and raw materials used. One definition of aerogels focuses on the process of their creation, stating that these can be defined as solid gels where the liquid media has been replaced by air, with minimal shrinkage of the solid open porous network.[14, 27] When the gel´s pores are filled with a liquid, it is called a "wet gel". If the fluid is water or alcohol, they are called hydrogels and alcogels respectively. [28-30] Aerogels are primarily mesoporous, with pore dimensions ranging from 2 nm to 50 nm. However, they may also contain macropores (over 50 nm) and micropores (below 2 nm), and the pore size distribution in these materials depends heavily on their synthesis. The physical and chemical properties, as well as the porous structure of aerogels, are largely defined by their solid backbone. In **Figure 1**, the classification of aerogels based on their constituents is observed.
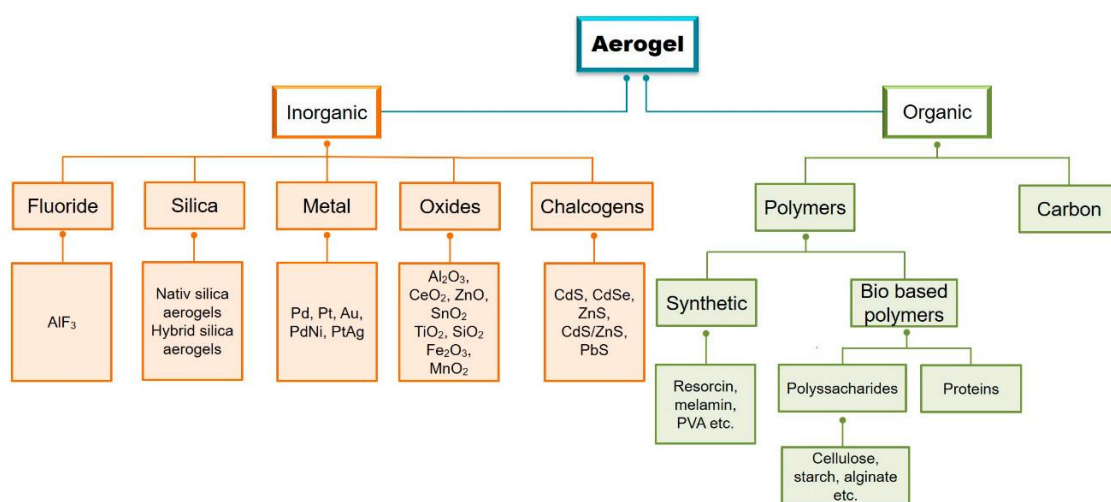

Figure 1 Classes of aerogels based on the nature of their constituents [18] (CC BY 4.0, https://creativecommons.org/licences/by/4.0/). All aerogels can be classified either as organic or inorganic.

2.1 Aerogels

Aerogels can be classified as either inorganic or organic materials based on the origin of their precursors. Silica aerogels currently dominate the aerogel market[31] while metal-oxide aerogels based on alumina (Al_2O_3), titania (TiO_2), and zirconia (ZrO_2) are still in the early stages of research. Organic aerogels can be created from resorcinol/formaldehyde (RF) and melamine/formaldehyde (MF) mixtures among others while biopolymers such as polysaccharides (cellulose, chitosan, alginate, among others) and proteins can be converted into aerogels. Carbon aerogels can be obtained from the pyrolysis of organic-based aerogels.[32-36] The synthetic route of each aerogel will influence its chemical and physical properties. Nonetheless, these have in common a high porosity, high specific surface area, and low densities, for some cases below the air density of 0.0012 g cm^{-3} under vacuum conditions.[14, 32] They can reach a thermal conductivity as low as 10 mW m^{-1} K^{-1}.[14] Their porous structure, large surface area, thermal stability, and chemical groups prone to functionalization make them ideal to catalyze various chemical reactions. The possibility to functionalize their surface or change the fundamental network structure by tuning the synthesis only increases the range of applications. Other applications include films, gas filters, sensors, carrying structures in the food and pharmaceutical industry [28, 29, 34, 37], batteries and capacitors, environmental remediation, and even spacecraft to capture stardust, among many others.[38, 39]

A wide range of organic and inorganic aerogels are synthesized through sol-gel chemistry. For those materials, their production comprises the synthesis of a precursor gel with desired properties, solvent exchange of the pore solvent with a target solvent, and drying. Here, the solvent is replaced by air while minimizing shrinkage.[29] While the creation of the precursor gel will define the structure of the aerogel-to-be, solvent exchange is required so the gel can be safely dried without the collapse of its porous structure, depending on the drying technique chosen.[14] These processes will be further explained in the following chapters.

2.1.1 Classical Sol-Gel Process

A sol, according to IUPAC, is considered a colloidal system of two or more components: a fluid, and dispersed molecular particles with dimensions close to 1 μm. Through a sol-gel process, a gel network is formed from the solution by a progressive change of the liquid precursor(s). The gel is characterized by the presence of a continuous macromolecular solid phase and the residual liquid sol.[26] By removing the latter, a final dried product can be obtained. During the sol-gel process, the mechanical resistance of the sol system increases as it transforms into a gel. This increased resistance to shear stress is intrinsically linked to the gelation process, which can be monitored by rheological methods.[14] For most aerogel classes,

such as inorganic and synthetic organic aerogels, their network is created by hydrolysis and condensation reactions between activated chemical precursors. The conditions at which the gel´s 3D network is formed determine the chemical and physical properties of the dried aerogel.[30, 40] The exact structure of the final gels can be considered a hybrid between polymeric and colloidal gels. This means that it can vary from the condensation of large clusters of colloidal particles to linear/branched polymeric chains formed from the condensation of small structures.[28] In **Figure 2**, the sol-gel process is described.
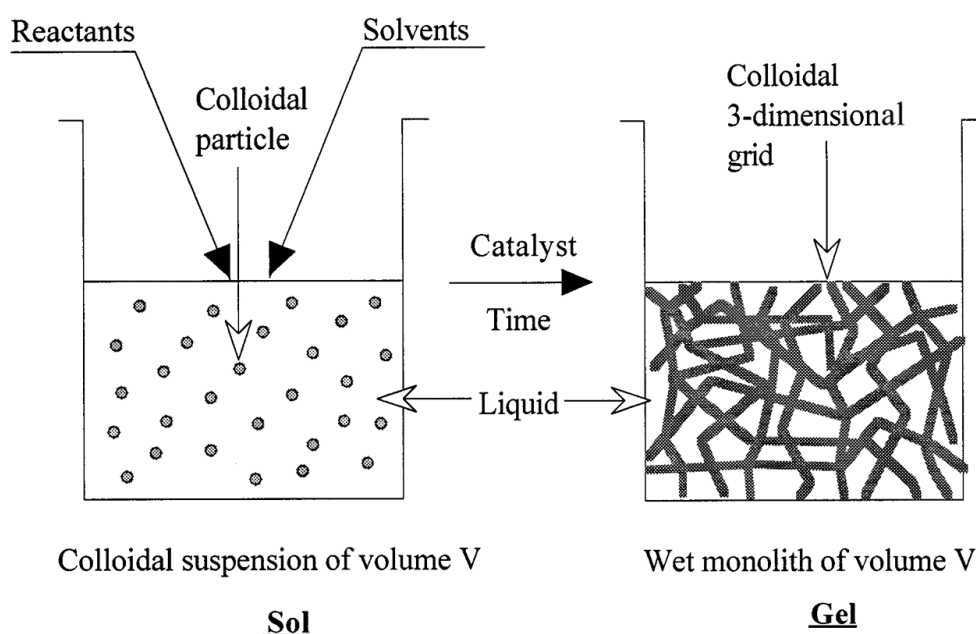
Figure 2 Classical sol-gel process.[29] Reprinted (adapted) with permission from Pierre, A.C. and G.M. Pajonk, Chemistry of Aerogels and Their Applications. Chem.Rev, 2002(102): p. 4243-4265. Copyright 2002 American Chemical Society; permission conveyed through Copyright Clearance Center, Inc.

Some relevant examples of chemical precursors include silicon and transition metal alkoxides for silica and metal oxide aerogels, resorcinol, isocyanates, and melamine among other organic molecules for synthetic organic aerogels.[41, 42] Their activation and reaction are highly dependent on temperature, pH, concentration, and solvent, among other factors, which will influence the properties of the synthesized aerogels.[43, 44]

2.1.2 Aging, Solvent Exchange and Drying of Wet Gels

After gelation, wet gels are left for aging to strengthen the network. The more time the gels are left in their mother solutions or other gelation media, the stiffer and stronger become their

2.1 Aerogels

porous networks.[45] After aging, it is important to adapt the gel´s solvent to the selected drying method to minimize shrinkage and modification of its porous structure. Once the gel is sturdy enough, it undergoes solvent exchange, where its pore solvent is substituted with another solvent. This process occurs when the gel is immersed in a bath of the desired solvent, allowing the solvent within the gel to diffuse and mix with the bath until equilibrium is reached. This is made possible by the open porous structure of the gel. To minimize shrinkage and retain the gel´s structure, careful consideration must be given to the selection of the solvent, as well as the soaking time, number, and volume of baths. The solvent chosen should balance its hydrogen bond ability and its dielectric constant. Extensive hydrogen bonding between the solvent and the gel´s polymer chains diminishes their aggregation during solvent exchange and reduces shrinkage. A lower dielectric constant may indicate a low polarity of the solvent, which enhances the polymer-polymer interactions in the gel and promotes its shrinkage.[46, 47] Although a multi-step, gradient solvent exchange can reduce the severity of the concentration gradient and shrinkage, it requires more time to replace the pore solvent with a liquid suitable for the chosen drying method.[48]

For all the previous classes of aerogel materials, the drying step is essential in converting gels into aerogels by replacing the liquid solvent with air with minimal shrinkage. Different techniques exist to achieve this step, and all of them should consider the same physical laws. The main factor responsible for gel shrinkage during drying is capillary pressure (Pc), which is influenced by the surface tension of the pore liquid (γ_{lv}), the pore radius (r_p), and the thickness of the surface adsorbed layer (δ). These relations are described by **Equation 1**.[49, 50]

$$\text{Pc} = \frac{-\gamma_{lv}}{(r_p - \delta)} \qquad\qquad \textbf{Equation 1}$$

The radius of the pores can be described by the relation between their pore volume (V_p) and surface area (S_p), described in **Equation 2**.[49]

$$r_p = \frac{2V_p}{S_p} \qquad\qquad \textbf{Equation 2}$$

At room temperature, the tensions between the liquid and vapor phases are inevitable and depend on factors such as the drying solvent, the drying rate, the permeability, and the pore size of the wet gel. If the pore is smaller than 200 Å, the pressures around the pore liquid are very high but, at larger dimensions, the cracking and shrinkage in the aerogel are less pronounced.

Three main types of drying can be applied to minimize shrinkage: supercritical drying (SCD); ambient pressure drying (APD) and freeze drying (FD), as described in **Figure 3**.[49, 50]
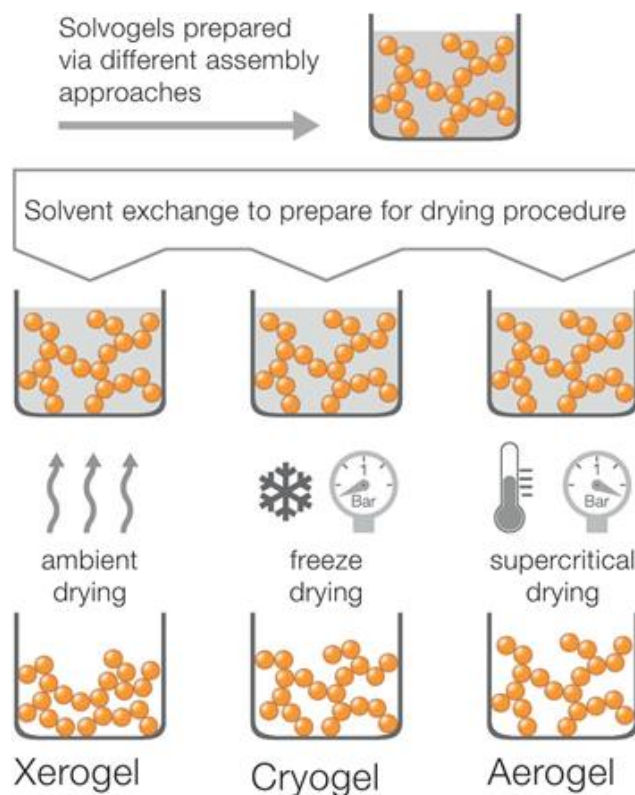

Figure 3 Different drying processes of wet gels and resulting structure.[30] Used with permission of JOHN/WILEY & SONS, INC, from *Modern Inorganic Aerogels*., Ziegler, C., et al., 56 / International ed. in English., 2017.; permission conveyed through Copyright Clearance Center, Inc.

APD is an attractive technique as it uses ambient temperature and pressure however, at these conditions, the capillary forces are too strong to produce an aerogel without significant shrinkage due to pore collapsing. This can be minimized with functionalization and network-strengthening techniques. The product from APD can be called a "xerogel".[49, 51] In FD (or lyophilization), the solvent in the gel is replaced by a solvent with a low expansion coefficient and high sublimation pressure. By freezing the liquid and then sublimating it under a vacuum, a "cryogel" is obtained. While this technique is widely used, there is a risk of crystallization of the pore liquid, which can induce cracking in the final material. As a result, the final products are mainly macroporous (pores up to 1 µm) with low surface area and degree of mesoporosity.[52-55]

Regarding SCD, the low-temperature variant (LTSCD) is the most widely used nowadays as it is safer and less costly than high-temperature methods. One of the most commonly used

alternatives is supercritical CO_2, which can reach a supercritical state at low temperatures (as low as 40 °C) and moderate pressures (as low as 80 bar), as shown in **Figure 4**. Supercritical CO_2 is directly injected into the autoclave and, after the complete replacement of the pore solvent by CO_2, the next steps include depressurization until room pressure and subsequent temperature decline.[49, 56] Under these conditions, the solvent is replaced by air with minimized shrinkage of the network, and the wet gel is converted into an aerogel.
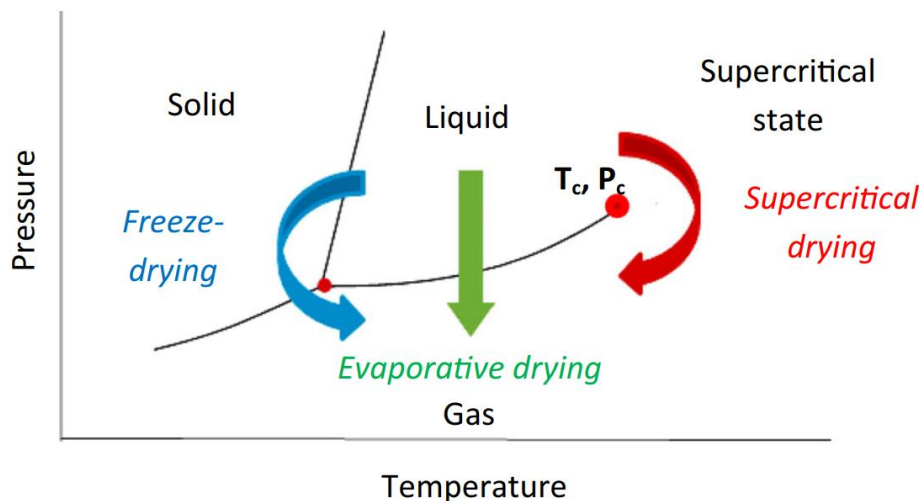
Figure 4 Phase diagram for drying methods.[57] Used with permission of JOHN/WILEY & SONS, INC, from *Cellulose II aerogels: a review*., Budtova, T., 26., 2019.; permission conveyed through Copyright Clearance Center, Inc.

The two main diffusion mechanisms between supercritical CO_2 and the pore solvent in the gel are Knudsen and surface diffusion. As these diffusion coefficients are not easily discernible (they increase along with temperature), it is difficult to predict how long the drying step should be to ensure complete solvent replacement. If the drying time is too short, non-transparent areas can be formed, and cracking can occur for silica aerogels, especially when the network´s bonds are weak and their clusters can be rearranged.[49, 50] This makes the supercritical drying step crucial in the synthesis of aerogels at low temperatures. It is important to notice that water and supercritical CO_2 are poorly miscible. As many aerogels form in aqueous media, water needs to be replaced by an organic solvent (ethanol, isopropanol, acetone, among others) so that SCD with carbon dioxide can be applied, and the drying accomplished. CO_2-dried aerogels achieve a higher microporosity and undergo low or no cracking due to lower stress in the network during the drying process. Any existing shrinkage is due to the rearrangement of aggregates during solvent replacement.[49, 58]

2.2 Cellulose

Cellulose is a biopolymer that has a simple chemical structure and from which aerogels can be synthesized. However, various types of "celluloses" exist, making it important to understand its nomenclature. The primary biological function of this biopolymer is structural, due to its strength and insolubility in water. The structure of its monomer is described in **Figure 5**.[59, 60]
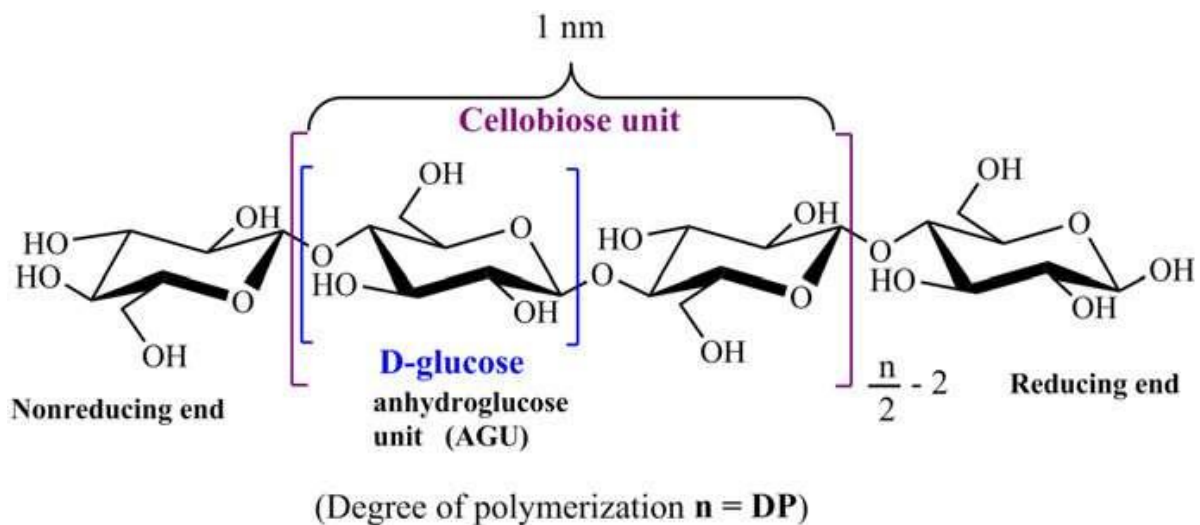

Figure 5 Cellobiose, composed by 2 units of glucose. Glucose is the monomer of cellulose.[61] Reprinted from Biotechnology Advances, 35, Coseri, S., *Cellulose: To depolymerize... or not to ?*, 255-261, Copyright (2017), with permission from Elsevier; permission conveyed through Copyright Clearance Center, Inc.

Glucose is the monomeric unit of cellulose and it can be classified into α or β depending on the position of the OH group in carbon one (C_1), if it is below or above the pyranose ring, respectively.[62] As shown in **Figure 5**, the pyranose rings are in a chair conformation and their OH groups are in the equatorial position. The hydrogens are in the axial position, which makes the surface of the ring hydrophobic.[59, 63] The combination of those units creates a poly 1→4-β-D-glucopyranose $(C_6H_{11}O_5)_n$ chain which also can be called a cellulose chain. Two monomer units together describe cellobiose. Depending on the organization and packing of these cellulose chains, they can be classified into seven different polymorphs: $I_α$; $I_β$; II; III_I, III_{II}, IV_I, and IV_{II}, as shown in **Figure 6**.[64]
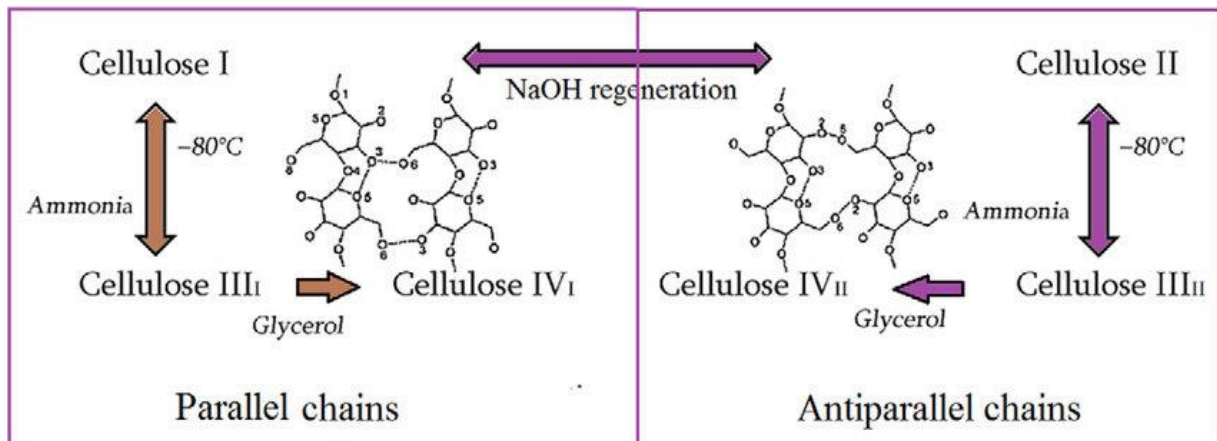
Figure 6 Interconversion between cellulose polymorphs and hydrogen bonding patterns for cellulose I and II.[65] Used with permission of Elsevier Science & Technology Journals, from *11 – Nanocellulose: Preparation methods and applications* , in *Cellulose-Reinforced Nanofibre Composites: Production, Properties and Applications.,* Nasir, M., et al., 2017.; permission conveyed through Copyright Clearance Center, Inc.

Native cellulose, as directly obtained from biomass, is crystalline and its chains are organized in parallel. While the cellulose found in algae and bacteria is mainly I_α, both I_α and I_β are present in higher plants. These structures are represented in **Figure 7**.
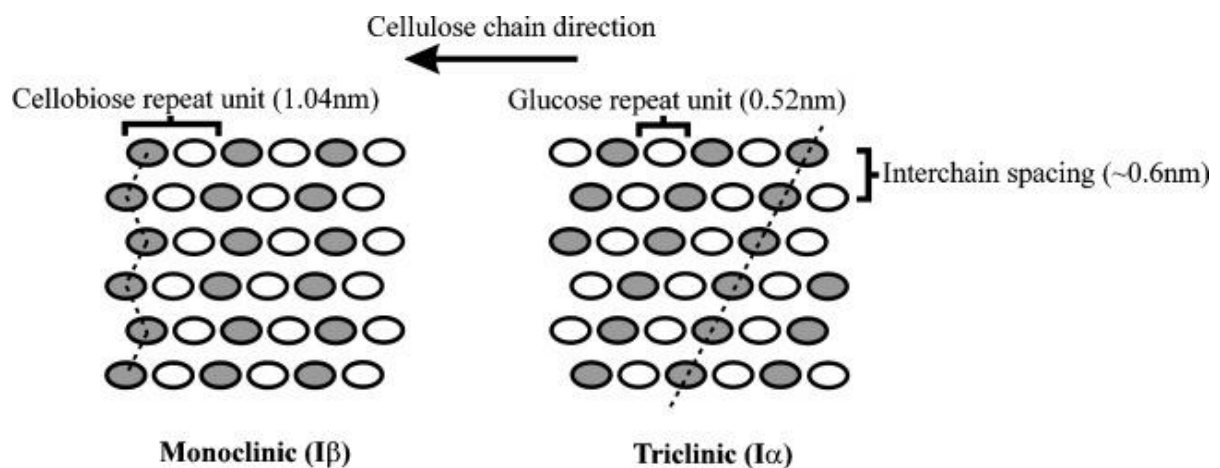
Figure 7 Difference in chain organization between cellulose I_α and I_β.[66] Used with permission of John Wiley & Sons - Books, from *Cellulose crystallites*., Fleming, K., D.G. Gray, and S. Matthews., 7., 2001.; permission conveyed through Copyright Clearance Center, Inc.

The main difference between these two polymorphs is their hydrogen bond patterns, with I_α having one chain in a triclinic unit cell (a meta-stable phase) and I_β containing two chains in a monoclinic unit cell. I_α can be converted into I_β by annealing at 270 °C and, in plant species

where both polymorphs co-exist, I_α might be more prone to attack when cellulose is extracted from biomass through chemical or enzymatic extraction processes.[59, 67]

Cellulose II is regenerated cellulose, that can be obtained through the process of mercerization or, more efficiently, through regeneration of cellulose I in a basic medium. In the first case, the fibers are swelled in a strong sodium hydroxide medium, and cellulose II is obtained. In the second one, the solubilization of native cellulose and its regeneration converts it into cellulose II. In cellulose II, its chains are organized in an antiparallel fashion and the extra hydrogen bond between chains makes this polymorph more thermodynamically stable and the conversion reaction irreversible. The chains are said to be parallel when the direction of the $1 \rightarrow 4$ chain is the same and antiparallel when these are in opposite directions.[68-70] Cellulose III can be obtained from celluloses I and II (III_I and III_{II}, respectively) by chemical treatment with ammonia or other amine compounds. At high temperatures and humidity, this reaction can be reversible while cellulose IV polymorphs are stable. These are obtained by conversion of celluloses III up to 260 °C in glycerol. While cellulose I and IV can be observed in nature, II and III are purely artificial. While having crystalline domains, cellulose also has amorphous phases. These contain a lower density of fibers, that are randomly organized. These regions are more prone to chemical attack and, depending on the conditions, can be degraded leaving only the crystalline domains.[64, 71] It is important to notice that even those amorphous regions still have a certain degree of order, so it cannot be considered a completely "amorphous" phase.[59]

The degree of polymerization (DP) is an important factor in the characterization of cellulose. It counts the number of anhydroglucose units in the cellulose chains, which range from 100 to 44000 depending on the biomass, extraction process, and treatment. These values are higher for cellulose I than for II. The influence of these factors is further observed in the determination of the index of crystallinity (*ICs*), which is another important trait of celluloses. The main techniques used to determine the DP are viscometry, gel permeation chromatography (GPC), and light scattering techniques but, due to the insolubility of cellulose in most media, specific preparation of the samples is required.[67, 72, 73] This is due to cellulose´s high molecular weight, high crystallinity, and strong hydrogen bond network (intra and intermolecular) that strongly attaches cellulose fibrils. Hydrophobic interactions and van der Walls forces further play a role in explaining this packing.[64, 74, 75]

2.2.1   Dissolution of Cellulose

Cellulose is not easily dissolved due to the presence of strong hydrogen bond networks, hydrophobic interactions between the surface of the glucopyranose rings, and other intermolecular interactions. Besides, the crystallinity of cellulose and the fact that it can only turn its 1-4 bond, as shown in **Figure 5**, limits the degrees of freedom for conformational changes and hinders the increase in entropy.[76]

The most widely used method of dissolution in the industry has been derivative, the viscose procedure. Here, cellulose is converted with CS_2 into the alkali-soluble cellulose xanthogenate and is regenerated by the addition of an acid solution. Besides the inherent toxicity and explosive nature of CS_2, this process produces high quantities of residues and degrades the cellulose backbone. For the past decades, non-derivative solvents have been developed that are capable of dissolving the cellulose without altering its chemical composition.[77, 78] Here, it is assumed a previous swelling phase, where the solvent molecules penetrate the cellulose amorphous region network, expand its volume, and facilitate further penetration and dissolution among the rest of the chain network.[79, 80]

A class of solvents uses non-organic compounds such as metal complex solutions and inorganic salt hydrate melts. The first type includes well-known complexes such as cuprammonium hydroxide (Cuam), cupriethylenediamine hydroxide (Cuen), and Cadoxen: $[Cd(H_2N(CH_2)_2NH_2)_3]$ $(OH)_2$, which are widely used for determination of the DP of cellulose in viscometry.[67, 81] Inorganic salt hydrates melts, such as $ZnCl_2.3H_2O$, $Ca(SCN).3H_2O$ and Li salts dissolve similarly.[82-84] Other solvents include LiCl/N,N-dimethylacetamide (LiCl/DMAc)[85], $TBAF \cdot 3H_2O$[86], N-methylmorpholine-N-oxide (NMMO)[87, 88], and ionic liquids such as was 1-allyl-3-methylimidazolium chloride (AMIMCl).[89, 90]

Most of these systems suffer from toxicity, high cost, difficult recycling processes, limited capacity for dissolution of cellulose according to its concentration or molecular weight, cellulose side reactions, and cumbersome upscaling.[77]

Another alternative is to use simply a sodium hydroxide aqueous solution, at low temperatures, to dissolve up to 8 wt.-% cellulose depending on its molecular weight. Common additives, such as urea and thiourea, can be added to improve dissolution. These turn this method into one of the cheapest, most accessible, and sustainable.

The method discussed here involves the creation of hydrates by dissolving NaOH in water. **Figure 8** shows the binary phase diagram where multiple stable and metastable hydrates can be found in the NaOH concentration range of 20 wt.-% to 70 wt.-%. For cellulose dissolution, the interesting concentration is below 20 wt.-%, where a eutectic mixture is found, (NaOH,

$5H_2O$; $4H_2O$). In **Figure 9**, A binary phase diagram of NaOH:water for that range can be observed. The hydrate structure and size depend on the NaOH:H_2O ratio and solution temperature.[76]

The ideal concentration range for hydrates with the right hydrodynamic diameter to penetrate first in the amorphous regions of cellulose and, from then, into more crystalline domains is between 7 wt.-% to 10 wt.-%. At higher concentrations, the hydrates are too small to effectively disrupt the hydrogen bonds between cellulose fibers, and, at lower concentrations, they are too big to penetrate the cellulose chains. Furthermore, it can be argued that a negatively charged cellulose at high pH is also more easily dissolvable. The maximum cellulose dissolution is achieved with a ratio of four moles of NaOH to one mole of a hydroglucose unit. This corresponds to a 7 wt.-% to 8 wt.-% cellulose concentration in a 7 wt.-% to 8 wt.-% NaOH-water solution, at negative temperatures.[76, 91] A representation of the possible structure of dissolved cellulose at these conditions is presented in **Figure 10**.
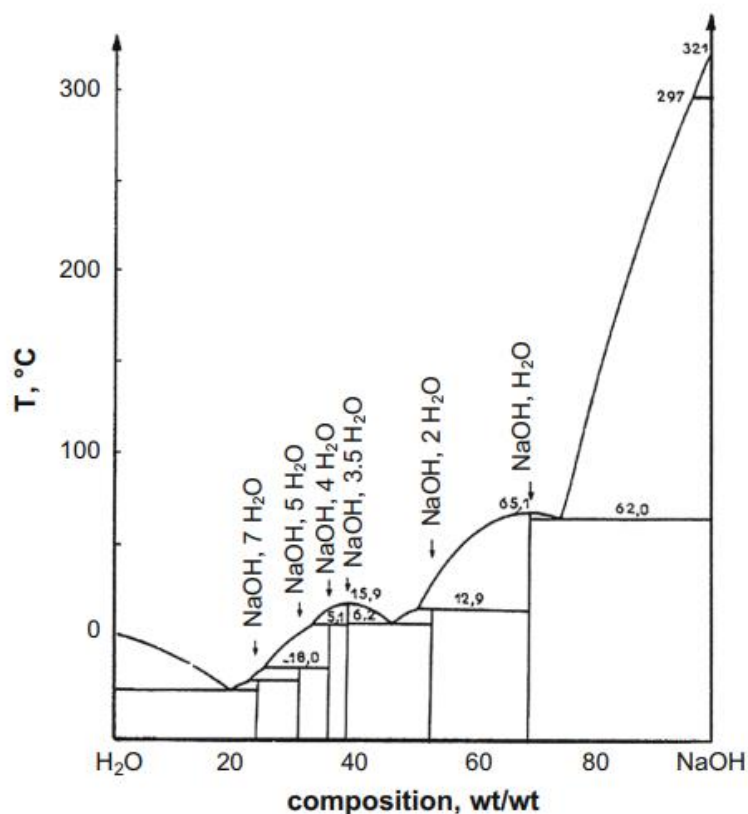
Figure 8 Binary phase diagram of NaOH and water. [76] Used with permission of Springer Nature BV, from *Cellulose in NaOH–water based solvents: a review*., Budtova, T. and P. Navard., 23., 2015.; permission conveyed through Copyright Clearance Center, Inc.

2.2 Cellulose

The reason for the better dissolution at low temperatures can be explained by the conditions at which the $NaOH:H_2O$ eutectic mixture can be reached, by the amphiphilic character of cellulose, and by its DP. At higher temperatures, the relative viscosity of the cellulose solution decreases due to the decrease of effectiveness of the solvent.[92] The hydrophobic regions of the cellulose fibers (centered on their pyranose rings) have stronger interactions at higher temperatures, increasing compaction on existing conglomerates. These forces will create new, smaller compact conglomerates and so, this viscous liquid transforms into a gel. A phase separation between a rich and poor fiber phase can be observed when gelation is induced by temperature as the solution becomes increasingly opaque. A higher DP also means that the fibers will more easily interact with one another, creating aggregates more difficult to dissolve. [76, 93, 94]
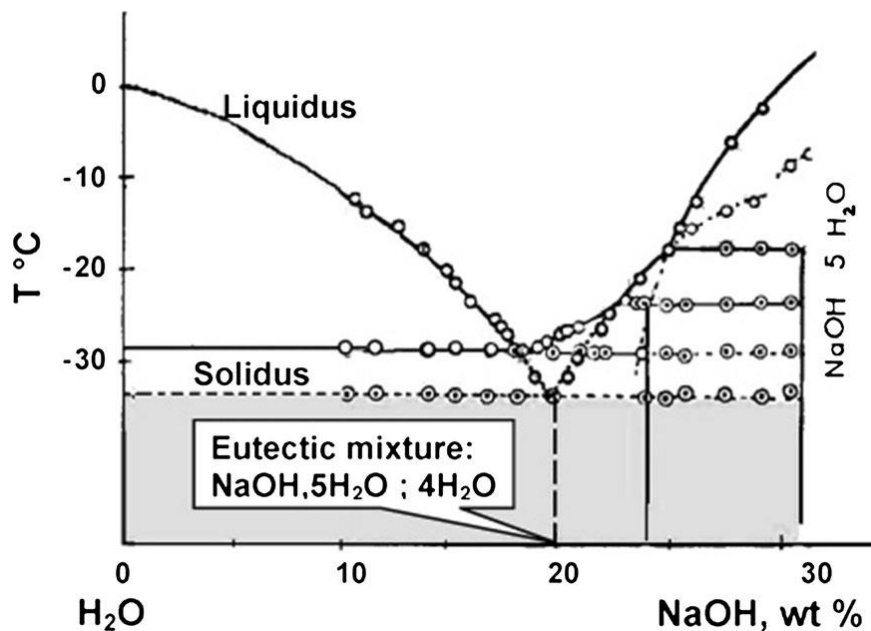
Figure 9 Binary phase diagram of NaOH and water for concentrations of NaOH below 30 wt.- %.[76] Used with permission of Springer Nature BV, from *Cellulose in NaOH–water based solvents: a review*., Budtova, T. and P. Navard., 23., 2015.; permission conveyed through Copyright Clearance Center, Inc.

Other authors proposed, alternatively, that gelation was due to the formation of new crystalline domains with increasing temperatures or due to the adsorption of CO_2 and the formation of carbonate bridges between cellulose chains.[95, 96]
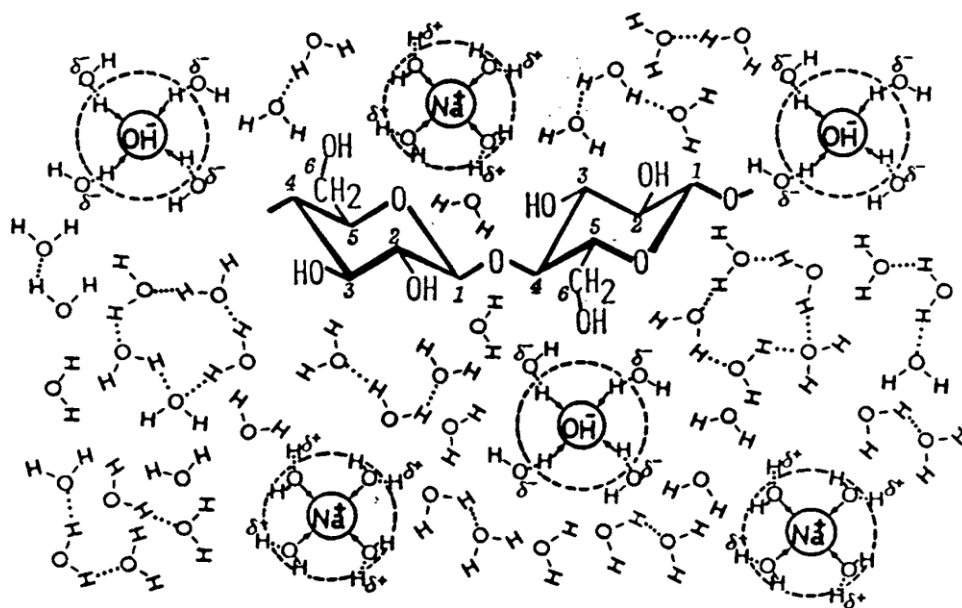
Figure 10 Tentative schematic representation of a structure of the dissolved cellobiose in NaOH-water solution.[76] Used with permission of Springer Nature BV, from *Cellulose in NaOH–water based solvents: a review*., Budtova, T. and P. Navard., 23., 2015.; permission conveyed through Copyright Clearance Center, Inc.

Another explanation may be related to the conformational changes of cellulose at different temperatures. At negative temperatures, the more polar configurations would be promoted and so, its interaction with the NaOH hydrates.[63] Alternative hypotheses include the exothermic overall character of the dissolution process (promoted at low temperatures) and the temperature-dependent nature of the NaOH hydrates, whose hydrogen bonds become weaker at higher temperatures as their network is gradually destroyed.[79]

Despite the effectiveness of the NaOH system in dissolving cellulose, this system is not stable and it can only dissolve cellulose fibers with low DP (no more than 300). These make it a very restrictive technique, not suitable for upscaling. To increase the range of celluloses that can be dissolved, amphiphilic additives such as urea, thiourea, and polyethyleneglycol (PEG) can be added while maintaining the same NaOH concentration.[97] Urea is an additive well known for its availability, non-toxicity, low cost, and abundant literature on its role in the synthesis of cellulose aerogels. The addition of urea in 12 wt.-% concentration to a 7 wt.-% NaOH aqueous solution provides a stable and effective dissolution media for cellulose at low temperatures (see **Figure 11**).
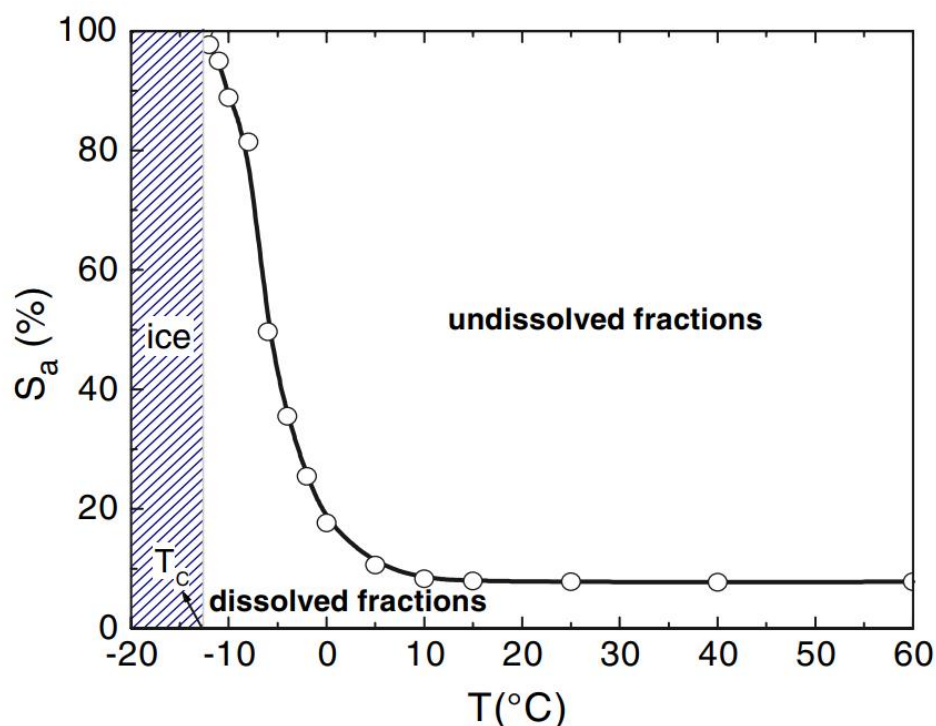
Figure 11 Solubility range of cellulose in 7 wt.-% NaOH, 12 wt.-% urea solution in water.[98] Used with permission of Springer Nature BV, from *Effects of temperature and molecular weight on dissolution of cellulose in NaOH/urea aqueous solution.*, Qi, H., C. Chang, and L. Zhang., 15., 2008.; permission conveyed through Copyright Clearance Center, Inc.

However, the exact role of urea in the process is still debatable. Song et al. showed through 13C CP/MAS solid-state NMR that, at urea concentration over 12 wt.-%, a peak associated with free urea appears and it is enhanced at higher concentrations. This concentration ensured maximum interaction between the cellulose-NaOH species and urea.[99]

Cai et al. defended that urea interacts with cellulose mainly through hydrogen bonds while Egal et al. argued that urea does not have any direct interaction with either NaOH or cellulose.[91, 100] Urea´s role as a disruptor of the hydrogen bonding network among water molecules is also contentious. Later research suggests that urea stabilizes the hydrophobic regions of cellulose due to its amphiphilic character. Xiong et al. through ^{13}C NMR studies, regarded that there were no hydrogen bonds between cellulose or NaOH and urea and that the latter acted as a weak disrupter of the hydrogen bond network between water molecules.[94] Nonetheless, urea is completely soluble in water and can self-assemble on the hydrophobic regions of cellulose, which reduces their interaction with the polar solvent. This, plus the hydrogen bonds formed between water, decreases the aggregation tendency between these regions, ensures a better dispersion of fibers, and delays gelation. This mechanism is similar to the ones observed for thiourea or PEG, which makes the cellulose dissolution process an enthalpy-driven exothermic

process with negative entropy.[63, 79] The negative entropy comes from the described self-assembly of all these particles. As both hydrophilic and hydrophobic regions of cellulose have to be stabilized by the solvent molecules, dissolution is favored when their mobility is reduced and less energy is present in the system. This can explain why dissolution occurs at low temperatures, as here macromolecules have a lower chance to interact with each other and the solvent, and additive molecules form large clusters around these fibers that ensure their dissolution.[94] In **Figure 12**, a molecular model of the interaction of cellulose with urea when dissolved can be observed. While difficult to demonstrate this experimentally, simulating studies based on molecular dynamics,[101-104] and the three-dimensional Reference Interaction Site Model support the role of urea as a stabilizer of the hydrophobic regions of cellulose.[105] The mechanisms behind the regeneration of dissolved cellulose and their influence on the formation of a porous wet gel are discussed in the next chapter.
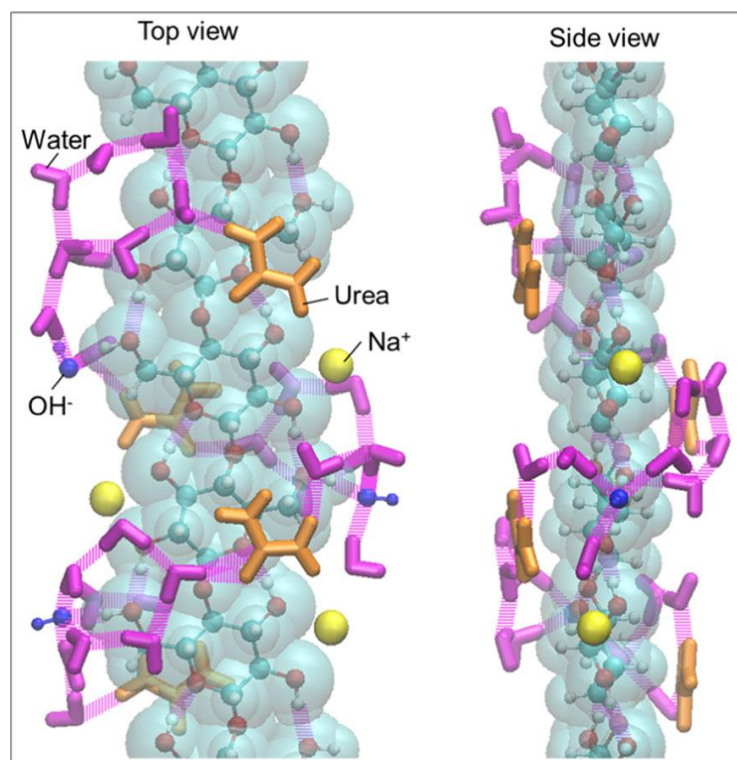
Figure 12 Molecular model of urea:cellulose:NaOH water system. As described, urea is present on the surface of the hydrophobic pyranose rings, while Na^+ and OH^- are at their edges.[105] Used with permission of Springer Nature BV, from *Thermodynamic analysis of cellulose complex in NaOH–urea solution using reference interaction site model.,* Huh, E., et al., 27., 2020.; permission conveyed through Copyright Clearance Center, Inc.

2.2.2 Regeneration of Cellulose

To create a 3D fibrillar gel network from the dissolved cellulose fibers, they should be regenerated through contact with a non-solvent. The gel formed can have many different shapes (beads, monoliths, sheets, fibers, among others) and properties based on the coagulant, temperature, time, and regeneration pathway. An understanding of the mechanisms of regeneration is essential to properly tune the morphology and properties of the cellulose aerogels. Furthermore, through chemical and physical modification, cellulose gels can be converted into composite and multifunctional materials. [77]

When in contact with a non-solvent, Na^+, OH^-, and urea move out of the cellulose solution while diffusion of the coagulant occurs in the opposite direction.[106] During gelation, a micro-phase separation occurs between the cellulose fibrils and the solvent that creates the 3D network of a wet gel. This phase separation can be observed by the increase of opacity in the gel and syneresis. The syneresis or shrinkage in the gel is related to the miscibility of cellulose with the coagulant and it can be analyzed using the Hildebrand (solubility) parameter (δ) or the Hansen parameters. These measure the attractive forces between solvents and respective solutes. The closer the solubility parameters, the more miscible the polymer and the solvent, and the lower the shrinkage in the gel. When regeneration occurs in water, the shrinkage is much lower than in ethanol, as the Δ_δ water:cellulose is 8.5 while ethanol:cellulose is 13.[106] This is also why the solvent exchange before drying should be done in multiple steps and an appropriate solvent should be chosen to minimize shrinkage.[46, 47]

The creation of a heterogeneous medium during gelation, with polymer-rich and polymer-poor regions, will influence the diffusion rate of the smaller molecules and, as a consequence, the speed of regeneration. For example, in a gel, the viscosity in its pores is lower than in a non-gelled cellulose solution, which leads to a higher mobility of Na^+ and OH^- ions in the former. At higher DPs and concentrations of cellulose fibers, there is an increased number of contacts and interactions between them which contributes to an increase in coagulation speed. At higher temperatures or higher concentrations of coagulants in the case of acids or salt solutions, diffusion is faster and the pores in the gel are bigger due to the fast precipitation of cellulose which do not have the time to organize themselves in a filigree porous structure.[76, 106] A faster diffusion is further related to larger dimensions, as less time is available for the fibers to reorganize into a more packed, smaller gel body.[107]

Depending on the speed of coagulation, the surface of the aerogel is dense while its interior presents a heterogeneous porous structure, mainly mesoporous. In the immediate surface of contact with the coagulant agent, diffusion is very fast. As a consequence, cellulose fibers

quickly agglomerate in the form of a thin skin of a few hundred nanometers.[106] In the interior, where coagulation is slower and is mainly controlled by diffusion, the filigree structure obtained from the reorganization of the cellulose fibers maximizes the surface area and the presence of smaller mesopores. With the increase of the gelation speed, a more macroporous internal structure is privileged with thicker fibrils and higher mechanical stability.[107-109]

Besides water, organic solvents can be used (acetone, alcohols, esters, among others), as well as acids (H_2SO_4, HCl, CH_3COOH, etc) and salt solutions (Na_2SO_4, NaCl, etc) as coagulation baths. It is interesting to notice that the polarity of these solvents will affect the crystallinity of the coagulated gels. When acids or salt solutions are employed, the cellulose fibers stack by their hydrophobic pyranose rings while their OH groups are oriented to the exterior. This trend will promote certain diffraction patterns. More hydrophobic surfaces are created when alcohols or acetone are used as coagulants.[110, 111] This, in conjugation with the coagulation speed, will determine the aerogel's mechanical properties.[69, 112] Adding salts to the cellulose solution before coagulation also influences aerogel properties. These salts can promote faster gelation or act as scaffolds for tailoring the porous structure.[113, 114] The higher the interaction of these ions with water (kosmotropes, in opposition to chaotropes), the higher the interaction between cellulose fibers. This is due to the decrease of the quality of the solvent which promotes a higher viscosity of the solution and faster precipitation.[115-117]

2.2.3 Cellulose in Biomass

Cellulose is a natural polysaccharide, that needs to be obtained from natural sources before handling. Polysaccharides are carbohydrate polymers based on sugars found in plants, animals, microorganisms, and fungi. They include homo-polysaccharides such as cellulose, starch, and chitosan,[22, 57] consisting of only one repeating unit, and biopolymers composed of more than one monomer repeating unit, such as alginate, carrageenans, and pectins, among others.[118-120] To obtain polysaccharide-based aerogels, polysaccharides are dissolved in a liquid medium, and a network is formed by their reaggregation when changing the medium conditions (pH, temperature, ionic force, addition of anti-solvent, and others).[21] Unlike the classic sol-gel process, there is no polymerization and, for most cases, cross-linking is not required as the starting solution contains polymeric chains and not a suspension of monomers/precursors. The regeneration of the biopolymeric chains depends on each polysaccharide but usually involves a non-solvent-induced phase separation.[14, 24]

2.2 Cellulose

Most of the mentioned polysaccharides are abundant in nature, with some comprising the most abundant composite on earth: the lignocellulosic polymer. Its general composition can be observed in **Figure 13**.
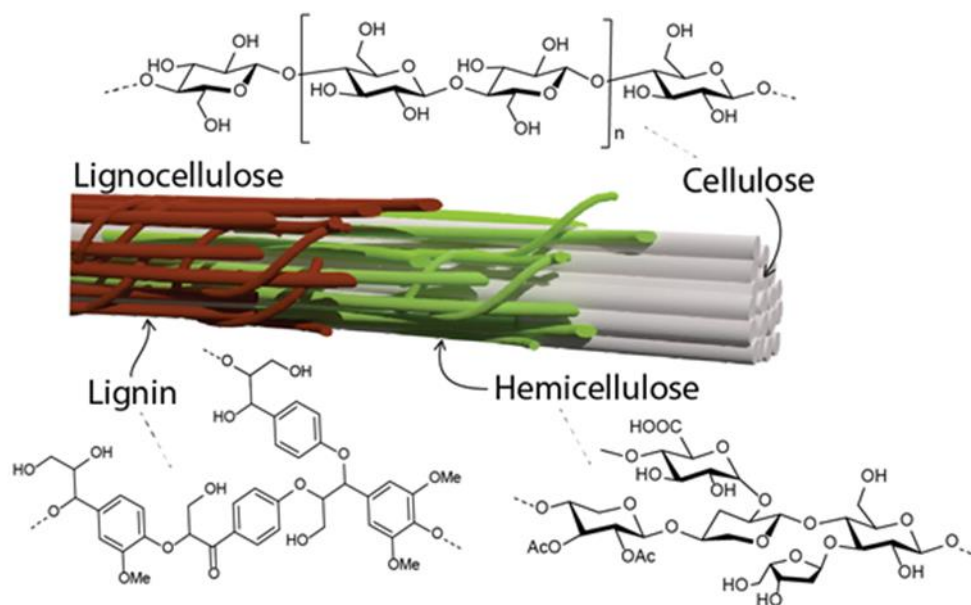
Figure 13 Lignocellulosic polymer composite and structure of its constituents.[121] Used (adapted) with permission of Springer Nature BV, from *Solar-driven reforming of lignocellulose to H2 with a CdS/CdOx photocatalyst*., Wakerley, D.W., et al., 2., 2017; permission conveyed through Copyright Clearance Center, Inc.

The lignocellulosic polymeric consists of a combination in varying proportions of cellulose, lignin, and hemicellulose, and is the main constituent of the plant kingdom. For the production of aerogels from this composite, two main alternatives exist: the aerogel can be produced directly from it or from the polysaccharides obtained from the fractioning of the lignocellulosic polymer. While cellulose aerogels have been under research for decades, lignin and hemicellulose aerogels have been more intensively studied recently.[19, 64, 122]

Chemical, physical, and biochemical methods can be applied to separate cellulose, lignin, and hemicellulose from the lignocellulosic polymer. All these polymers are known for their biodegradability, non-toxicity, renewability, and abundance. Hemicellulose composes 20- 30 wt.-% of lignocellulosic biomass and, as observed for many other biopolymers, its composition varies widely depending on its source.[64, 123] Due to its low molecular weight (MW), easily hydrolysable chemical bonds, and chemical variability, hemicellulose has very low mechanical properties which hinder its conversion into monolithic aerogels.[24, 123, 124]

Lignin is also an irregular polymer, but its structure is more stable than hemicellulose. It comprises 20 to 30 wt.-% of woody plants, where it fulfills structural and defense functions due to its recalcitrant nature. Lignin is a phenolic polymer, composed of p-coumaryl, coniferyl, and sinapyl alcohols. These differ in the number of methoxy groups and are present in different proportions depending on the plant species and extraction method. It is one of the most relevant residues from the paper milling industry but it can also be purposely extracted from biomass through alkali and sulfite processes, and organosolv techniques, among others. While it is used as a binder and additive for animal feed and composite industries, it is mainly combusted for energy production.[24, 125] Recently, research has focused on valorizing this residue into more high-value products such as fine chemicals, adhesives, and other advanced materials. One of these is aerogels. Most lignin aerogels are created through crosslinking with formaldehyde and other components such as tannin, phenol, or resorcinol to create a stable porous network.[18, 126] Many of these aerogels have relatively high thermal conductivities (40- 50 mW m^{-1} K^{-1}) and densities (0.2-0.4 g cm^{-3}). Nonetheless, they can be mixed with other biopolymers like alginate and reach surface areas as high as 550 m^2 g^{-1}. Due to their natural hydrophobic properties and high carbon content, they might be particularly interesting for thermal insulation or supercapacitors, but more research is still required.[24, 126]

Despite all these properties, cellulose presents some advantages compared to lignin and hemicellulose. It is not only the most abundant biopolymer on earth, but its linear and consistent chemical structure can be accurately characterized and manipulated, something that is still a challenge for irregular polymers such as hemicellulose and lignin. Additionally, the methods to extract chemically pure cellulose from biomass are at a higher scientific and technical development compared to the extraction of other lignocellulosic polymers.

Therefore, based on cellulose properties, its well-tested extraction processes, and extensive research on cellulose aerogels, cellulose is particularly interesting for the synthesis of aerogels.

2.2.4 Coating of Cellulose

Cellulose, as well as cellulose aerogels, are known for their hydrophilicity and flammability which hinder their application as thermal insulators. To solve these issues, various strategies have been developed to improve insulation properties and stabilize the aerogels in the long term by surface coating. For instance, a protective coating or a filler can be added to the material to enhance fire resistance. These additives can act by releasing inert products, creating free radical scavenging compounds to inhibit the combustion reaction, and forming a protective layer, among others. Common alternatives involve oxidation, adding silane groups (silanization)[127-

2.2 Cellulose

129], carbon chains (esterification, graft polymerization)[130], or phosphorous or boric-based moieties on the cellulose´s surface are common alternatives.[131] These methods protect the oxygen groups in cellulose, further improving the material´s resistance to moisture and combustion.[132, 133]

In recent years, biobased non-toxic alternatives have been under scrutiny, such as tannic, phytic acids, and isoborbide, among others. One interesting alternative is lignin because, as discussed in previous chapters, it is highly abundant, and its phenolic structure enables the formation of a char layer that can protect the more combustible cellulose (up to 41% of char residue after combustion).[134] Its antioxidative properties also indicate resistance against the radical reactions of combustion. Modifying lignin with phosphoric-nitrogen or silica groups further enhances its natural fire and moisture resistance.[135-137]

Lignin could then act as a modification agent of cellulose to improve its resistance against water and fire. However, the interaction of lignin with cellulose and with modifying agents is hindered by its complex irregular chemical structure (see **Figure 14**) which is influenced by multiple factors, including the source of biomass and its treatment.[138]
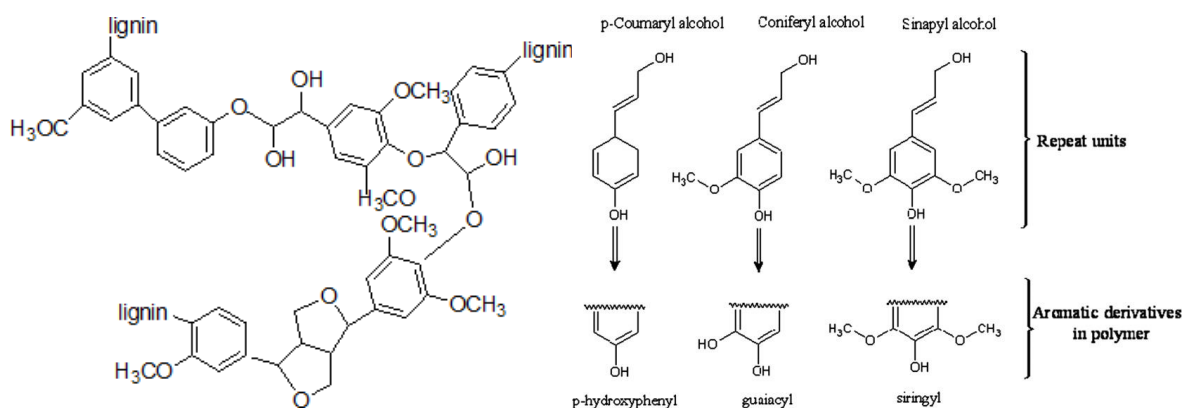
Figure 14 On the left, general structure of lignin.[136] Used with permission from Springer Nature BV, from *Recent Developments in Flame-Retardant Lignin-Based Biocomposite: Manufacturing, and characterization.,* Solihat, N.N., et al., 30., 2022. On the right, the structures of the repeat units of lignin and their derivatives.[126] Used with permission of Elsevier Science & Technology Journals, from *Lignin–phenol–formaldehyde aerogels and cryogels.,* Grishechko, L.I., et al., 168., 2013. Permissions conveyed through Copyright Clearance Center, Inc.

Lignin extracted using sulfur methods (Kraft and sulfite lignin) contains up to 3 wt.-% and 8 wt.-%, of sulfur content, respectively. These materials are not pure but present higher molecular weights and OH moieties than lignin produced through sulfur-free processes (soda

and organosolv lignin). Costes et al. verified that organosolv lignin was less thermally stable due to the relative content in carboxylic and phenolic groups than Kraft lignin.[137] While sulfur-containing methods are applied to hard and softwood, sulfur-free processes are used on agriculture residues. The lignin obtained from the latter processes is more hydrophobic than the one obtained from the former.[136]

Due to its hydrophobicity, lignin can only be dissolved in organic solvents or basic aqueous solutions. Depending on its relative chemical compositions, the solubility of lignin ranges significantly. Fitigău et al. concluded that Kraft lignin had a maximum solubility at an acetone:water mixture of 50 vol.-% while for soda lignin, it was found at 90 vol.-%.[139] The dissolution of the widely commercially available Kraft lignin in ethanol:water mixtures, alkali water, and other solvents has been particularly studied as well as its comparison with other classes of lignin.[140-142] The conditions for lignin precipitation when in basic media and the relations between the pKa of its phenolic groups, the pH, temperature, and the ionic force of the solution are still not well understood. Generally, at higher salt concentrations, the conversion of lignin into larger particles and conglomerates that precipitate occurs at higher pHs. This is due to the electrostatic interactions between salt ions and dissociated phenolic and carboxylic groups of lignin, which promote lignin protonation and consequent precipitation.[143-145] These mechanisms are essential to quantify how much lignin can be dissolved in a basic solution and remain dissolved after neutralization.

Furthermore, unmodified lignin agglomerates on the polymer matrix may not interact strongly enough if this matrix is hydrophilic and no chemical bonding is applied. This poor interfacial adhesion may lead to leaching and a decrease in the mechanical resistance of the material.[146, 147] On the interaction of lignin with cellulose fibers, it was found that lignin can adsorb on cellulose (especially in complexation with $CaCl_2$) as conglomerates, but most of it leaches after washing.[148, 149] Computational studies indicate that the adsorbed lignin interacts through its OH groups with the OH groups of cellulose, by electrostatic dipole-dipole interactions, while its phenol rings tend to be parallel to the cellulose chains.[150]

In the synthesis of cellulose aerogels, the influence of lignin on the cellulose solution and the cellulose aerogel body has been studied. Costa et al. found that the dissolution of cellulose in NaOH media was promoted due to the amphiphilic properties of Kraft lignin, which acted as urea.[151] On the other hand, Sescousse et al. noticed the opposite trend when organosolv lignin was used while observing lignin leaching during coagulation (more leaching and higher pores were observed with decreasing acid concentration in the regeneration bath).[152] Similar observations were recorded by other researchers when lignin-cellulose composites were

formed, in monolith or bead shape.[153] The aerogels with lignin became more hydrophobic and presented lower thermal conductivity but its leaching and formation of bigger pores decreased specific surface area.[24, 154]

In the next chapters, the properties of cellulose aerogels are described.

2.3 Cellulose Aerogels

As was observed, cellulose has a versatile structure that makes it prone to modification treatments. A wide range of cellulose materials exist, from which cellulose aerogels can be produced. Due to the inter-changeability of terms to describe similar but different compounds, these will be described in this chapter. Different cellulose materials can be classified and created depending on the cellulose extraction process from a cellulosic precursor (such as biomass) and the cellulose´s DP.[64, 65]

2.3.1 Cellulose I Aerogels

Nanocellulose fibers are extremely small, with dimensions lower than 100 nm. Cellulose nanofibers (CNFs) and nanocellulose crystals (CNCs) are obtained mainly from plant biomass while bacterial cellulose (BC) is synthesized by bacteria cultures, as shown in **Figure 15**.[74, 155-157] CNFs, also known as microfibrillated cellulose (MFC), contain crystalline and amorphous domains and can have high aspect ratios with a length of up to tens of micrometers and a width between 10 nm and 100 nm. These high aspect ratios are created using energy-intensive mechanical equipment on pulp or cellulose residues.[158-160] However, separating cellulose nanofibers from the tightly packed natural fibrils is energy-intensive and costly. Chemical treatments such as acid hydrolysis, TEMPO oxidation, and enzymatic action can be applied to functionalize cellulose´s surface and facilitate the defibrillation process.[75, 160]
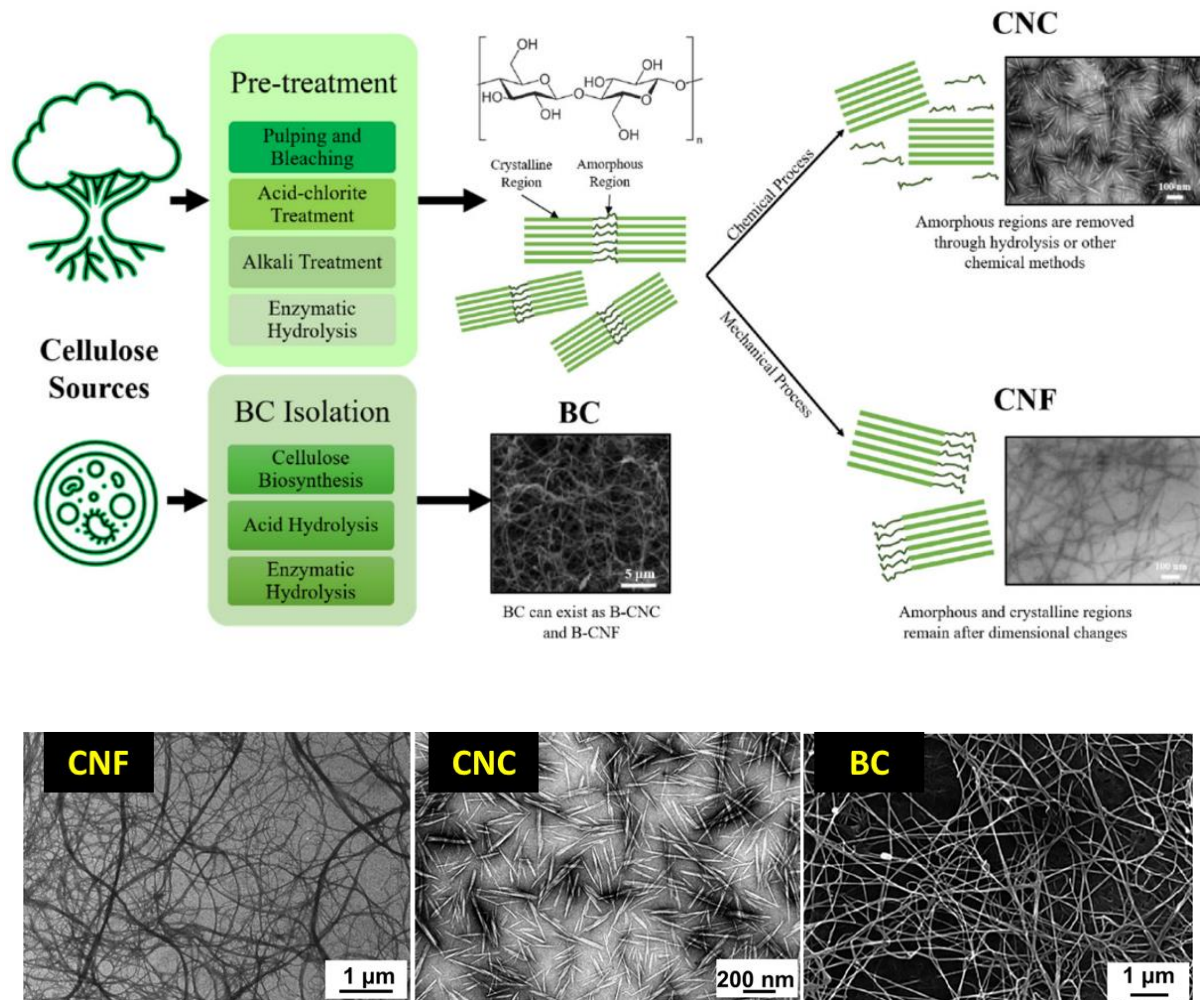
Figure 15 General processes for the production of CNF, CNC, and BC, as well as SEM pictures of these materials.[157] (CC BY 4.0, https://creativecommons.org/licences/by/4.0/)

In the case where the width of the fibers is also in the nano-scale they are called nanocellulose crystals. CNCs are obtained from enzymatic or acid hydrolysis (the most common due to higher yields) of biomass or other cellulose-rich materials. This process removes the amorphous regions of the cellulose microfibrils and determines the shape and dimension of the resultant crystalline rod-like product. Besides, strong acids such as sulfuric and phosphoric acids functionalize the surface of the cellulose nanocrystals, stabilizing them in water suspensions.[158, 160] CNCs have a width of 3 nm to 50 nm, and a length between 50 nm to 500 nm and are known for their high tensile strength, aspect ratio, and thermal stability. However, extracting CNCs is inefficient, time-consuming, and costly, resulting in low production yields. [75, 161]

Despite their high production costs, CNCs and CNFs have numerous applications in various industries, from the biomedical to the production of sensors, catalysts, and filters, among others.

Because of their hydrophilic nature, low density, and toughness, they make excellent building blocks for hydrogels and aerogels. CNCs gel in water at concentrations greater than 10 wt.-% and its gelation conditions depend on the ionic strength of the water solution and if additives are added. CNFs, with their longer fibers, create more flexible gels at concentrations between 0.05 wt.-% and 6 wt.-%.[75, 158] The resultant aerogels have porosities over 90% and surface areas as high as 600 $m^2\,g^{-1}$ (slightly higher for CNCs than CNFs), resulting from porous fibrillar networks. Due to their very low density, high porosity, and mesoporous structure, these aerogels have very low thermal conductivities ($\approx 25\,mW\,m^{-1}\,K^{-1}$). Further functionalization or composite creation improves hydrophobicity, mechanical properties, or electrical conductivity.[158]

As discussed above, despite its properties, the production of all classes of nanocellulose is costly and its upscaling is still not feasible. On the other hand, biobased cellulose II aerogels, whose cellulose I precursor can be easily extracted from biomass in the form of pulp or microcrystalline cellulose (MCC), can be synthesized. These extraction processes are well developed and commonly used in industry.[64]

As in the case of other biobased aerogels, the synthesis of cellulose II aerogels involves dissolution, regeneration, neutralization, and drying with possible solvent exchange depending on the coagulation system.[21]

The following chapter will focus on the properties of cellulose II aerogels.

2.3.2   Cellulose II Aerogels

Besides the already described cellulose I aerogels, cellulose II aerogels can be synthesized. As in the previous chapters, the final properties of cellulose aerogels are heavily influenced by factors such as DP and concentration of cellulose, solvent, coagulation conditions, solvent exchange process, and parameters of drying. Nonetheless, after over 20 years of research, some general properties and trends can be noted. Cellulose aerogels have low densities, up to 0.25 $g\,cm^{-3}$, which increase proportionally with cellulose´s content in the aerogels. The increase in cellulose concentration creates a stiffer aerogel structure, with a higher compressive modulus (from 5.2 kPa to 16.67 MPa), and induces a higher resistance to shrinkage during the wet gel´s processing and drying.[57, 162, 163] The stress-strain dependence of cellulose aerogels has three regimes: a linear elastic region from which the Young modulus can be calculated and where the aerogel can still recover its shape, a stress plateau where plastic yield is reached and cell walls start collapsing and a densification region where deformation start to compress the aerogel irreversibly, with consequent destruction of its porous structure.[164, 165]

Regarding their specific surface areas, they range from 100 m^2 g^{-1} to 500 m^2 g^{-1}, with low influence of the cellulose concentration. Here, coagulation mechanisms, shrinkage, and dissolution methods play a bigger role.[82, 164-166] Cai et al. studied the influence of the regeneration (coagulant agent, temperature) and drying conditions on the internal properties of cellulose aerogels, whose density (from 0.10 g cm^{-3} to 0.58 g cm^{-3}) and specific surface area (from 260 m^2 g^{-1} to 410 m^2 g^{-1}) ranged widely.[167] Other researchers reached similar conclusions.[168, 169]

For thermal conductivity, lower values are obtained by reducing the solid backbone of the aerogel (lower density) or by shifting the pore size to the lower values in the mesoporous region. Most samples present a thermal conductivity between 25 mW m^{-1} K^{-1} and 45 mW m^{-1} K^{-1}, and only cellulose composites with silica were able to create hydrophobic materials whose thermal conductivity was lower than the 25 mW m^{-1} K^{-1} of air at STP conditions (18 mW m^{-1} K^{-1}). As a reminder, current alternatives such as mineral wool and glass fiber present thermal conductivities from 30 mW m^{-1} K^{-1} to 50 mW m^{-1} K^{-1}, with polyurethane foams as low as 26 mW m^{-1} K^{-1}.[162, 166, 170, 171] Cellulose fibers, per se, have a thermal conductivity of 40 mW m^{-1} K^{-1}, in the same range as some cases where they are dissolved and converted into aerogels.[11]

Those cellulose-silica composites (where silica fills most of the bigger pores of the cellulose network) and cellulose aerogels with cross-linking agents achieve a higher fraction of mesopores, with the consequent increase in the surface area (from 250 m^2 g^{-1} to 750 m^2 g^{-1}). Despite having similar or improved thermal conductivity properties compared to current market alternatives, cellulose II aerogels are still not super-insulators. The presence of too-thick pore walls or too-large macropores hinders the achievement of superinsulation properties.[57, 163] If aerogels are produced from non-fully dissolved solutions, composites are created where cellulose I and II co-exist. These materials are characterized by a higher degree of crystallinity, stiffer structures that provide higher strength[172-174] and similar specific surface areas (140-340 m^2 g^{-1}) to fully dissolved cellulose solutions.[175]

Besides, moisture increases the thermal conductivity of the aerogels due to water adsorption and hornification of the porous structure. This leads to the closing of the pores, thicker pore walls, and consequent higher thermal conductivity. If aerogels can be produced at a mass scale, their improved performance increases their industrial appeal. In the next chapters, the scaling of the synthesis of aerogels from laboratory to technical scale is discussed.

2.4 Upscaling Processes of Cellulose Aerogels

Most of the aerogels discussed earlier were only produced at a laboratory scale. To reduce production costs and increase their industrial appeal, aerogel synthetic procedures need to be adapted to a technical scale. Cellulose wet gels are produced in four main shapes: beads, sheets, monoliths, and fibers, as these are best suited for most applications. However, only commercial equipment exists for the production of beads and fibers. Up to now the production of a strong gel body in a monolithic shape is time-consuming. For thin sheets, a prototype apparatus for the production was designed, the CAProLi (**C**ellulose **A**erogel **Pro**duction **Li**ne) at the German Aerospace Center, among other works.

2.4.1 Manufacturing of Beads

The upscaling of cellulose gel beads (> 10 μm) or particles can be performed using different technologies, many of which are shown in **Figure 16**. Each creates particles with different dimensions, shapes, morphology, and size distribution. The first class of methods forms the particles by creating an emulsion in a liquid phase that is immiscible with the cellulose solution[176-178], while the second class of techniques forms cellulose solution droplets in a gaseous phase and creates particles by their fall into a regeneration bath.[21, 179] The size and shape of the particles are determined by the viscosity of the solutions, their surface tensions, the stirring speed of the bath, and the chemical interactions between the two phases.[21, 180]
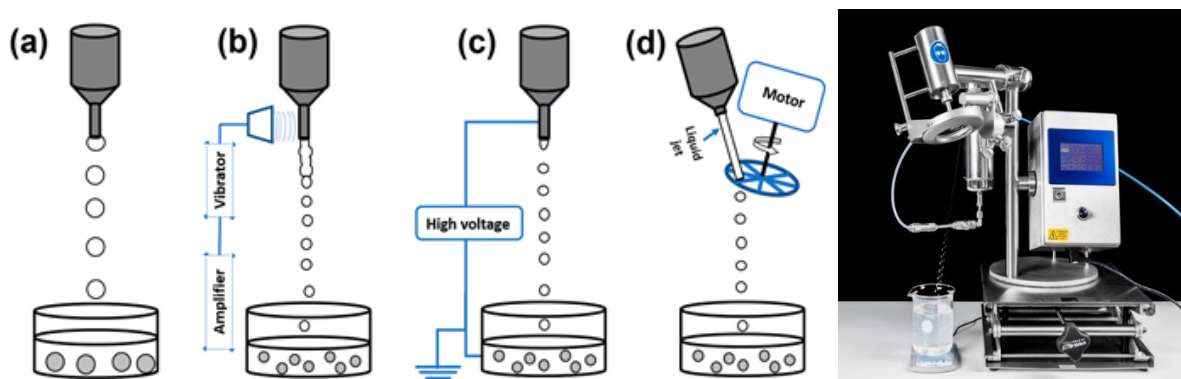
Figure 16 On the left, different techniques used for production of cellulose wet gel beads: dropping method (a), vibrating nozzle (b), electrostatic (c) and mechanical cutting (d). On the right, a JetCutter® in action.[21] (CC BY 4.0, https://creativecommons.org/licences/by/4.0/)

If the stirring rate is too high, it can lead to the distortion of the droplet´s spherical shape, and if it´s too low, non-gelled droplets can coalesce and form aggregates. This trend in stirring is universal for all upscaling techniques.[176]

On the second class of techniques, the conventional dropping method is the most widely used at the laboratory scale. Here, droplets are produced at the tips of nozzles connected to solution-filled containers and continuously fall freely into a regeneration bath. As gravity and the surface tension of the solution are the only forces applied, these droplets have a size of a few millimeters, generally bigger than the nozzle diameter.[179] Factors such as the nozzle diameter, solution viscosity, surface tension, and drop height, among others will influence the shape and size of the particles. If the stability of the droplets is low, they will flatten when encountering the regeneration bath. Besides, the droplets need time to turn their typical pear-like shape when released from the nozzle into a spherical one. The relation between these factors, namely the importance of the viscosity to the surface tension of the droplet (Ohnesorge number, Oh), the importance of inertia to the viscosity of a falling droplet (Reynolds number, Re), and the shape of the beads have been systematically investigated using alginate solutions as models.[181, 182]

This method has a low production capacity but can be slightly improved by using multiple nozzles or adding pressure to increase the dropping speed (the added pressure reduces the particle size).[176] For upscaling the production, a series of techniques were developed where monodisperse particles can be produced and are classified by how they cut the liquid jet: vibrating nozzle, electrostatic, spraying/atomization, and mechanical cutting.[21, 179] These techniques are limited to low-viscosity solutions, are prone to clogging, and produce only small particle sizes (from 300 μm to 1500 μm). These limitations hinder their application even when lab-scale equipment is already commercially available.[21, 176]

The mechanical cutting method is based on the mechanical cutting of the pressurized jet fluid when extruded through a nozzle. The JetCutter® from geniaLab® is one of the best-known equipment following this process. Here, a rotating wired disk cuts the jet into equal particles which develop into spherical droplets while falling into the regeneration bath. By selecting the nozzle diameter, jet speed, cutting frequency, and disk, among other parameters, spherical particles from a few hundred micrometers to a few millimeters can be produced in kilo batches in an economical and fast manner.[179, 180] Besides this high production rate, beads can be produced from solutions with wide viscosity ranges. The inclination of the nozzle and the thickness of the cutting wires can minimize cutting losses during the process but spray losses, which increase with decreasing viscosity of the solutions, cannot be minimized.[21] Schroeter

et al. used the JetCutter® to create cellulose beads from cellulose dissolved in urea:NaOH:water solvent. They successfully synthesized cellulose aerogel beads with production rates as high as 4.1 kg hydrogel/h, high sphericity between 0.92-0.96, and specific surface areas around 400 m^2 g^{-1}.[183]

Based on the determination of optimum parameters for cellulose aerogel bead production using the JetCutter®, this technology can be used to upscale the synthesis of aerogels from both commercial and biobased sources.

2.4.2 Manufacturing of Fibers

The production of cellulose fibers has been of interest in the industry for many decades due to their biodegradability, safety, and comfort when compared to traditional synthetic fibers. Various solvent systems such as the viscose process, ionic liquids, and LiCl/DMAc systems, among others, are used in this process. In all cases, the wet-spinning method creates these fibers by purging the cellulose solution through a nozzle in a regeneration bath (directly or in the air). The regenerated cellulose fiber is then stretched and passes through multiple baths filled with a coagulant agent or water to neutralize and remove salts or residues. The fiber is then collected and dried.[184, 185] A scheme of this process can be observed in **Figure 17**. The viscosity of the solution, the draw ratio of the spinning, the molecular weight, and the distribution of cellulose in the solution are essential parameters. A solution should not be so viscous to clog the nozzle but should have enough cohesive strength between the cellulose molecules to create a stable fiber that can be stretched. The draw ratio (stretching speed after gel formation over the initial extrusion speed) is particularly important as it imparts the mechanical properties of the fibers: a higher ratio leads to a higher orientation of the fibers and increased crystallinity.[186]
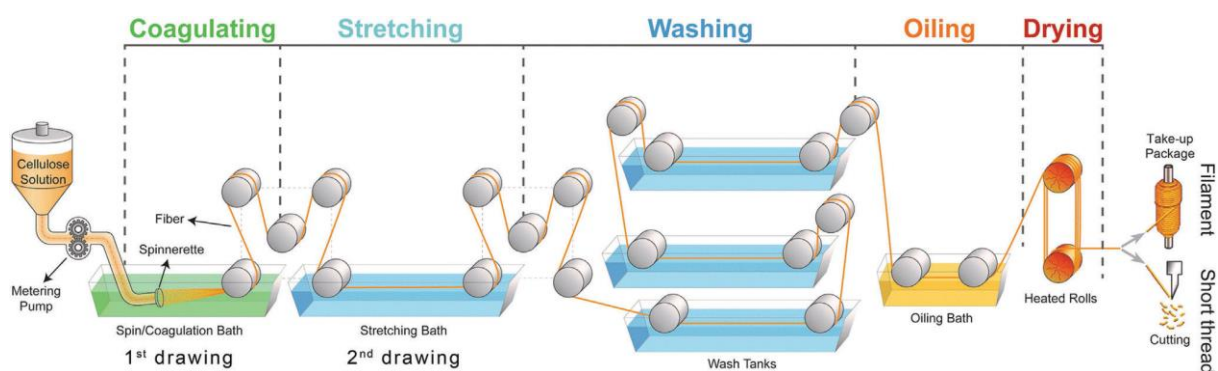
Figure 17 Schematic illustration of the production of regenerated cellulose fibers by wet-spinning.[187] (CC BY 3.0, https://creativecommons.org/licences/by/3.0/)

For an alkali:urea aqueous system, where the radial regeneration of the fiber from the surface to the interior is diffused-based, it is important to use a residence time long enough to ensure complete gelation. A slower regeneration-induced bath is helpful to better align the cellulose fibers with the stretching direction, improving their mechanical properties.[184, 187] The lower the DP of cellulose, the easier it dissolves, but it might negatively affect the chain entanglement and subsequent stretching capacity. If its molecular weight is too high, the entanglement is so intense that it hampers the fiber´s stretching process with a negative influence on its mechanical properties. A higher pumping speed facilitates stretching, increases the fiber´s orientation, and reduces the diameter of the gel fiber.[184, 186, 187]

Cellulose fibers have already been created by dissolving cellulose in Water:NaOH solutions with additives such as urea and thiourea, and by coagulating them in a strong acidic media. Those fibers were found to have a homogeneous structure with a slight fibrillary orientation.[188] Most of these studies concentrated on the mechanical properties of the fibers and indicated that low jet drawing ratios and higher post-drawing ratios lead to improved tensile properties. These studies used water baths at different temperatures for washing, but further batch-wise washing was performed after the fibers were collected.[189, 190]

Some authors focused on developing cellulose aerogel fibers using salt-based dissolution methods such as $Ca(SCN)_2 \cdot 4H_2O$ and $ZnCl_2$, lab-scale wet-spinning apparatus, and coagulation in organic solvents. The materials obtained were mesoporous and presented a high surface area (100- 250 m^2 g^{-1}) and low density (below 0.13 g cm^{-3}).[185, 191-194] Karadagli et al. obtained strong fibers (up to 6.4 MPa) for over 90% porosity.[191] All these synthetic routes, however, require high temperatures for coagulation (from 95 °C to 115 °C for calcium thiocyanate and from 50 °C to 70 °C for zinc chloride). More recently, patents have been focused on the development of cellulose fibers using the water:NaOH:urea dissolution system. Meifang et al. developed patents for porous cellulose gel fibers production using conventional wet-spinning technology in different regeneration baths, cellulose concentrations, and spinning processes. The fibers produced were highly porous (> 85%) with high specific surface areas (100- 400 m^2 g^{-1}), with higher values when thiourea was added and when coagulation was smoother.[195, 196]

While lab-scale equipment can have a 100 mL capacity, technical scale production lines exist with a production capacity of up to 2 L. Based on this background, wet-spinning could be used to create cellulose fibers from both commercial and biobased sources for aerogel production.

In the next chapter, the reasons behind the choice of hemp and flax as sources of cellulose and how to extract it are discussed.

2.5 Cellulose from Biowaste

Biobased wastes should be used as resources for the development of high-value materials such as aerogels. For the production of cellulose aerogels, it is of great interest to use biowastes with a high content of cellulose, that are widely available, can be easily processed, are moisture resistant, and have biological activity.

2.5.1 Hemp and Flax

Crops, such as hemp and flax, shown in **Figure 18**, are known for their outstanding durability and strength, benefiting the mechanical properties of their extracted cellulose.[197-199]

Figure 18 On the left, a field of hemp and, on the right, a field of flax.[200, 201] (CC BY-SA 3.0, https://creativecommons.org/licenses/by-sa/3.0/)

Industrial hemp (*Cannabis Sativa*) has been used for millennia for various purposes, including fiber and seed production. More recently, it has also been used for its medical compounds such as terpenes and phenolic molecules. Unlike marijuana, hemp does not contain more than 0.2 wt.-% to 0.3 wt.-% of the intoxicating tetrahydrocannabinol (THC) and is a source of non-intoxicating cannabidiol (CBD).[202, 203] Hemp seeds are composed of 30 wt.-% protein, 25 wt.-% starch, and 30 wt.-% oil. 90 wt.-% of this oil is composed of unsaturated fatty acids. These oils are used in energy production, cosmetics, and food industries while the protein-rich cake can be used as animal feed.[204]

The stalk of the hemp plant can be separated into bast fibers (20 wt.-% to 35 wt.-%) and hurds (up to 75 wt.-%)[205], as shown in **Figure 19**. In the phloem, bundles of primary bast fibers run across the length of the plant, with secondary bast fibers present at the cambium. The xylem and the pith layers are composed of hurds. Each elementary fiber that comprises the bundles is multi-layered, with primary and secondary walls (split into three sub-layers). These fibers are

bounded together by the middle lamella, mainly composed of lignin, while the S2 sub-layer is the richest in cellulose (each layer has a slightly different chemical composition). The cell wall layers are composed of nano-sized cellulose chains (microfibrils) which self-organize into macrofibrils through interaction with hemicellulose and lignin.[197, 206] Bast fibers are mainly used for textiles, composites, and building applications while hurds are applied as animal bedding. While the former has a high content of cellulose compared to hemicellulose and lignin (64 wt.-% to 78 wt.-%; 16 wt.-% to 22 wt.-% and 3 wt.-% to 6 wt.-%, respectively), hurds are more diverse in their composition (48 wt.-% for cellulose, 21 wt.-% to 25 wt.-% for hemicellulose, and 17 wt.-% to 19 wt.-% for lignin). A higher cellulose content is related to higher strength and Young´s modulus, longer cell length, and lower microfibrillar angle (angle between microfibrils and fiber axis).

Stem	Bundle	Elementary fiber
Diameter from 0.6 to 4.5 cm [32].	50 µm.	10 µm [32].
(a)	(b)	(c)
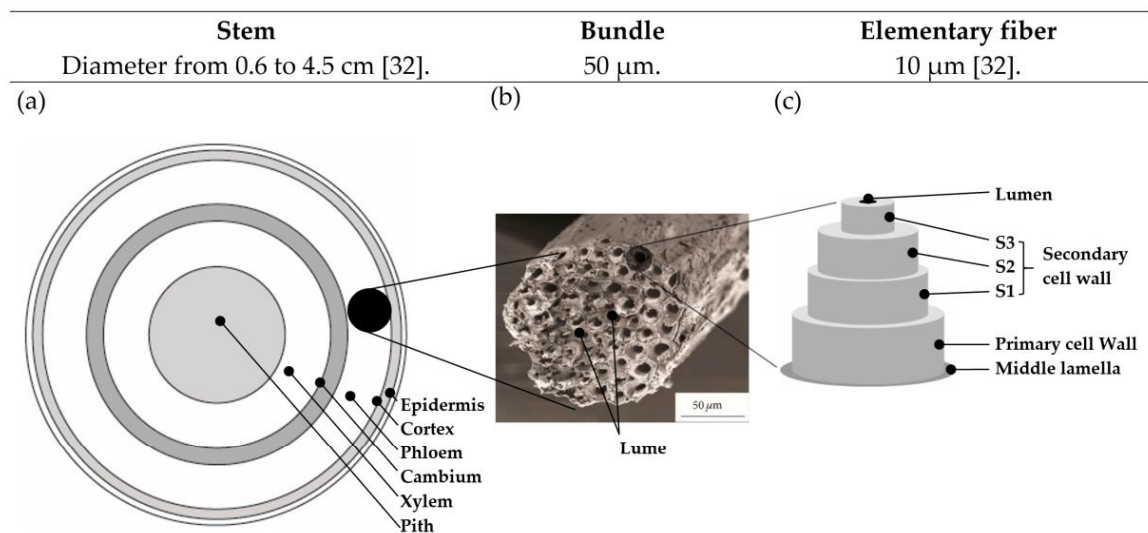
Figure 19 Structure of the stem of hemp. The waste bast fibers are obtained from the phloem of the plant and are organized in a complex multi-layered structure. The secondary wall, namely the S2 layer, is where most cellulose is found.[197] (CC BY 4.0, https://creativecommons.org/licences/by/4.0/)

Hemp and flax have some of the highest Young´s modulus and cellulose content among natural fibers, comparable with glass fibers while having a low density.[197, 199] Hemp bast fibers were tested as thermal insulators due to their low thermal conductivity of 44 mW m^{-1} K^{-1}.[207] While the hurd has a similar composition compared to other energy crops, the higher cellulose content in hemp bast fibers makes them more interesting for the production of biofuels like bio-ethanol, biogas, and building blocks for chemistry. This also makes these fibers a suitable starting point for cellulose extraction and its conversion into cellulose aerogels.[205, 206]

To separate the bast fibers from the hurd, retting is applied. This is a process where the plant is left on the field (dew-retting) or in a water tank (water-retting) after harvesting (at flowering) to favor the degradation of pectin and other components responsible for the binding of the bast and hurd components by microbial activity. Environmental conditions, the microbial population, the retting method, and the crop maturity at harvest will influence the efficacy of this procedure. However, retting is a time-consuming process (up to three weeks) that contributes to water pollution and provides fibers of inconsistent quality. After retting, specialized equipment is used to scutch (break into small pieces the hurds) and decorticate (separate the hurds from the bast fibers) the hemp fibers.[202, 207, 208]

Flax, *Linum usitatissimum L.*, has been used for thousands of years and different strands were developed to obtain fibers and linseed oil. This linseed oil mainly comprises linolenic acid (40 wt.-% to 60 wt.-%), which is particularly relevant for food, feed, and technical industries.[209-211] The internal organization of flax is very similar to the one observed in **Figure 19** for hemp, with the presence of fiber bundles in the phloem of the plant and with each fiber-containing primary and secondary cell walls.[198, 212, 213] Exceptions are the lack of secondary bast fibers and the fact that the woody core in flax is named "shive" and not "hurd".[214] The orientation of the microfibrils changes depending on the layer and the development phase of the plant. The bast fibers have a high content of cellulose, 60 wt.-% to 85 wt.-%, compared to hemicellulose, 14 wt.-% to 26 wt.-%, and lignin, 1 wt.-% to 3 wt.-%, which contributes to a high Young modulus (up to 60 MPa) and tensile strength (up to 1500 MPa). These values are similar to the ones found in hemp bast fibers.[198, 212, 213]

After harvesting, dew or water retting is applied, followed by scutching and decortication. The long technical fibers (up to 30 cm) can be applied in textiles, composites, and in the building and manufacturing industries among other applications while the shorter fibers, tow, and other residues are used for low-value applications or considered as residues.[212, 213] The resistance of this crop to heavy metals and the minimum input needed to grow it makes flax an interesting tool for phytoremediation, agro-mining, and other environmental applications.[215]

The integrity of hemp and flax bast fibers is essential for composite and other applications but, in their mechanical processing, their cell wall structure may be damaged. This decreases the mechanical strength of the fibers. These fractured fibers, as well as those that are too short (scutching and hackling tow), are considered wastes or are used in low-value applications such as animal bedding or heat.[208, 214, 216, 217] The fact that the fiber´s properties are variable and dependent on all the abiotic factors that affect the plant development (nutrients, water availability, soil temperature, among others), retting and processing is the major drawback in

the valorization of these resources. Other disadvantages are their highly anisotropic nature, low thermal stability, and low mechanical properties compared to synthetic fibers. To increase production yields for seeds, fibers, and metabolites, genetic and agriculture studies have been developed. The development of strands that produce larger seeds and have a higher cellulose content are just some of the desired goals.[203, 218] Besides, chemical and physical treatment of these fibers may improve their adherence to polymer matrixes in composites among other modifications depending on the final application.[197, 199, 212]

Considering the production numbers for these crops, the shorter and mechanically damaged fibers discarded alongside the hemp and flax processing are an important resource that can be valorized for high-value applications. It is possible to separate the stalk into strands by using mechanical forces and avoiding retting but a larger amount of mechanically damaged fibers is produced.[214]

Their high content in crystalline cellulose, low density, abundance, and good mechanical properties make them promising starting points for developing biobased cellulose aerogels following a circular biobased economic perspective.

In the next chapter, it will be discussed how cellulose can be obtained from these wastes.

2.5.2   Extraction of Cellulose

Different techniques can be applied to extract cellulose from agricultural residues such as hemp and flax waste bast fibers. Although retting degrades some of the lignin and hemicellulose in the waste fibers, this process provides inconsistent results and is time-consuming. Enzymes such as laccases and lignin peroxidases can be used, but most extraction methods are chemically based. These involve treating the fibers in acid or alkali media combined with bleaching reactions using hydrogen peroxide, sodium chlorite, or other reactants.[214]

Kopania et al. studied the effect of different basic and acid methods to extract cellulose from hemp and flax straw. The fibers were delignified in sodium hydroxide or sodium hydroxide plus hydrogen peroxide before further delignification using oxygen, sodium chlorite, and acetic acid. It was found that the combination of NaOH and H_2O_2 achieved higher yields of cellulose extraction (over 70 wt.-%) and lignin removal than if NaOH was used alone. A multi-step treatment was found more effective in obtaining highly pure non-degraded cellulose.[219] Sodium hydroxide and hydrogen peroxide were used by other researchers who extracted pure cellulose, with a lignin content ranging from 2 wt.-% to 10 wt.-%, from both flax and hemp.[220, 221] The advantages of using sodium hydroxide are its low cost, less corrosiveness compared to acid alternatives, and its applicability at room pressure, from short periods up to

some hours at mild temperatures (from 25 °C to 150 °C). These methods are particularly suitable for agricultural residues such as waste fibers.[222, 223] Other alkali salts can be used, such as potassium and ammonium hydroxides, with CaOH being widely used due to its easy recovery, low cost, and less corrosiveness. Nonetheless, NaOH is the most efficient in the extraction of cellulose and it is not as expensive nor requires harsh conditions like ammonium hydroxides.[223] Sodium hydroxide acts on the chemical link between hemicellulose and lignin, breaking the ester group between ferulic acid and the carbohydrates. These links can be observed in **Figure 20**.[222, 223]
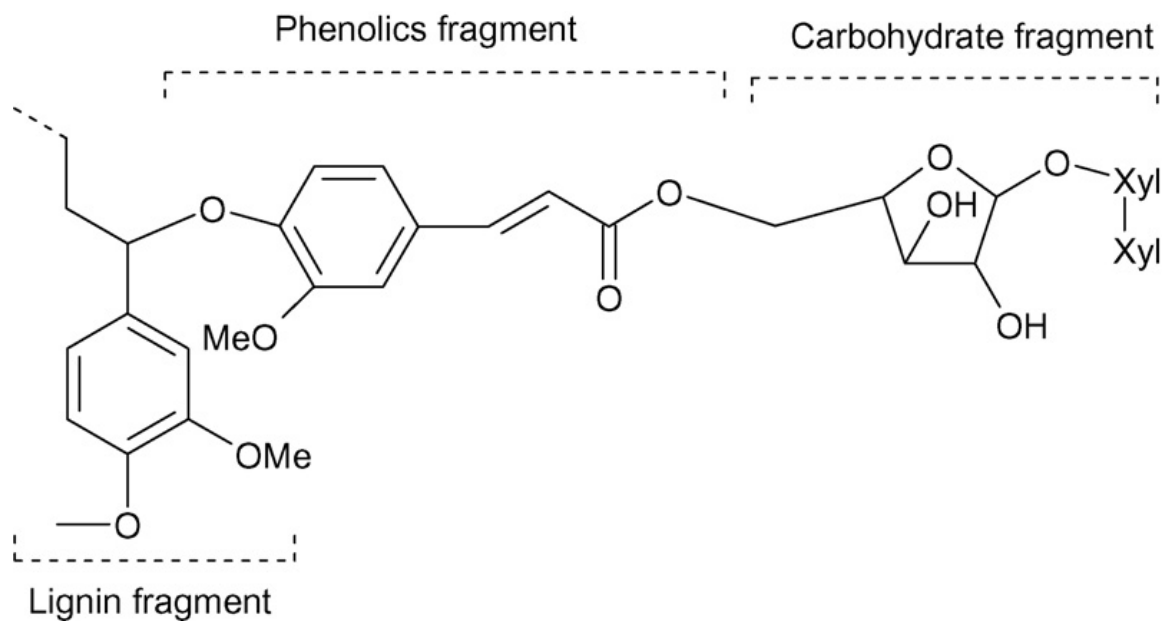
Figure 20 The phenolic fragment (ferulic acid) is connected with the lignin fragment through an acid-labile ether bond, and with the carbohydrate hemicellulose (arabinoxylan) fragment., through an alkali-labile ester bond.[224] Used with permission of Elsevier Science & Technology Journals, from *Lignin in straw of herbaceous crops*., Buranov, A.U., and Mazza, G., 28., 2008; permission conveyed through Copyright Clearance Center, Inc.

By breaking this link, hemicellulose is prone to degradation, and lignin dissolves in the alkali medium. These biopolymers, dissolved in oligomeric form, can be isolated and further degraded through chemical or biological methods for sugars, bulk chemicals, and materials production. From a circular biorefinery perspective, the severity of the alkali treatment can be modulated to control the degree of degradation of lignin and hemicellulose required for their final application while extracting pure cellulose. The phenolic monomers and ferulic acid formed from the hydrolysis of the ester link are also interesting building blocks to be valorized.[223]

Furthermore, sodium hydroxide swells the lignocellulosic polymer, increasing its contact area and accessibility within the solution. The crystallinity of cellulose may decrease, as well as its degree of polymerization, if NaOH concentration is over 4 wt.-% and temperature is over 100 °C. This is due to the promotion of a self-catalyzing "peeling" reaction, where the reducing ends of cellulose suffer β-alkoxy-carbonyl elimination. The most important parameters to define in this process are temperature (20 °C to 180 °C), concentration of NaOH (0.5% to 10% w/v), solid:liquid ratio (10% to 30% w/v), and residence time (0.5 h to 18 h). Under this range, 50 wt.-% to 80 wt.-% of lignin and hemicellulose are removed from the lignocellulosic polymer. These parameters can be optimized to maximize yields of cellulose extraction and minimize the consumption of energy, time, and materials. The smaller the particle size, the more efficient the process, but it becomes costly to mill biomass below 2 mm.[223]

However, there are some disadvantages to this method, such as the treatment of the process residues, the recycling of the reactants, and the lack of effectiveness at solid loads higher than 15 wt.-%. Without the addition of an oxidizing agent, the reaction can take days, and the removal of other biopolymers is not complete.[222] To increase cellulose yields and promote the further degradation of lignin into high-value phenolic molecules, hydrogen peroxide is widely used as an additive for the sodium hydroxide treatment. One of these mechanisms are exemplified in **Figure 21**.[225]
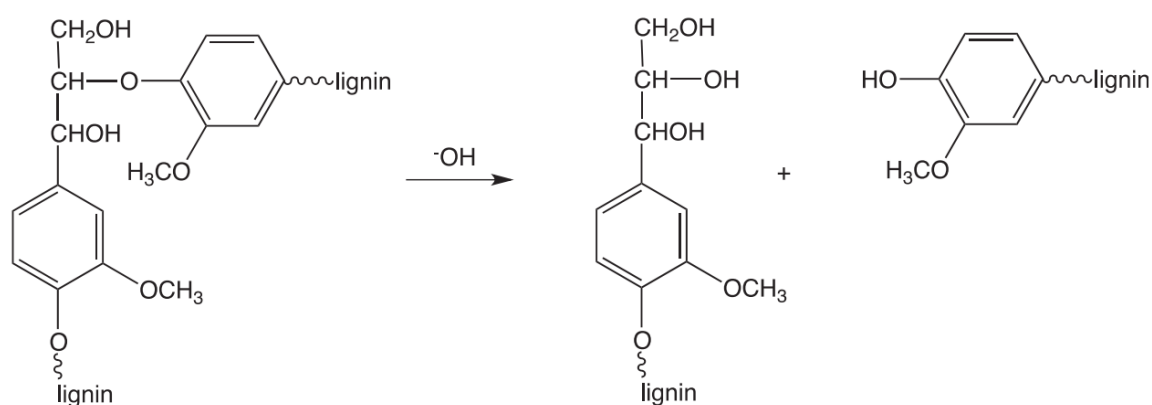
Figure 21 Hydrolysis of the α-ether link in lignin at basic conditions after addition of an oxidative agent.[125] Used with permission of Elsevier Science & Technology Journals, from *2 Extraction and Types of Lignin,* in *Lignin in Polymer Composites*., Chung, H., and Washburn, N. R., 2016; permission conveyed through Copyright Clearance Center, Inc.

Hydrogen peroxide is environmentally benign, accessible, easy to use, and causes significant degradation of lignin in both phenolic and non-phenolic structures (oxygen is not capable of

doing it). The mechanisms for this degradation are complex and highly dependent on the pH, temperature, and source of the biomass. The optimum pH for this reaction is 11.5, where the dissociation of H_2O_2 into OOH^- is maximized. The conjugate base perhydroxyl anion is the active nucleophile in the oxidation of phenolic and non-phenolic lignin, as well as in the degradation of the aromatic rings.

Higher temperatures favor the dissociation of hydrogen peroxide and the lignin phenols, which are responsible for lignin´s degradation. However, if the temperature is too high, it can lead to the degradation of cellulose, as well as higher energy consumption.[225]

Various researchers have studied the effect of different cellulose extraction methods on the properties of the corresponding cellulose aerogels. Nguyen et al. conducted experiments to test alkaline, acid, and acidified glycerol treatment methods on barley straw. From the extracted cellulose, aerogels were produced as a constant 5 wt.-% cellulose concentration and a temperature of 100 °C for two hours. The results showed that fibers obtained from the alkali treatment (2 wt.-% NaOH) had the lowest lignin content compared to other methods (6 wt.-% vs. 10 wt.-%), but also the lowest cellulose content (71 wt.-% vs. 74 wt.-% for diluted acid and 80 wt.-% for acidified glycerol). A lower quantity of lignin led to aerogels with lower shrinkage and density, higher porosity, and lower specific surface areas.[226] In another study, Freitas et al. compared alkali hydroxide, subcritical water extraction, and ultrasound-reflux heating methods, followed by bleaching, in extracting cellulose from rice straw. The alkali method (NaOH 4.5 wt.-%, 100 °C, 3 h) followed by bleaching (100 °C, 4 h) was found to be the most efficient in extracting cellulose (73.4 wt.-%, vs. 62 to 69 wt.- %), while also obtaining the lowest content in lignin and ashes. The hemicellulose content was still significant (10 wt.-% vs. 4 to 16 wt.-%).[227] Based on these findings, a two-step extraction process with sodium hydroxide and bleaching at basic conditions could be applied to extract cellulose from hemp and flax bast waste fibers and produce cellulose aerogels.

After this description of the sources of cellulose, its characteristics and extraction process as well as the synthesis routes that can be used to convert it into aerogels, the next chapter focuses on the thermal insulation properties of aerogels and how they can be used as suitable thermal insulators.

2.6 Principle of Thermal Insulation

The thermal conductivity of a material determines how well it can insulate against heat. Several factors influence the overall thermal conductivity (λ_{tot}) as described in **Equation 3**[10], namely: thermal conductivity of the solid fraction (λ_{solid}); thermal conductivity of the gaseous fraction (λ_{gas}); radiation thermal conductivity (λ_{rad}); convection thermal conductivity (λ_{conv}); thermal conductivity from the interaction between the previous factors ($\lambda_{coupling}$) and the leakage thermal conductivity (λ_{leak}). As the λ_{leak} is based on the air and moisture leakage that occurs when a pressure difference exists and the structure of thermal insulators does not present the cavities necessary for its occurrence, it can be neglected. The same can be said for $\lambda_{coupling}$ due to its high complexity and difficult determination.[10, 228, 229]

$$\lambda_{tot} = \lambda_{solid} + \lambda_{gas} + \lambda_{rad} + \lambda_{conv} + \lambda_{coupling} + \lambda_{leak} \qquad \textbf{Equation 3}$$

Only the first two terms are related to conduction phenomena, which means the direct transference of thermal energy across atomic or molecular collisions (λ_{solid} is based on the atomic vibrations present in the lattice structure while λ_{gas} originates from the collision of the gaseous molecules). The emission of electromagnetic waves in the range of the infrared contributes to λ_{rad}. The movement of air or moisture alongside its thermal mass (convention currents) relates to λ_{conv}. The minimization of these parameters is essential to achieve a low thermal conductivity.[10, 12] Besides this property, thermal insulators should be fire-resistant, durable enough to resist stresses and their implementation process, and resistant to microbial activity.[12]

A material is considered a thermal insulator if its thermal conductivity is below 0.1 W m^{-1} K^{-1}, with most commercial options falling between 30 mW m^{-1} K^{-1} and 40 mW m^{-1} K^{-1}. A super thermal insulator would reach values lower than the 26 mW m^{-1} K^{-1} of air.[14]

As most aerogel´s pores are below 1 μm and the mean free path of air molecules at ambient pressure is between 64-68 nm[230], heat transfer in the gaseous phase is mostly molecular, according to the Knudsen effect. This occurs when gas molecules have a higher probability of shock with the pore wall than with another molecule, minimizing the air thermal conductivity which becomes proportion to the air pressure. If bigger macropores are present, as occurs often for polysaccharide-based aerogels, a diffusion heat transfer is observed. Here gas molecules mostly collide with each other, making λ_{gas} the same as in the free gas, independently of the gas pressure at ambient conditions. A smaller pore size profile is associated with a lower

2.6 Principle of Thermal Insulation

thermal conductivity, and, if the pore emissivity and solid-state thermal conductivity remain low by a higher opacity and lower density, respectively, aerogels can achieve overall values of thermal conductivity lower than 20 mW m^{-1} K^{-1} at STP, as observed in some studies.[10, 14, 231]

At the laboratory scale, the methods to measure thermal conductivity are mostly dynamic and often lack accuracy due to the low quantity of samples that can be analyzed and the complex working equations involved in thermal conductivity calculation. These include the hot-wire, hot-strip, and hot-disc methods, among others. These discrepancies can be greatly reduced if larger quantities, such as the ones produced with the JetCutter®, and stationary methods are used to determine thermal conductivity. These include, as examples, the guarded-hot-plate and the heat-flow-meter and are known for their straightforward determination of thermal conductivity.[231-233]

Regarding biobased aerogels, some polysaccharides can be converted into superinsulator aerogels. Pectin and alginate aerogels reach thermal conductivities as low as 15 mW m^{-1} K^{-1} and 18-20 mW m^{-1} K^{-1}, respectively, as well as nanocellulose aerogels due to their nanoporous structure, and resultant sharp pore size distribution and low density.

However, cellulose II aerogels, unless hydrophobized or in a composite with silica, have thermal conductivity values never below 25 mW m^{-1} K^{-1}.[234, 235] Karadagli et al. synthesized cellulose aerogel monoliths and recorded a linear relation between their thermal conductivity and cellulose content. Their thermal conductivity ranged from 40 mW m^{-1} K^{-1} to 75 mW m^{-1} K^{-1}, to 1 wt.-% and 7 wt.-% cellulose concentration, respectively.[191] Nguyen et al. developed a 2 wt.-% cellulose aerogel whose thermal conductivity was 32 mW m^{-1} K^{-1} and 29 mW m^{-1} K^{-1} if coated with methyltrimethoxysilane.[170] Similar values, from 30 mW m^{-1} K^{-1} were recorded by Rudaz in cellulose aerogels synthesized using different methods and cellulose concentrations.[166] It should be noted that a direct comparison between these results is not possible due to the use of different equipment, techniques, and synthetic routes. Even the temperature, atmospheric pressure, and altitude at which the measurement was performed have an influence.[232, 236]

The reduction of the thermal conductivity (λ) of the cellulose aerogels can be achieved through two routes: through the reduction of the cellulose concentration in the aerogel (decreases the solid backbone contribution) and through the decrease of the number of macropores over 70 nm, according with the Knudsen effect (decreases the gas conduction contribution).[10, 24, 237] Another important factor, in the case of beads, is their shape. The more homogeneous, smaller, and spherical the beads, the higher degree of compaction is achieved by reducing the

free space available and more accurate values can be obtained.[238, 239] Consequently, optimization of JetCutting parameters is essential.

2.6 Principle of Thermal Insulation

3. Experimental Part

3.1 Materials and Characterization Methods

3.1.1 Materials

Sodium hydroxide (NaOH, ACS grade), trisodium citrate (Na$_3$Cit, anhydrous, EMPROVE$^®$ ESSENTIAL, USP, FCC), and glacial acetic acid (pure) were purchased from VWR. Cellulose medium fibers (MC, product number: C6288, DP of 153), urea, sodium chloride, and sodium sulfate were purchased from Sigma-Aldrich. MC was extracted from cotton linters. Hydrochloric acid (37%) was obtained from Panreac-AppliChem. Anhydrous citric acid, KOH pellets and H$_2$O$_2$ (30 wt.-%) were purchased from Merck-Millipore. Lactic acid (90% in water) was purchased from Bernd Kraft. Two different lignins were used in these experiments: Indulin AT lignin (Ind, kraft lignin from pine, from Ingevity) and Protobind^{TM} 1000 lignin (P1, soda lignin from wheat straw, from PLT Innovations). Deionized water was used for all the experiments. Ethanol (99%) denatured with 1% methyl ethyl ketone or petroleum ether Th. Geyer was used for the solvent exchange process. CO$_2$ for supercritical drying was supplied by Air Liquid. All reactants were used without further purification. Flax and hemp crops based on agriculture bast waste fibers have been provided from Assistant Professor Sepideh Pakpour (PhD), University of British Columbia, Okanagan Campus, Kelowna, Canada.

3.1.2 Viscometry and Rheometry

Determining the degree of polymerization (DP) of celluloses and measuring the rheological properties of their solutions is a crucial quality control method. It helps to understand the concentration of cellulose solution needed for effective manipulation and conversion into aerogels of the desired shape and properties.

The DP of the celluloses was determined using a viscometer from SI analytics (50110 I). This determination was performed by the research group of Prof. Annette Schmidt at the University of Cologne, Faculty of Mathematics and Natural Sciences, Department of Chemistry, using a previously developed method[72].

The Haake^{TM} Mars^{TM} 60 rheometer by Thermo Scientific^{TM} was used to investigate the viscoelastic properties of cellulose solutions. The dynamic viscosity measurements were conducted with a plate-plate geometry (titanium) with a diameter of 35 mm and a gap of 0.8 mm. Viscosity analysis was performed with a steady shear rate from 1 to 1000 1 s^{-1}. The viscosity values at a shear rate of 1000 1 s^{-1} were used to compare the cellulose solutions. The

same setup was used for static viscosity tests (1 s^{-1} sheer rate), temperature dependence tests (1 s^{-1} sheer rate, 3 °C min^{-1}) and to determine the gel point (oscillating frequency of 1 Hz). The gel point is the point at which a gel starts to form due to incipient chemical or physical polymer network formation. The gel point is identified as the point at which the storage modulus (G´, representing elastic behavior)) becomes greater than the loss modulus (G´´, representing viscous behavior).[240]

3.1.3 Optical Microscopy and Shrinkage Behavior

It is important to record the shape and shrinkage of the aerogels during their processing to determine if they are deformed and to what extent. The homogeneity of their shape is essential for industrial applications, and their shrinkage causes energy and resource losses. To classify the efficiency of the dissolution conditions applied, it is necessary to evaluate the dissolution state of cellulose fibers.

A Zeiss Axiocam 208 color optical microscope was used for the morphological and dimension analysis of bead (laboratory and technical scale) and fiber samples. Laboratory scale beads were analyzed across all stages of processing (acidic wet gel, hydrogel, alcogel, and aerogel), while for technical scale beads and fibers, only aerogel samples were studied. For monoliths, their dimensions were measured optically with a digital caliper ($\pm$ 0.1 mm) across all stages of processing. For fibers, only their aerogels were measured optically with a ruler ($\pm$ 0.5 mm).

The total shrinkage of laboratory scale beads (S) was calculated using **Equation 4**, where D_0 and D_1 represent the average diameter of the regenerated acidic wet gel and the average diameter of the aerogel after supercritical drying respectively. Each average diameter was determined by measuring over 25 beads for each sample. For the fiber samples, D_0 corresponds to the nozzle diameter used.

$$S(\%) = \frac{(D_0 - D_1)}{D_0} \times 100 \qquad\qquad \textbf{Equation 4}$$

For monolith samples, shrinkage was calculated by replacing D_0 for the volume of cellulose solution used for each sample (V_0) and D_1 for the volume of the dried aerogel obtained (V_1) in **Equation 4**. To analyze the dissolution state of cellulose, the ZEISS Axioscope 5 microscope was used. Bright-field (BF) images were taken due to the transparency of the observed cellulose fibers and the occurring light reflection. The sheets had an irregular shape due to difficulties in removing them from the CAProLi and in assuring a homogeneous distribution of the cellulose

solution on the equipment. As a consequence, it was not possible to measure their shrinkage and dimensions.

3.1.4 Pycnometry and Porosity Determination

The properties of aerogels are influenced by the fraction of solid content and the space available in their open porous structure. Pycnometry techniques can quantify the solid and free space in aerogels and their porosity.

The skeleton density (ρ_s) of biomass samples, celluloses, and aerogels was determined using a helium pycnometer Accupyc II 1340 from Micromeritics. This method is based on the volume displaced in a container by adding a known mass of a sample. By measuring the displaced fraction ten times and knowing the volume of the container (V=1.3273 cm^3), an average volume of the sample and its ρ_s was obtained. The samples were crushed and the crucible filled up to 75% before the measurement.

For the envelope density (ρ_e) of the aerogels, a Geopyc 1360 sand pycnometer from Micromeritics was used. A pressure of 25 N and 51 N was applied when laboratory scale beads and monolith fragments were analyzed, respectively. A glass container was first filled up to 50 vol.- % with DryFlo®, a solid displacement medium, and preliminary compaction was performed to establish a zero-volume baseline. Afterward, the sample was added until filling up to 25 vol.-% of the displacement medium. The displacement volume of the medium was measured ten times, and an average envelope density value was obtained.

The sand pycnometer could not be applied to beads produced using the JetCutter® or to fibers due to their small dimensions. For aerogel fiber samples, the average envelope density was calculated using the volume and mass measured for multiple fibers. For aerogel beads produced with the JetCutter®, the target theoretic density (ρ_t) was first calculated by dividing the mass (m) of each component in cellulose solutions of different concentrations by the volume (V_0) of the dissolution medium (see **Equation 5**).

$$\rho_t = \frac{m_{NaOH} + m_{Urea} + m_{H_2O} + m_{Cellulose}}{V_0} \qquad \textbf{Equation 5}$$

The density of the dissolution medium (NaOH:urea aqueous solution) used for all experiments was 1.11 g cm^{-3}. It is assumed that there is no volume change if salts and cellulose are added to the dissolving medium. The estimated actual envelope density of the aerogels was measured by dividing ρ_t by the volume shrinkage ratio, VS_r, of the beads from acidic wet gel to aerogel,

as observed in **Equation 6**.[183] The acidic wet gel dimensions were determined by the JetCutter®, and the aerogel dimensions were determined according to the method described in **Chapter 3.1.3**. From these, the VS_r was calculated.[241]

$$\rho_e = \frac{\rho_t}{VS_r} \qquad\qquad \textbf{Equation 6}$$

The porosity ($P(\%)$) of the aerogel samples was calculated by applying their respective envelope, (ρ_e), and skeleton densities, ρ_s, using **Equation 7**.

$$P(\%) = \left(1 - \frac{\rho_e}{\rho_s}\right) \times 100 \qquad\qquad \textbf{Equation 7}$$

The aerogel sheets had an irregular shape due to difficulties in removing them CAProLi and in assuring a homogeneous distribution of the cellulose solution on the equipment. As a consequence, it was not possible to measure their envelope density and porosity. As only one coated monolith as produced was produced for each set of parameters, no variation in dimension or shrinkage was measured.

3.1.5 Infrared Spectroscopy (FTIR)

Infrared spectroscopy is a useful tool for quality control and evaluating the presence of impurities in aerogel samples and cellulose extracted from biomass. These impurities can be originated from the synthesis or extraction processes, respectively. Fourier transform infrared (FTIR) spectra were recorded in the range of 400 to 4000 cm⁻¹ using a Bruker-Tensor 27 instrument with a resolution of 4 cm⁻¹. An attenuated total reflectance module was used, and the spectra were analyzed to identify the chemical functional groups present in biomass samples, celluloses, and aerogels.

3.1.6 X-ray Diffraction (XRD)

To evaluate the purity of the cellulose extracted from the biomass wastes and the degree of crystallinity in the aerogel samples, X-ray diffraction is used. XRD measurements were carried out using a Brucker D8 ADVANCE A25 diffractometer to record the diffraction data from 5° to 80° 2 θ with a step size of 3° min⁻¹. The measurements were performed with Cu-Kα radiation

Experimental Part

(λ = 1.5406 Å) at a standard parameter of 35 kV and 30 mA for the signal crystal reflection mode. The empirical Segal method (see **Equation 8**) was used to calculate the crystallinity index (IC_S) of cellulose in biomass samples, celluloses, and aerogels. In this method, I_{am} is the intensity of the amorphous fraction diffraction pattern of the cellulose when 2θ is 18° and I_{200} is the maximum intensity of the peak plane (200).[242-245] For the cellulose aerogels, I_{am} was obtained when 2θ is 16°.[114, 192] The background in the diffractogram was not removed for this calculation.[246]

$$IC_S = \frac{I_{200} - I_{am}}{I_{200}} \times 100$$

Equation 8

3.1.7 Scanning Electron Microscopy (SEM)

SEM is used to study the microstructure of biomass samples, celluloses, and aerogels. In the case of aerogels, SEM is used to analyze both the exterior and interior surfaces to gain knowledge about their porous structure and understand their properties better.

To evaluate the microstructure of the samples, a scanning electron microscope Zeiss-Ultra 55 with a Gemini column operated by 2-6 kV was used. For all aerogel samples and to prevent deformation of the cellulose filigree structure, small fragments in the millimeter range were cut under liquid nitrogen. These fragments and other biobased materials were deposited on a carbon pad, which was attached to the sample holder. To avoid charging the sample surface during SEM analysis, the samples were coated with platinum, for 90 sec, at 0.04 mbar and 21 mA, using a BALTEC SCD 500 sputter coater. An aperture diameter of 7.5 µm or 10 µm, without using the high current mode, was applied.

3.1.8 Physisorption Measurements

Physisorption technologies can be used to describe the diversity of nanopores present in aerogel samples and to measure their total volume and surface area. These characteristics are intrinsically linked with the effectiveness of aerogels as thermal insulators and their use in other industrial applications.

Nitrogen adsorption-desorption measurements at 77 K were performed with a Micromeritics Tristar II 3020 instrument while the data was analyzed using the *MicroActive* (*v5.02*) software from Micromeritics. The Brunauer-Emmett-Teller (BET) model was used to measure the specific surface area in a partial pressure range between 0.05 and 0.3 (p/p_0). The total pore

volume was obtained from the N_2 adsorption isotherms at a partial pressure of 0.98, and the pore size distribution was calculated using the Barrett-Joyner-Halendar (BJH) model from the desorption branch of the isotherms. For sample preparation, the aerogels were degassed at 110 °C and 0.00133 kPa for five hours using a Micromeritics Smart VacPrep Gas Adsorption Sample Preparation Device. Two measurements were taken for all aerogel samples, while single measurements were taken for aerogel fiber and coated aerogel bead samples.

3.1.9 Thermogravimetric Analysis

The thermogravimetric profiles obtained from biomass samples, celluloses, and aerogels serve as a quality control instrument. This technique detects the presence of residual biopolymers in extracted celluloses and aerogels. The thermogravimetric analyses were conducted using a NETZSCH STA 449F3 thermal analyzer in an argon atmosphere. The samples were placed in an open Al_2O_3 crucible and were heated up to 600 °C at a rate of 5 K minute^{-1}. For the wet cellulose aerogel beads coated with lignin, the same conditions were applied, except the maximum temperature was 250 °C.

3.1.10 Heat Flow Meter (HFM)

The heat flow meter method was used to measure the thermal conductivity of the aerogel beads produced with JetCutter®. This property is crucial in assessing the performance of materials as thermal insulators.

The thermal conductivity measurements were performed with an HFM 446 S from NETZSCH for biomass samples, celluloses, and aerogel beads produced from JetCutter®. The sample was placed in a mold of size 15x15 and left for 16 h at 50°C to remove any moisture from the samples. Additional sample was then added to fill any voids in the mold and ensure homogeneous distribution. The sample was covered with aluminum foil and placed in the HFM. Measurements were set at 25 °C and 10 °C, with an applied pressure of 2.1 kPa and a heating rate of 2 K min^{-1}. These tests were conducted in Habsheim, France, at an altitude of 245 m, with the ambient temperature ranging from 18° to 21°C, the air humidity from 41% to 61%, and the atmospheric pressure from 1006 mbar to 1015 mbar. After the measurement, the sample was discarded as the compression applied during the measurement could have altered the internal porous structure of the sample.

3.1.11 Moisture Absorption, Water Uptake Tests, and Contact Angle Measurement

These different methods were used to investigate how water affects the properties of aerogels and if their coating with lignin improves their resistance against it.

The moisture absorption of aerogel beads synthesized from hemp and flax-extracted cellulose, and commercial cellulose was recorded. In an alternating climate chamber MKF 56 from BINDER, 0.5 to 1.5 g of sample were exposed to 63% humidity for 24 h. After 24 hours, the weight, dimensions, and density of the samples were registered. This value of humidity was chosen because it was above the 60% limit of comfort recommended for buildings and when microbial growth starts to be strongly promoted.[247-249]Water uptake tests were conducted on cellulose aerogel beads produced with the JetCutter® with and without being coated with lignin. In the test, 0.25 g of beads were immersed in a 100 mL water bath, for 24 hours, at 40 °C. Afterward, the solution was filtrated, the excess of water was removed from the beads and these were weighted to determine the amount of water absorbed. Water angle contact tests were performed on lignin-coated aerogel monoliths. In those experiments, one droplet of water was dropped on the monolith´s surface to record the time required for its absorption and, in the case of hydrophobicity, measure the water contact angle. The images were recorded with a TOMLOV DM101 Digital USB Microscope 500X camera.

3.2 Extraction of Cellulose

In this chapter, first, it is described the preparatory processes of the raw materials, biomass waste fibers, for the extracting of cellulose. Then, the procedure for dissolving cellulose is described in detail along with the conditions used for synthesizing cellulose aerogel beads, monoliths, sheets, and fibers. Afterward, the methodologies used at both laboratory and technical scales for each shape are presented. At last, the laboratory procedures that are used for lignin coating of cellulose wet gel samples are described.

Laboratory scale

Milling

For preparation, hemp and flax waste fibers (HF and FF, respectively) were cut into small fragments of 1 to 2 cm and then milled into small particles using an SR200 rotor beater mill by Retsch® with a 0.2 mm sieve. Liquid nitrogen was added regularly to keep the fibers stiff and avoid overheating. The received waste fibers had a size of 50 cm.

3.2 Extraction of Cellulose

Extraction Process I – Alkali Hydrolysis

In a round bottom flax, 50 g of the biomass particles were soaked in 900 g of 8 wt.-% sodium hydroxide solution and left at room temperature for 16 hours, under stirring. The mixture was then heated at 60 °C under stirring for three hours and, after cooling to room temperature, it was neutralized with acetic acid to pH 7. The small particles were collected by filtration and washed several times with distilled water until the supernatant became colorless. Afterward, they were washed with ethanol and later rinsed with acetone to remove any remaining organic residues and water so their drying at 50 °C under vacuum was faster. The quality of the first extraction process was evaluated by characterizing the alkali-treated hemp and flax intermediates with FTIR.

Extraction Process II – Bleaching

The product from the alkali hydrolysis extraction process was placed into a round bottom flask containing 900 g of 5 wt.-% potassium hydroxide solution. After dispersion, 45 mL of 30 wt.- % hydrogen peroxide in water was added and the mixture was left at room temperature for 16 hours, under stirring. During this period, the fibers became dull white in color. To complete the bleaching process, the mixture was heated at 60 °C for three hours under stirring. After cooling to room temperature, the fibers were neutralized, washed, and dried as in alkali hydrolysis.

The total extraction yield was 72 wt.-% for hemp cellulose (HC) and 63 wt.-% for flax cellulose (FC), respectively.

Technical Scale

A series of laboratory scale tests were conducted to develop the technical scale extraction procedure. The tests were performed only on hemp fibers (HF) due to their higher yield of cellulose extraction. HF were cut into small fragments measuring 1 to 2 cm and milled using a food chopper C1801 from Nestling® for 20 cycles. This equipment was used to evaluate if longer fibers could be used for cellulose extraction while saving time and resources in milling larger quantities of biomass fibers for extraction at technical scale. The resulting milled fibers were above 1 mm. Each cycle consisted of 30 seconds of milling at speed III, followed by two minutes of rest to avoid overheating. The same proceeding described previously regarding alkali hydrolysis and bleaching was applied to these milled fibers, except for the following points: volume of solution (100 mL), stirring speed (no stirring vs. 450 rpm), and residence time in alkali and/or bleaching medium before heating (16 h; 6 h; 3 h; 1 h).

At the technical scale, the proportions of reactants in the alkali hydrolysis and bleaching steps remained unchanged, but an 1800 mL bath was used for 100 g of particles (< 0.2 mm or > 1 mm). Before heating was applied, the residence time of the fibers was three hours in both extraction steps. The three-hour heating treatment took place in an autoclave A40, with a capacity of 2 L, built by the former company for supercritical drying equipment and aerogels production, Separex, from Nancy, France. In **Figure 22** the equipment is shown. It contains a mechanical stirrer and a thermostat with a limited stirring speed of 450 rpm. To start the process the suspension was placed in the reactor and, after its closing, the thermostat was activated to reach 60 °C without exceeding the desired temperature. After three hours at 60 °C, the reactor was left to cool down. Only afterward, the tap was opened to avoid pressure drops, and the mixture was removed, neutralized, and washed as previously described.

Figure 22 The A40 autoclave equipment from Separex was used for the heating stages of the cellulose extraction from hemp bast waste fibers. An 1800 mL bath was used in the 2 L reactor, where 100 g of milled fiber particles (< 0.2 mm or > 1 mm) were added. The heating phases of the extraction process (three hours at 60°C) were performed here, under 450 rpm of stirring.

3.3 Dissolution of Cellulose

Seven grams of sodium hydroxide were dissolved in 81 g of distilled water and, when cooled down to room temperature, cellulose fibers were added with varying concentrations, ranging

3.3 Dissolution of Cellulose

from 2 wt.-% to 7 wt.-%. The suspension was stirred for ten minutes to promote the swelling of the cellulose. The next step involved cooling the mixture in an ice bath to 0 °C and stirring it for one hour. Afterward, twelve grams of urea were added to this mixture, and stirring continued for another hour. The dissolution of urea is an endothermic reaction. The solution was further stirred at room temperature for ten minutes and it was observed to be opaque. The solution was then stored at -20 °C for 16 hours, and, after thawing at room temperature, it became a clear pale-yellow viscous liquid. This batch-wise method to dissolve cellulose was used for all cellulose aerogel syntheses presented in this work, adapting the quantities of reactants used for laboratory and technical scales.

To generate a high-quality, fast continuous cellulose dissolution process, a series of experiments were designed using a 7 wt.-% commercial cellulose solution.

In the first set of trials, the batch-wise process was used, but the storage period at -20 °C was reduced to 2 h, 1 h, or 30 min. In the second set of trials, a slightly variated process was tested: In the alkali medium, the cellulose fibers were added at the same time as the urea and mixed for 30 min over a KP 283 cooling plate from Fryka Kältetechnik GmbH as shown in **Figure 23**. This equipment can decrease the temperature of its plate to temperatures below 0 °C, which enables the continuous mixing of the solution at those temperatures.
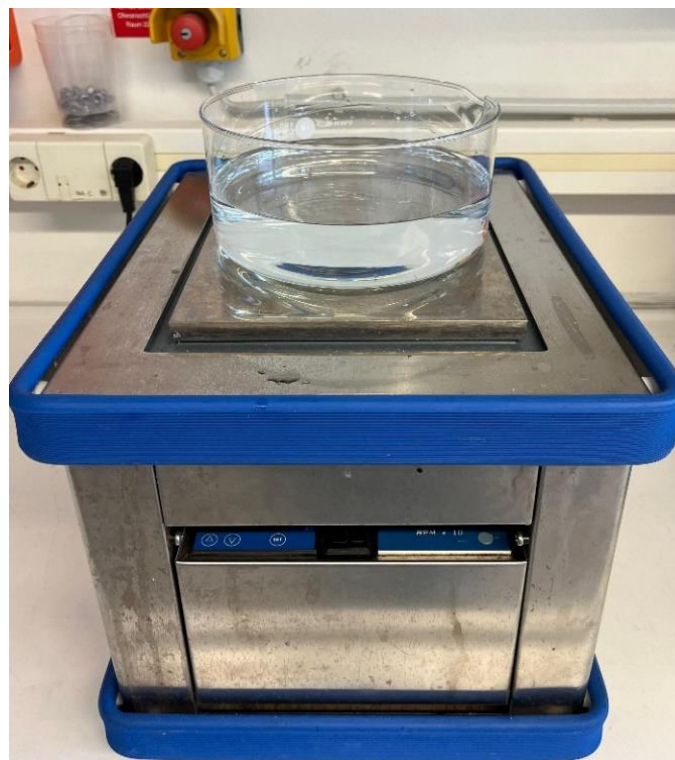
Figure 23 KP 283 cooling plate from Fryka Kältetechnik GmbH, with a NaCl-saturated water bath.

The solution was stirred in a flask (or beaker) placed in a NaCl-saturated water bath to support the homogeneous temperature conditions in the flask (or beaker). The solution was first stirred at -12 °C, -10 °C, -7 °C or -5 °C and then further stirred at room temperature for another 10 min to complete dissolution, when it was ready to use. Below -12°C, the freezing point of the solution was reached, and no stirring was performed.[113]

3.4 Manufacturing of Cellulose Aerogel Monoliths

Laboratory Scale

To produce monoliths, a thawed cellulose solution, from 3 wt.-% to 7 wt.-% concentration was stirred for ten minutes to homogenize it, after that, it was sonicated for 15 minutes to remove any bubbles. For some samples, 1 wt.- % or 2 wt.-% of one of the following three different sodium salts was dissolved in the cellulose solution: sodium chloride (NaCl), sodium sulfate (Na_2SO_4), and trisodium citrate (Na_3Cit). Sodium salts were chosen to study the variation of anions with different charges (from -1 to - 3), both organic and inorganic. Part of this work was carried out under supervising a master thesis.[262] The solution was transferred to cylindrical polypropylene containers with a diameter of 31 mm and filled with a height of 20 mm. If any air bubbles were observed, the solution was centrifuged at 1000 rpm for five minutes to eliminate them. After that, the solution was kept at 50 °C for 30 minutes to form a weak gel network. Afterward, it stood at room temperature until it reached a stable non-wobbling structure. The developed weak wet gels were placed in a gelation bath consisting of 90 vol.-% ethanol and 10 vol.-% acetic acid or lactic acid and stored for two days until a strong regenerated wet gel was obtained. The gel bodies were washed five times (1:5 ratio wet-gel to water, vol.- %) with distilled water for salt removal and neutralization. A five-step solvent exchange process was applied from water to ethanol (1:2 ratio wet-gel to solvent, vol.- %). Then the samples were dried in a 60 L autoclave for nine hours under $scCO_2$, at 115 bar between 25 °C and 60 °C. No technical scale approach was applied.

3.5 Manufacturing of Cellulose Aerogel Beads

3.5.1 Nozzle-Tip Technology

A cellulose solution, from 2 wt.-% to 7 wt.% concentration was used after thawing, stirring, and sonication. It was transferred to an open polypropylene plastic container, with ten nozzle

tips (diameter of 1 mm). The solution was dripped through the nozzles into a stirring regeneration bath composed of a 2 M acid aqueous solution, as seen in **Figure 24**.
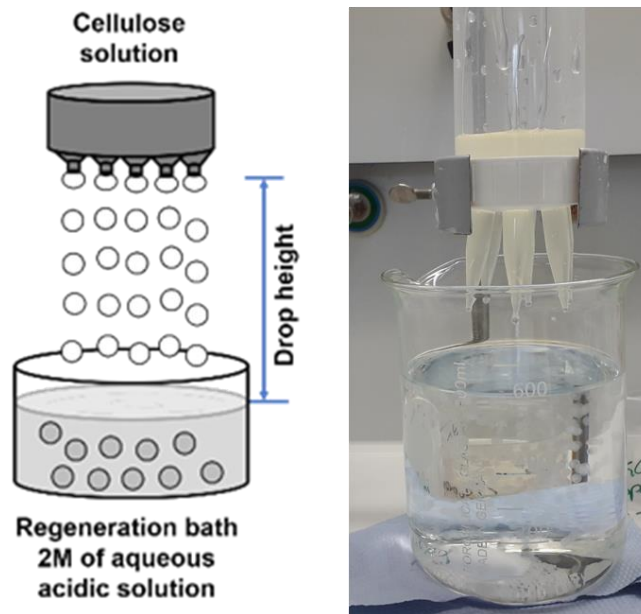
Figure 24 On the left, schematic diagram of a conventional multi-nozzle dropping technique[250] (CC BY-NC 4.0, https://creativecommons.org/licenses/by-nc/4.0/) and, on the right, the same technique is applied using acetic acid as regeneration bath.

The drop height was 2 cm, and the droplets gelled to white beads. After gelation, the beads were washed five times with deionized water (1:5 ratio wet-gel to water, vol.- %), with each cycle composes of stirring for 30 minutes in fresh deionized water to remove the salts and neutralize the pH. Solvent exchange and drying were followed according to **Chapter 3.4**

3.5.2 Jet-Cutting Technology

After bringing a cellulose solution to room temperature, it was mixed to promote homogenization. The cellulose concentrations used ranged from 5 wt.-% to 7 wt.- %. In this phase, 2 wt.-% of NaCl or sodium citrate was dissolved in 5 wt.-% cellulose solutions. Sonification was not possible due to the large volumes of solution (up to 3 L) used.

The storage container of the JetCutter® was filled batch-wise with 1 L of solution. The density and mass flux of the solution at 0.5 bar and 1 bar were measured to select the appropriate pressure to apply. To produce droplets continuously, a 2 M acid aqueous bath (acetic or lactic acid) of 10 L was used for the regeneration bath. After every 2 L of solution cut, 250 mL of acid was added to the regeneration bath to maintain the pH constant and compensate for the

water input from the newly formed wet gel cellulose beads. The bath was stirred at 50 rpm to avoid deformation and agglomeration of the beads. Waste solution from the cutting process collected in the protective disk was re-used. Bead collection and placement in a water bath occurred every ten minutes.

For these experiments, a nozzle diameter of 500 μm, a cutting disk with 24 wires, each with 0.15 mm thickness, an angle between the nozzle and the cutting disk of 10°, and a mass flux from 0.8 g s^{-1} to 1.5 g s^{-1} were fixed. The drop height of 110 cm was used for 6 wt.-% and 7 wt.-% cellulose concentrated solutions while 60 cm was used when 5 wt.-% cellulose solutions were cut. The process is shown in **Figure 25**.

Figure 25 On the left, the JetCutter® in action, and, on the right, a detail of the cutting of a 7 wt.-% cellulose solution.

After the regeneration of the cellulose beads, they were washed in tap water until pH was neutralized. Subsequently, two washes with distilled water were applied to remove salts (1:2 ratio beads to water, vol.-%).

Further solvent exchange and drying were followed by the previously described procedures in **Chapter 3.4**.

3.6 Manufacturing of Cellulose Aerogel Sheets

A cellulose solution, from 3 wt.-% to 7 wt.% concentration was used after thawing, stirring, and sonication. Once the cellulose solution was homogenized, the gel sheets were made directly with the CAProLi device as shown in **Figure 26**. The device included a conveyor belt, three flattening rolls, a mixing unit connected to a slit die, and a cutting wheel. In this work, only the conveyor belt and the flattening rolls were used to create the aerogel sheets. The time for the solution to become a stable gel body was 140 seconds at the lowest belt velocity. In the first step, the gel solution was poured over the belt. For some solutions, 2 wt.-% NaCl was added and dissolved beforehand. Then, the cellulose solution was evenly distributed with a dough scraper. The solution was transported to the first flattening roll, which defined the thickness of the sheet with a gap of 0.3 mm. After the cellulose solution was flattened by the first roll, a mixture of 80 vol.-% ethanol and 20 vol.-% lactic acid was sprayed continuously over the highly viscous cellulose solution until the end of the conveyor belt to start gelation.

Figure 26 Cellulose **A**erogel **Pro**duction **Li**ne (CAProLi), the experimental apparatus for the production of wet gel sheets.

Lactic acid was favored as the evaporation of the acid component has to be reduced to a minimum. The higher acid concentration of 20 vol.-% accelerated the gelation velocity, resulting in a stronger gel body at the end of the conveyor belt. The second and third flattening

rolls were used as wetting rolls to help distribute the gelation agent over the weak gel body. At the end of the conveyor belt, the gel body in sheet form was cut into several pieces to be transferred into a water bath for washing and neutralization. Further sample preparation for supercritical drying with CO_2 was followed as described in **Chapter 3.4**. Part of this work was carried out under supervising a master thesis.[295]

3.7 Manufacturing of Cellulose Aerogel Engineered Fibers

A cellulose solution prepared of 6 wt.-% or 7 wt.-% concentration was poured into a 100 mL storage container in the wet-spinning machine LabLineCompact as shown in **Figure 27**.

Figure 27 LabLineCompact, the experimental apparatus for the production of wet gel cellulose fibers.

The fibers were spun out using metal 23 AWG (American Wire Gauge) dispensing needles with an inner diameter of 0.33 mm and 0.5 mm. The pump revolutions ranged from 0.45 min^{-1} to 1.1 min^{-1}, while the take-up speed was between 3 m min^{-1} to 6 m min^{-1} to ensure stable continuous spinning. The fibers were solidified in a 2 M acetic acid coagulation bath of 25 L volume at various take-up speeds. The fibers were collected into deionized water containers and underwent neutralization, solvent exchange, and drying, following the procedure described previously in **Chapter 3.4**.

3.8 Lignin Coating of Cellulose Aerogels

The coating aimed to produce hydrophobic cellulose aerogel surfaces. To coat cellulose aerogels at laboratory scale, lignin was dissolved in an EtOH/H_2O mixture of 80:20 vol.-% or a basic water solution.

Beads were produced following the procedure described in **Chapter 3.5.2** from a 7 wt.-% cellulose solution, while monoliths were manufactured following the procedure described in **Chapter 3.4**, from a 7 wt.-% cellulose solution**.** In both cases, lactic acid was used in the coagulation baths.

When coating was carried out by dissolving lignin in ethanol/water solutions (80:20 vol.-%), a 100 mL EtOH/H_2O solution was prepared, and lignin powder (soda or kraft) was added. The dispersion was left for 24 hours to dissolve completely. After 24 hours, 10 g of cellulose alcogel beads were added and left for 24 hours to adsorb the lignin on the cellulose body. Depending on the amount of lignin added, the ratio of lignin to cellulose wet gel beads (wt.-%) was 1:50, 1:20, 1:10, and 1:5. Afterward, the beads were moved to an acetone bath, which was replaced three times to ensure that no residue of desorbed lignin or other solvents remained. The samples were dried following the protocol found in **Chapter 3.4**.

When coating with lignin was carried out by dissolving lignin in a basic water solution, a 0.2 M NaOH solution was prepared, and lignin powder (soda or kraft) was added to reach a concentration of 2 wt.-%. The solution was left standing for 24 hours to ensure complete dissolution of lignin. After 24 h, HCL (37 wt.-%) was added to neutralize the solution. Although a slight color change was noted, from very dark brown to light brown, complete dissolution remained. From this mother solution, fractions were mixed with deionized water and diluted until their volume was 100 mL, to which 10 g of alcogel beads were added. The beads stayed for 24 hours in the lignin bath. Depending on the amount of lignin present in the coating solution, the ratio of lignin to cellulose wet gel (wt.-%) was 1:50; 1:20; 1:10, and 1:5. When alcogel monoliths (17 g) were coated, the volume of lignin solution (only soda lignin was added) was 170 mL. The monoliths stayed four days in those baths, two days with each phase upside down, to promote adsorption along the gel body. Afterward, the gels were moved to an acetone bath, where solvent exchange and drying followed the same steps as in coating with EtOH/H_2O solutions. Due to improved results, only samples coated with the soda lignin P1000 were fully characterized.

3.9 Overview of all Samples

The following tables describe all the samples prepared and their relevant parameters for the scientific discussion ahead. They are organized in the following themes: Cellulose extraction (**Table 1**), cellulose dissolution and solutions (**Table 2**), cellulose aerogel beads and monoliths (**Table 3**), cellulose aerogel fibers (**Table 5**), and lignin coated aerogels (**Table 6**).

3.9 Overview of all Samples

Table 1 Samples and respective synthesis parameters for biomasses, extracted celluloses and intermediates.

Chapter	Sub-Chapter	Sample	Source of Cellulose	Extraction Process	Residence time before heating phases / hour	Fiber Dimensions / mm	Stirring / 450 rpm	Manufacturing Scale
4.1 Extraction of Cellulose	**4.1.1** Laboratory Scale	**Hemp fibers (HF)**	-	-	-	-	-	-
		Flax fibers (FF)						
		Hemp-extracted alkali treated supernatant (HAS)	Hemp	Alkali treatment	16	< 0.2	Yes	Laboratory
		Flax-extracted alkali treated supernatant (FAS)	Flax					
		Hemp-extracted cellulose (HC)	Hemp	Alkali treatment followed by bleaching				
		Flax-extracted cellulose (FC)	Flax					
		Commercial cellulose (MC)	Commercial	-	-	-	-	-

Chapter	Sub-Chapter	Sample	Source of Cellulose	Extraction Process	Residence time before heating phases / hour	Fiber Dimensions / mm	Stirring / 450 rpm	Manufacturing Scale
4.1 Extraction of Cellulose	**4.1.2** Technical Scale	**Hemp-extracted alkali treated fibers (HAT)**[*] **HAT-16 h**	Hemp	Alkali treatment	16	> 1	Yes	Laboratory
		HAT-6 h			6			
		HAT-3 h			3			
		HAT-1 h			1			
		HC-16 h		Alkali treatment (3h residence time before heating phase) followed by bleaching	16			
		HC-6 h			6			
		HC-3 h			3			
		HC-1 h			1			
		HAT-NS		Alkali treatment	3		No	Laboratory
		HAT-TS				> 1	Yes	Technical
		HAT-TS-M				< 0.2		
		HC-NS		Alkali treatment (3h residence time before heating phase) followed by bleaching		> 1	No	Laboratory
		HC-TS					Yes	Technical
		HC-TS-M				< 0.2		

[*] For the samples HAT-16 h, HAT-6 h, HAT-3h, and HAT-1h, the respective supernatants (HAS) were analyzed with FTIR as well.

3.9 Overview of all Samples

Table 2 Samples and respective synthesis parameters for cellulose solutions from different cellulose sources and after addition of salts.

Chapter	Sub-Chapter	Sample	Source of Cellulose	Concentration Cellulose / wt.-%	Dissolution Temperature / °C	Time of Residence / hour	Form of Dissolution	Salt added to solution
4.2 Dissolution of Cellulose	-	**MC7-16 h**	Commercial	7	-20	16	Batch-wise	-
		MC7-1 h				1		
		MC7-0.5 h				0.5		
		MC7-0 h				0		
		MC7_- 10 °C			-10	0.5	Continuous-wise	
		MC7_- 7 °C			-7			
		MC7_- 5 °C			-5			
		HC3	Hemp	3	-20	16	Batch-wise	
		HC4		4				
		HC5		5				
		HC6		6				
		HC7		7				
		F2	Flax	2				
		F2.5		2.5				
		F3	Flax	3				

Chapter	Sub-Chapter	Sample	Source of Cellulose	Concentration Cellulose / wt.-%	Dissolution Temperature / °C	Time of Residence / hour	Form of Dissolution	Salt added to solution
4.3 Regeneration of Cellulose	**4.3.1** Addition of Salts in the Cellulose Solution	**MC7-1NaCl**	Commercial	7	-20	16	Batch-wise	1 wt.-% of NaCl
		MC7-1Na₂SO₄						1 wt.-% of Na₂SO₄
		MC7-1Na₃Cit						1 wt.-% of Na₃Cit
		MC7-2NaCl						2 wt.-% of NaCl
		MC7-2Na₂SO₄						2 wt.-% of Na₂SO₄
		MC7-2Na₃Cit						2 wt.-% of Na₃Cit

Table 3 Samples and respective synthesis parameters for cellulose aerogel monoliths and beads, at laboratory and technical scale.

Chapter	Sub-Chapter	Sample	Source of Cellulose	Shape	Concentration Cellulose / wt.-%	Regeneration Medium	Salt added to solution	Manufacturing Scale
4.3 Regeneration of Cellulose	**4.3.1** Addition of Salts in the Cellulose Solution	**MCM7**	Commercial	Monolith (M)	7	50°C for 30 min; EtOH: Acetic Acid (90:10 vol.-%)	-	Laboratory
		MCM7-1NaCl					1 wt.-% of NaCl	
		MCM7-1Na₂SO₄					1 wt.-% of Na₂SO₄	

3.9 Overview of all Samples

Chapter	Sub-Chapter	Sample	Source of Cellulose	Shape	Concentration Cellulose / wt.-%	Regeneration Medium	Salt added to solution	Manufacturing Scale
4.3 Regeneration of Cellulose	**4.3.1** Addition of Salts in the Cellulose Solution	**MCM7-1Na₃Cit**	Commercial	Monolith (M)	7	50°C for 30 min; EtOH: Acetic Acid (90:10 vol.-%)	1 wt.-% of Na₃Cit	Laboratory
		MCM7-2NaCl					2 wt.-% of NaCl	
		MCM7-2Na₂SO₄					2 wt.-% of Na₂SO₄	
		MCM7-2Na₃Cit					2 wt.-% of Na₃Cit	
	4.3.2 Acidic Conditions of the Regeneration Bath	**MCB7-HCl**	Commercial	Bead (B)	7	2 M Hydrocloric Acid aqueous solution	-	Laboratory (Nozzle-tip)
		MCB7-HAc/ MCB7*				2 M Acetic Acid aqueous solution		
		MCB7-HLac				2 M Lactic Acid aqueous solution		
		MCB7-HCit				2 M Citric Acid aqueous solution		
4.4 Manufacturing of Cellulose Aerogel Beads	**4.4.1** Laboratory Scale	**FCB2**	Flax	Bead (B)	2	2 M Acetic Acid aqueous solution	-	Laboratory (Nozzle-tip)
		FCB2.5			2.5			
		FCB3			3			
		HCB4	Hemp		4			
		HCB5			5			
		HCB6			6			

Chapter	Sub-Chapter	Sample	Source of Cellulose	Shape	Concentration Cellulose / wt.-%	Regeneration Medium	Salt added to solution	Manufacturing Scale
4.4 Manufacturing of Cellulose Aerogel Beads	**4.4.2** Technical Scale	**MCB7-JC**	Commercial	Bead (B)	**7**	2 M Acetic Acid aqueous solution	-	Technical (JetCutter®)
		HCB6-JC	Hemp		6			
		MCB6-JC	Commercial					
		MCB6-HLac-JC	Commercial			2 M Lactic Acid aqueous solution		
		MCB5-JC			5			
		MCB5-1NaCl-JC				2 M Acetic Acid aqueous solution	1 wt.-% of NaCl	
		MCB5-1Na₃Cit-JC					1 wt.-% of Na₃Cit	
		MCB5-2NaCl-JC					2 wt.-% of NaCl	
		MCB5-2Na₃Cit-JC					2 wt.-% of Na₃Cit	
4.5 Manufacturing of Cellulose Aerogel Sheets	-	**HCM3**	Hemp	Monolith (M)	3	50°C for 30 min, EtOH: Acetic Acid (90:10 vol.-%)	-	Laboratory
		HCM3-2NaCl					2 wt.-% of NaCl	
		MCS7-2NaCl	Commercial	Sheet (S)	7	50°C for 30 min, EtOH: Lactic Acid (80:20 vol.-%)		Technical (CAProLi)
		HCS3-2NaCl	Hemp		3			

*   Samples MCB7-HAc is known as MCB7 from **Chapter 4.4** onwards as 2 M acetic acid bath is used as standard gelation bath.

3.9 Overview of all Samples

Table 4 Samples and respective synthesis parameters for cellulose aerogel fibers.

Chapter	Sample	Source of Cellulose	Shape	Concentration Cellulose / wt.-%	Regeneration Medium	Nozzle Diameter / mm	Pumping Speed / mL min^{-1}	Manufacturing Scale
4.6 Manufacturing of Cellulose Aerogel Engineered Fibers	**MCF6_0.5**	Commercial	Fiber (F)	6	2 M Acetic Acid aqueous solution	0.5	0.75	Laboratory (LabLineCompact)
	MCF7_0.5			7		0.5		
	MCF7_0.33			7		0.33		
	HCF6_0.5	Hemp		6		0.5		
	HCF7_0.33			7		0.33		
	HCF7_0.5			7		0.33		

Table 5 Samples and respective synthesis parameters for lignin-coated cellulose aerogel beads and monoliths, using different coating approaches.[*]

Chapter	Sub-Chapter	Sample	Shape	Regeneration Medium	Lignin Used	Dissolution Medium	Coating Medium	Ratio lignin:cellulose / wt.-%
4.7 Lignin Coating of Cellulose Aerogels	**4.7.2** Chemical Interaction of Lignin with Wet Cellulose Gel	**Indulin AT (In)**	-	-	-	-	-	-
		P1000 (P1)	-	-	-	-	-	-

Chapter	Sub-Chapter	Sample	Shape	Regeneration Medium	Lignin Used	Dissolution Medium	Coating Medium	Ratio lignin:cellulose / wt.-%
4.7 Lignin Coating of Cellulose Aerogels	**4.7.2** Chemical Interaction of Lignin with Wet Cellulose Gel	**MCB7-JC-NC**	Bead (B)	2 M Lactic Acid aqueous solution	-	-	-	-
		MCB7-JC-P1-80:20-1:50			Soda Lignin - P1000 (P1)	Ethanol:water bath, 80:20 (vol.-%)	Ethanol:water bath, 80:20 (vol.-%)	1:50
		MCB7-JC-P1-80:20-1:20						1:20
		MCB7-JC-P1-80:20-1:10						1:10
		MCB7-JC-P1-80:20-1:5						1:5
		MCB7-JC-In-80:20-1:50			Kraft Lignin - Indulin AT (In)			1:50
		MCB7-JC-In-80:20-1:20						1:20
		MCB7-JC-In-80:20-1:10						1:10
		MCB7-JC-In-80:20-1:5						1:5
		MCB7-JC-P1-Alkali-1:50			Soda Lignin - P1000 (P1)	0.2 M NaOH aqueous solution	Neutralized water	1:50
		MCB7-JC-P1-Alkali-1:20						1:20
		MCB7-JC-P1-Alkali-1:10						1:10
		MCB7-JC-P1-Alkali-1:5						1:5

3.9 Overview of all Samples

Chapter	Sub-Chapter	Sample	Shape	Regeneration Medium	Lignin Used	Dissolution Medium	Coating Medium	Ratio lignin:cellulose / wt.-%
4.7 Lignin Coating of Cellulose Aerogels	**4.7.2** Chemical Interaction of Lignin with Wet Cellulose Gel	**MCB7-JC-In-Alkali-1:50**	Bead (B)	2 M Lactic Acid aqueous solution	Kraft Lignin - Indulin AT (In)	0.2 M NaOH aqueous solution	Neutralized water	1:50
		MCB7-JC-In-Alkali-1:20						1:20
		MCB7-JC-In-Alkali-1:10						1:10
		MCB7-JC-In-Alkali-1:5						1:5
	4.7.3 Lignin coated Cellulose Aerogels	**MCM7-NC**	Monolith (M)	50°C for 30 min, EtOH: Lactic Acid (90:10 vol.-%)	Soda Lignin - P1000 (P1)	0.2 M NaOH aqueous solution	Neutralized water	-
		MCM7-P1-Alkali-1:50						1:50
		MCM7-P1-Alkali-1:20						1:20
		MCM7-P1-Alkali-1:10						1:10
		MCM7-P1-Alkali-1:5						1:5

* While ethanol was used in all previous chapters, the final solvent of the samples of Chapter **4.7** before supercritical drying was acetone.

4. Results and Discussion

The results and discussion are divided into five main sections. In the first section, cellulose extraction from hemp and flax bast waste fibers (see **Chapter 4.1**) at laboratory and technical scales is discussed. Secondly, the dissolution of cellulose (see **Chapter 4.2**) and the influence of different regeneration conditions on the properties of cellulose aerogels are discussed in **Chapter 4.3**. By using the data collected in **Chapter 4.3**, the third section focuses on the manufacturing of beads (see **Chapter 4.4**), sheets (see **Chapter 4.5**), and fibers (see **Chapter 4.6**). The fourth section focuses on the coating of cellulose aerogels with lignin (see **Chapter 4.7**) to improve their resistance to moisture. The last section (see **Chapter 4.8**) deals with the economic and environmental impacts of the development of a continuous industrial aerogel production system. The chapters and sub-chapters from each topic can be consulted in **Table 6**.

Table 6 Topics discussed in **Chapter 4**

Chapter	Sub-Chapter		Corresponding Chapters in Experimental Part
4.1 Extraction of Cellulose	**4.1.1** Laboratory Scale		**3.2** *
	4.1.2 Technical Scale		**3.2**
4.2 Dissolution of Cellulose	-		**3.3** **
4.3 Regeneration of Cellulose	**4.3.1** Addition of Salts in the Cellulose Solution		**3.4**
	4.3.2 Acidic Conditions of the Regeneration Bath		**3.5.1**
4.4 Manufacturing of Cellulose Aerogel Beads	**4.4.1** Laboratory Scale		**3.5.1**
	4.4.2 Technical Scale		**3.5.2**
4.5 Manufacturing of Cellulose Aerogel Sheets	-		**3.6**
4.6 Manufacturing of Cellulose Aerogel Engineered Fibers	-		**3.7**
4.7 Lignin Coating of Cellulose Aerogels	**4.7.1** Moisture Influence		**3.5**
	4.7.2 Chemical Interaction of Lignin with Wet Cellulose Gel		**3.8**
	4.7.3 Lignin coated Cellulose Aerogels		
4.8 Economic and Environmental Impact	-	-	-

    *   Applied as well in the synthesis of samples in chapters **4.4**, **4.5**, and **4.6** according to their manufacturing scale.

   **   Applied as well in the synthesis of all samples from chapters **4.3** to **4.7**.

4.1 Extraction of Cellulose

In this chapter, the characteristics of the hemp and flax bast waste fibers and their extracted cellulose at the laboratory scale are described and discussed. The adaptation of the extraction method to technical scale and its challenges are further discussed.

4.1.1 Laboratory Scale

After alkali treatment and bleaching, 63 wt.-% of the flax fibers and 72 wt.-% of the hemp fibers remained in the form of white cellulose. Considering that 65 wt.-% to 75 wt.-% of these waste bast fibers are composed of cellulose [212, 251], these yields confirmed the high efficiency of this extraction method. The difference in yield between the two fibers could be related to their different cellulose content, which is highly dependent on each plant and its development. The skeleton density, the density of the material´s solid backbone without considering the free space, shall be constant for different celluloses, independently of their source. Nonetheless, small differences exist as the biomass fibers are not purely composed of cellulose and different degrees of cellulose crystallinity will influence this value. In general, a higher crystallinity leads to higher skeleton density due to more packing.[252] **Table 7** presents the skeleton densities and crystallinity indexes of the biomasses used, the extracted celluloses (HC and FC, from hemp and flax respectively), and commercial cellulose (MC).

Table 7 Skeleton densities and crystallinity indexes of biomass fibers and of celluloses (extracted and commercial)

Fibers and Celluloses	Skeleton Density / g cm^{-3}	ICs / %
HF	1.47	78.26
FF	1.44	80.22
HC	1.50	87.03
FC	1.55	86.19
MC	1.52	87.55

The skeleton density increased slightly during the extraction process from fiber to cellulose (from 1.47 g cm^{-3} to 1.5 g cm^{-3} and from 1.44 g cm^{-3} to 1.55 g cm^{-3}, for hemp and flax respectively) and the celluloses obtained had a skeleton density close to the 1.5 g cm^{-3} of

4.1 Extraction of Cellulose

standard cellulose density found in literature and measured for MC.[251] As the concentration of cellulose was already very high in the fibers (from 65 wt.-% to 75 wt.-%, with the content of hemicellulose from 10 wt.-% to 20 wt.-% and of lignin from 2 wt.-% to 2.5 wt.-%)[212], it was expected that their density would be close to the standard cellulose and would increase during the extraction process as hemicellulose and lignin would be removed. The high content of cellulose in the biomass fibers and the quality of the extraction of cellulose were evaluated by the FTIR spectra of the samples, in **Figure 28**.
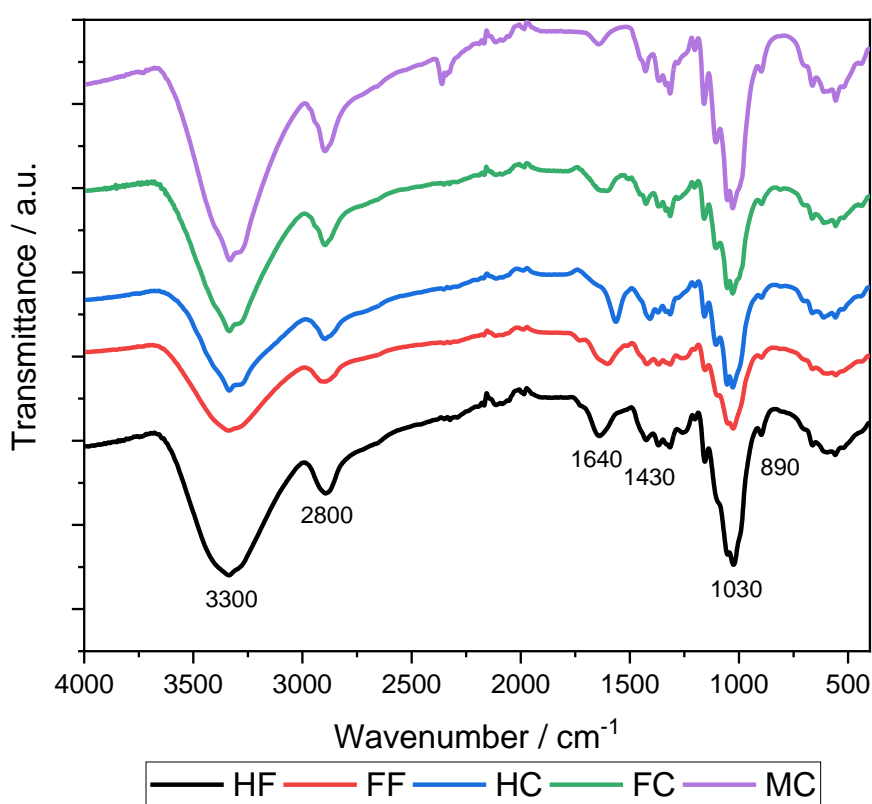
Figure 28 FTIR spectra of biomass fibers (black for HF; red for FF) and of celluloses (blue for HC; green for FC and purple for MC)

Both in the fibers and in their extracted celluloses spectra, at 3300 cm^{-1} and 2800 cm^{-1}, there were signals corresponding to the O-H and C-H stretching vibrations, respectively, and at 1640 cm^{-1} a small band associated with the presence of water adsorbed on the hydrophilic surface of cellulose. The bending of the CH and CH$_2$ groups was recognized at 1430 cm^{-1}, at 1030 cm^{-1} the CO stretching, and, at 890 cm^{-1}, the CH deformation.[243, 251] Each one of these bands was recognizable in the FTIR spectrum of commercial cellulose, which demonstrated the high content of cellulose in the waste fibers and the purity of the extracted

cellulose. For the extracted celluloses, no signal was present at 1730 cm^{-1}, typical of acetyl groups of hemicellulose and lignin´s esters, nor at 1533 cm^{-1}, from C=C present in lignin´s aromatic rings[242]. Those peaks had a small presence in the biomass spectra but disappeared after the extraction process. The broadening of the peak 1640 cm^{-1} for the extracted celluloses could be due to the presence of residual lignin, which has a signal at 1595 cm^{-1} from C=C aromatic stretching, or from the presence of water entrapped in the cellulose matrix, with a signal at 1600 cm^{-1}.[253, 254] Despite this, the alkali treatment and further bleaching were successful in the isolation of cellulose and no major differences were observed between FC, HC, and MC.

The FTIR spectra of the first supernatant from the alkali treatment of biomasses were measured to evaluate the efficiency in removing hemicellulose, lignin fragments, and reactants used in the extraction procedure. These are shown in **Figure 29.**
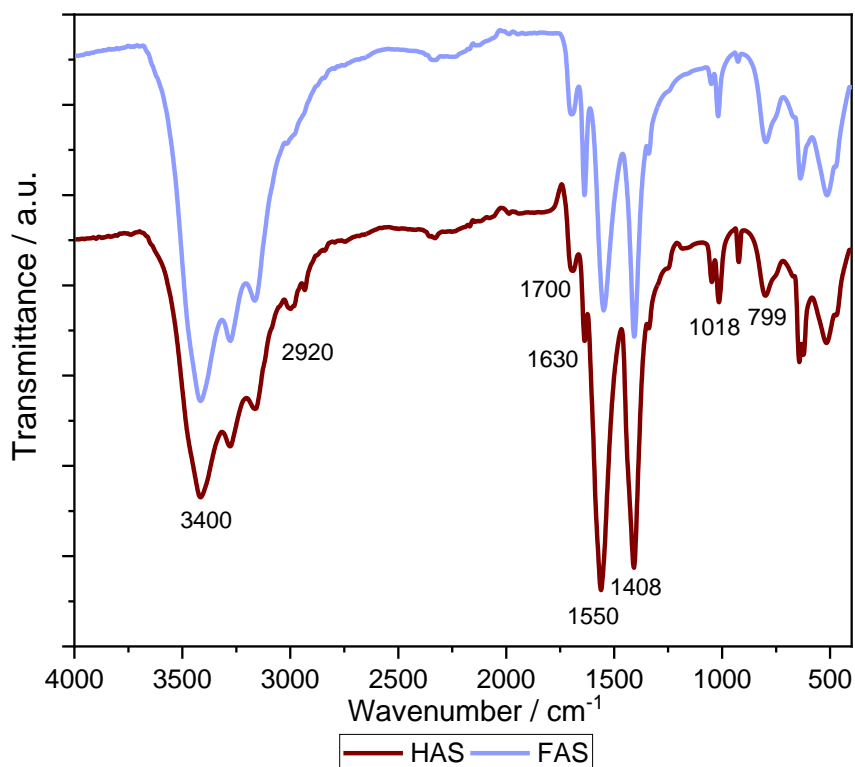
Figure 29 FTIR spectra of the first supernatant from the alkali treatment of hemp (wine red for HAS) and flax (light purple for FAS) fibers.

The main differences to the previous spectra were the presence of a very low signal at 1018 cm^{-1}, of two intense peaks at 1550 cm^{-1} and 1408 cm^{-1}, and the shift of some bands recognizable in **Figure 28** (band at 3400 cm^{-1} with shoulders at lower values). The presence of

4.1 Extraction of Cellulose

the residues of the undesirable biopolymers was found in the peaks at $3400 \, cm^{-1}$ (alcoholic and phenolic OH stretching), at $2920 \, cm^{-1}$ (C-H stretching from aromatic methoxy groups from lignin), and at $1630 \, cm^{-1}$ (C=O stretching from α,β-unsaturated aldehydes or ketones or C=C from alkenes). The carboxyl group from the acetic acid used in the neutralization was detected at $1700 \, cm^{-1}$. The C-C stretching from lignin's aromatic rings was at the origin of the strong peak at $1550 \, cm^{-1}$. The peaks in the region between $1385 \, cm^{-1}$ and $1250 \, cm^{-1}$ were characteristic of hemicellulose, especially when alkali extracted. C-O stretching from alcohol or ether groups was visible at $1018 \, cm^{-1}$ while, at $799 \, cm^{-1}$, the peak corresponded to the deformation vibrations from C-H groups in the aromatic rings of lignin.[255-257] The first supernatant already contained most impurities and removed organic molecules for both HF and FF. After washing, the alkali-treated biomasses were bleached and pure cellulose was obtained. This trend was further observed from the analysis of the XRD spectra.

As the relative weight of cellulose in the samples increased along the extraction process, it was expected that the bands associated with cellulose became better defined in the XRD pattern. Indeed, as shown in **Figure 30**, for hemp and flax fibers, it was evident that cellulose was present.

Important diffraction planes associated with cellulose were detected for HF and FF. They dominated the diffractogram while not being at their highest definition due to the presence of hemicellulose and lignin. As these last two do not have a crystalline structure, they broadened the visible signals without originating defined peaks of their own. A peak at 16.5° 2θ reflection with a shoulder to its left was assigned to an agglomeration of the signals from the crystalline planes (1$\bar{1}$0) (from 14.5° to 15.3°) and (110) (from 15.7° to 16.3°). The signal with the highest intensity, at 22.7°, was related to the (200) crystallographic plane of cellulose, and the plane (004) was associated with the signal at 35.1°. These signals are characteristic of cellulose I[242, 243] The signals at 15.1° and 16.5° were better separated in the flax spectrum but the difference was small compared to hemp. After the chemical treatment of the biomass fibers, the cellulose could be extracted in its crystalline form which originated XRD diffractograms with a higher definition of its peaks.
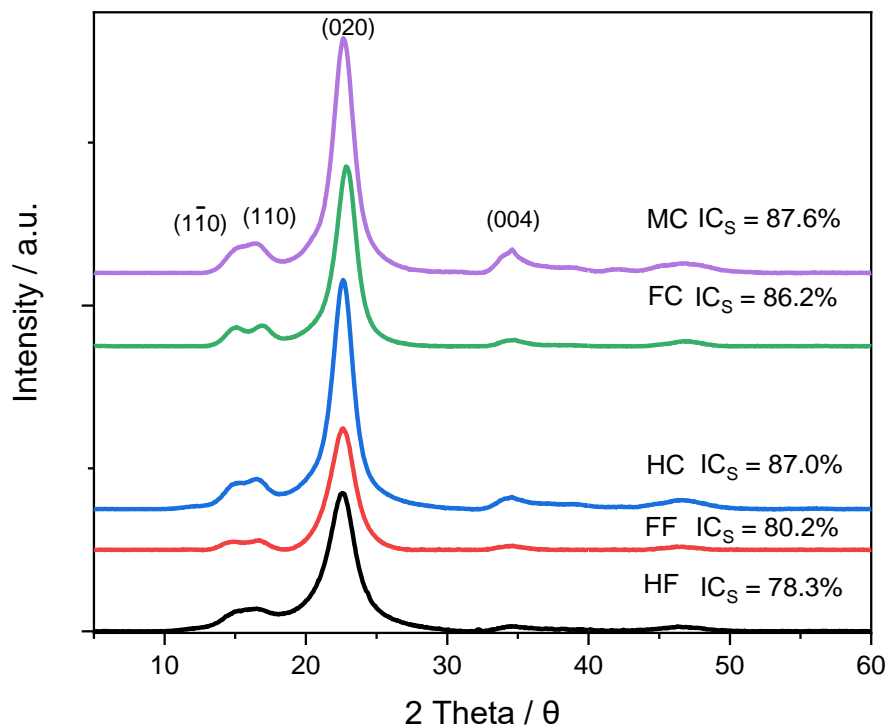
Figure 30 XRD diffractograms and respective crystallinity indexes (IC_S) of biomass fibers (black for HF; red for FF) and of celluloses (blue for HC; green for FC and purple for MC).

The peaks around 15° became deconvoluted, appearing at 15.1° and the other at 16.5°, corresponding to the mentioned ($1\bar{1}0$) and (110) planes. The peak at 22° increased its intensity, demonstrating that crystalline cellulose was in a state of high purity and that the other biopolymers were removed. The region at 18 ° also presented a smaller relative intensity, associated with the amorphous phase of the cellulose I. The crystallinity of the samples was calculated using **Equation 8**.

While the fibers had a high level of crystallinity due to their rich composition in cellulose (78.3% and 80.2% for hemp and flax respectively), the isolation of cellulose without degradation and the removal of the other biopolymers increased these values to 87.0% and 86.2%, respectively. These were close to the 87.6% obtained from MC. These data suggested that the structural properties and purity of the extracted celluloses were independent of the biomass used and were similar to the commercial cellulose used as standard.

In the SEM photographs of **Figure 31**, the fibers are visibly heterogeneous in nature. They had different diameters and sizes, ranging hundreds of μm. The lignocellulosic polymer was intact,

4.1 Extraction of Cellulose

and its surface was smoother or rougher depending on the concentration of waxes, pectins, and other impurities.[258] Flax fibers presented a rougher surface compared with hemp fibers.
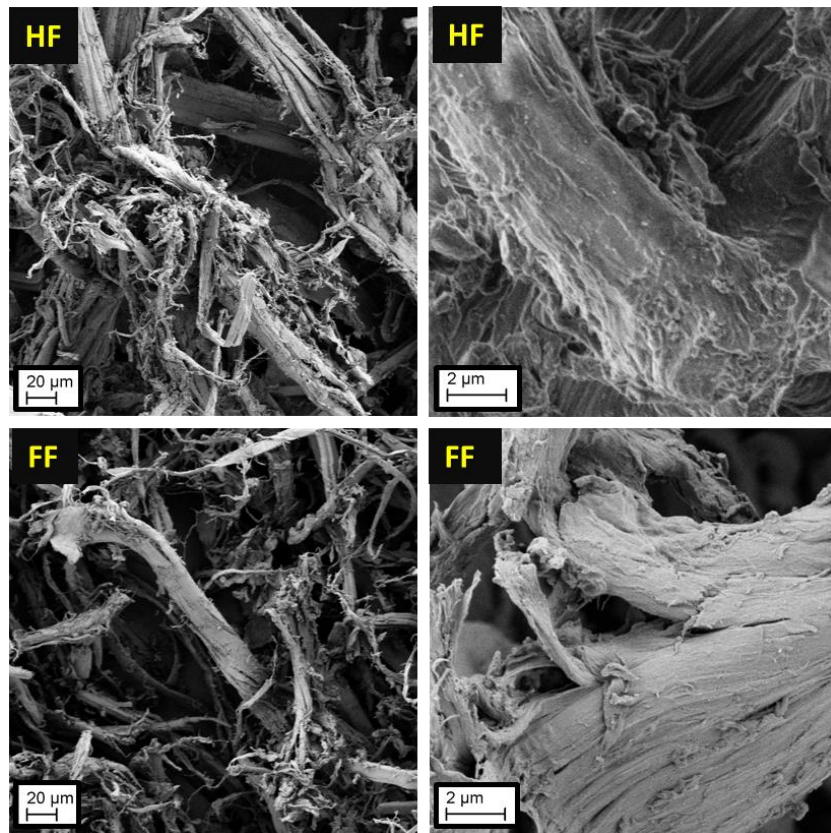
Figure 31 SEM images of hemp (HF) and flax (FF) waste bast fibers, at different magnifications.

After alkali treatment and bleaching, cellulose remained while other biopolymers, waxes, and residual organic compounds were removed. In **Figure 32**, long fibers of crystalline cellulose are visible. This agreed with the data obtained from other characterization techniques such as FTIR and XRD, which indicated an overwhelming presence of cellulose, with a high degree of crystallinity. The cellulose fibrils were so packed due to the attractive interaction between them that their dimensions could not be measured. Those fibers were composed of crystalline cellulose I.
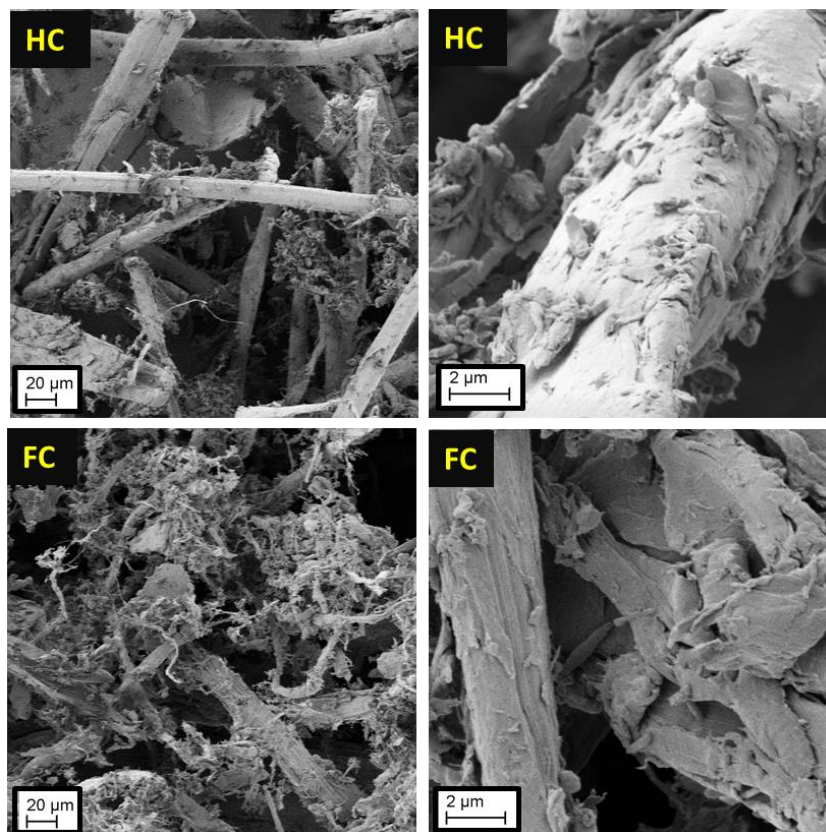
Figure 32 SEM images of hemp (HC) and flax (FC)-extracted cellulose after alkali treatment and bleaching of biomass fibers, at different magnifications.

In **Figure 33**, the thermal behavior of the different samples can be observed. The samples presented three main areas of weight loss. The first, between 40 °C and 100 °C, corresponded to the evaporation of water, with a weight loss between 1.77% and 4.89%. In the second area, from 200 °C to 380 °C, a sharp decline in the sample weight was recorded due to the degradation of cellulose and other remaining biopolymers. A stabilization curve was recorded from 380 °C to 600 °C, mainly due to the remaining residue carbonization into char.[242] Except for HC, degradation for all biomass-based samples started at 215 °C and reached 50% between 310 °C and 350 °C, where a linear region characteristic of cellulose degradation was found. This latter range encompasses the cleavage of the glucosidic bonds and dehydration reactions of cellulose´s glucose monomers[242, 259] While hemicellulose and lignin have decomposition ranges between 180 °C and 350 °C and between 250 °C and 600 °C, respectively, no significant weight decline outside of the classical cellulose range was observed in the extracted celluloses. This confirmed the efficiency of the cellulose extraction method and the thermal stability of the obtained products.[243, 258]
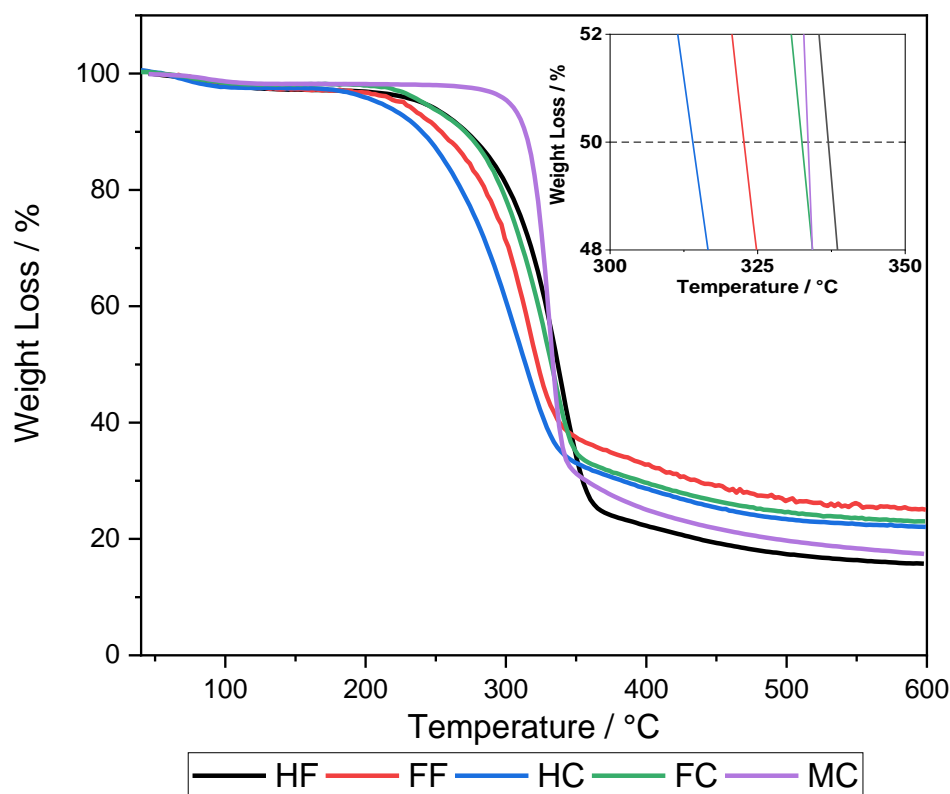
Figure 33 Thermal gravimetric profile of biomass fibers (black for HF; red for FF) and of celluloses (blue for HC; green for FC, and purple for MC).

The differences between the profiles of each sample were influenced by the presence or absence of other biopolymers and the cellulose structure. In the case of flax, its fibers reached 50% degradation at a lower temperature than its extracted cellulose due to the presence in the first of easily degradable hemicellulose (322 °C vs. 332 °C, respectively). Furthermore, FF had a higher amount of char residue than FC due to the presence of highly recalcitrant lignin (24.9% vs. 22.9%, respectively). MC was the sample whose degradation started later, at 260 °C, and had one of the lowest amounts of residue (17.3%) due to its purity, high degree of crystallinity, and homogeneity of its cellulose fibers. HC´s degradation started at 180 °C, reached 50% mass loss at a lower temperature than HF (310 °C vs. 340 °C, respectively), and produced more char residue. This trend was the opposite of what was recorded for flax. The size and inhomogeneity of the cellulose fibers, which could have suffered some degradation, could have contributed to the lower thermal stability of HC.[222]

Results and Discussion

4.1.2 Technical Scale

The extraction of cellulose at laboratory scale from hemp and flax bast waste fibers was effective but required adaptation to be applied at larger scales.

Figure 34 shows that the infrared spectra of hemp alkali-treated intermediates, according to residence time before the heating phase, were similar regardless of the residence time.
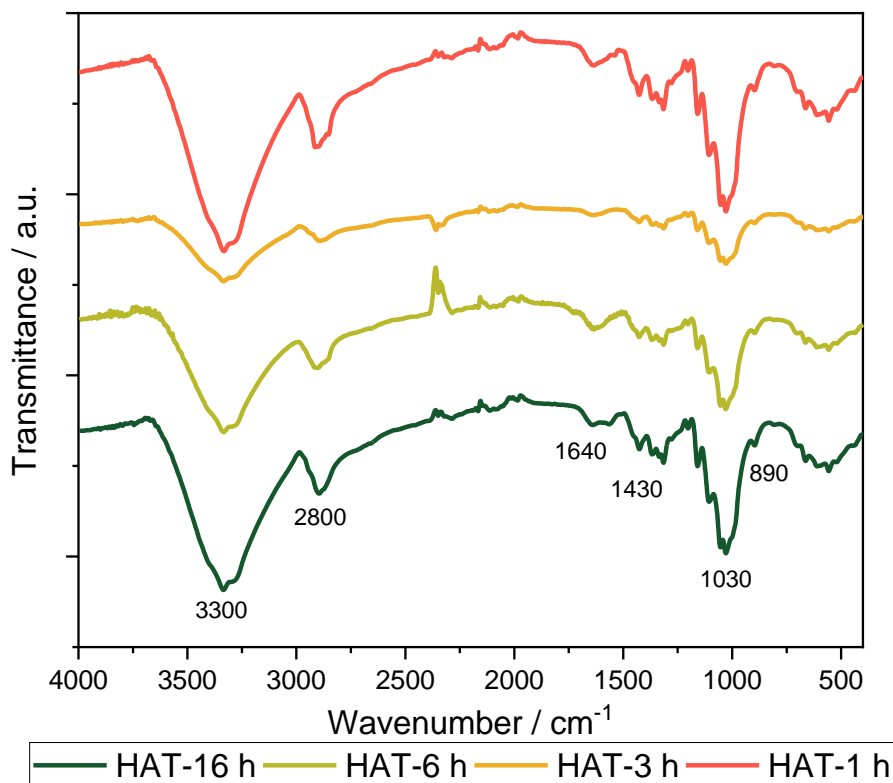
Figure 34 FTIR spectra of hemp alkali-treated intermediates (HAT), according to residence time (dark green for 16 h; light green for 6 h; orange for 3 h, and red for 1 h) before the heating phase. The hemp fibers were milled to > 1 mm before the alkali treatment.

Cellulose-related signals such as the vibrations of the OH, CH, CH_2, and other functional groups from the pyranose ring (identified in the previous section) were visible. Some signals from remnants of lignin were still present. In all cases, the peak at 1640 cm^{-1}, which was related to water adsorption on the hydrophilic surface of the residue, still had a shoulder between 1500- 1595 cm^{-1}, due to aromatic ring vibrations from residual lignin.[256] This was least pronounced for HAT-3 h. Nonetheless, these intermediates were significantly pure as many of the hemicellulose, waxes, lignin, and pectins of the lignocellulosic polymer were washed out.

4.1 Extraction of Cellulose

Signals of these removed biopolymers were present in the FTIR spectra of the first supernatants, in the appendix (see **Figure 109**).

When the residence time for the alkali treatment was fixed at three hours, due to limited presence of lignin in HAT-3 h, and the duration of the bleaching step was modified, as observed in **Figure 35**, no significant differences were observed in the FTIR spectra of the celluloses.
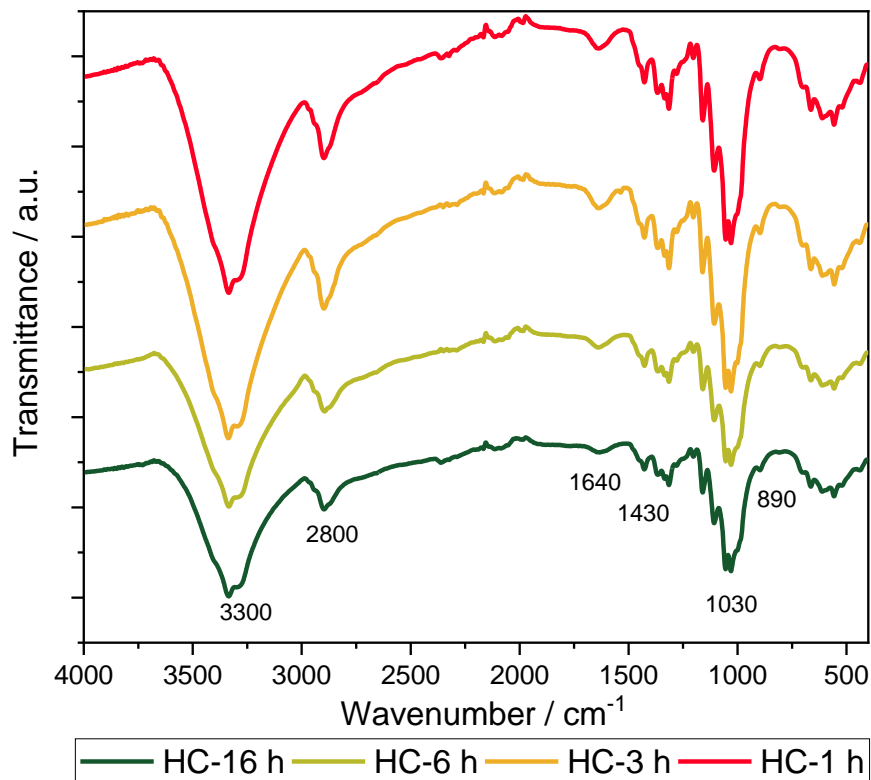
Figure 35 FTIR spectra of hemp-extracted cellulose samples (HC), according to bleaching residence time (dark green for 16 h; light green for 6 h; orange for 3 h, and red for 1 h) before the heating phase. The hemp fibers were milled to > 1 mm before the alkali treatment, whose room temperature residence time was three hours.

Compared to their alkali-treated correspondent, the FTIR spectra became sharper and the cellulose-associated peaks became more pronounced as they became purer. Based on this chemical analysis, three hours was established as the residence time for both the alkali treatment and the bleaching steps at room temperature, before the respective heating phases of 3 h, at 60 °C.

In the appendix (see **Figure 110**), it is shown that the lack of stirring did not affect the quality of the cellulose obtained. These results were surprising as it was expected that a fast stirring would promote the dispersion and size reduction of the cut fibers. The more available area

would enable a more effective interaction between the fibers and the reaction media and the consequent extraction of undesirable biopolymers and molecules. However, the alkali and bleached spectra were almost identical, independently of the existence of stirring. Both alkali residue spectra became sharper after the bleaching step due to the removal of the remaining lignin and other impurities. It could mean that the fibers had a dimension (> 1 mm) small enough to be effectively surrounded by the reaction mixture and that the kinetics of the reaction were not a limiting factor.[223] This would entail that further mixing would not improve the speed or quality of the extraction process. Nonetheless, the non-stirred cellulose fibers were significantly bigger than the stirred ones, which hindered their dissolution. Stirring facilitated the de-fibrillation of the bast fibers, reducing their size and facilitating their dissolution for aerogel production.[19] It also ensured that the extraction conditions remained constant across the full height of the reactor, which is particularly important at technical and industrial scales where bigger volumes are handled. If not, a phase separation could occur between purer and less pure cellulose fibers and the reproducibility and reliability of the extraction process would have been put at stake.[21]

The FTIR spectra of the upscaled samples can be observed in the appendix (see **Figure 111**). No significant differences were perceived between the alkali-treated residues and the cellulose samples between the scales. This indicated that the extraction method was successfully upscaled without compromising the quality of the final cellulose product. The same results were obtained when finely milled fibers (0.2 mm) were used, as observed in the appendix (see **Figure 111**).

In **Figure 36**, the XRD patterns of cellulose samples according to residence time for bleaching (after three hours of alkali treatment) can be observed. These were very similar among themselves and were characteristic of cellulose I. [217, 237, 240]

The IC_S of all cellulose samples ranged between 89% to 95% and did not vary significantly between residence times. These were comparable to the 87.6% obtained from MC. A similar trend was observed when the XRD patterns were compared between the stirred or non-stirred process, as in the appendix (see **Figure 116**). Using three hours as room temperature residence time for alkali treatment and bleaching, the IC_S obtained from laboratory and technical scales (TS) were the same, and the crystallinity of the alkali-treated residues was also similar, as shown in the appendix (see **Figure 117**). The alkali intermediates had a high degree of crystallinity. The alkali treatment step removed most of the amorphous components of the lignocellulosic polymer, resulting in a higher increase in the IC_S of the samples than the bleaching step. As bleaching mainly removed the remaining lignin, which comprised 3.5% to 5.7% of these fibers, only a slight increase in crystallinity was observed.[197, 205]
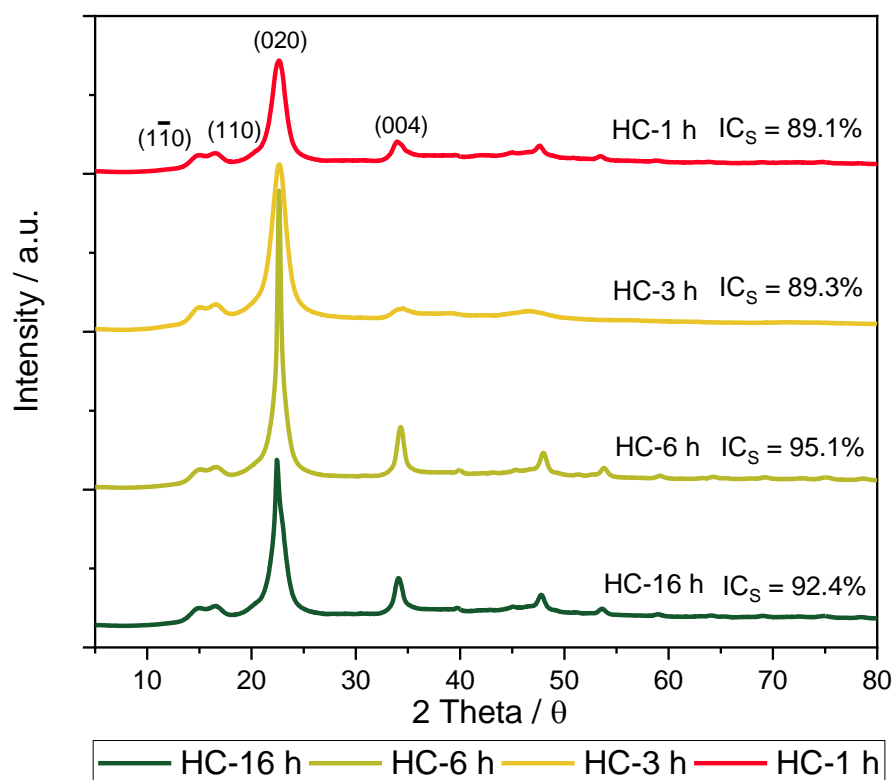
Figure 36 XRD diffractograms and respective crystallinity indexes (IC_S) of hemp-extracted cellulose samples (HC), according to bleaching residence time (dark green for 16 h; light green for 6 h; orange for 3 h, and red for 1 h) before the heating phase. The hemp fibers were milled to > 1 mm before the alkali treatment, whose room temperature residence time was three hours.

This series of experiments indicated that a suitable method to extract cellulose from hemp bast fibers was developed by adapting the standard, laboratory scale methodology. Not only was it performed in a fraction of the time (three hours for residence time at room temperature instead of 16 h), with a consequent reduction in costs and labor, but also the cellulose obtained maintained a similar degree of chemical purity and high crystallinity. The dimensions of the milled fibers used in these tests (> 1 mm) did not affect the quality of the cellulose obtained but hindered their dissolution and conversion into aerogel. However, the extraction was successful as well, at a technical scale, with finely milled (< 0.2 mm) fiber particles and dissolution was possible.

4.2 Dissolution of Cellulose

Figure 37 shows microscope pictures of a 7 wt.-% commercial cellulose solution (MC7), after selected storage periods at -20 °C. After one hour, the contours of the few visible structures could not be defined at any magnification, which indicated that they were dissolved.[260] These structures were cellulose fragments with swollen sections and flat rings. When the solution stayed for half an hour, some of those fragments became clearly defined, with visible longer and thinner fibers. This indicated a decrease in the quality of dissolution. When the solution was not stored (0 h), many well-defined undissolved fibers were observed.
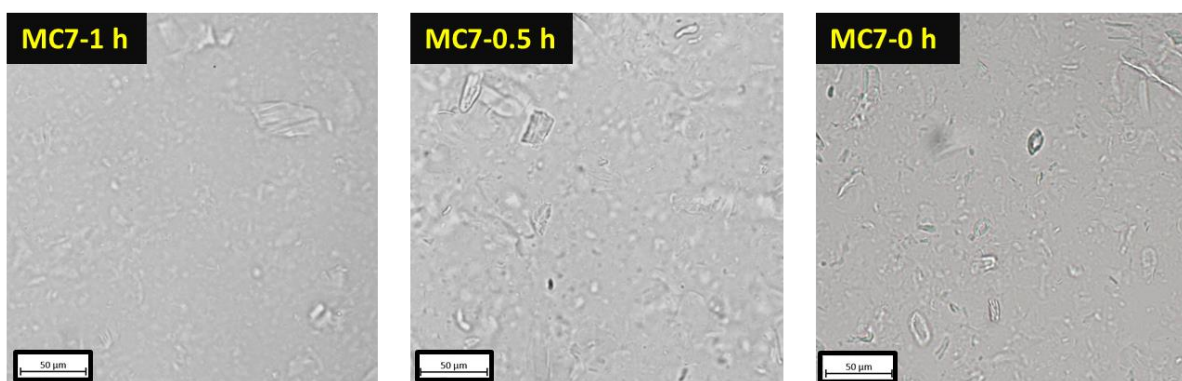
Figure 37 Microscope pictures of 7 wt.-% commercial cellulose solutions (MC7) stored for different residence times at -20 °C (1 h; 0.5 h, and 0 h).

It is known that during dissolution, the swelling and shearing during the process lead to the formation of swollen sections, flat rings, and fragments from the cellulose fibers that can remain undissolved and visible, as shown in **Figure 37**.[98, 159, 260] These results showed that successful dissolution was achieved by storing the solution at -20°C for at least one hour. In **Figure 38**, pictures of the cellulose solutions continuously stirred and dissolved at different temperatures show that higher temperatures gave less transparent solutions.

4.2 Dissolution of Cellulose
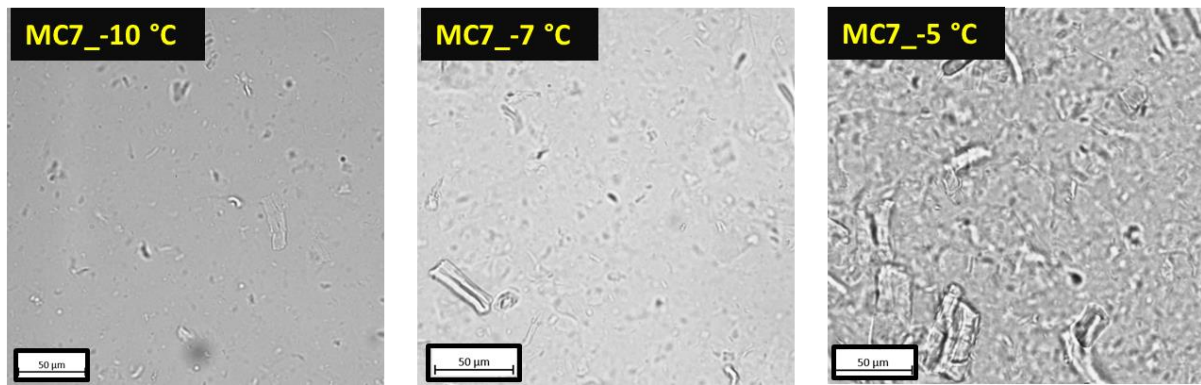
Figure 38 Microscope pictures of 7 wt.-% commercial cellulose solutions (MC7) continuously dissolved at different temperatures (-10 °C; -7 °C, and -5 °C).

As shown above, with increasing temperatures, the number of visible structures and their definition increased. At -10 °C, a good state of dissolution was observed, with bigger particles that remained undissolved. Other researchers have successfully used this temperature to dissolve cellulose.[107, 261] At -7 °C, more and better-defined structures were visible while, at -5 °C, the state of dissolution was very low. This conformed with the conditions at which efficient dissolution of cellulose in this system was observed in other studies.[76, 79, 98, 261]

In the appendix (see **Figure 122**), the dynamic viscosity of the tested solutions is shown. Samples with standard (16 h) and one hour of residence time at -20 °C had a viscosity of 0.29 Pa.s. For different temperatures, their difference in viscosity was low, from 0.24 Pa.s to 0.26 Pa.s. The solution where cellulose was dissolved at -20 °C for 30 min has a viscosity of 0.19 Pa.s, the value with the highest deviation from the viscosity of the standard solution. The different viscosity was explained by a lower amount of dissolved material which un-homogeneously spread in the solution. It indicated that the viscoelastic properties of the cellulose solutions prepared with different residence times a -20 °C and temperatures were similar.

The results showed that efficient dissolution of cellulose was achieved at a maximum temperature of -10 °C, after 30 min of continuous stirring. This reduced the time and energy required to prepare cellulose solutions, making it more attractive to the industry. However, for volumes over 1 L, specific equipment needs to be used, and the solution should remain at - 10 °C for a longer period to ensure complete cellulose dissolution. The acquisition or development of industrial reactors that can achieve those low temperatures and their integration in a continuous process for the synthesis of cellulose aerogels is a challenge. As a consequence, storing solutions at freezing conditions remains the easiest solution for most industries, even

though it is a batch-wise process. It is essential to ensure complete dissolution of the cellulose fibers to minimize waste and avoid a higher crystallinity of the synthesized aerogels. A higher crystallinity induces a higher solid thermal conduction of the aerogels, decreasing their performance as thermal insulators. This feedback is useful in the upscaling of the production of cellulose aerogels while enabling the complete dissolution of cellulose at the lowest cost possible.

Furthermore, the results obtained from the molecular weight of the extracted celluloses and their influence on the viscosity of the respective cellulose solutions, are discussed. Depending on the degree of polymerization of the celluloses, their concentration in the solutions for the production of aerogels needed to be adapted. In **Figure 39** the shear viscosity profiles are shown of hemp-extracted cellulose solutions at different concentrations.
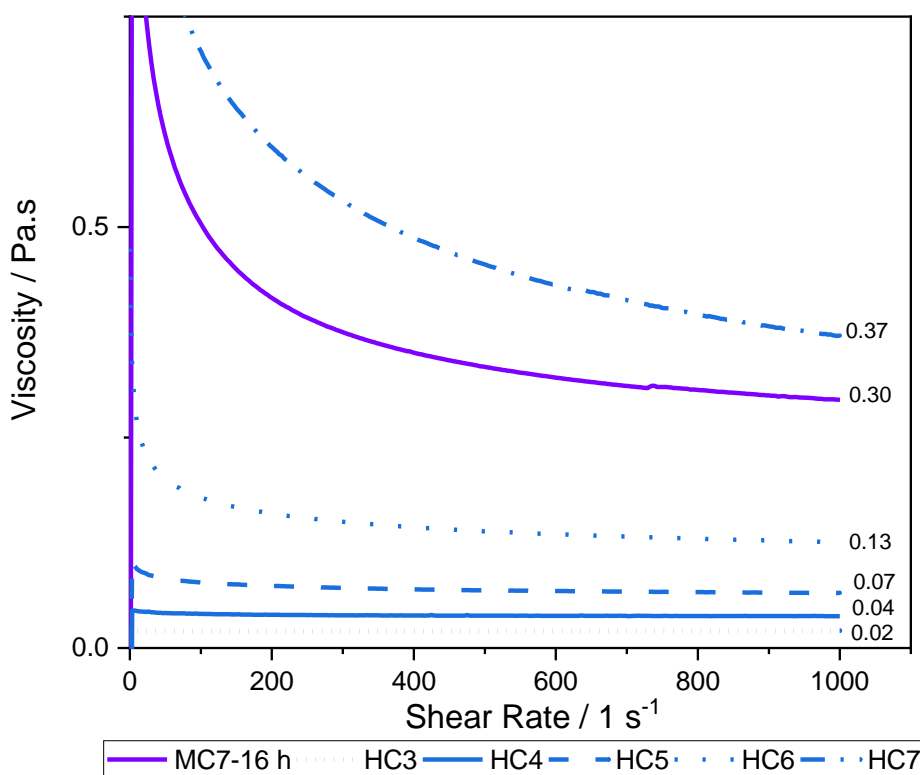
Figure 39 Dynamic viscosity of a 7 wt.-% commercial cellulose solution (purple for MC7-16 h) and of hemp-extracted cellulose (HC) solutions at different weight concentrations (short dotted blue line for 3 wt.-%, HC3; solid blue line for 4 wt.-%, HC4; dashed blue line for 5 wt.-%, HC5; dotted blue line for 6 wt.-%, HC6, and dashed-dotted blue line for 7 wt.-%, HC7). Celluloses were dissolved and the solutions were prepared after storage at -20 °C for 16 hours.

4.2 Dissolution of Cellulose

For all cases, the viscosity had higher values at low shear rates and decreased as the force applied in the solution was increased. This phenomenon is called shear thinning and, after 400 s^{-1}, it was less pronounced, stabilizing the viscosity. As the forces applied to the solution increased, the intertwined cellulose fibers were disrupted and disentangled. This decreased their opposition to the force applied and the viscosity of the solution. For more concentrated solutions, where fibers were more prone to entanglement, the increase in shear rates induced a more drastic reduction in their viscosities.[240, 262]

Higher concentrations of HC increased the solution´s viscosity, especially after the critical overlap concentration (c*). HC3, HC4, HC5, and HC6 solutions were described as diluted solutions, where cellulose fibers had enough space to avoid interactions and whose viscosity depended only on the number of coils present. It explained why for those samples the viscosity remained fairly constant with increasing shear rates. Over c*, whose exact determination was not performed, the fibers interacted with each other and could not be considered discrete. This imparted a higher viscosity dependence on the cellulose concentration.[240] This was why the viscosity difference between HC5, HC6, and HC7 was higher than between HC3 and HC4. The higher viscosity of HC7 compared to MC7 was in line with the respective obtained values of DP (341 and 152 respectively). These data showed that hemp cellulose solutions had similar viscoelastic properties to the ones prepared with MC. For flax-extracted cellulose solutions, as observed in **Figure 40,** higher viscosities were obtained. In this case, FC3 presented a viscosity higher than MC7-16 h, by the higher DP of FC (1328) compared to MC and HC. The high molecular weight of FC fibers meant that these occupied a higher volume in the solvent and, therefore, smaller concentrations were required to reach c* and consequent higher viscosities. It explained the sharp decrease in shear viscosity with increasing shear rates at very low concentrations.
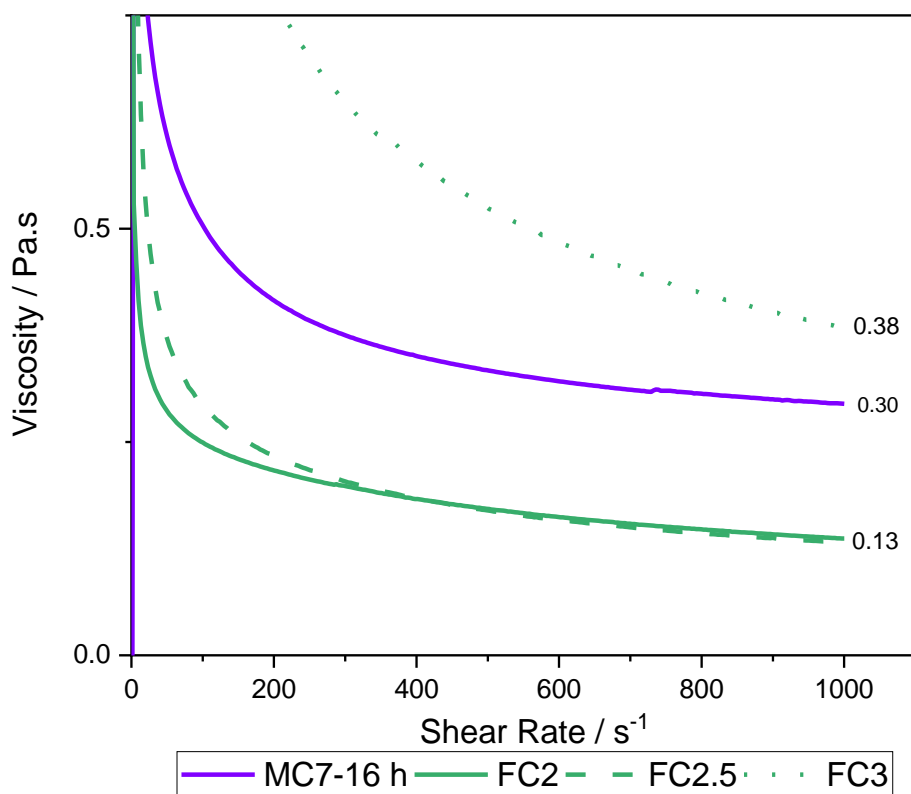
Figure 40 Dynamic viscosity of a 7 wt.-% commercial cellulose solution (purple for MC7-16 h) and of flax-extracted cellulose (FC)solutions at different weight concentrations (solid green line for 2 wt.-%, FC2; dashed green line for 2.5 wt.-%, FC2.5, and dotted green line for 3 wt.-%, FC3). Celluloses were dissolved and the solutions were prepared after storage at -20 °C for 16 hours.

4.3 Regeneration of Cellulose

This chapter focuses on how modifying the cellulose regeneration methodologies influences the properties of the resultant aerogels. The goal of these studies was to optimize the properties of the cellulose aerogels synthesized, namely by maximizing the active surface area and shifting the pore size distribution to lower values, and to adapt some of the synthetic procedures for technical scale. The influence of adding different salts to the cellulose solution (see **Chapter 4.3.1**), and using different acids as regenerating baths (see **Chapter 4.3.2**) are discussed in this section.

4.3.1 Addition of Salts in the Cellulose Solution

The addition of salts to cellulose solutions and their influence on the properties of the resultant aerogels are not fully understood and are a topic of scientific discussion. For scale-up processes, the viscosity of the cellulose precursor solution and the gelation time are of relevance. It is for example relevant to prepare fast-gelling solutions used for the CAProLi wet cellulose gel sheet production.

The influence on the viscosity of a 7 wt.-% commercial cellulose solution, at different salt concentrations (1 and 2 wt.-%) is shown in **Figure 41**. The viscosity of the cellulose solution increased with the amount of added salts, therefore a maximum of 2 wt.-% was suitable.
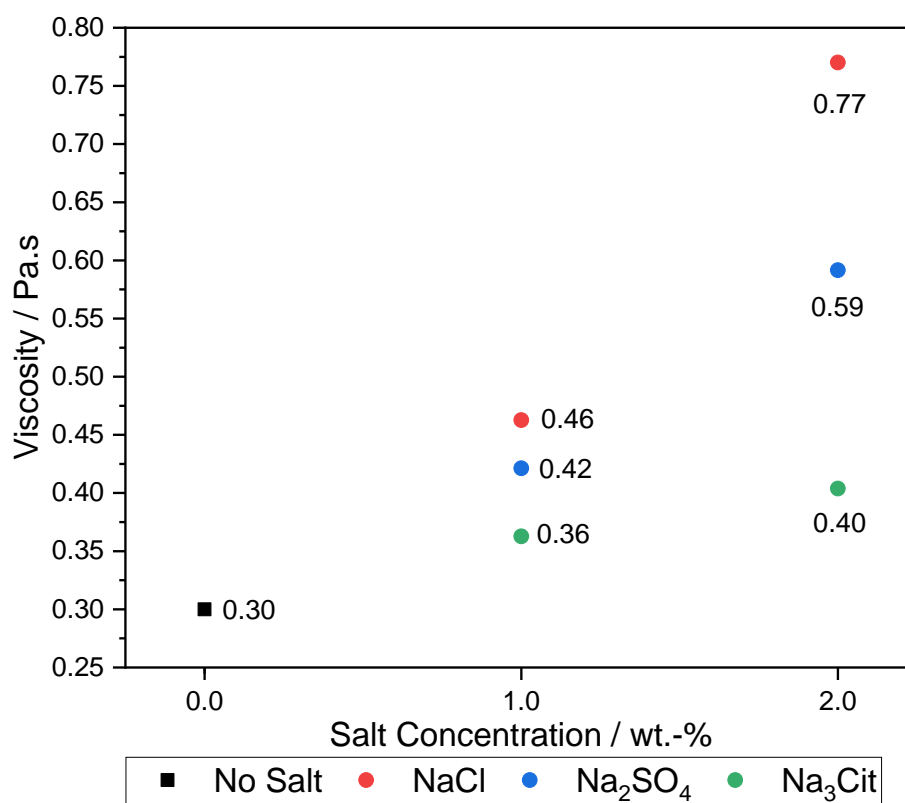
Figure 41 The dynamic viscosity of a 7 wt.-% commercial cellulose solution without (black square for "No Salt"), and after addition of sodium salts at different concentrations (red circle for NaCl; blue circle for Na_2SO_4, and green circle for Na_3Cit). Cellulose was dissolved and the solutions were prepared after storage at -20 °C for 16 hours.

The dynamic viscosity increased for all salts when 1 wt.-% of salts was added, with only small variations between 0.36 Pa.s and 0.46 Pa.s. The addition of 2 wt.- % NaCl was more effective in increasing the viscosity than the addition of 2 wt.- % Na_2SO_4 (0.77 Pa.s to 0.59 Pa.s) while

the viscosity using 2 wt.- % Na_3Cit was slightly higher than the value of viscosity obtained from the cellulose solution with no added salt (0.4 Pa.s). For the static viscosity (see Appendix and **Figure 123**) the same trend was observed for all salts, especially at 2 wt.-% and for NaCl and Na_2SO_4.

At low salt concentrations, the salt added was not enough to compete with cellulose for water, and so did not significantly affect its state of dissolution. If more salt was added, more ions would be solvated by water and the association between the cellulose chains would be promoted, increasing the solution´s viscosity. The differences between the various salts could be explained by using weight percentages to quantify the addition of salt instead of molar ratios. For comparison, for the same mass of salt added to the solution, the molar ratio of Cl^- :SO_4^{2-} :Cit^{3-} present in the solution was 4.4:1.8:1. Na^+, for the same order of anions, had molar ratios of 4.4:3.7:3. This trend can be observed in **Figure 42**.
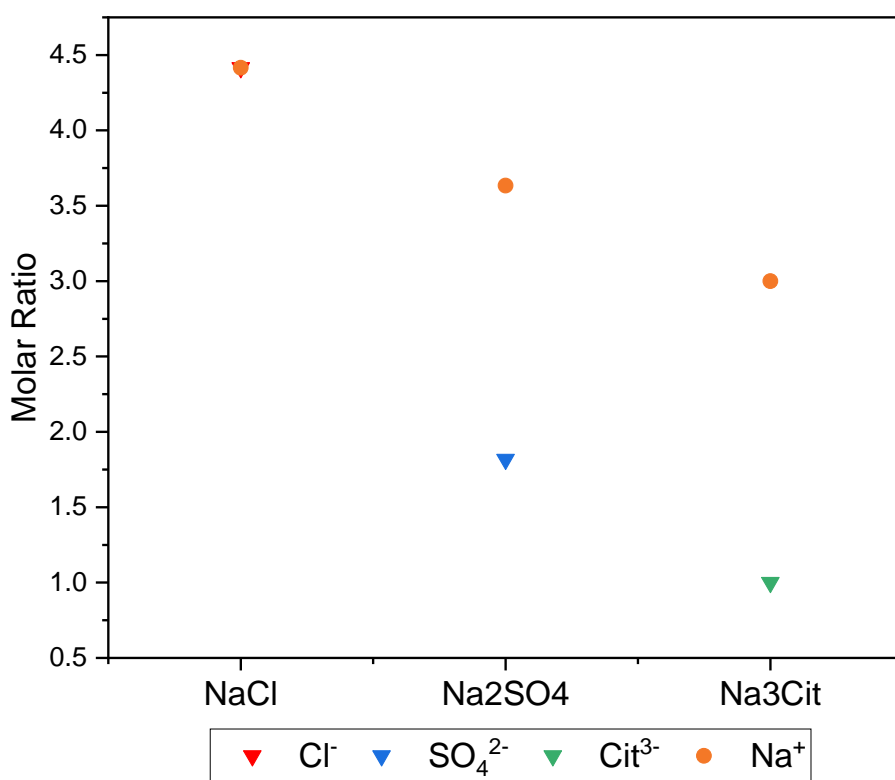
Figure 42 Molecular ratio of different anions and cations per gram of salt added to a 7 wt.-% commercial cellulose solution (red triangle for Cl^-; blue triangle for SO_4^{2-}; green triangle for Cit^{3-}, and orange circle for Na^+). These values were adjusted for Na_3Cit as standard. Cellulose was dissolved and the solutions were prepared after storage at -20 °C for 16 hours.

4.3 Regeneration of Cellulose

Thus, for the same mass of salt added, NaCl had a higher molar presence in the solution than the other salts, which contributed to the capture of more water molecules and led to a bigger increase in viscosity. However, the difference in a molar ratio between ions was not the only explanation. In addition, the different charges and structures of the anions and their interaction with cellulose in basic media played a decisive role.

These anions are known as kosmotropic (promote order) and create strong hydration spheres due to their high charge. These water molecules are removed from the vicinity of the cellulose chains, which increase the viscosity of the solution.[263-265] However, if this was the only factor, citrate, with a -3 charge, would promote the highest increase in viscosity, but that was not observed. The size of the anion increases from Cl^- to SO_4^{2-}, and Cit^{3-}, and so does its polarizability. In the case of citrate, its charge density is symmetrical, which favors a less orientation-dependent binding. Therefore, in this cellulose dissolution medium, citrate could interact with urea or the more hydrophobic regions of cellulose, while sulfate and chloride were excluded from the cellulose interaction zone.[266, 267] Citrate stabilized the cellulose:NaOH:urea complex while promoting the separation of the cellulose fibers due to its -3 charge. This could explain why adding a small quantity of sodium citrate had a limited influence on the viscosity of the solution, due to competition between Cit^{3-} and Na^+ ionic effects. It would further explain why an inverse Hofmeister series was observed, and why increasingly smaller ions, with more concentrated charges, had stronger hydration shells.[115, 263] Depending on the charge of their surface and their hydrophilic/hydrophobic character, the anions could interact differently with different sections of the cellulose chains. Other factors such as the thermodynamics of the solution, viscosity, mass partition coefficients, and more should be considered.[268] Following the trend observed for the viscosity, the gel point changed with the addition of salts as observed in **Figure 43**. After 1 wt.-% of NaCl and Na_2SO_4 addition, the gelation decreased from 483 s to 180 s and 307 s, respectively. A further reduction was observed at 2 wt.-%, to 0 s and 17 s, respectively. This was in line with their strong interaction with water, which increased the viscosity of the solution and promoted faster gelation.[114, 269] An opposite trend was observed for citrate, where the gel point increased from 483 s to 1092 s (1 wt.-%) and 692 s at 2 wt.-%. From 1 wt.-% to 2 wt.-%, the gel point decreased for all salts, but citrate still promoted a longer gelation time than the sample without salt. These results supported the role of citrate, a big and polarizable organic anion, as a stabilizer of the cellulose dissolution complex.
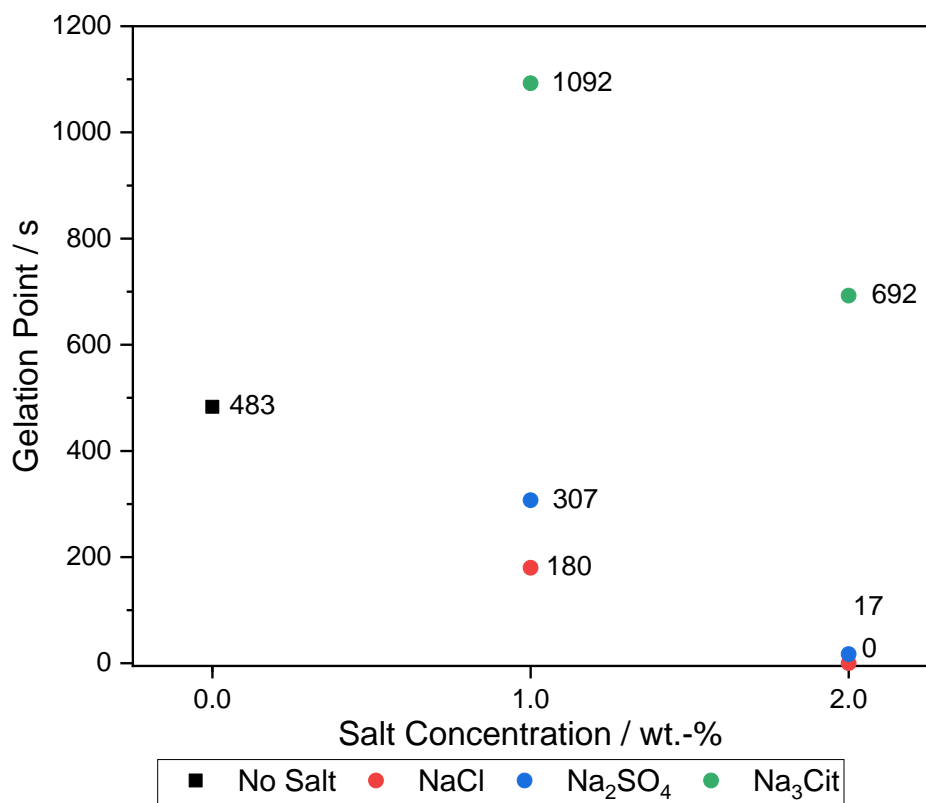
Figure 43 The gel point of a 7 wt.-% commercial cellulose solution without (black square for "No Salt"), and after addition of sodium salts at different concentrations (red circle for NaCl; blue circle for Na$_3$SO$_4$, and green circle for Na$_3$Cit). Cellulose was dissolved and the solutions were prepared after storage at -20 °C for 16 hours.

The influence of the temperature on the viscosity of the cellulose solution and how the addition of salts affected it was also evaluated. If no salt was added, the viscosity remained constant with increasing temperature and slightly increased during cooling. This did not contribute to the creation of a stable gel. The addition of salts, as shown in **Figure 44**, increased significantly the viscosity of the solution after a heating/cooling cycle. The addition of sodium chloride increased the viscosity of the cellulose solution, starting at 30 °C, up to 47 Pa.s and stabilizing it at 32 Pa.s in the cooling phase. The increase at lower temperatures was explained by its higher molar concentration and stronger association with water compared to the other salts. When sodium sulfate and sodium citrate were used, the viscosity increased more steadily at 40 °C, reached 36 Pa.s and 43 Pa.s at 50°C, respectively, and decreased during the cooling phase down to 25 Pa.s and 35 Pa.s, respectively. In the cooling phase for sodium citrate, the values of viscosity ranged from 27 Pa.s to 40 Pa.s until stabilizing close to 36 Pa.s, at 30 °C. Due to the interactions between citrate and cellulose, a smoother cooling gradient might be needed to

ensure isothermal conditions in the solution. Otherwise, temperature gradients can be present in the fluid, leading to the variations in the viscosity readings found in **Figure 44**.[270] For all salted solutions, higher temperatures, in combination with water-binding ions, deteriorated the dissolution state of cellulose, increasing the viscosity of the solution and promoting gel formation. The hystereses observed for all cases was explained by van der Walls forces, electrostatic interactions as well as hydrogen bonding between cellulose chains. These stabilized the gel during the cooling step.[261]
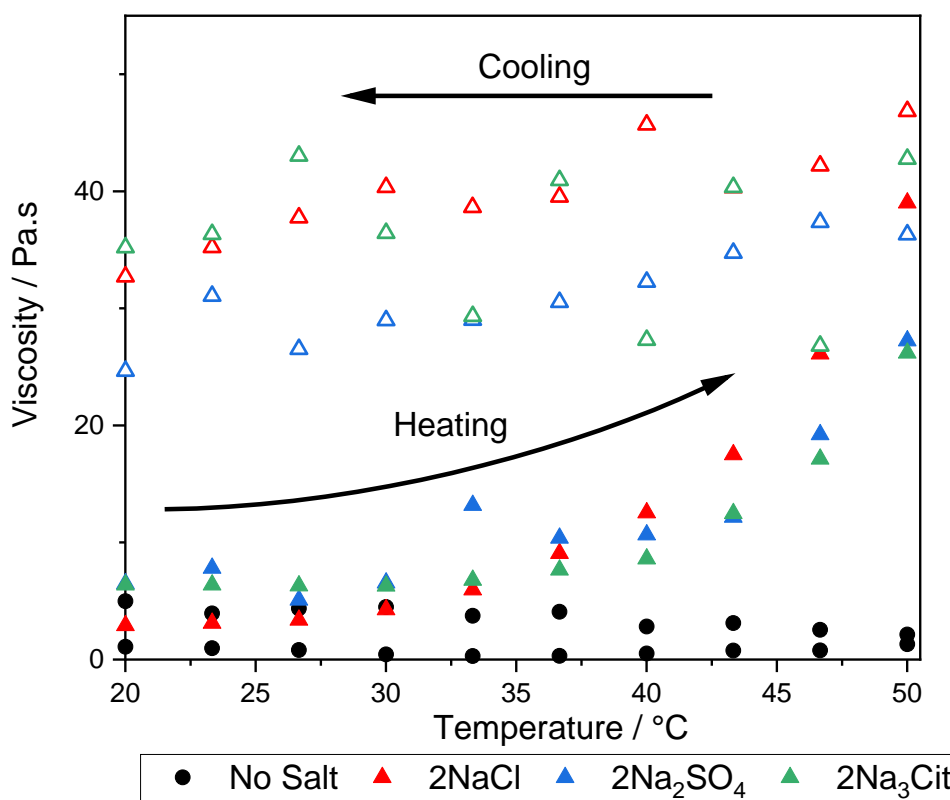
Figure 44 Evolution of 7 wt.-% commercial cellulose solution viscosity without (black circle for "No Salt"), and after addition of sodium salts at 2 wt.-% salts (red symbols for NaCl; blue symbols for Na_2SO_4, and green symbols for Na_3Cit) during a heating (closed symbols) and cooling cycle (open symbols). Cellulose was dissolved and the solutions were prepared after storage at -20 °C for 16 hours.

Based on these results, 7 wt.-% commercial cellulose solutions with or without these salts at different concentrations were converted into cellulose aerogel monoliths (MCM7). All monolithic samples were white and cylindrical. In **Figure 45**, a representative example is shown. The shape of the monolith was not perfectly cylindrical with different shrinkage behavior on the top wall and bottom face of the monolith.

Results and Discussion

When sodium chloride or sodium sulfate was added, a strong gel body was formed faster and, although shrinkage still took place, the shape was better preserved. During solvent exchange, salt crystallites could be present on the surface of the monoliths. This phenomenon was observed for all salts, with a stronger presence when a higher salt concentration was used. This happened due to the lower solubilization of salts in ethanol and indicated an inhomogeneous salt distribution in the samples.
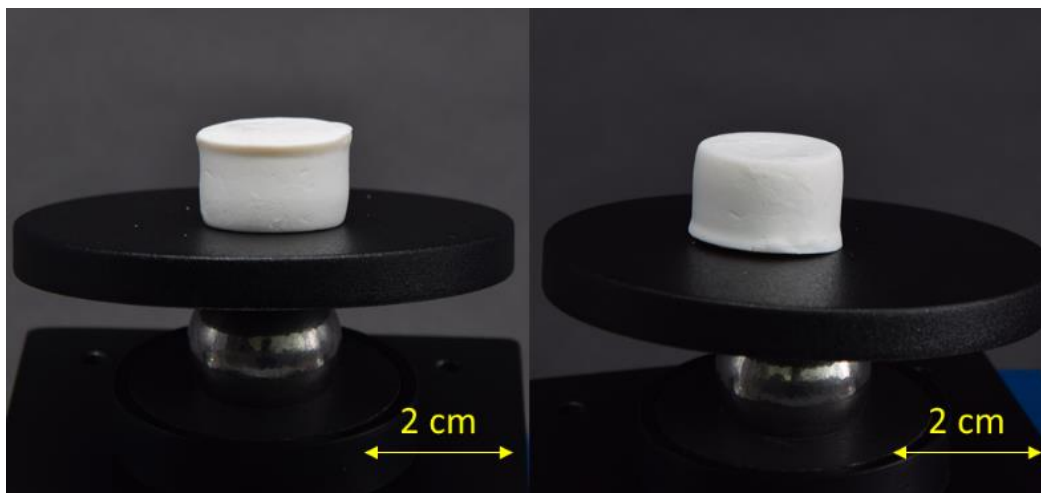
Figure 45 Pictures of a 7 wt.-% commercial cellulose aerogel monolith (MCM7-2Na$_3$Cit) upright (left) and up-side down (right).

Despite the apparent differences, the addition of salt had a low influence on the shrinkage in volume of the monoliths, as shown in **Table 8**. After 1 wt.- % of NaCl and Na$_2$SO$_4$ addition, the volume shrinkage increased from 49.40% of the blank sample to 56.81% and 53.66%, respectively. At 2 wt.-%, these values were 48.82% and 50.86%, respectively. It was assumed that competition existed between a strong gel body promotion, that preserved the monolith´s structure and reduced shrinkage, and the creation of pores by the scaffold effect. The addition of salt captured water and led to the fast association between cellulose fibers, resulting in a more resistant cellulose network against the osmotic pressure in gelation.[107] However, as the salts were removed during the neutralization phase, empty spaces were created that were more prone to induce shrinkage around their cellulose walls. The fast creation of the cellulose network played a major role when higher concentrations of salt were added, while the scaffold effect was more relevant at lower salt concentrations.[113, 114]

4.3 Regeneration of Cellulose

Table 8 Properties of 7 wt.-% commercial cellulose aerogel monoliths (MCM7) synthesized from solutions without and after addition of salts at different wt.-% concentrations. Information on the specific surface area and total pore volume of the aerogels is presented later.

Samples	Volume Shrinkage / %	Envelope Density / g cm^{-3}	Porosity / %	Average Pore Size / nm
MCM7	49.40±4.10	0.17	88.96	14.67
MCM7-1NaCl	56.81±2.47	0.17	88.97	17.18
MCM7-1Na$_2$SO$_4$	53.66±2.71	0.16	89.74	21.29
MCM7-1Na$_3$Cit	48.62±0.82	0.16	89.68	13.58
MCM7-2NaCl	48.82±0.91	0.16	89.54	17.42
MCM7-2Na$_2$SO$_4$	50.86±1.08	0.17	88.68	14.76
MCM7-2Na$_3$Cit	57.07±0.82	0.23	84.92	11.88

In the case of Na$_3$Cit, shrinkage increased with its concentration due to citrate´s bigger dimensions and because it hindered the creation of a stable gel body as shown in **Figure 45**. The pores created around the citrate anion were bigger than Cl$^-$ and SO$_4^{2-}$, which meant that shrinkage was magnified at higher salt concentrations. The uncertainty in the shrinkage among different salts could be linked to their inhomogeneous distribution in the gel body.

As shown in **Figure 46**, the difference in shrinkage between the samples reduced as the gel was converted into an aerogel. The 2 wt.-% of NaCl and Na$_2$SO$_4$ addition yielded less shrinkage at the hydrogel, alcogel, and aerogel phases, than 1 wt.-% while the opposite was observed for Na$_3$Cit. This was related to the previously discussed trends.

Despite these differences in shrinkage, the envelope density, and porosity remained constant for most samples, independently of the addition of salts in different concentrations. The density values ranged from 0.16 g cm^{-3} to 0.17 g cm^{-3}, with porosity values between 88.68% and 89.74%. The skeleton density was constant at 1.52 g cm^{-3}. These values were within the range for cellulose aerogel monoliths where salts were added during their synthesis.[113, 114] The only exception was for 2 wt.-% Na$_3$Cit, where the density was 0.23 g cm^{-3} and the porosity 84.92%. This was due to the higher shrinkage observed for the sample, which densified its porous structure. Another cause could have been an inhomogeneous distribution of the salt across the gel body, which might have a negative influence on the porous structure of the aerogel.
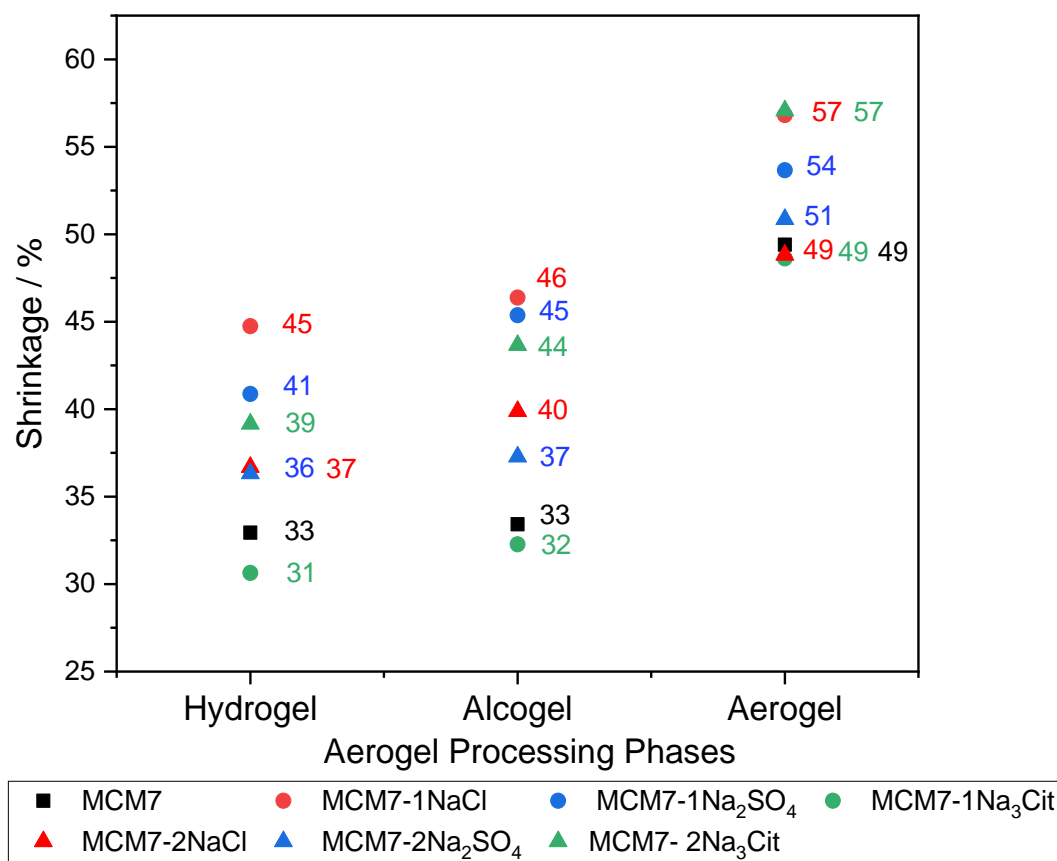
Figure 46 Shrinkage of 7 wt.-% commercial cellulose monoliths across different processing phases. These were synthesized from solutions without (black square for MCM7), and after addition of sodium salts (red symbols for NaCl; blue symbols for Na_2SO_4; green symbols for Na_3Cit) at different concentrations (circle for 1 wt.-%, and triangle for 2 wt.-%).

The addition of different salts at various concentrations did not influence the FTIR spectra of the synthesized aerogels, but differences were observed when cellulose I (MC) was converted into cellulose II in the aerogels. This is shown in **Figure 47.** The broad peak at 3300 cm^{-1} from O-H stretching became broader in the monoliths, with some distinction between different OH vibrations, due to the reinforcement of intra and inter-molecular hydrogen bonding.[271] For the bands presented at lower wavelengths, they were classified according to their functional groups and associated crystalline polymorphism (cellulose I or II). The peak at 1430 cm^{-1} from the CH_2 bending was characteristic of cellulose I and had a lower intensity in the aerogels while the signal from CH bending at 1370 cm^{-1} had the opposite evolution. The signal at 1160 cm^{-1} (C-O-C asymmetric stretching) had a lower intensity in the aerogels compared with MC. The signal at 1030 cm^{-1}, corresponding to ring asymmetric stretching of C-O, remained constant across the samples while a slight shift for lower frequencies and higher intensity was recorded

at 890 cm^{-1} (vibration in the glycosidic links) when cellulose was converted into an aerogel.[242, 243, 271, 272] The conversion of cellulose I into II during regeneration changed the tridimensional configuration of the cellulose fibers. This led to different hydrogen bond interactions and consequent vibrational modes between the spectra of MC and the aerogels.[272, 273] The lack of differences between aerogel samples indicates that the salts removed during washing and solvent exchange.
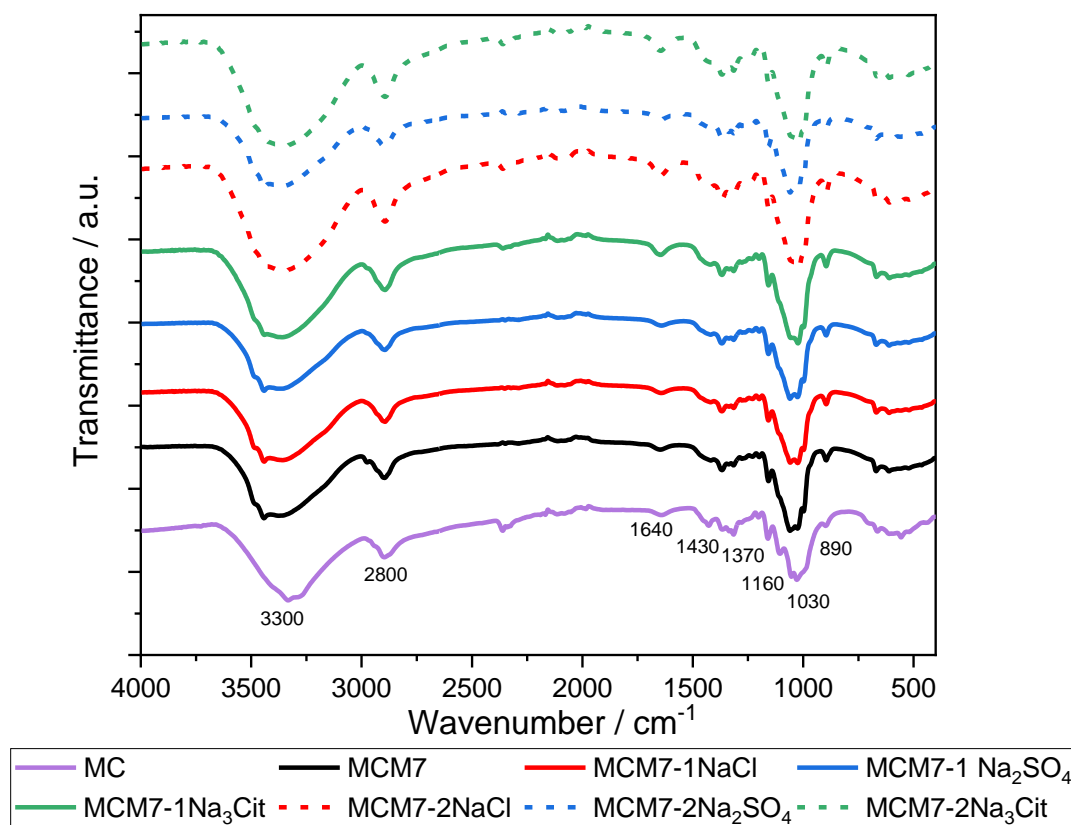
Figure 47 FTIR spectra of 7 wt.-% commercial cellulose aerogel monoliths from solutions without (black for MCM7), and after addition of sodium salts (red for NaCl; blue for Na_2SO_4; and green for Na_3Cit) at different concentrations (solid line for 1 wt.-%, short dashed line for 2 wt.-%). Commercial cellulose (MC) appears in purple.

Crystalline salts in the cellulose solutions could have influenced the crystallinity of the synthesized cellulose aerogel monoliths. Besides, if not well washed, those residues would be visible in the XRD diffractograms. However, no significant differences were observed between the XRD profiles of the monoliths and, in **Figure 48,** only representative samples formed with NaCl are shown. The peaks from the aerogel samples were broader and less intense than those detected for MC, due to the dissolution of the crystalline cellulose which became amorphous. Some shifts in the peaks 2θ were detected in the monolithic samples compared to MC and were

Results and Discussion

explained by the conversion of cellulose I into cellulose II. Cellulose II planes were identifiable in the aerogels where the peak corresponding to the plane ($1\bar{1}0$) shifted to 12.3° while the most intensive peak at 21.8° was related to planes (110) and (020) (20° and 22° respectively). The signal of the plane (004) shifted to 35.1°. The amorphous cellulose region in the aerogels was found at 16° and was more preeminent than in MC, at 18°, due to the lower content in crystalline planes.[256, 283] **Equation 8** was applied to study the evolution of the crystallinity during the creation of the aerogels.
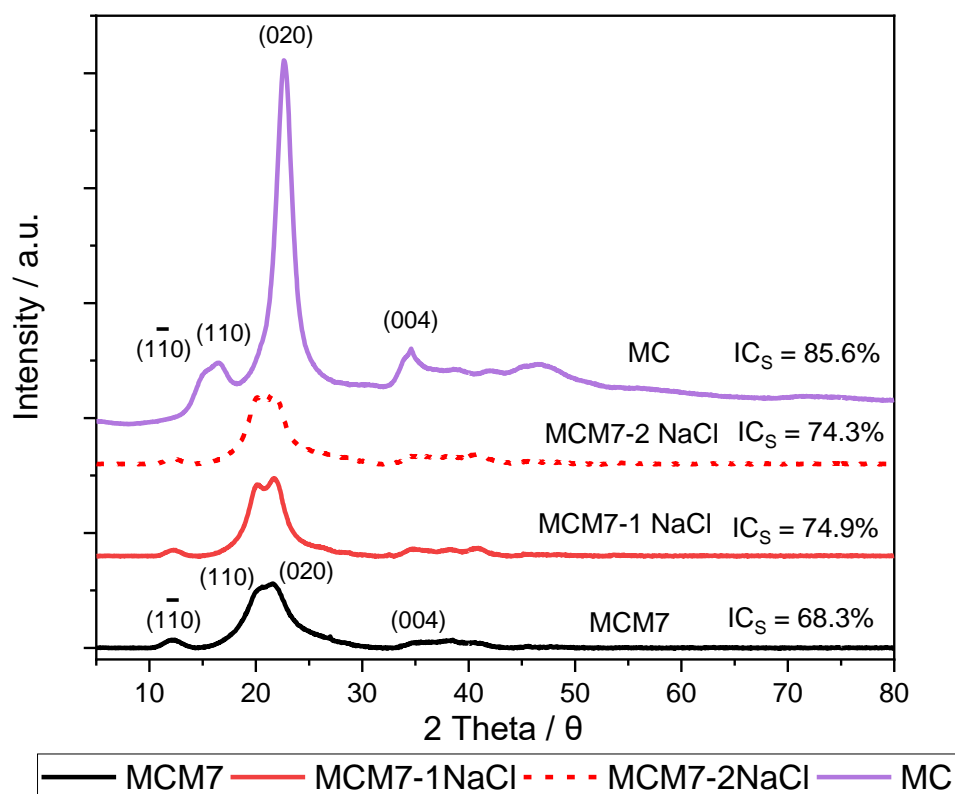
Figure 48 XRD diffractograms and respective crystallinity indexes (IC_S) of 7 wt.-% commercial cellulose aerogel monoliths from solutions without addition of salt (black for MCM7), and after addition of NaCl (red for NaCl) at different concentrations (solid line for 1 wt.-%, short dashed line for 2 wt.-%). Commercial cellulose (MC) appears in purple.

When cellulose was dissolved and converted into an aerogel, a significant decrease in crystallinity was registered, following the conformation change of the cellulose´s structure from cellulose I to II. This evolution in the XRD patterns was in the same range as in the literature.[109, 114, 188] It should be noted that **Equation 8** slightly overestimates the crystallinity values for more amorphous samples, which may lead to differences between values found in other references.[243, 245] Adding salts increased the crystallinity index compared to

the blank sample (from 68.3% to 74%-75%). The anion species added or the salt concentration did not influence that increase. Introducing salts led to a higher polarity in the media and favored the packing of cellulose fibers through hydrogen bonds during regeneration. These packing patterns followed the planes (110) and (020), which became better defined and contributed to higher crystallinity.[110, 111] This was observed by Parajuli et al.[113, 114]

The porous structure of these materials was significantly distinct between their surface and interior body. In **Figure 49**, the surface of MCM7 and of a representative aerogel monolith synthesized after the addition of salt (MCM7- 2NaCl) are shown. The exterior surfaces were compact, with a wide range of pore sizes. The surface of MCM7-2NaCl was more homogeneous and had smaller pores than MCM7. This trend was observed for all samples where salt was added, independently of their ions and concentration. The reasons for this difference could be found in the regeneration kinetics of the cellulose body.[107, 252] Monoliths needed multiple days to create a stable wet gel body. Under an acidic ethanol solution, the cellulose fibers at the surface quickly re-organized into a compact dense network of pores, whose densification continued as the gelation occurred in the interior of the monolith. As the addition of salts increased the gelation speed, the surface of the affected aerogels suffered more densification during gelation than the one from the blank aerogel, which needed more time to achieve a stable structure .[107] As a phase separation was formed between a cellulose-rich and cellulose-poor solution, the fibers in the interior had more time to reorganize into fibrillar networks with thinner pore walls, and more dispersed structures.[106]
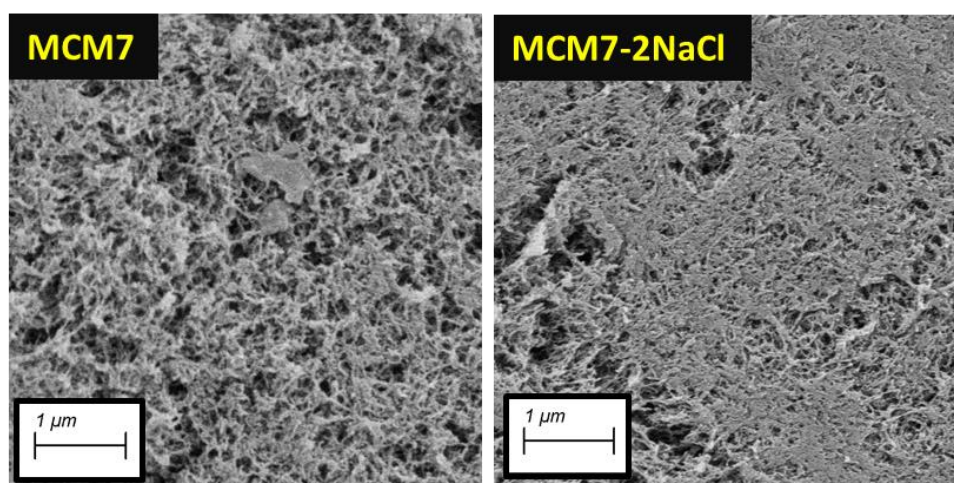
Figure 49 SEM picture of the exterior surface of 7 wt.-% commercial cellulose aerogel monoliths from solutions without addition of salt (MCM7), and after addition of 2 wt.-% sodium chloride (MCM7-2NaCl).

Results and Discussion

Indeed, using the samples where Na₃Cit was used as representative examples, the addition of salts at different concentrations led to changes in the porous structure of the aerogels. This is shown in **Figure 50**.
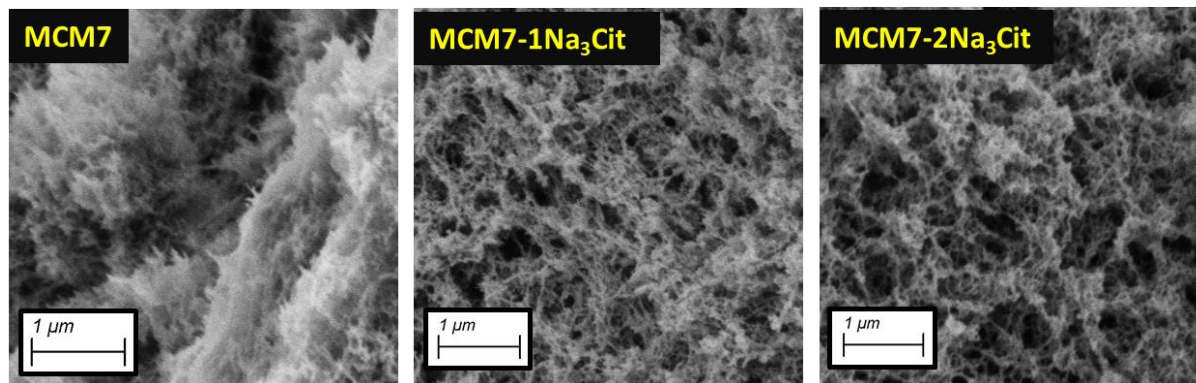
Figure 50 SEM pictures of the interior surface of 7 wt.-% commercial cellulose aerogel monoliths from solutions without addition of salt (MCM7), and after addition of 1 wt.-% and 2 wt.-% sodium citrate (MCM7-1Na₃Cit and MCM7- 2Na₃Cit, respectively).

In the blank sample, MCM7, a dense fibrillar network existed with some bigger pores. With increasing concentrations of Na₃Cit, bigger pores became more preeminent. This was observed for NaCl and Na₂SO₄ as well. These empty spaces were associated with salt-rich areas, whose salts were removed during the washing and solvent-exchange steps.[113] These new cavities increased with the size of the anion, as shown in **Figure 51**.
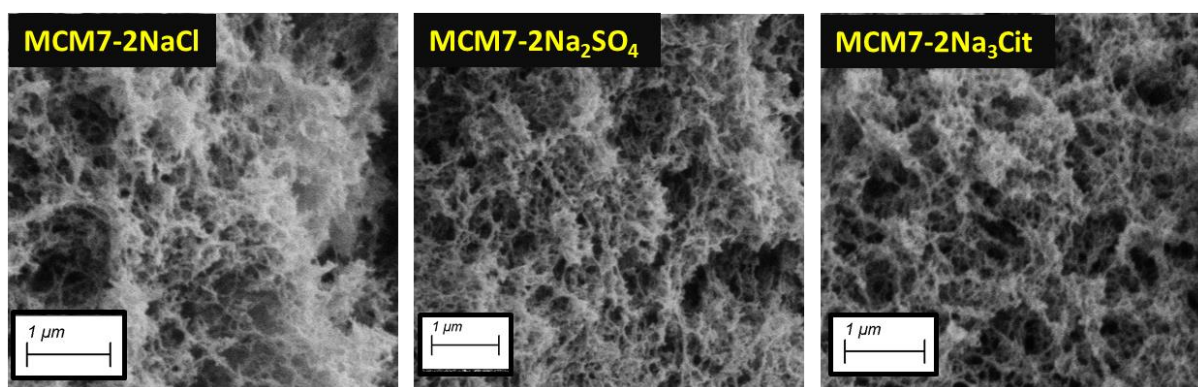
Figure 51 SEM pictures of the interior surface of 7 wt.-% commercial cellulose aerogel monoliths from solutions after addition of 2 wt.-% sodium chloride (MCM7-2NaCl), sodium sulfate (MCM7- 2Na₂SO₄) and sodium citrate (MCM7- 2Na₃Cit).

While some of the bigger cavities could be from inhomogeneities in the gel body, the porous structure became looser and less compact as the anion added increased its size: $Cit^{3-} > SO_4^{2-}$

>Cl$^-$. This was related to the influence of these salts on the gelation mechanism and the formation of the porous network, as observed in **Figure 43**. Additionally, Cl$^-$ left smaller pores in the aerogel´s network when removed than SO$_4{}^{2-}$ and Cit^{3-}. An increasing gelation speed in addition to the presence of removable anions, promoted a looser fibrillar structure, with thin pore walls, in conjugation with bigger cavities as observed in **Figure 51**. Without these salts, cellulose structures with denser packing had been observed in previous studies and other samples examined in this work.[107, 109, 179] For the case of Na$_3$Cit, the scaffold effect and the creation of bigger cavities counterbalanced its smoother gelation and densification of the aerogel structure.

Nonetheless, adding salts did not significantly affect the value of porosity of the aerogels compared to the blank sample, despite an apparent increase in the presence of larger cavities. This could indicate that any increase in the number of larger pores was not significant, not homogeneous, or that its effect was attenuated by the creation of smaller pores when the added anions were removed. In the case of 2 wt.-% Na$_3$Cit, the wider presence of these larger cavities and less compact network could explain a lower mechanical resistance towards shrinkage, resulting in a reduction in porosity and an increase in density compared to MCM7. The SEM pictures indicated that the addition of salts influenced the porous structure of the monoliths depending on their structure and application quantity. Their influence was further analyzed in the physisorption studies. The adsorption and desorption profile of N$_2$ on the porous structure of the monoliths are shown in **Figure 52**. Each sample had different adsorption capacities, but all could be classified as type IV isotherms, as described by IUPAC.[91] These curves are characterized by having a saturation plateau at 0.7-1 (P/P^0), which is formed due to pore condensation, and hysteresis. This behavior indicated a mesoporous nature for these aerogels with a wide range of pore sizes, in line with what was found in other studies.[113, 167]The existence of hysteresis under these adsorption conditions is related to delayed pore condensation in mesopores whose size exceeds 4.5 nm. The hysteresis shape provided further information on the network structure of the aerogels. The desorption behavior of nitrogen was influenced by the existence of pores whose access to the exterior was only through narrow necks of different sizes and distributions. The samples MCM7-2NaCl and MCM7-1Na$_2$SO$_4$ presented the highest adsorption capacities, while the remaining have similar profiles. While the blank sample and the monoliths associated with NaCl had an H2(b) hysteresis, the other aerogels had intermediate hysteresis between H1 and H2(b), with a low influence of the salt concentration.[274]
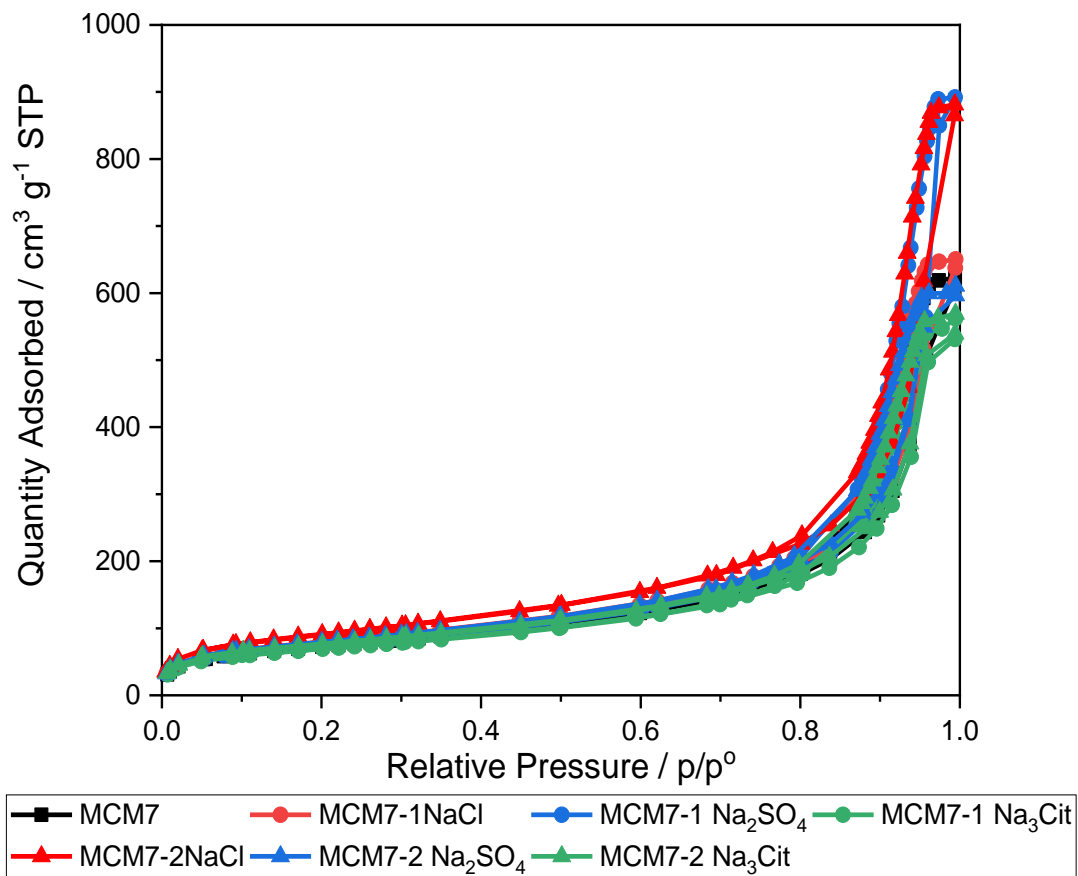
Figure 52 N₂ adsorption-desorption isotherms of 7 wt.-% commercial cellulose aerogel monoliths from solutions without (black for MCM7), and after addition of sodium salts (red for NaCl; blue for Na₃SO₄, and green for Na₃Cit) at different concentrations (circle for 1 wt.- %; triangle for 2 wt.-%).

Figure 53 shows that the specific surface area of MCM7 was 259 m^2 g^{-1}, while all the samples where salt was added ranged from 244 m^2 g^{-1} to 307 m^2 g^{-1}. Adding sodium chloride led to a slight increase in the specific surface area, from 259 m^2 g^{-1} to 284 m^2 g^{-1} (1 wt.- % NaCl) and 307 m^2 g^{-1} at 2 wt.-% NaCl. A smoother growing trend was observed for Na₂SO₄, where the surface area increased to 271 m^2 g^{-1} and 286 m^2 g^{-1}, at 1 wt.-% and 2 wt.-%, respectively. This was consistent with work performed by Parajuli et al., where the removal of smaller ions during the neutralization of the gels created smaller pores and increased the specific surface area and total pore volume of the aerogels.[114]
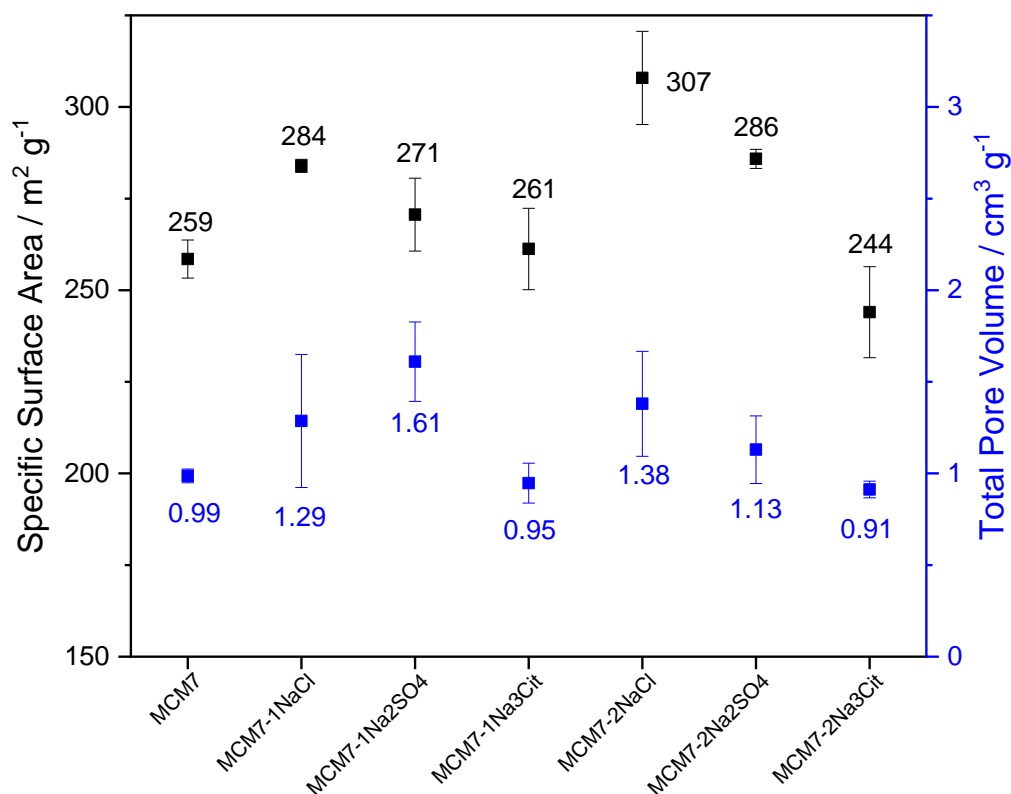
Figure 53 Specific surface area and total pore volume of 7 wt.-% commercial cellulose aerogel monoliths from solutions without (MCM7), and after addition of sodium salts (NaCl, Na_2SO_4, and Na_3Cit) at different concentrations (1 wt.-% and 2 wt.-%).

For Na_3Cit, the surface area remained constant at 261 m^2 g^{-1} at 1 wt.-% and decreased to 244 m^2 g^{-1} at 2 wt.-% due to its higher density and presence of small cavities, which decreased the number of pores available and consequent surface area. The total pore volume followed similar behaviors but within a smaller range of values (from 0.91 cm^3 g^{-1} to 1.38 cm^3 g^{-1}) and with higher uncertainty. This was in line with what had been observed in the previous pages and the literature.[113, 114, 165, 166]

Figure 54 shows the pore size distribution of the samples. Most of the pores detected were mesopores (from 2 nm to 50 nm) with some presence of macropores. The profiles were similar among the aerogels, but some important differences were observed. When 1 wt.-% Na_2SO_4 or 2 wt.-% NaCl was added, a plateau was reached at the top of their distribution curves instead of a sharp point. Those samples had a higher proportion of larger mesopores and a broader distribution, which led to the higher adsorption registered in their isotherms. MCM7-2NaCl had the highest specific surface area, which could explain the higher concentration of pores. For MCM7-2Na2SO4, the pore size distribution is similar to that of MCM7. Minor changes in the

concentration of these salts in the cellulose solution have a relevant influence on the pore size distribution of their resultant aerogels, but a clear understanding of their mechanisms is still lacking in the literature.[113, 114] Regarding the Na$_3$Cit samples, their profiles were the sharpest ones with no relevance to the concentration added.
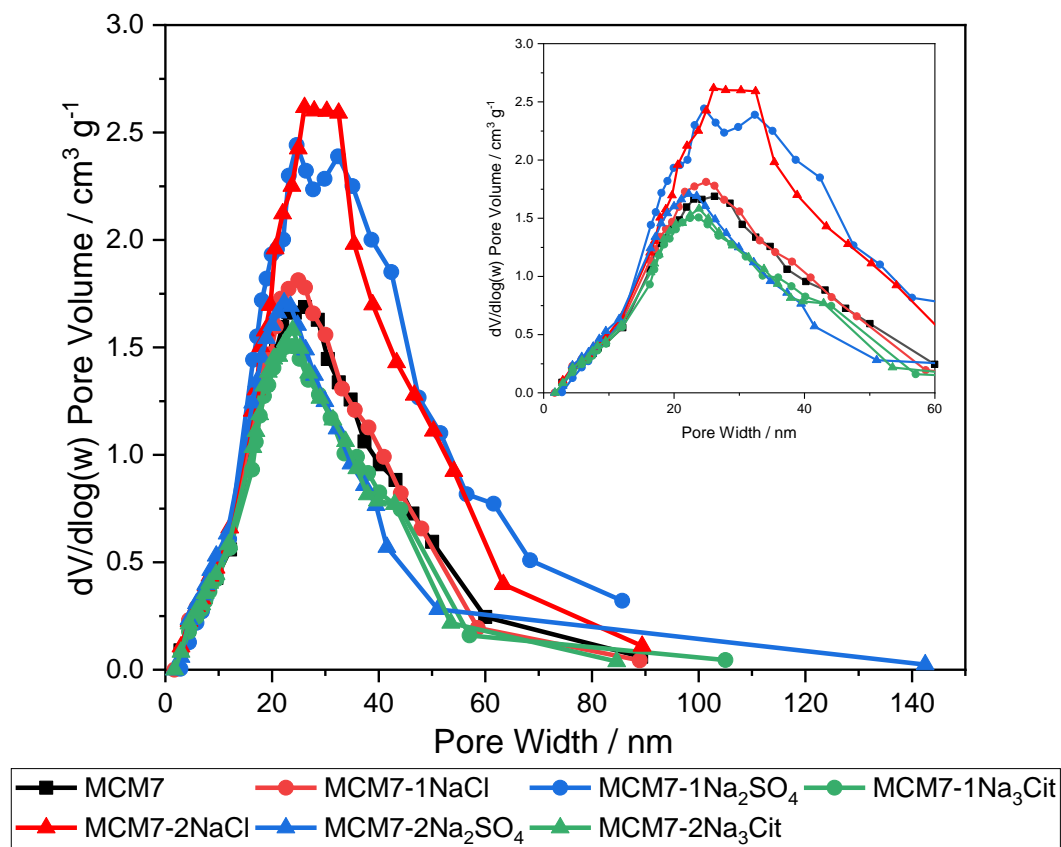
Figure 54 Pore size distribution of 7 wt.-% commercial cellulose aerogel monoliths from solutions without (black for MCM7), and after addition of sodium salts (red for NaCl; blue for Na$_2$SO$_4$, and green for Na$_3$Cit) at different concentrations (circle for 1 wt.- %; triangle for 2 wt.- %).

The pore size distribution affected the average pore size of the samples, as shown in **Table 8**. In MCM7, the average pore size was 14.67 nm and increased to 17 nm when NaCl was added, with no influence from the salt concentration. It indicated that the creation of a plateau at its pore size distribution at 2 wt.-% NaCl was compensated by the creation of smaller pores when NaCl was removed during the processing of the gels. For MCM7-1Na$_2$SO$_4$, the pore size increased to 21.29 nm and decreased for MCM7-2Na$_2$SO$_4$ to 14.76 nm. For Na$_3$Cit, the average pore size consistently decreased to 13.58 nm and 11.88 nm, from 1 wt.-% to 2 wt.-%. Most of this reduction was caused by a decrease in the presence of macropores, as shown in **Figure 54**. It could be that the bigger mesopores were absorbed by bigger cavities not detected by the

physisorption technique (limited to 100 nm).[175, 275, 276] It would mean that, in conjugation with the creation of pores from the removal of the citrate anion, the relative weight of smaller pores would increase, leading to a smaller average pore size. Overall, sodium chloride and sulfate addition to the cellulose solution increased the specific surface area of the monoliths. The trisodium citrate addition resulted in a sharper pore size distribution and a smaller average pore size.

In **Figure 55**, the thermogravimetric profile of MCM7 and the monoliths produced from cellulose solutions with salts can be found. As MC was composed of highly crystalline cellulose I, while the aerogel monoliths contained more amorphous cellulose II, it was expected that degradation would occur earlier for the latter.
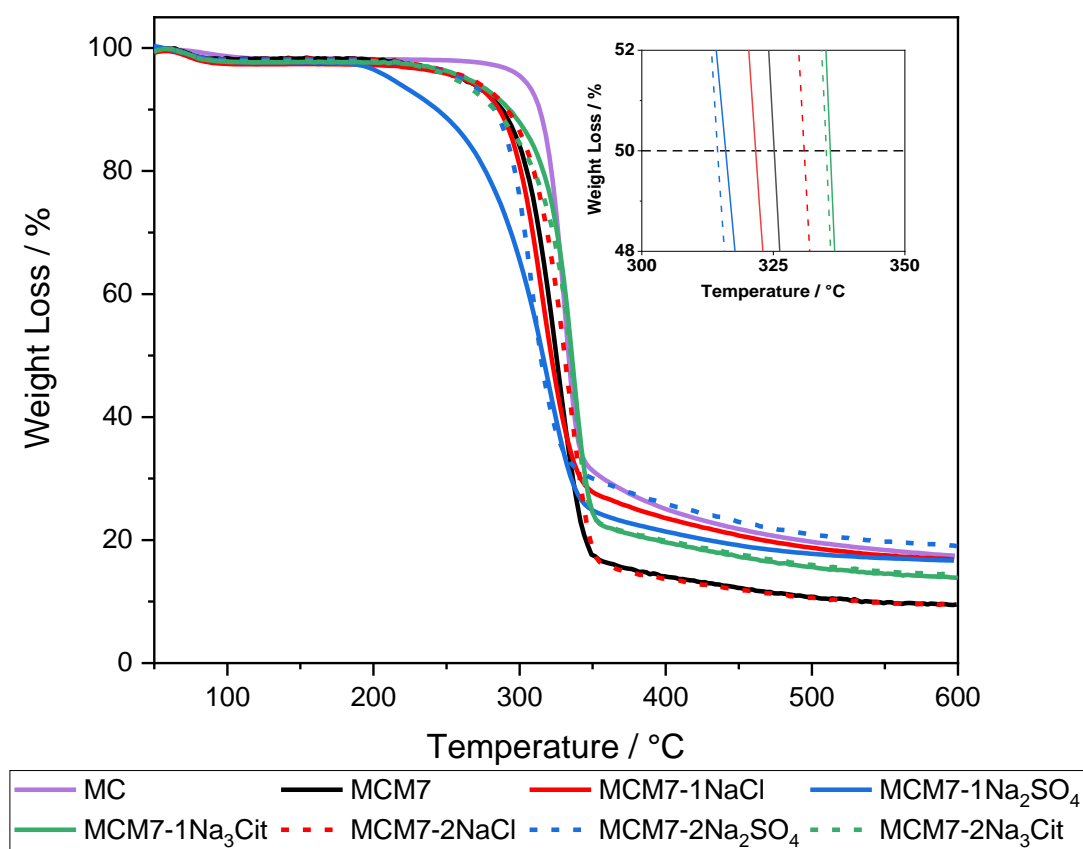
Figure 55 Thermal gravimetric profiles of 7 wt.-% cellulose aerogel monoliths from solutions without (black for MCM7) and with addition of salts (red for NaCl, blue for Na_2SO_4, and green for Na_3Cit) at different concentrations (solid line for 1 wt.-%, short dashed line for 2 wt.-%). Commercial cellulose (MC) appears in purple.

A higher content of the crystalline phase is associated with a higher degree of hydrogen bonds between cellulose chains. Therefore, more packed structures need more energy to be

degraded.[251, 277] The profiles were very similar, with no significant influence from the addition of salts, and contained the characteristic profile of cellulose samples.[242, 251] All samples reached 50% degradation between 300°C and 340 °C, with some differences between the salts added depending on their influence on the porous structures of the aerogels. For all samples, except for MCM7-1Na$_2$SO$_4$, significant mass loss starts at 250 °C, typical for cellulose II. The mass decline observed from 205°C to 250 °C for MCM7-1Na$_2$SO$_4$ could correspond to the crystal-phase transition from T-Na$_2$SO$_4$ to γ- Na$_2$SO$_4$, indicating an inhomogeneous distribution of the salt and its residual presence in the sample.[278]. Parajuli et al. verified a slight increase in the thermal stability of the samples when chloride-based salts with different cations were added (Na$^+$, K$^+$, Ca^{2+}, Mg^{2+}, Li$^+$). This indicated that the cations and anions interact differently with the cellulose fibers[114-116].
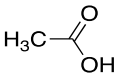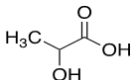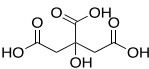
This study on the influence of adding sodium salts on cellulose solutions and their aerogels indicated that those anions influence the gelation speed of a cellulose solution while slightly improving the aerogel's properties. NaCl and Na$_2$SO$_4$ addition up to 2 wt.-% led to an increase in the gelation speed (down to 0 s) while preserving the density and increasing the specific surface area up to 300 m^2 g^{-1}. On the opposite side, trisodium citrate slowed the solution gelation, and reduced the surface area of the resultant cellulose aerogels while sharpening their pore size distribution and reducing the relevance of macropores. The reasons behind these trends lay in how the anions, with different charges and dimensions, competed with cellulose for the water in the dissolution media. Cl$^-$ and SO$_4^{2-}$, with stronger hydration shells, more easily decreased the quality of the dissolution media and promoted the regeneration of cellulose than citrate whose organic character made it more prone to interact with cellulose.[263, 264, 268] The removal of the anions during the washing of the monoliths created new pores whose sizes were proportional to the dimensions of the anions. The salts had limited influence on the chemical composition, crystallinity, and thermal behavior of the cellulose aerogel monoliths. While the fundamental mechanisms of the interaction of these salts with cellulose and with the water:urea:NaOH components of the dissolution medium still have to be further studied, this work provides recipes to quickly increase the gelation speed of solutions while preserving or even improving the properties of the resultant aerogels. This is a powerful tool for upscaling in industrial environments and modulating the internal structure of the aerogels.

4.3.2 Acidic Conditions of the Regeneration Bath

In **Table 9**, it is shown some of the most important properties in 2 M aqueous solutions of the different acids tested.

Table 9 Structure and general properties of 2 M acidic aqueous solutions.[250] (CC BY-NC 4.0, https://creativecommons.org/licenses/by-nc/4.0/)

Name of Acids (abbreviation)	Structure	pKa[279]	pH	Density / g cm^{-3}
Hydrochloric acid (HCl)	H-Cl	-7	-0.3	1.03
Acetic acid (HAc)	H$_3$C—C(=O)OH	4.76	2.23	1.01
L(+)-Lactic acid (HLac)	H$_3$C—CH(OH)—C(=O)OH	3.86	1.78	1.04
Citric acid (HCit)	HO$_2$C—CH$_2$—C(OH)(CO$_2$H)—CH$_2$—CO$_2$H	3.09; 4.75; 6.41	1.39	1.15

The values for the density and pH were similar across the different bathes. The pH of the organic acids was higher than that of HCl due to their lower dissociation rates. The densities were close to 1 g cm^{-3}, with citric acid being the densest (1.15 g cm^{-3}). The chemical structure of the molecules ranged from simple H-Cl bonds to organic structures with numerous functional groups such as OH and COOH. These factors influenced the final structure of the aerogel beads. The aerogel beads, shown in **Figure 56**, were all white and spherical, with a slight oval deformation in the HCit samples. Due to the slow speed of gelation observed in HCit baths, the soft-gelled beads deformed when they collided with each other during regeneration.
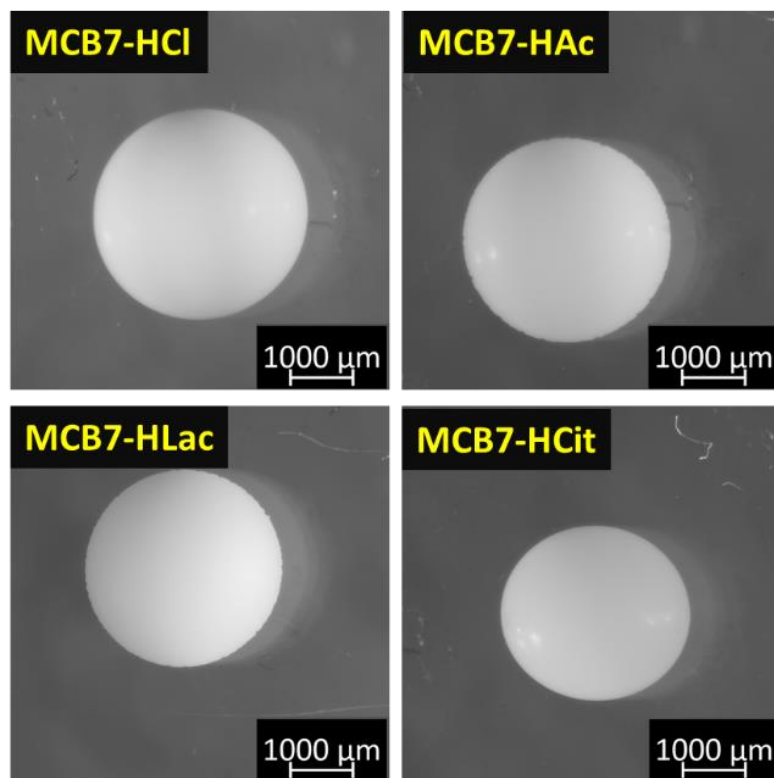
Figure 56 Optical microscope pictures of 7 wt.-% commercial cellulose aerogel beads (MCB7) gelled in different regeneration bathes (HCl, HAc, HLac, and HCit).[250] (CC BY-NC, https://creativecommons.org/licenses/by-nc/4.0/)

In **Table 10**, it is visible that the aerogel beads had diameters close to 3 mm (from 2.86 mm in MCB7-HCit to 3.28 mm in MCB7-HAc), with the size difference depending on the acid bath used. The differences observed could be explained by each acid´s different diffusion rates and functional groups. During the regeneration of cellulose beads, a two-phase separation occurred between a rich-cellulose phase formed from the precipitation and association of cellulose fibers through hydrogen bonds (the gel) and a poor-cellulose phase, where fibers were still in solution. The cellulose chains assembled differently depending on the diffusion mechanisms between the acidic molecules in the gelation bath, which penetrated the bead, and cellulose´s solvent components, which diffused into the bath. A higher rate of diffusion led to faster cellulose precipitation. A slower diffusion rate proportionated more time for the gelation of the droplets and the reorganization of the cellulose chains into smaller beads, with a stiffer structure. The coagulation speed was influenced by differences in pH and viscosity between the solutions and the miscibility of the cellulose with the regeneration bath.[46] Besides, the organic acids here discussed present carboxylic and OH functional groups, that are known for their high hydrogen-bond donor-acceptor properties. These can easily interact with the OH groups in cellulose, affecting its regeneration.[250]

109

4.3 Regeneration of Cellulose

Table 10 Properties of 7 wt.-% commercial cellulose aerogel beads (MCB7) gelled in different regeneration bathes (HCl, HAc, HLac, and HCit). Information on the specific surface area and total pore volume of the aerogels is presented later.[250] (CC BY-NC, https://creativecommons.org/licenses/by-nc/4.0/)

Sample	Average Bead Diameter / mm	Diameter Shrinkage / %	Envelope Density / g cm^{-3}	Porosity / %	Average Pore Size / nm
MCB7-HCl	3.25±0.07	15.05±1.94	0.18	88.19	23.46
MCB7-HAc	3.28±0.10	12.77±2.70	0.21	85.94	25.16
MCB7-HLac	3.15±0.07	13.65±2.01	0.21	86.24	24.89
MCB7-HCit	2.86±0.11	13.86±3.44	0.23	85.15	21.88

The beads produced immediately after gelation in HCl had the largest diameter due to their fast coagulation. The HCl bath presented the lowest pH, and the lowest density, and the small dimensions of the Cl$^-$ anion enabled it to promote a fast gelation. Other acids produced smaller beads, with citric acid inducing the lowest diameter. Its pH was similar to the ones observed for acetic or lactic acid but its higher viscosity and density hindered the diffusion of the citrate anions through the bead. Indeed, during the production of beads in the citric acid bath, it was noticed that the cellulose droplets remained for a few minutes on the surface of the bath and a visible polymer-phase separation was formed (see **Figure 57**).

Besides, the different acidity constants created citrate anions that were not fully dissociated. These bigger, organic conjugated bases could interact with the OH groups in the cellulose chains and between themselves through hydrogen bonds and other weak forces such as electrostatic and van der Walls. These further contribute to create smaller beads. The influence of the hydrogen-bond donor-acceptor groups in the other organic acids was not as pronounced as in HCit.[280-282]

The bead´s size decreased due to shrinkage across the other processing steps. All beads shrank, having a total shrinkage from 12.77% for MCB7-HAc to 15.05% for MCB7-HCl. At these small dimensions, the concentration gradient between the bead´s core and its surface was limited. This reduced the stress caused by molecular diffusion and induced a similar shrinkage across all samples.[47, 107, 109] However, shrinkage was directly proportional to the strength of the acid, assuming monovalent ion formation. HCl, with the lowest pKa and faster gelation,

created a porous structure more prone to shrinkage while the acetic acid-induced network was more stable and resistant.[250]
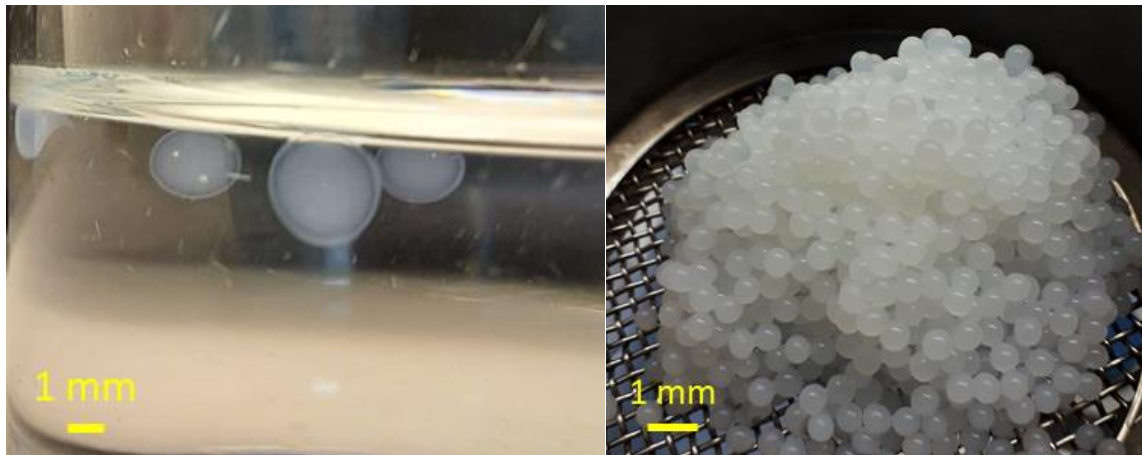
Figure 57 On the left, is a detail of the gelation of cellulose beads in a citric acid bath (MCB7- HCit). It is visible an outer shell of a cellulose-rich phase (transparent) and a poor-cellulose phase in the bead´s core (whitish). On the right, the same beads after 30 minutes in the acid bath to ensure complete gelation. The beads were white and opaque.

Regarding the skeleton density, as no difference was recorded between samples, a value of 1.523 g cm^{-3} was used for calculating porosity. This value was close to the one obtained from MC, of 1.524 g cm^{-3}, and found in the literature.[251, 283] The commercial cellulose was composed of cellulose I and, when dissolved, changed to the more stable cellulose II structure. This more amorphous, less packed cellulose polymorph composed a significant fraction of the aerogels, contributing to their lower skeleton density.[252, 284]

In comparison, the envelope density for these samples was much lower, from 0.18 g cm^{-3} in MCB7-HCl to 0.23 g cm^{-3} in MCB7-HCit. This indicated that the density of the aerogels was influenced by their high porosity, as more space was occupied by open-air than by the solid fraction of the network. The smaller the bead, the higher its envelope density due to a larger compaction of its cellulose fibers and the lower its porosity. The values of porosity for the samples, which ranged from 85.15% in MCB7- HCit to 88.19% in MCB7-HCl. Their difference was small, presenting porosities typical for cellulose aerogel produced from similar synthetic routes.[57, 162, 167] The fast counter-diffusion gelation rate in HCl provided the highest porosity. A faster cross-linking between cellulose chains decreased their agglomeration time, originating thinner cellulose walls, larger cavities, and higher porosity.[107, 109]

The FTIR spectra for all the cellulose aerogel beads were similar (see appendix in **Figure 112**), showing only signals from cellulose II as described in the previous chapters. This indicates that

impurities were removed during the washing steps. The diffractograms of MC and from a representative acid (MCB7-HAc), as the use of different acids did not affect the crystallinity of the beads, are shown in the appendix (see **Figure 118**). Some shifts in the peaks 2θ were detected in MCB7-HAc compared to MC and were explained by the conversion of cellulose I into cellulose II. When that cellulose was dissolved and converted into an aerogel, it registered a significant decrease in crystallinity (from 87.55% to 68.33%), which followed the conformation change of the cellulose´s structure from cellulose I to II. This evolution in the XRD patterns was in the same range as in the literature.[109, 114, 188]

In **Figure 58**, the exterior surface of the aerogel beads gelled in different acidic media can be observed in SEM pictures. The surface presented densely packed cellulose fibers, with bigger pores in MCB7-HCl compared with the beads from other bathes. In the latter, the microfibrils had coagulated into dense regions where most pores were below the macroporosity range. As previously discussed, this was related to different coagulation speeds. The surfaces were homogeneous with some regions with small fibers conglomerates or small cavities due to inhomogeneities in the cellulose distribution in the falling solution droplets. As there existed polymer-rich and polymer-poor regions in the droplet, different diffusion rates were present in the beads which could explain slightly different packaging on their surface.[107]
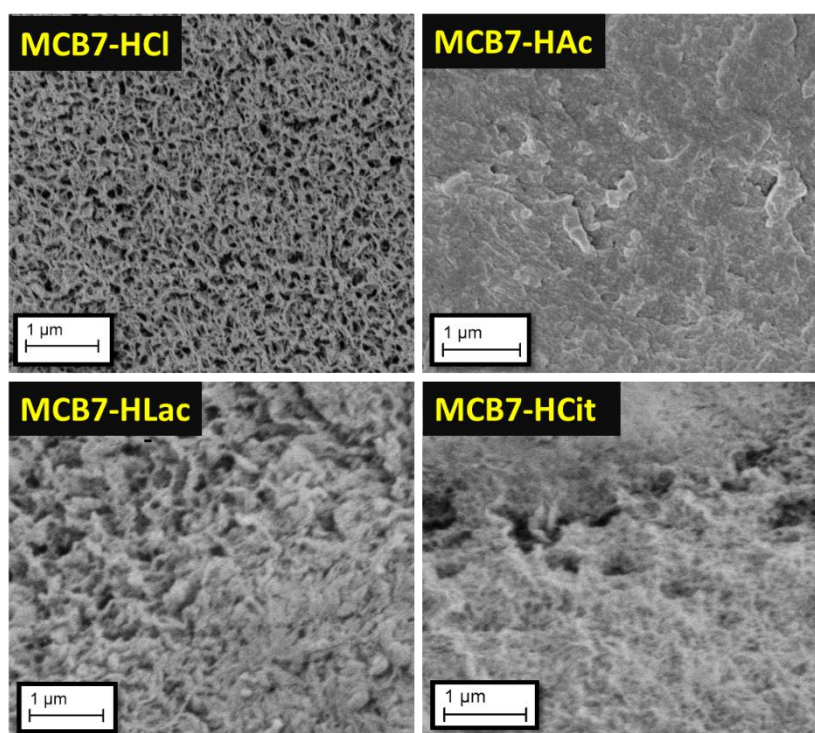
Figure 58 SEM images of the exterior surface of 7 wt.-% commercial cellulose aerogel beads (MCB7) gelled in different regeneration bathes (HCl, HAc, HLac, and HCit).

Results and Discussion

The same trends were identified in the interior of the beads. In **Figure 59**, the highly porous microfibrillar networks were found across all cellulose aerogel samples.[88, 285] The structures were less compacted, with pores and cavities from the macroscale to the nanoscale, while the random fibrillar network was more dispersed with thinner walls. For all aerogels, the structures in the interior of the bead were less dense than on its surface, but they were more compact in the samples formed in organic acids than in MCB7- HCl. This phenomenon occurred due to the faster gelation of the fibers on the surface of the bead. As the gelation of the bead´s core was slower, cellulose fibrils had more time to agglomerate and create fibrillar networks with smaller pores. In the case of organic acids, these interior structures achieved a higher degree of compaction and detailed porous network due to their lower gelation speed and higher interaction with the cellulose fibrils compared with HCl. Besides, the densification of the surface of the gels continued as gelation proceeded in the interior of the beads. [89]
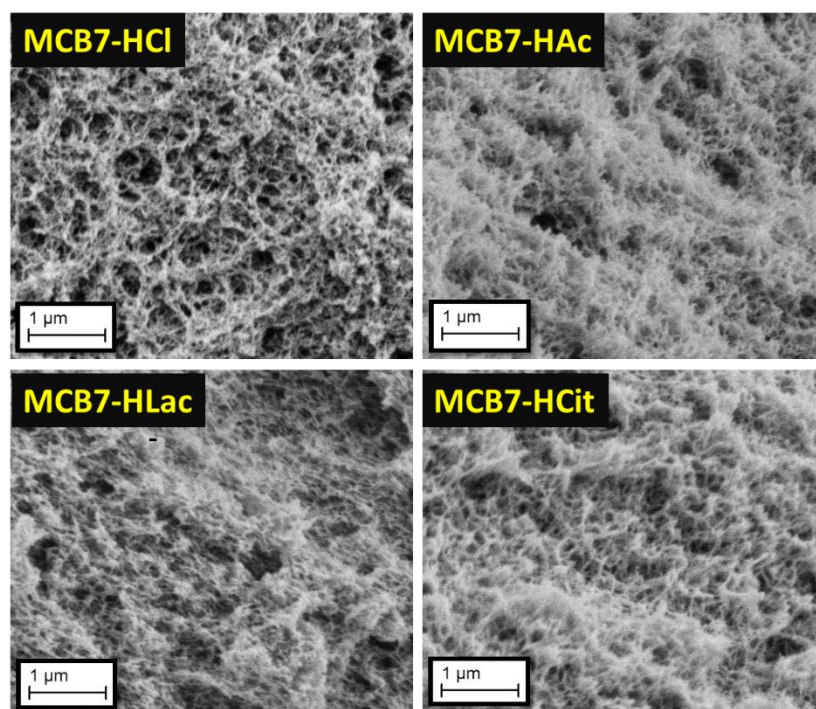
Figure 59 SEM images of the interior surface of 7wt.-% commercial cellulose aerogel beads (MCB7) gelled in different regeneration bathes (HCl, HAc, HLac, and HCit).

For the microstructural analyses, it has to be considered that the cellulose aerogels are soft and ductile materials. Therefore, the artifacts should also be carefully taken care of.[82] Thanks to developed expertise, the porous structure of the aerogels was preserved for study.

4.3 Regeneration of Cellulose

In the appendix (see **Figure 124**), the N_2 adsorption capacities of the aerogels can be observed. Each sample had different adsorption capacities but were all classified as type IVa isotherms, as described by IUPAC.[276] The observed hystereses in **Figure 124** were classified as H2(b), associated with pore-blocking for a wide distribution of pore neck widths.[275, 276] If the aerogels have a more uniform range of mesopores and a steeper, narrower, desorption, their isotherms might be closer to the H1 shape, as in MCB7-HCit, or a combination between that category and H2(b) hysteresis, as for the remaining samples produced in organic acids.[274, 286, 287] Aerogels produced in organic acids had a significantly higher adsorption capacity compared to those produced in HCl, and this was related to the porous matrix formed in each case. **Figure 60** shows the influence of these differences on the total pore volume and surface area of the samples.
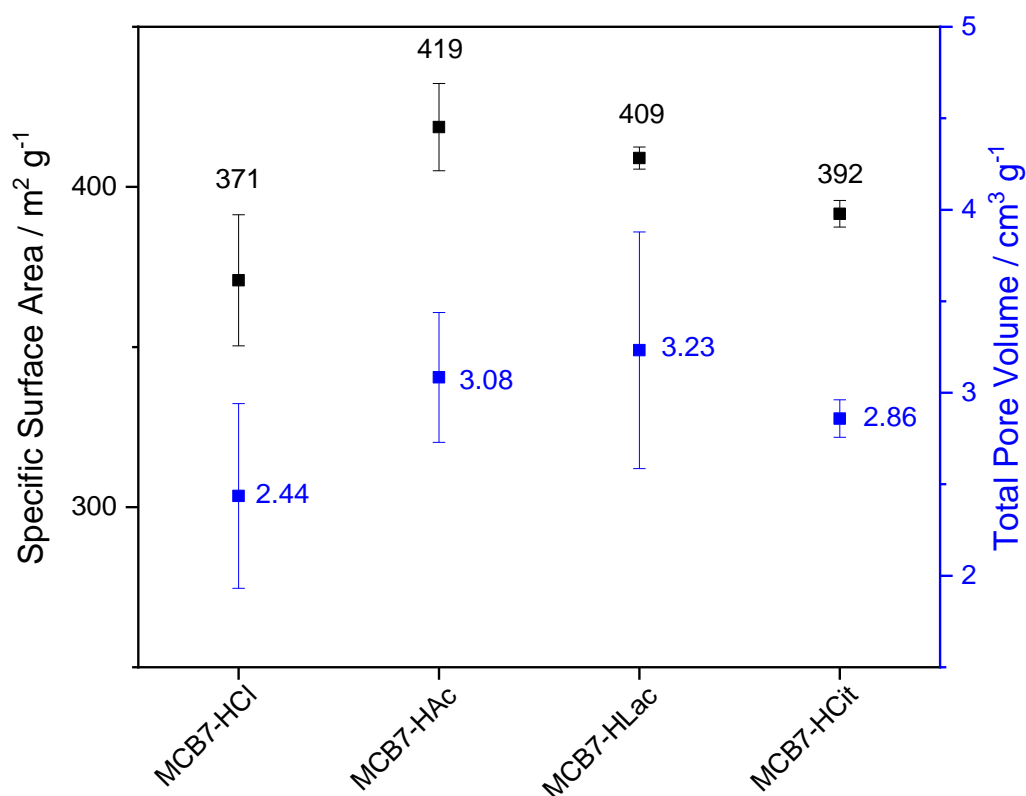
Figure 60 Specific surface area and total pore volume of 7 wt.-% commercial cellulose aerogel beads (MCB7) gelled in different regeneration bathes (HCl, HAc, HLac, and HCit).

While the beads formed in hydrochloric acid presented a BET of 371 m^2 g^{-1}, those values increased to 419 m^2 g^{-1}, 409 m^2 g^{-1}, and 392 m^2 g^{-1} in HAc, HLac, and HCit respectively. Similarly, the total pore volume increased from 2.44 cm^3 g^{-1} in HCl to 3.08 cm^3 g^{-1}, 3.23 m^3 g^{-1}, and 2.86 cm^3 g^{-1} for beads synthesized in HAc, HLac, and HCit, respectively. These surface

area values were in the range of the ones found for other cellulose aerogel beads and films in similar studies.[107, 110, 167] These numbers agreed with what was observed in the SEM pictures. Specific surface areas were higher than the ones observed in the previous chapter for the monoliths but a direct comparison was not possible. As it was used a different coagulation system (acetic acid ethanol bath after heating) for monoliths and the samples have different surface area/volume ratios, these originated different regeneration kinetics during gelation and properties among the synthesized cellulose aerogels.[126] Beads formed in HCl presented bigger pores in their interior, creating a smaller surface area and concomitant total pore volume. On the other hand, the filigree structure observed in the beads formed in the organic acid solutions contained smaller pores, which increased their available surface area and the total volume of the porous fraction. The more hydrogen-bond donor-acceptor groups in the organic acid, the higher the degree of nano-fibril densification. This could eliminate small pores and close the entrances of other pores. This led to smaller decreases in specific surface area and total pore volume for citric and lactic acid compared to HAc. These trends influenced the pore size distribution of the aerogels and their average pore size. The first parameter is expressed in **Figure 61**.

The vast majority of the pores were in the mesoporous regions (2 nm to 50 nm) for all samples, with a smaller fraction in the macroporous region (over 50 nm) and a low contribution from the microporous region (less than 2 nm). This expressed the mesoporous character of cellulose aerogels.[162, 191, 288] As the aerogels formed in organic acids had a higher total pore volume than MCB7-HCl, they had a more intense dV/dlog(W) pore volume across different pore sizes. The pore size distribution for all samples was centered between 20 nm and 40 nm, but depending on the acid used, this profile shifted for higher or lower values. From MCB7- HCl to the samples produced in other acids, the profiles sharpened in the mesoporous area and a constant decrease in the proportion of volume occupied by macropores occurred. MCB7-HCit presented the sharpest profile, with a shift for smaller pores and the lowest presence of macropores. This is in line with the steeper desorption observed in the isotherms of the aerogels synthesized in organic media, in **Figure 124**. These different profiles slightly influenced the average pore size. Gelled aerogels in HCl had an average pore size of 23.46 nm, while in HAc and HLac they had average pore sizes of 25.16 nm and 24.89 nm, respectively. The decrease in the number of macropores in MCB7-HAc and MCB7-HLac was not enough to compensate for the shift of the peak of the curves to bigger pores. HCit induced the lowest pore size, at 21.88 nm.
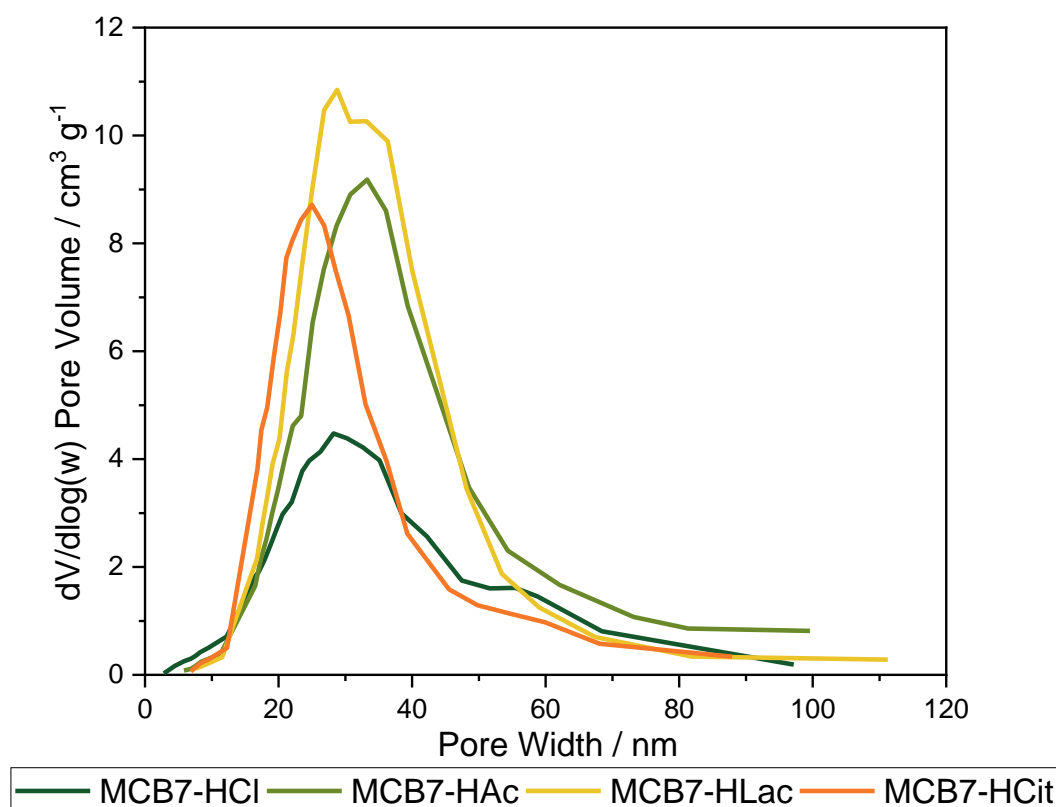
Figure 61 Pore size distribution of 7 wt.-% commercial cellulose aerogel beads (MCB7) gelled in different regeneration bathes (dark green for HCl; light green for HAc; golden for HLac, and orange for HCit).[250] (CC BY-NC, https://creativecommons.org/licenses/by-nc/4.0/)

These results indicated that the porous network and morphology of the aerogels can be tailored depending on the acid type in the regeneration bath and its diffusion speed into the cellulose solution. If the final product should have a higher content of macropores for the desirable application, it is more appropriate to use a strong acid such as HCl or H_2SO_4 which promotes a fast gelation and the creation of a less dense porous structure with bigger pores. The choice of an organic acid leads to a longer time for the regeneration of the cellulose fibrils, giving them time to aggregate and create a denser structure, with a higher content on meso and micropores. The thermal profile of the samples is shown in the appendix (see **Figure 120**).

All the samples presented the three main areas of weight loss associated with cellulose, as previously described. A first, between 40 °C and 100 °C, was recorded due to evaporation of water. Afterward, the profiles remained stable until reaching 240 °C for the cellulose beads and 250 °C for MC. There started a very pronounced mass reduction from 55.60% to 69.74%, where thermal degradation of the cellulose fibers occurred.[242, 251, 289] At this point, the higher

CI$_S$ of MC enabled it to have a higher thermal stability. The aerogel samples achieved 50% weight loss at 325 °C while MC reached at 335 °C.

After those points, the degradation rate was reduced, with the creation of char and the release of H_2O, CO, and CO_2.[277] MC presented the smallest amount of residue (17.44%) while aerogel´s residue ranged from 21.02% when regenerated in HCl to 26.55% in HCit. This was explained by the different envelope densities between samples. The more compact the sample, the stronger the interactions between the cellulose fibrils and correspondent higher content in biochar and smaller in volatiles. MC had a higher IC_S but its non-gel structure could have influenced the low final residue content. The choice of a different organic acid as a regeneration bath did not significantly influence the thermal profile of the aerogels.

In summary, different organic acid solutions were prepared as regeneration bathes for aerogel bead synthesis. The size of the organic conjugate base and their functional groups influenced the diffusion rate between the dissolution and coagulation systems. Weaker acids with bigger organic conjugated bases imposed a higher density on their solutions, interacted more with the cellulose fibers through hydrogen bonds and electrostatic interaction, and decreased their rate of diffusion into the interior of the bead. Organic acids produced denser, less porous aerogel beads but with a network containing smaller pores than HCl. This led to higher specific surface area and total pore volume in the former. Among the organic acids, HCit promoted the sharpest profile of pore distribution with smaller mesoporous in comparison with the other organic alternatives. However, its higher density lead to the deformation of the shape of the beads, which hinders its use at a technical scale. As a consequence, acetic and lactic acid were chosen as regeneration baths in the synthesis of aerogels. No significant influences were recorded regarding thermal stability, chemical composition, and crystalline structure among the studied samples. It was concluded that, depending on the final application of the aerogels and the desired range of pore sizes, different acids can be used to tailor the aerogel´s structural and morphological properties. This new tailoring tool diversifies the industrial applications of these materials while providing a safer and more environmentally friendly alternative to the more hazardous inorganic acid alternatives.

4.4 Manufacturing of Cellulose Aerogel Beads

In this chapter, it is discussed the synthesis of cellulose aerogel beads at laboratory and technical scales. In **Chapter 4.4.1**, aerogel beads were synthesized using extracted cellulose from hemp and flax bast waste fibers. Their properties were studied and compared to the properties of commercial cellulose-based aerogels. In **Chapter 4.4.2**, selected recipes for the synthesis of

commercial and hemp-extracted cellulose aerogels were scaled up using the JetCutter®. Their properties were compared to their lab-scale batches. Besides, it was studied how the influence of the cellulose concentration, the coagulation bath, and the addition of salts to cellulose solutions infuenced the thermal conductivity of the synthesized aerogels. These experiments were performed at a technical scale, using the JetCutter®.

4.4.1 Laboratory Scale

Depending on the DP of each cellulose source, different cellulose concentrations were used for the preparation of cellulose solutions and the synthesis of aerogels. **Figure 62** shows the aerogel beads, which were white and spherical while differing in size and surface shape.
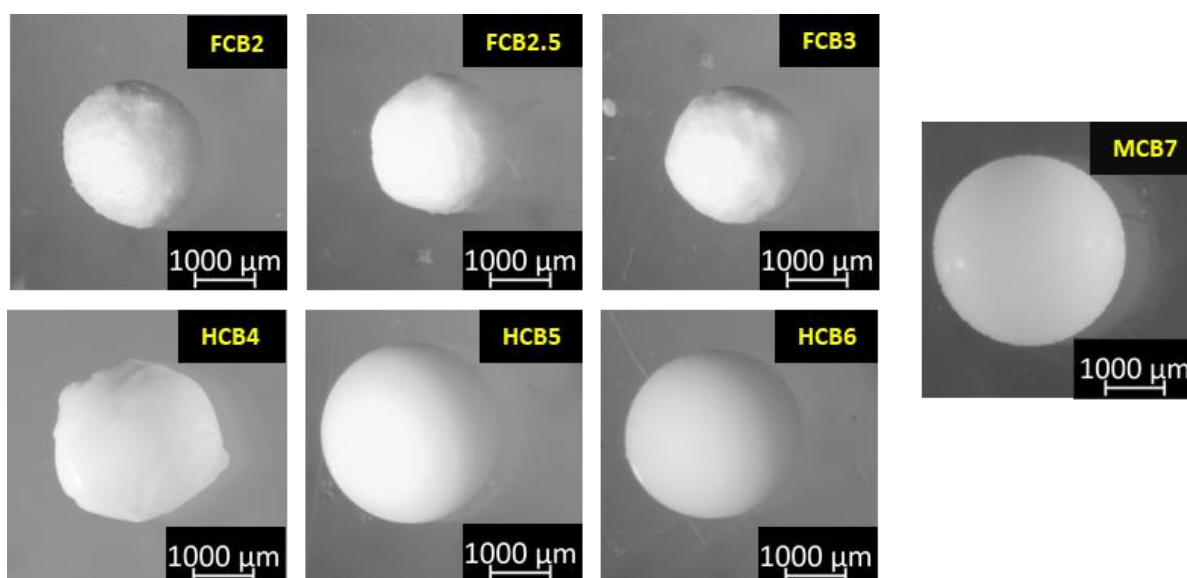
Figure 62 Optical microscope pictures of cellulose aerogel beads produced from flax-extracted (FCB), hemp-extracted (HCB), and commercial cellulose (MCB) at different cellulose concentrations (from 2 wt.-% to 7 wt.-%).

For the FCB samples, increasing the cellulose concentration resulted in more spherical beads and smoother surfaces. The diameter of the beads remained constant between 2.2 mm and 2.27 mm. The same trend was observed for the hemp samples but there was a steadier increase in the average diameter (from 1.80 mm to 3.08 mm). HCB6 had a similar shape and size compared to MCB7. These differences between HCB and FCB samples were due to the different DP of their celluloses and how it influenced the droplet stability. When the cellulose concentration was not high enough, the falling droplet did not sustain a spherical shape against the surface tension of the gelation bath and created a deformed gel.[181, 182]

Results and Discussion

Increasing the cellulose concentration helped the droplets sustain the shock when entering the regeneration bath, promoting faster gelation of the bead and preserving its sphericity.[176, 183] Higher cellulose concentrations also led to less shrinkage in the neutralization, solvent exchange, and drying of the gels, which explained the increasing sizes of the hemp beads with increasing concentrations. For the synthesis of cellulose solutions with similar viscoelastic properties, a lower concentration of FC was used, as it had a higher DP than HC. This turned the beads produced from FC more prone to shrinkage, with smaller dimensions and more homogeneous diameters across different concentrations compared to hemp samples.[88]

The skeleton density of the aerogel beads had minor differences between different celluloses, being constant across all the concentrations. FCB samples had a skeleton density of 1.51 g cm^{-3} while HCB and MCB samples had 1.52 g cm^{-3}. Any increase in the amorphous fraction of cellulose in the aerogels due to cellulose regeneration led to slight modifications of the skeleton density in compared with the pre-dissolved cellulose.[284] In **Table 11**, the properties of the aerogel synthesized from different cellulose sources are shown.

Table 11 The properties of cellulose aerogel beads produced flax-extracted (FCB), hemp-extracted (HCB), and commercial cellulose (MCB) at different cellulose concentrations from 2 to 7 wt.-%). Information on the specific surface area and total pore volume of the aerogels is presented later.

Samples	Average Bead Diameter / mm	Envelope Density / g cm^{-3}	Porosity / %	Average Pore Size / nm
FCB2	2.35±0.11	0.12	92.05	16.83
FCB2.5	2.23±0.14	0.15	90.08	17.00
FCB3	2.37±0.08	0.20	86.86	16.75
HCB4	1.80±0.20	0.15	90.19	24.20
HCB5	2.86±0.16	0.21	86.19	24.78
HCB6	3.08±0.23	0.18	87.87	24.22
MCB7	3.28±0.10	0.21	85.94	25.16

FCB samples had an envelope density in the range of 0.12 g cm^{-3} to 0.20 g cm^{-3}, with a significant increase in density from 2 wt.-% to 3 wt.-%. As the fibers presented a higher DP,

smaller increases in cellulose concentration influenced the envelope density of the samples. HCB samples registered a short variation between different concentrations, from 0.15 g cm^{-3} to 0.21 g cm^{-3}, reaching HCB5 with the same density as MCB7. The higher density of HCB5 compared to HCB6 could be related to a higher shrinkage and densification of HCB5 beads. The flax cellulose-based samples had a higher porosity (from 86.86% to 92.05%) than the HCB and MCB samples due to the lower concentration of cellulose used. Nonetheless, HCB samples had high porosities between 86.19% and 90.19%. The higher the cellulose concentration, the lower the porosity as more space was occupied by the increase of the cellulose solid backbone in the aerogel. These values were comparable with the 85.94% from MCB7 and with results obtained in the literature.[165, 167]

The FTIR spectra profiles of HCB and FCB were the same as MCB7, indicating that the aerogels only contained cellulose with a high degree of purity. As the spectra were the same for samples from the same source, only representative spectra from HCB and FCB aerogels are shown in the appendix (see **Figure 113**). The spectra showed that only cellulose was present in the beads and no signs of hemicellulose or lignin. Some differences were noted between the celluloses and respective aerogels, as described in previous chapters.[271] The signal at 1600 cm^{-1} from hemp cellulose, which corresponds to the presence of water in the cellulose, was shifted to 1640 cm^{-1} in the beads as the former corresponded to the presence of water entrapped in the cellulose matrix while the latter was due to its adsorption on the cellulose chains.[253]

The changes in the crystalline structure of the cellulose when converted into an aerogel are shown in the appendix (see **Figure 119**). As previously observed, all aerogel signals had a lower intensity than the original celluloses and corresponded to cellulose II.[258, 289] When cellulose was converted into an aerogel, it resulted in a decrease in crystallinity by 15% (from 85% to 70%) across all samples.

Figure 63 shows the exterior (E) and interior (I) surfaces of HCB samples and MCB7. HCB4- E had well-visible pores, and thin pore walls, and HCB5-E and HCB6-E had smaller pores and thicker cellulose fibrils due to an increased cellulose concentration. HCB5-E had a more compact surface than HCB6-E, despite its lower content in HC. This might have occurred due to differences in the diffusivity of the regeneration bath between the two samples. The range of DP of the hemp cellulose might be broad enough to induce slightly different gelation behaviors depending on the concentration of cellulose used.[89] The packing was still inferior to MCB7- E, which used a higher cellulose concentration.

Results and Discussion

For the interior of the beads, an increase in the concentration of HC led to fewer cavities, smaller pores, and a denser 3D network of fibers. The porous structure observed in HB6-I was similar to the one found in MCB7-I. The fibers were so packed due to the attractive interaction between the cellulose fibers that it was not possible to directly measure their dimensions.
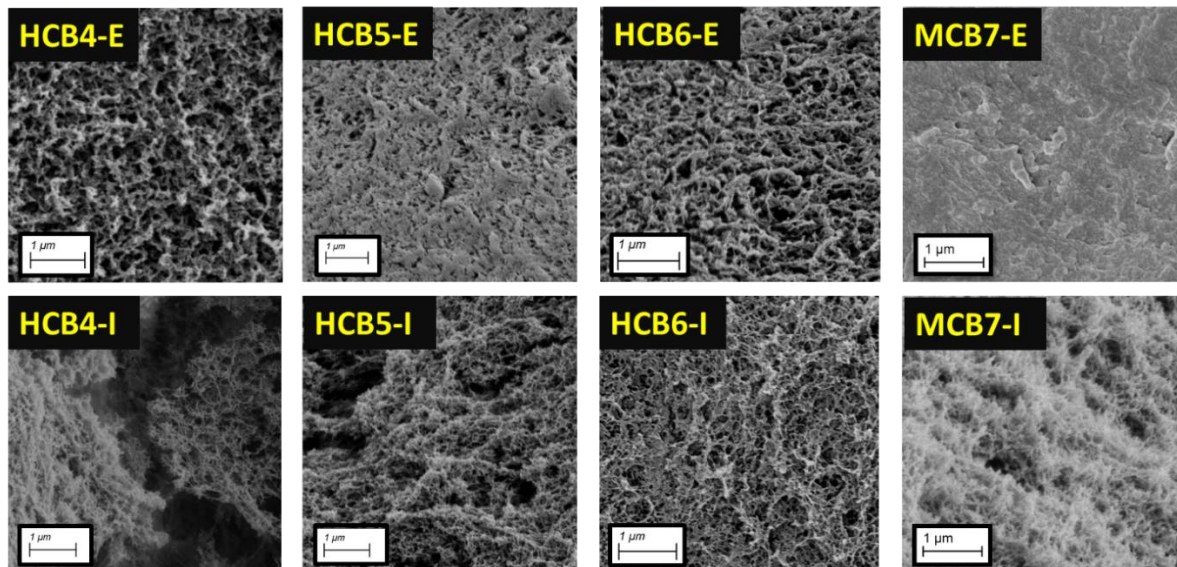
Figure 63 SEM images of the exterior (E) and interior (I) surfaces of hemp-extracted cellulose aerogel beads (HCB) at different cellulose concentrations (from 4 wt.-% to 6 wt.-%) and of commercial cellulose aerogel at 7 wt.-% (MCB7).

A similar tendency was observed for the FCB aerogels but with some differences due to the different molecular weights of their cellulose, as shown in **Figure 64**. The fibers present in the network were longer and more intertwined than in the HCB samples. An increase in the cellulose concentration led to a higher uniformity of the surface of the beads, with a reduction of visible pores and cavities. This behavior has already been observed by other researchers.[285, 290] Despite its low concentration, the cellulose network in the interior of the beads was denser, with big macropores and thick walls comprised of long fibers. The interior structure of FCB3- I was similar to the one obtained in MCB7-I, which was due to the higher DP of flax cellulose than the one of MC.
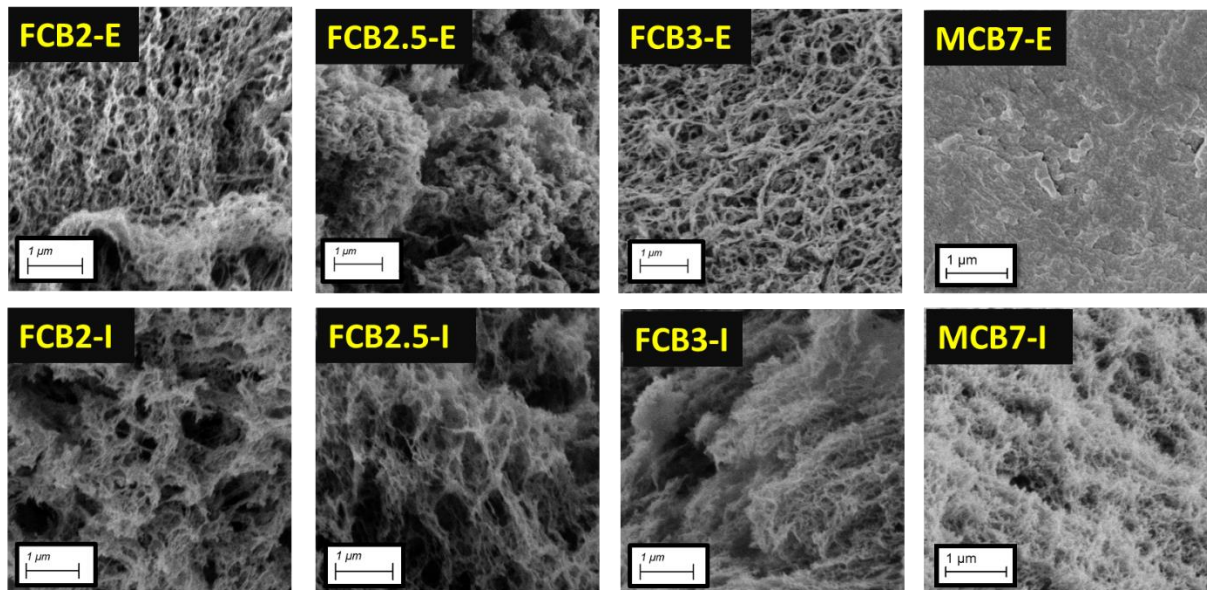
Figure 64 SEM images of the exterior (E) and interior (I) surfaces of flax-extracted cellulose aerogel beads (FCB) at different cellulose concentrations (from 2 wt.-% to 3 wt.-%) and of commercial cellulose aerogel at 7 wt.-% (MCB7).

The difference between the fiber organization on the surface and the interior of the beads was related to the cellulose coagulation mechanism. The fast coagulation of cellulose at the surface of the solution droplet when entering the acidic bath gave little time for the fibers to assemble. Depending on the cellulose concentration, it gave origin to different structures. For beads with low cellulose concentration, larger pores and thinner pore walls were created while, for higher concentrations, the surfaces were more homogeneous, compacted, and with smaller pores. The diffusion rate of the coagulation bath to the interior of the bead enabled a slow gelation, which provided time for the reorganization of the cellulose fibers. In all sample's interiors, this led to dispersed cellulose networks with smaller and more numerous pores. The higher the cellulose concentration, the denser the porous network.[89, 107]

Each sample had different adsorption capacities. Their isotherms were classified as type IV with hystereses with shapes between H1 and H2(b), as described by IUPAC, and with a mesoporous structure.[276] The isotherms are shown in the appendix (see **Figure 125**). The results indicated that the adsorption behavior of the samples was independent of the cellulose concentration. FCB samples presented a saturation point close to 1000 cm^3 g^{-1} while HCB and MCB7 aerogels had similar values from 1750 cm^3 g^{-1} to 2000 cm^3 g^{-1}. This confirmed that the aerogel samples from hemp-extracted and commercial celluloses had similar properties.

Results and Discussion

Stepper desorption was observed for HCB and MCB7 samples, which indicated a sharper, more homogeneous pore distribution compared to FCB aerogels, as observed in the SEM pictures. **Figure 65** presents the active specific surface area and the total pore volume of the synthesized aerogels.
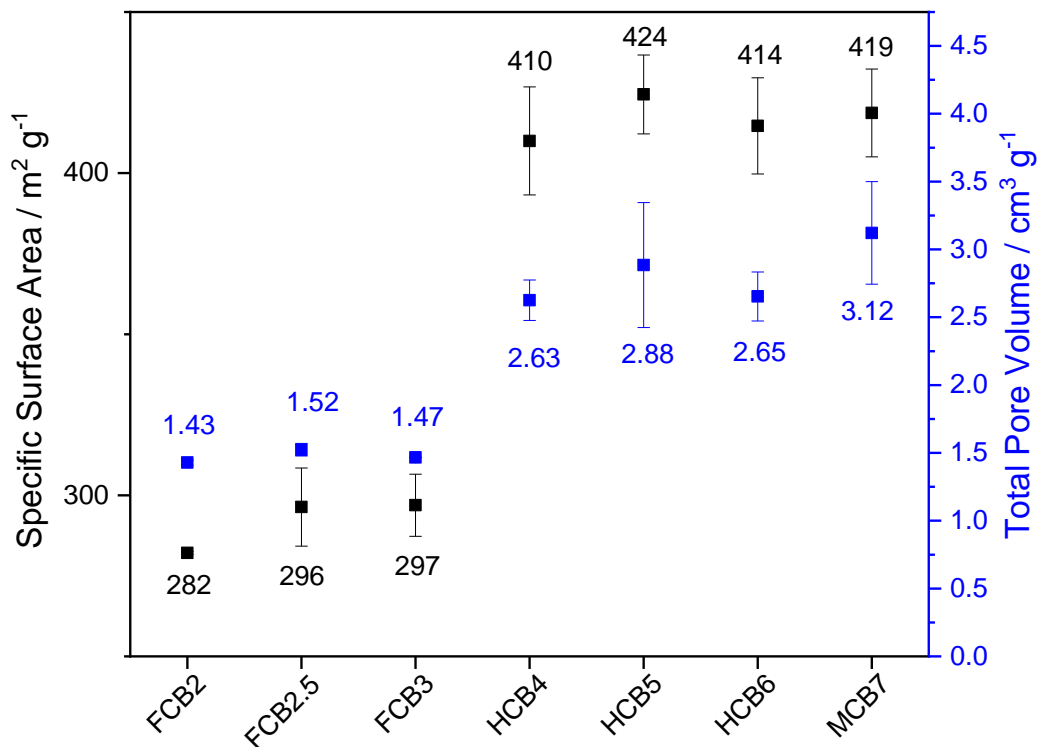
Figure 65 Specific surface area and total pore volume of cellulose aerogel beads produced from flax-extracted (FCB), hemp-extracted (HCB), and commercial cellulose (MCB) at different cellulose concentration (from 2 wt.-% to 7 wt.-%).

FCB samples had, across different concentrations, constant values for specific surface area (from 282 m^2 g^{-1} to 297 m^2 g^{-1}) and total pore volume (from 1.43 cm^3 g^{-1} to 1.52 cm^3 g^{-1}). These were considerably lower than the values obtained for MCB7 and HCBs. For these, the specific surface area ranged from 410 m^2 g^{-1} to 424 m^2 g^{-1}, with a higher variation in total pore volume, from 2.63 cm^3 g^{-1} and 2.88 cm^3 g^{-1} for HCB samples and 3.12 cm^3 g^{-1} for MCB7. These values were in the same range, from 300 m^2 g^{-1} to 400 m^2 g^{-1}, found in the literature for cellulose aerogels obtained using a similar synthetic route.[106, 107, 167] Other works reported the stability of the specific surface areas for cellulose aerogels synthesized from the same cellulose source, but with different cellulose concentrations.[290]

4.4 Manufacturing of Cellulose Aerogel Beads

The similarity between the HCB samples and MCB7 was related to the DP of their cellulose fibers. As the cellulose fibers extracted from hemp presented similar dimensions as MC, the cellulose solutions produced from each source of cellulose, at the same concentration, had the same viscoelastic properties. As a consequence, the aerogels synthesized from those solutions had similar properties. As FC had a higher DP, less cellulose concentration was used to obtain a solution as viscous as the ones created from HC and MC. Longer cellulose fibers and lower cellulose concentrations produced beads with smaller dimensions and bigger pores, with subsequent lower specific surface area and total pore volume.

Regarding the pore width range, the aerogel beads had a large concentration of mesopores and a significant amount of macropores. These distributions can be observed in **Figure 66.**
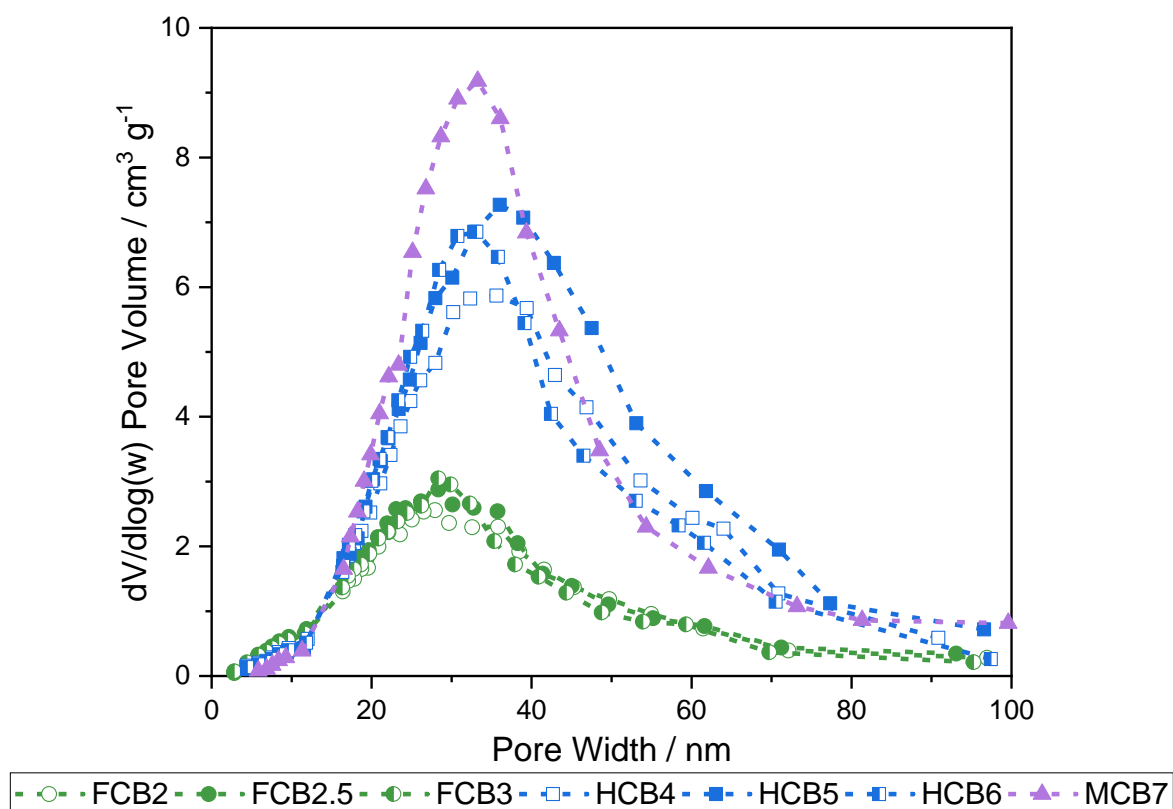
Figure 66 Pore size distribution of cellulose aerogel beads produced from flax-extracted (green for FCB), hemp-extracted (blue for HCB), and commercial cellulose (purple for MCB) at different cellulose concentration (empty circle for 2 wt.%; filled circle for 2.5 wt.-%; semi-filled circle for 3 wt.-%; empty square for 4 wt.-%; filled square for 5 wt.-%, semi-filled square for 6 wt.-%, and filled triangle for 7 wt.-%).

Results and Discussion

FC beads had an average pore size of 17 nm and a smooth pore size distribution. They presented a slow decline in adsorbed volume with increasing pore widths and, just as observed in the SEM pictures, they had a high proportion of bigger mesopores due to their cellulose higher DP and lower cellulose concentration used. HCBs had a steeper distribution curve and a lower proportion of macropores in comparison with FCBs, while still significant.

Few differences existed between HCB samples, having an average pore size of 24.5 nm. MCB7 had an average pore size of 25 nm and the highest proportion of mesopores than all other samples. Its steeper profile contained a higher proportion of smaller mesopores and a lower proportion of macropores, which explained its higher adsorption capacity. The difference between MCB7 and HCBs was related to the higher heterogeneity of HC fibers compared with MC. Small differences in size and distribution of those fibers in solution promoted a less homogeneous 3D cellulose network and a broader pore size distribution profile. Nonetheless, their properties were still similar.

In the appendix (see **Figure 121**), the thermogravimetric profiles of the tested celluloses are compared to representative profiles of the correspondent aerogels, as these latter profiles were independent of cellulose concentration. It was noticed that degradation started sooner for MCB7 than for MC (250 °C vs. 300 °C, respectively). The same was observed for FCB2 and FC. This was because cellulose aerogels consist of cellulose II, which has a significantly lower crystallization degree. This higher proportion of amorphous cellulose had a smaller degree of aggregation and was more prone to thermal degradation.[291] FCB2 presented a lower amount of char at 600 °C than HCB6 and MCB7 due to the lower amount of cellulose used and consequent lower density. Regarding the hemp beads, these reached 50% degradation at the same temperature as MCB7 and both contained similar values of char residue. This agreed with the previous data that indicated that these two sets of samples had very similar properties. The start of a significant mass loss in MCB7 occurred later in comparison with HC (240 °C vs. 200 °C, respectively), due to the removal of hemicellulose residues in the latter that could induce a sooner thermal decomposition or due to restructuration of the crystalline and fiber structure during the regeneration and coagulation phases of the cellulose gel formation.[106] Overall, the thermogravimetric profiles between samples synthesized from different celluloses and cellulose concentrations were not significantly different.

The synthesized aerogels had a high porosity (over 85%) and specific surface area (over 280 m^2 g^{-1}). Hemp-extracted cellulose aerogels and commercial cellulose-based aerogels had similar properties, such as a surface area of 400 m^2 g^{-1}, due to similar DP of the cellulose sources. It indicated that biowastes could be used as a source of cellulose for the synthesis of

aerogels with slight or no structural differences compared to the aerogels produced from commercially sourced cellulose. Lower cellulose concentrations were used for the flax-based cellulose solution preparation due to the higher DP of FC. These solutions produced lighter beads, with bigger pores and lower surface areas. These data reinforced the importance of the molecular weight of cellulose on the viscoelastic properties of the respective solutions and the final characteristics of the synthesized aerogels. It should be noted that these values might change slightly depending on the batch of waste fibers used and the cellulose extraction due to natural variations in the biomass composition.

4.4.2 Technical Scale

Based on the data discussed in **Chapter 4.1.2**, HB6, and MCB7 samples were synthesized at technical scale, using the JetCutter®.

The MCB7-JC beads had various shapes, ranging from spherical to oval, as in **Figure 67**. Due to the large volume of solution used, the distribution of cellulose was not uniform. The less viscous droplets were more likely to deform when entering the regeneration bath, resulting in the observed deformed shapes. For hemp-extracted cellulose, the 6 wt.-% concentration used resulted in fragments of varying sizes and shapes alongside spheroid beads, as observed in **Figure 67**.
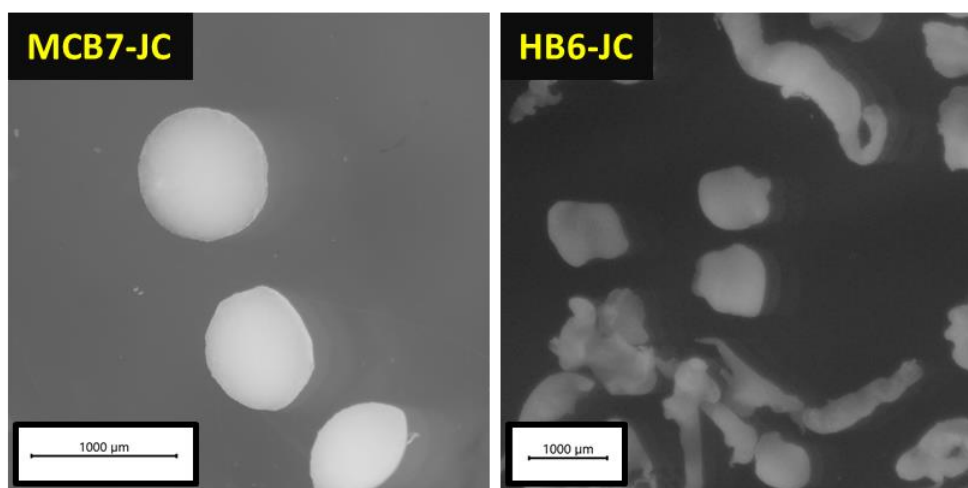
Figure 67 Optical microscope pictures of cellulose aerogel beads synthesized from a 6 wt.-% hemp-extracted cellulose solution (HCB6-JC) and from a 7 wt.-% commercial cellulose solution (MCB7- JC) at technical scale using the JetCutter® (JC).

This indicated that the viscosity of the cellulose solution droplet was not high enough to maintain a spherical shape when entering the coagulation bath. To optimize the shape of the

beads, the cellulose concentration in the solution could be increased to induce a higher viscosity or the kinetic energy of the droplet could be reduced while falling into the coagulation bath by decreasing the drop height or the flux speed.[181, 182] The average diameter of the MCB7-JC sample was 0.85 mm, and the envelope density was 0.15 g cm^{-3}, with a porosity of 90.33%. The porosity was higher than the 87.87% (with a density of 0.18 g cm^{-3}) observed for the laboratory scale correspondent. These values are shown in **Table 12**.

Table 12 Properties of cellulose aerogel beads synthesized from 7 wt.-% commercial cellulose solution (MCB7) and a 6 wt.-% hemp-extracted cellulose solution (HCB6) at laboratory and technical scale, using the JetCutter® (JC). Information on the specific surface area and total pore volume of the aerogels is presented later.

Samples	Average Bead Diameter / mm	Envelope Density / g cm^{-3}	Porosity / %	Average Pore Size / nm
MCB7	3.28±0.10	0.21	85.94	25.16
HCB6	3.08±0.23	0.18	87.87	24.22
MCB7-JC	0.85±0.09	0.15	90.33	25.60
HCB6-JC	0.76±0.13	0.07	95.34	25.70

The difference could be explained by the different influences of shrinkage on the samples. For smaller droplets (< 1 mm), the diffusion force between the core and the surface of the beads was more limited than at the laboratory scale beads (3 mm). This reduced the shrinkage and better preserved the porous structure of the wet gel across the neutralization and solvent exchange steps.[47] For HCB6-JC, the average diameter of the spheroid beads was 0.76 mm, while there were fragments with a wide variety of sizes. Its envelope density was lower than the one of MCB7-JC (0.07 g cm^{-3} vs. 0.15 g cm^{-3}, respectively) due to the lower concentration of cellulose used, which also explained its higher porosity compared to MCB7- JC, 95.3 % vs. 90.3% respectively. No change was recorded for the skeleton density (1.52 g cm^{-3}). As for MCB7-JC, a reduction in density and an increase in porosity occurred when the synthesis of hemp-extracted cellulose aerogel beads was performed at a larger scale. This was due to the minimization of shrinkage as explained above.

In the SEM pictures of MCB aerogels, shown in **Figure 68**, the exterior and internal porous structure of the sample changed when the synthesis was upscaled.
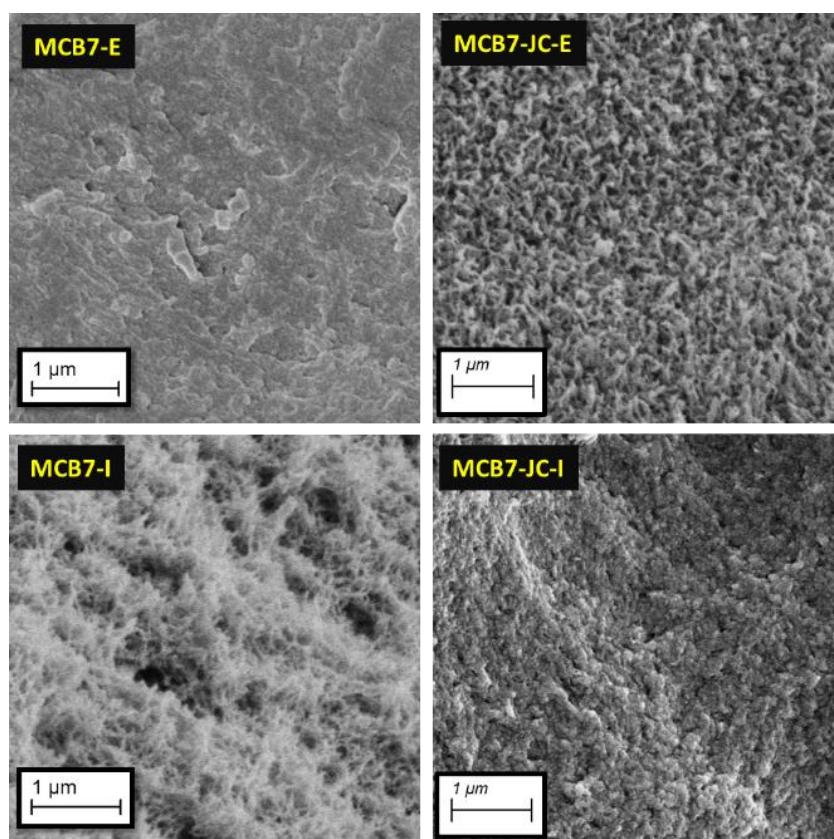
Figure 68 SEM pictures of the exterior (E) and interior (I) surfaces of cellulose aerogel beads synthesized from a 7 wt.-% commercial cellulose solution at laboratory scale (MCB7) and technical scale (MCB7-JC), using the JetCutter® (JC).

On the exterior, the surface became more porous than at laboratory scale. In the interior, the pores were smaller, with the existence of globular structures, in comparison with the dense fibrillated structures observed in MCB7. Due to the micrometer dimensions of the sample, an accurate cut of the bead was difficult. This could explain some of the higher compaction observed in the interior of MCB7-JC. Besides, the fast gelation of the droplets and the densification of the resultant gels as they remained in the regeneration bath could have created the compact fibrillar structures observed in their interior. On the exterior surface, as the cellulose concentration was lower than in the interior due to the cohesive forces applied in the droplet, the "freezing" of the cellulose fibers created a packed network with bigger pores than the ones observed for larger beads. For the latter, the regeneration speed was not so high, and the cellulose distribution in the droplet´s interior was more homogeneous.[107, 292] For the case of the hemp cellulose-based beads, as observed in **Figure 69**, some different trends were evident when upscaling was applied.
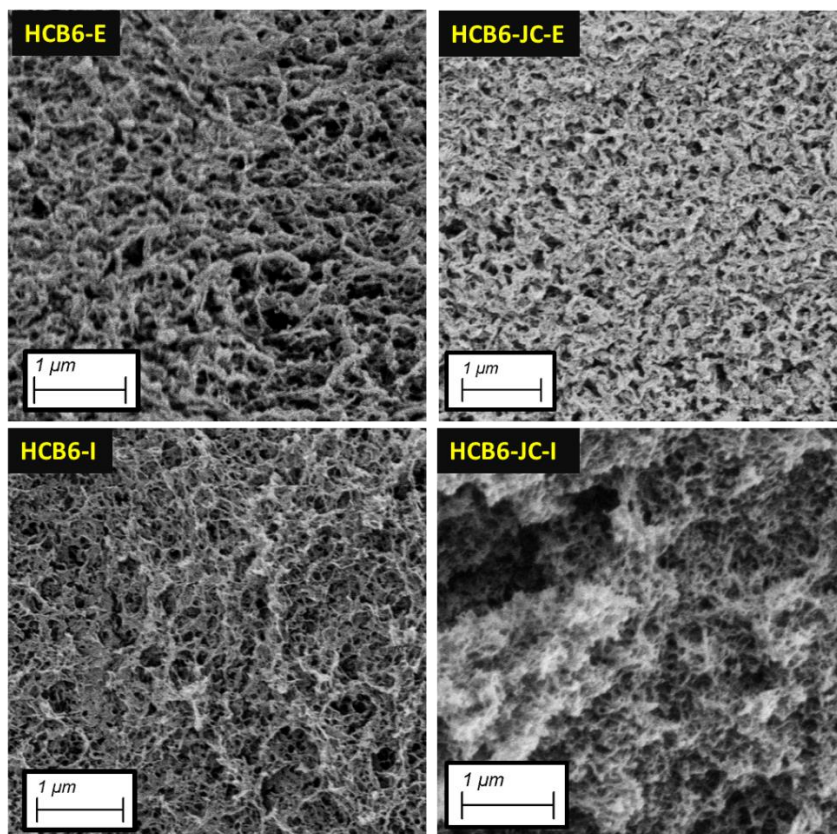
Figure 69 SEM pictures of the exterior (E) and interior (I) surfaces of cellulose aerogel beads synthesized from a 6 wt.-% hemp-extracted cellulose solution at laboratory scale (HCB6) and technical scale (HCB6-JC), using the JetCutter® (JC).

The exterior surface of both samples, HCB6 and HCB6-JC, had a similar porous structure, with slighter smaller pores and cavities for HCB6-JC. Here, the densification of the surface due to the extended presence of the beads in the regeneration bath might have been more relevant than for MCB7- JC. The samples synthesized with JetCutter® had a similar surface, after suffering a fast gelation that did not reorganize the cellulose fibers into more compact structures as in MCB7. From the laboratory to the technical scale, most of the internal structure of the aerogel remained composed of mesopores and thin pore walls. The presence of bigger cavities in HCB6- JC compared to HCB6 could be the product of the presence of air bubbles that could not be removed through sonification due to the volume of solution used or from deformation of the get structure during regeneration, as observed in **Figure 67**. These would have influenced the data collected through physisorption as well.

Few changes were observed in the data collected from physisorption for MCB samples, as visible in **Figure 70**.
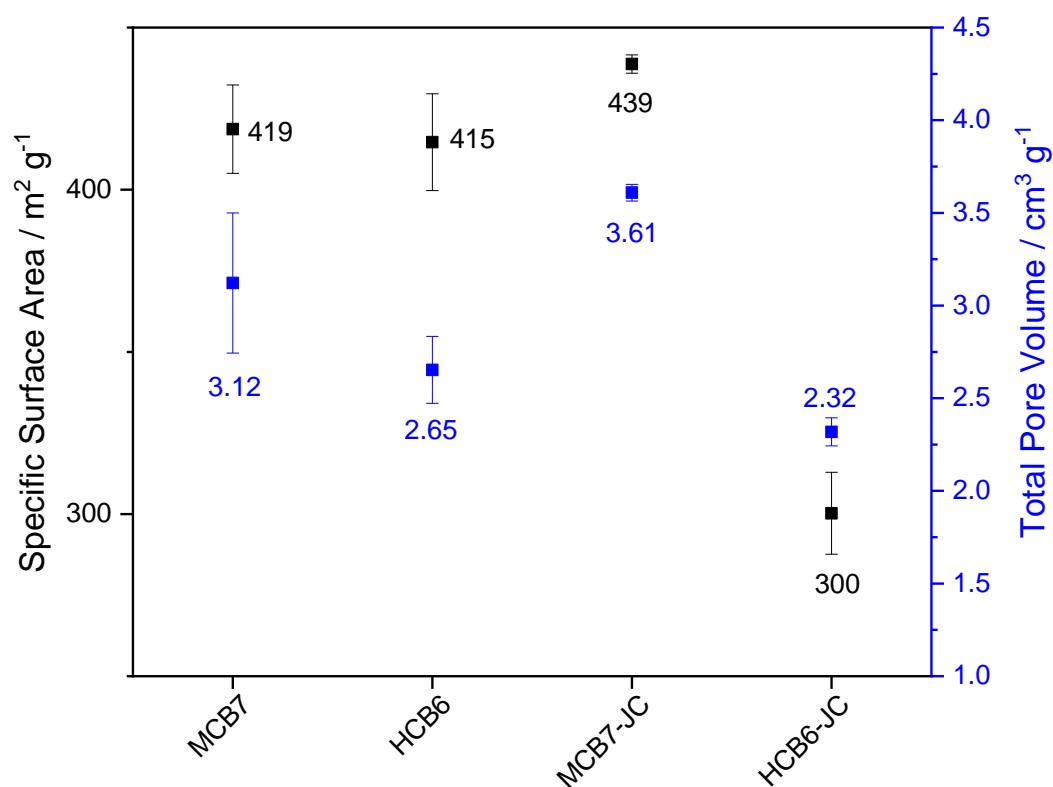
Figure 70 Specific surface area and total pore volume of cellulose aerogel beads synthesized from a 7 wt.-% commercial cellulose solution (MCB7) and a 6 wt.-% hemp-extracted cellulose solution (HCB6) at laboratory and technical scale, using the JetCutter® (JC).

By having a higher resistance to shrinkage and higher porosity, MCB7-JC achieved a higher specific surface area (439 m² g⁻¹ vs. 419 m² g⁻¹) and total pore volume (3.61 cm³ g⁻¹ vs. 3.12 cm³ g⁻¹) compared to MCB7. However, the opposite trend was observed for HC samples, which showed a slight decrease in total pore volume (from 2.65 cm³ g⁻¹ to 2.32 cm³ g⁻¹) while a more significant decrease in surface area was registered, from 415 m² g⁻¹ to 300 m² g⁻¹. These trends corresponded with the pore size distribution of the samples, as expressed in **Figure 71**. The mesoporous character of the aerogel beads was preserved in the upscaling as observed in their type IV (a) isotherms, in the appendix (see **Figure 126**). JC samples have a shorter plateau than their laboratory counterparts, showing a small deviation from the H2(b) hysteresis shape. This could be caused by changes in the dynamics of cellulose regeneration between the two synthesis scales. In the average pore size distribution, shown in **Figure 71**, few differences exist between MCB7 and MCB7-JC. For MCB7-JC, the profile was sharper, with a higher fraction of pores in the 30 nm to 40 nm range than MCB7. This was caused by the less pronounced shrinkage in the MCB7-JC which better preserved the porous structure and bigger mesopores.

Results and Discussion

Due to this, bigger pores survived the synthesis which led to a slightly higher average pore size than at the laboratory scale (25.60 nm vs. 25.16 nm). The upscaling of the process preserved the mesoporous character of the cellulose aerogels produced from commercial cellulose while decreasing the density and increasing the specific surface area.
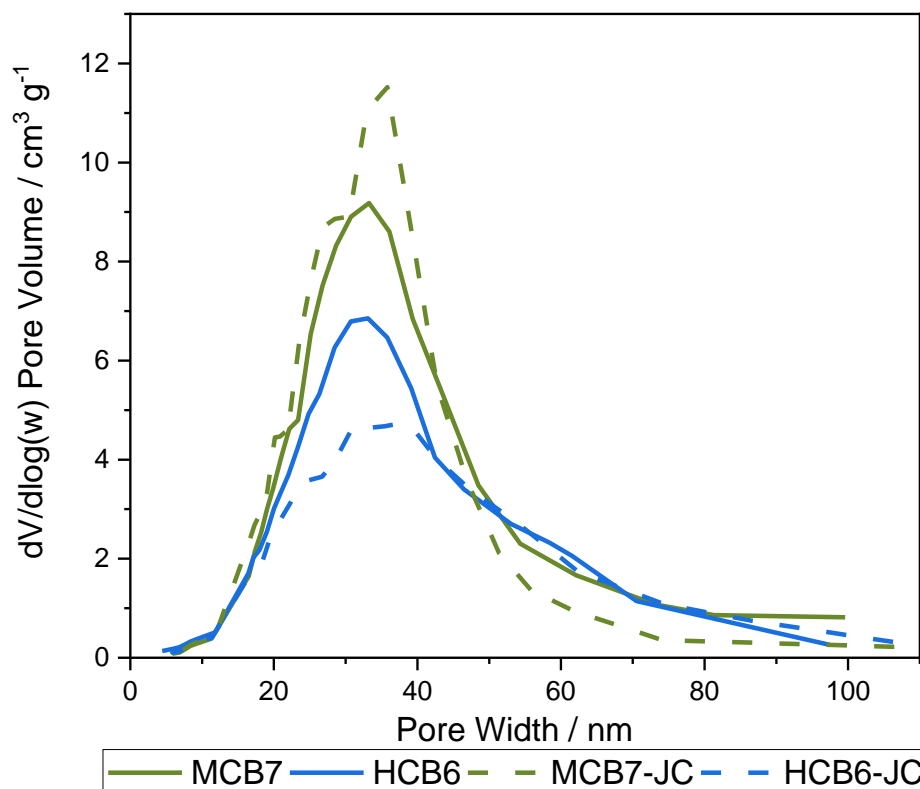
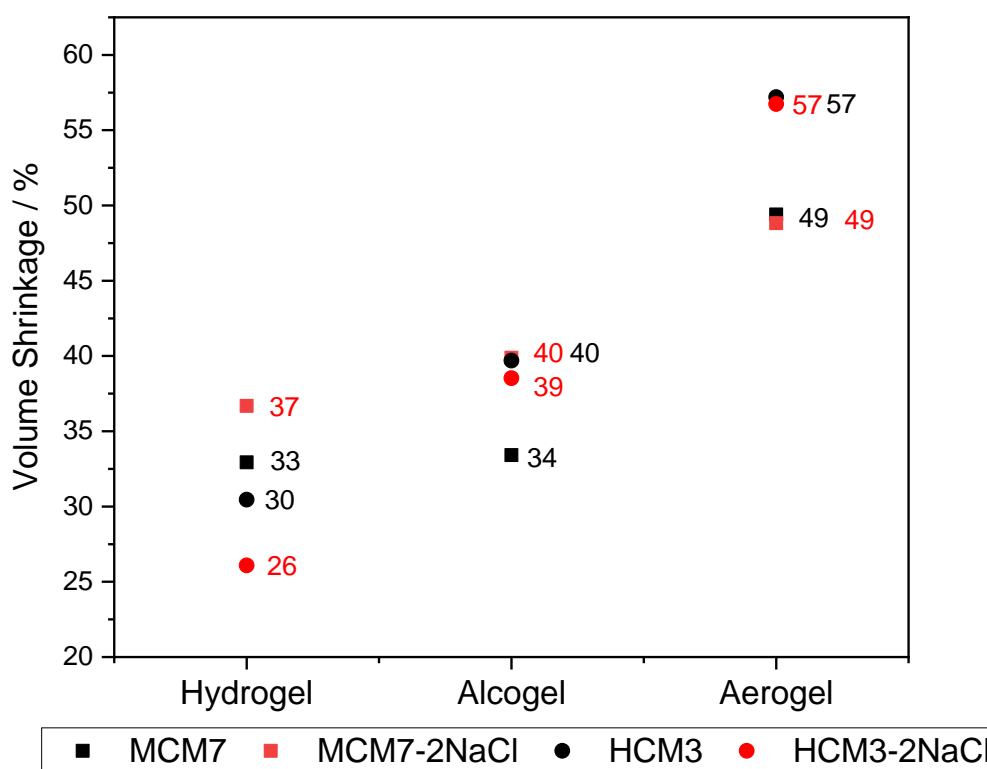**Figure 71** Pore size distribution of cellulose aerogel beads synthesized from a 7 wt.-% commercial cellulose solution (green for MCB7) and a 6 wt.-% hemp-extracted cellulose solution (blue for HCB6), at different scales (solid line for laboratory scale and dash line for technical scale, using the JetCutter®, JC).

For the HC beads, the profile suffered a significant decrease in the proportion of mesopores when the beads were produced with the JetCutter®. Besides, a plateau was observed in the range of 30 nm to 40 nm for HCB6-JC. These changes were related to the cutting parameters used. The shape of the HCB6-JC was not homogeneously spherical, and cellulose residues were present due to the squashing of cellulose solution droplets when entering the coagulation bath. This created random cellulose fibril aggregates alongside wet gels with distorted shapes and networks, with bigger cavities and pores. These aggregates were mixed with the aerogels and further artificially decreased the values of specific surface area and pore volume measured. Optimization of the cutting parameters, such as reducing the jet speed and increasing the

4.4 Manufacturing of Cellulose Aerogel Beads

cellulose concentration in the solution, would preserve a spherical shape of the droplets and the gel structure of the beads, and decrease the cellulose waste mixed with the aerogels.

For both MCB7-JC and HCB6-JC, the thermal conductivity was 42.7 mW m^{-1} K^{-1}, which was in line with what has been recorded by other researchers for similar materials.[171, 191, 288] Nonetheless, Nguyen et al. and Rudaz. were able to create cellulose aerogels, using similar synthetic processes, with values as low as 30 mW m^{-1} K^{-1}.[166, 170] The origin of these discrepancies was found in the myriad of factors that influence the thermal conductivity of an aerogel. Different dissolution and regeneration conditions, source and DP of cellulose, drying conditions, and even the method used to determine thermal conductivity influence this property.[166, 191, 232] The thermal conductivity of the synthesized aerogels was lower than that of MC, whose thermal conductivity was 92.5 mW m^{-1} K^{-1}, thanks to the creation of a porous structure and the reduction of the crystallinity of cellulose during the conversion of cellulose I into cellulose II.[63] These decreased the contribution of the solid backbone and the gas conductivity factors for the thermal conductivity of the aerogels. Despite these, the thermal conductivity recorded for the aerogels was comparable to mineral wool and cellulose fibers used for insulation.[11, 288] For the case of HCB6-JC, its thermal conductivity was higher than the 38.7 mW m^{-1} K^{-1} recorded for the non-milled hemp bast fibers. This was caused by cellulose waste mixed with the aerogel beads which increased thermal conductivity. At the same time, hemp bast waste fibers have an inherent porous structure which makes them suitable bio-insulants.[207, 293]

It was concluded that the upscaling of the selected recipes from laboratory to technical scale preserved and even improved the aerogel cellulose bead properties when synthesized from MC. However, the same cannot be said for HC, as the lack of optimized synthesis parameters for the JetCutter® produces aerogels with worse properties than HCB6. More experiments would be required to improve the shape and properties of HCB6-JC. This work highlights the importance of the cutting parameters in minimizing waste, maximizing the production of homogeneous spherical beads, and consequent preservation of the properties of the aerogels. The thermal conductivity values recorded for the aerogels were in the same range as current market alternatives, which hinders the competitiveness of this new product. The presence of bigger macropores and cavities, not detected by the physisorption measurements, in both samples, counterbalanced any difference in the detected pore size distribution. While MCB7- JC had a higher surface area and sharper pore size distribution than HCB6-JC, they had the same thermal conductivity. Using different regeneration baths, lowering cellulose concentrations, and adding salts could further reduce the thermal conductivity of the synthesized aerogels.

Results and Discussion

The results of applying those perspectives on alternative recipes are here reported and discussed. In the upscaling of the synthesis of cellulose aerogels, the consumption of solvents such as water and ethanol became more significant. **Figure 72** shows the total and discriminated consumption of water and ethanol for the neutralization and solvent exchange of aerogel beads per liter of cellulose solution.
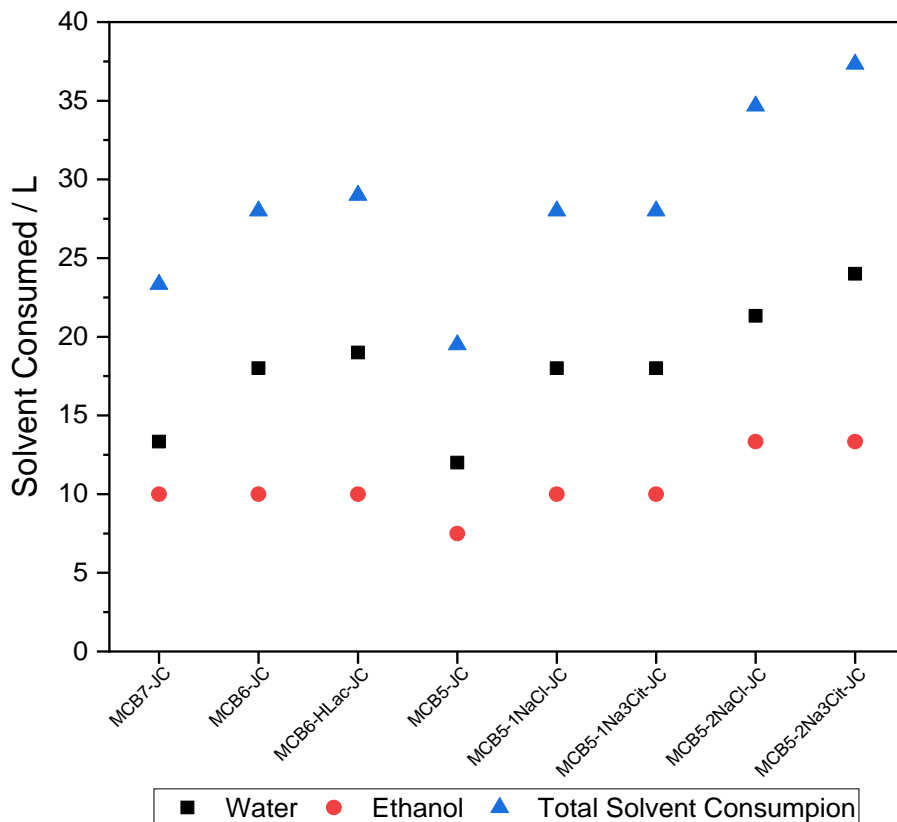
Figure 72 Individual consumption of solvents (black square for water, and red circle for ethanol) and their total consumption (blue triangle) for the neutralization and solvent exchange of cellulose aerogel beads produced at technical scale, using the JetCutter® (JC), per liter of cellulose solution.

There was a higher water consumption than ethanol because the former was used for the neutralization and solvent exchange while ethanol was used only in the latter step. While the average consumption of ethanol was 10 L, with little variation between samples, the water consumption was not constant. The addition of higher quantities of salt to 5 wt.-% cellulose solutions led to higher water consumption to neutralize their cellulose aerogel beads. For 2 wt.-% salt concentration, higher water consumption was required for Na_3Cit than NaCl due to the buffer effect caused by the citrate anion that delayed the neutralization of the cellulose wet gels. More water was consumed for MCB6-JC and MCB6- HLac-JC (18 L) than for

4.4 Manufacturing of Cellulose Aerogel Beads

MCB7-JC (13 L) and MCB5-JC (12 L). These differences might have originated from different rates of solution loss during the cutting. While most of the cellulose solutions were converted into droplets that fell into the acid bath, some of them were lost in the form of aerosol or droplets that fell outside of the bath due to occasional abrupt changes in the viscoelastic properties of the solutions. As time progressed, the solutions became less homogeneous due to decreasing cellulose dissolution quality. This caused momentary losses during their cutting as it was difficult to continuously correct the pressure applied promptly. As these losses were not quantified and the values presented in **Figure 72** are normalized per liter of solution cut, some deviations between samples might be found. Regarding MCB5-JC, a higher ratio of cellulose waste and shape deformation of its beads could have increased the diffusion rates during neutralization, requiring less water to reach a neutral pH. An average total consumption of 28.5 L $\pm$ 5.7 L of solvents per L of cellulose solution was found for these samples, with significant variation when salts were added. The sustainability and production cost would have been improved by the recycling of the solvents. The mixture of ethanol and water during solvent exchange could be separated by distillation while the acidic salty water obtained from neutralization could be purified with electrochemical methods such as electrodialysis to remove salts and electrochemical oxidation to degrade urea.[294, 295]

The viscoelastic properties of the cellulose solutions affected the shape of the produced beads. As shown in **Figure 73**, the shape of the beads was influenced by their cellulose concentration.
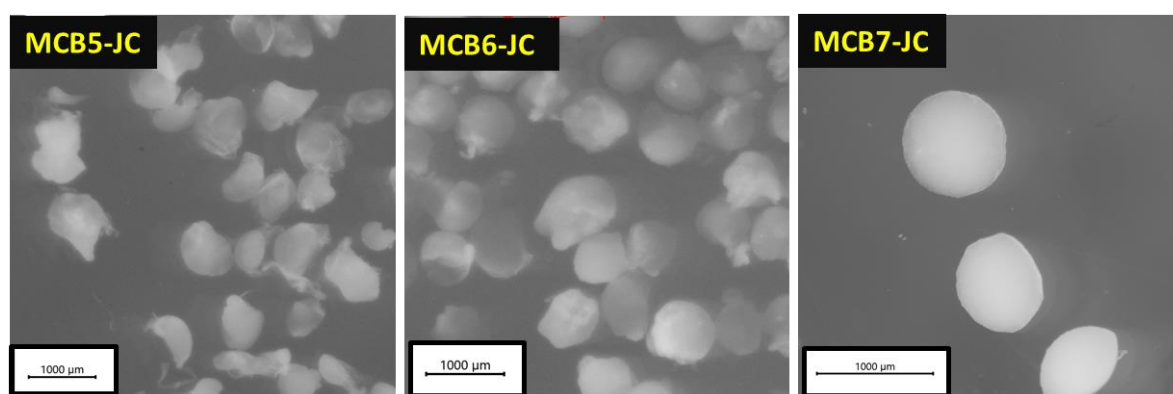
Figure 73 Optical microscope pictures of commercial cellulose aerogel beads (MCB) at different cellulose concentrations (from 5 wt.-% to 7 wt.-%) at technical scale, using the JetCutter® (JC).

As the concentration of cellulose increased, the shape of the aerogel beads evolved from deformed spheroids, with the presence of fragments, to more spherical beads. The deformation observed for MCB5-JC and MCB6-JC was due to the low viscosity of their solutions which

could not sustain the impact when entering the coagulation bath. Modification of the cutting parameters was not enough to improve the shape of MCB5-JC and MCB6-JC beads as the reduction of the dropping height was not effective and the use of a lower jet flux while producing more spherical beads, increased the production of waste and the clogging of the nozzle. Baldur et al. achieved better-shaped beads using the same procedure for cellulose dissolution, cutting parameters, and cellulose concentrations.[183]

In his work, a 30 wt.-% aqueous H_2SO_4 solution was used as a coagulation bath. This promoted a fast gelation of the droplet and the creation of an outer shell that preserved the spherical shape of the wet gel bead. In this work, it was used a 2M acetic acid aqueous bath, which promoted a smoother regeneration and, as a consequence, did not inhibit shape deformation of the non-fully coagulated beads during cutting. No difference in shape was observed between MCB6-JC and MCB6-HLac-JC, which indicated that both lactic and acetic acid at 2M concentration in water were not effective in preserving the shape of the wet gel beads. The addition of salts to the 5 wt.-% cellulose solution improved the shape of the beads, as observed in **Figure 74**.
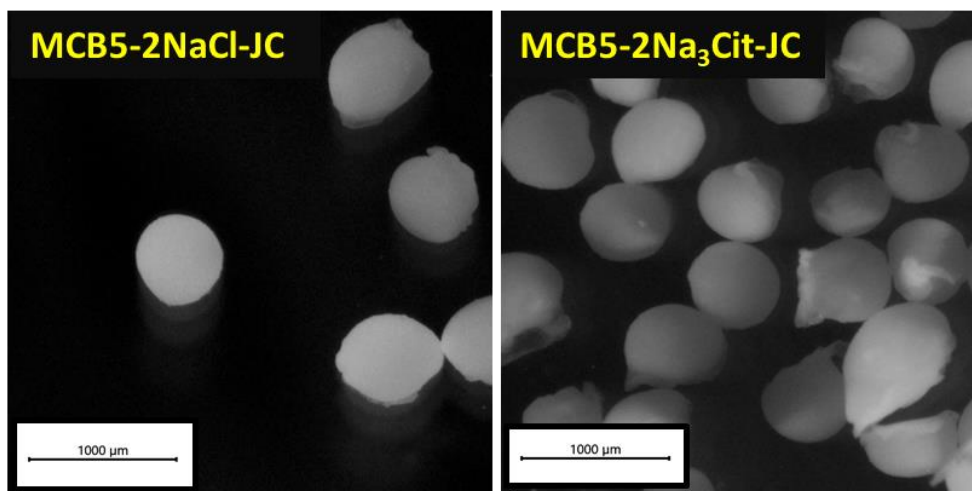
Figure 74 Optical microscope pictures of 5 wt.-% commercial cellulose aerogel beads (MCB5) produced at technical scale, using the JetCutter® (JC). Prior to gelation, 2 wt.-% NaCl (MCB5-2NaCl-JC) or Na_3Cit (MCB5- 2Na3Cit-JC) were added to the cellulose solutions.

For both MCB5-2NaCl-JC and MCB5-2Na3Cit-JC, the fraction of fragments was reduced while better sphericity was obtained. These salts increased the viscosity of the solution (especially NaCl), as discussed in **Chapter 4.3.1,** but also increased its surface tension.[296]Therefore, the droplets resisted the impact entering the coagulation bath and better preserved a spherical shape while a lower cellulose concentration was used. A lower cellulose concentration led to a decrease in the average diameter of the beads. This was due to the cutting process, as a less

viscous solution was more easily cut into smaller droplets in the JetCutter®. There was no direct influence of cellulose concentration on the envelope density of the samples, as observed in **Table 13**.

Table 13 Properties of commercial cellulose aerogel beads (MCB) produced at technical scale, using the JetCutter® (JC), at different cellulose concentrations (from 5 to 7 wt.-%). For selected samples, NaCl or Na_3Cit were added to their cellulose solutions before gelation, at 1 or 2 wt.- %. For MCB6- HLac-JC, a 2 M aqueous lactic acid solution was used as regeneration bath, while a 2 M acetic acid solution was used for all other samples. Information on the specific surface area and total pore volume of the aerogels is presented later.

Samples	Average Bead Diameter / mm	Envelope Density / g cm^{-3}	Porosity / %	Average Pore Size / nm
MCB7-JC	0.85±0.09	0.15	90.33	25.60
MCB6-JC	0.64±0.11	0.22	85.79	25.94
MCB6-HLac-JC	0.60±0.03	0.30	80.43	25.75
MCB5-JC	0.66±0.08	0.23	85.08	27.36
MCB5-1NaCl-JC	0.59±0.06	0.37	75.90	27.06
MCB5-1Na₃Cit-JC	0.62±0.07	0.24	83.98	25.30
MCB5-2NaCl-JC	0.62±0.08	0.26	83.05	28.27
MCB5-2Na₃Cit-JC	0.62±0.08	0.37	75.61	33.68

The envelope density ranged from 0.15 g cm^{-3} to 0.37 g cm^{-3}, with little influence from the addition of salts, different cellulose concentrations, or the use of lactic acid in the coagulation bath. This corresponded to values in porosity that ranged from 76% to 90%. These differences were related to the method used for envelope density determination. The loss of material during cutting created smaller droplets than theoretically expected, leading to the overestimation of the values of envelope density and consequent underestimation of the values of porosity for the aerogels. These inconsistent cutting losses were particularly high when less viscous solutions were used, and when salts were added (due to the faster gelation). This explained why MCB5- JC samples presented higher values of envelope density than aerogels with higher content in cellulose (6 wt.-% and 7 wt.-% cellulose concentrations). Envelope density could

have been determined through the packing density but this value was of difficult calculation and its use would have been an approximation without an experimental basis.[239, 297] For MCB7-JC, less production of wastes and cutting losses resulted in a lower density (0.15 g cm^{-3}) and bigger beads (0.85 mm) compared to the other samples. In **Figure 75**, the exterior and interior surfaces of aerogel cellulose beads with different cellulose concentrations can be observed.
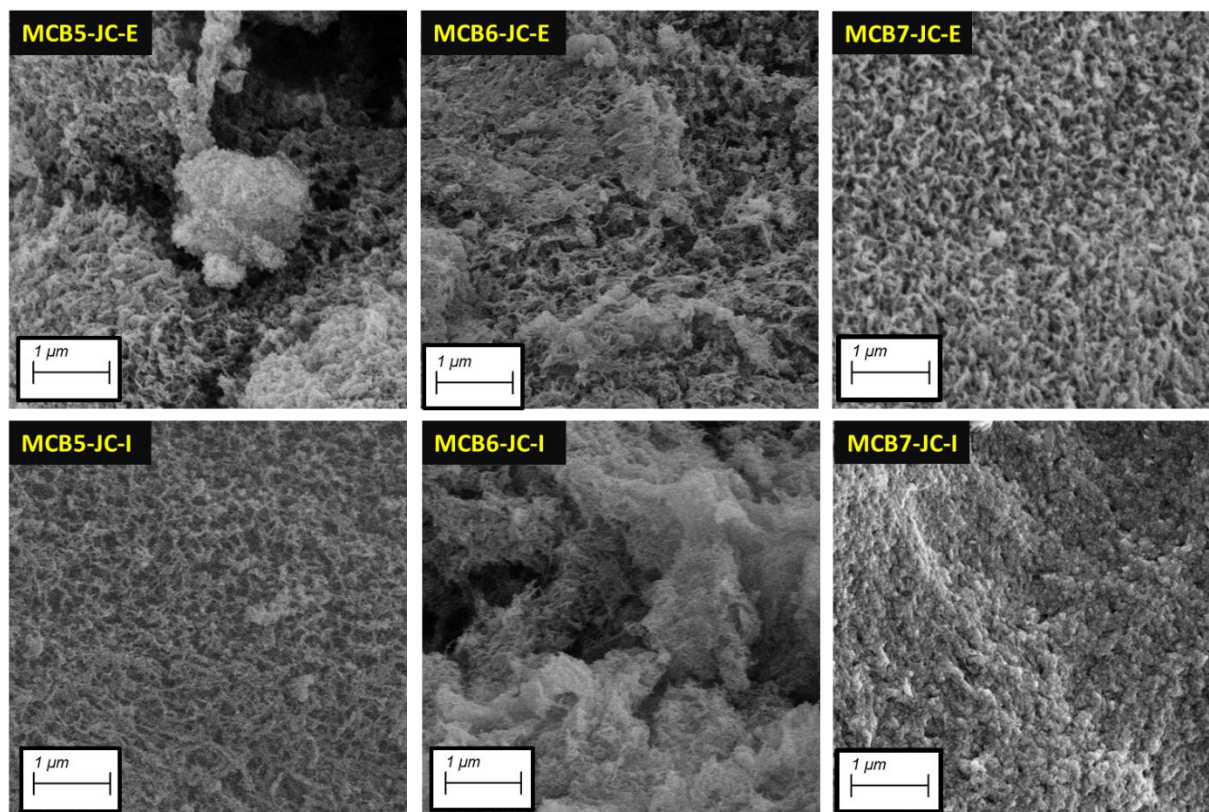
Figure 75 SEM pictures of the exterior (E) and interior (I) surfaces of commercial cellulose aerogel beads (MCB) at different cellulose concentrations (from 5 wt.-% to 7 wt.- %) produced at technical scale, using the JetCutter® (JC).

The exterior surface of the aerogels was compact and porous, and with decreasing cellulose concentration, the pores increased in size, cavities appeared, and the cellulose network became thinner. This was in line with what was observed in the previous chapters and the literature.[107, 114, 253] The surface became more irregular at lower cellulose concentrations due to the lower viscosity of the droplets during cutting. As they could not resist so effectively their entrance into the regeneration bath, their shape suffered deformation.[181, 182] In the interior of the beads, a similar behavior was observed. While at MCB7-JC-I, an intricated and compact structure was observed, this became increasingly populated by bigger pores, cavities, and a less

homogeneous fibrillar network in MCB6-JC and MCB5-JC. No significant differences between MCB6-JC and MCB6-HLac-JC were registered in their morphology. In **Figure 76**, it is visible the influence of the addition of salt to 5 wt.-% cellulose solutions on their resultant aerogels.
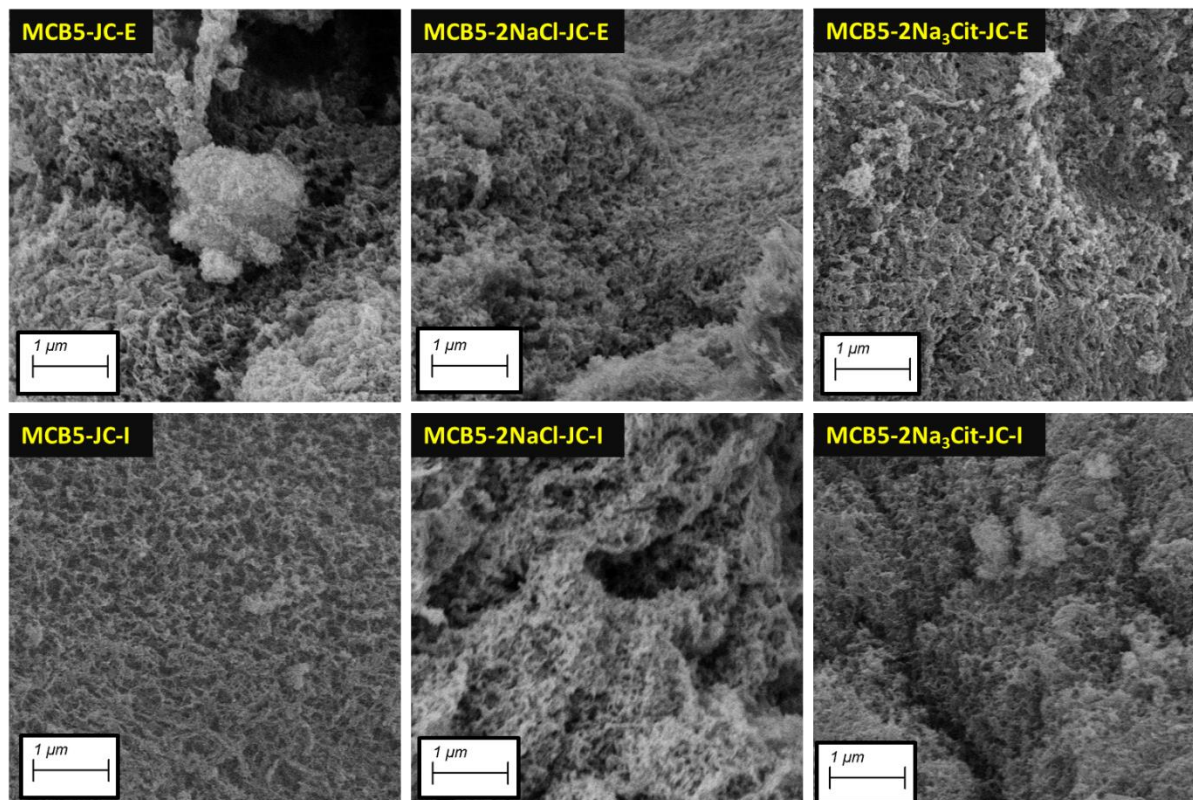
Figure 76 SEM pictures of the exterior (E) and interior (I) surfaces of 5 wt.-% commercial cellulose aerogel beads (MCB5) produced at technical scale, using the JetCutter® (JC). Prior to gelation, 2 wt.-% NaCl (MCB5-2NaCl-JC) or Na$_3$Cit (MCB5- 2Na$_3$Cit-JC) were added to the cellulose solutions.

Adding 2 wt.- % NaCl or Na$_3$Ci resulted in more compact and homogeneous external surfaces. However, cavities were visible in the interior. While the addition of salts influenced the gelation speed and, through its scaffold effect, more pores and cavities were created, the stable gel body formation was faster for these small beads than for a monolith. In this case, the droplet gelled and its cellulose fibers continued agglomerating in the acid bath before the beginning of the neutralization.[107] That is why there were not so many cavities in the aerogel where salt was added compared to what was observed in **Chapter 4.3.1**. The more homogenous surface was due to the increase of surface tension of the cellulose solution droplets after salts addition, which helped them sustain the entrance in the regeneration bath and inhibited shape deformation. The

inhomogeneous distribution of ions in small droplets played a role in the gel structures formation.[292]

The differences in the internal and external porous structure of the aerogels affected the specific surface area and pore size distribution of these materials. They were considered mesoporous materials, as shown by the isotherms IV (a) in the appendix (see **Figure 127**). Most isotherms have very short plateaus compared to the samples synthesized in the laboratory for this work. Their hystereses had a shape intermediate between H2(b) and H3, being the latter characteristic of materials with macropores that are not filled during the adsorption phase.[276] Only MCB7-JC and MCB6- HLac-JC have a longer plateau and a steeper desorption line, indicating a narrower pore size distribution. This was in line with what was observed in SEM pictures. The specific surface area and total pore volume of the aerogels are shown in **Figure 77**.
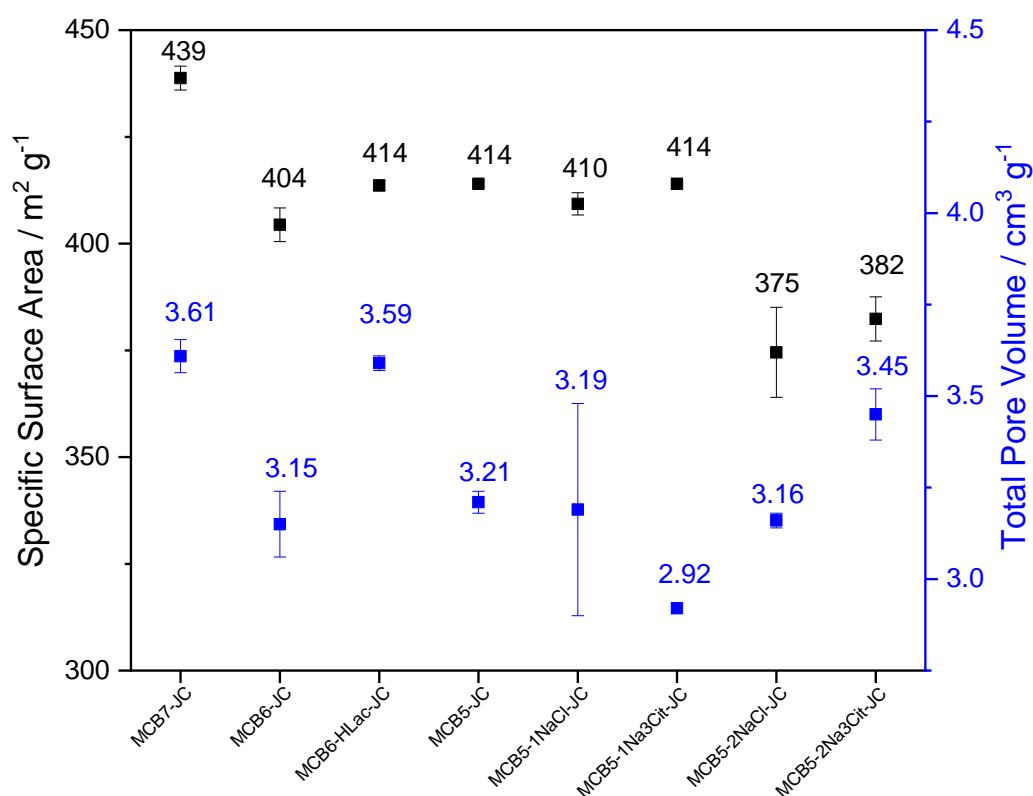
Figure 77 Specific surface area and total pore volume of commercial cellulose aerogel beads produced at technical scale, using the JetCutter® (JC), from cellulose solutions of different concentrations without the addition of salt (from 5 wt.-%, to 7 wt.-%). For selected samples, NaCl or Na₃Cit were added to their cellulose solutions before gelation, at 1 or 2 wt.-%. For MCB6- HLac-JC, a 2 M aqueous lactic acid solution was used as regeneration bath, while a 2 M acetic acid solution was used for all other samples.

4.4 Manufacturing of Cellulose Aerogel Beads

Most samples, except MCB5-2NaCl-JC, MCB5-2Na$_3$Cit-JC, and MCB7-JC, had a specific surface area close to 410 m^2 g^{-1}. These values were independent of cellulose concentration, the acid used in the regeneration bath, or 1 wt.-% salt addition. These were in line with what has been observed in this work (see **Chapters 4.3.1** and **4.3.2**) and the literature.[57, 107, 166, 298] The total pore volume ranged from 2.92 cm^3 g^{-1} to 3.61 cm^3 g^{-1} for all samples. When the salt concentration was increased from 1 wt.-% to 2 wt.-%, it was observed a decrease in specific surface area (375 m^2 g^{-1} and 382 m^2 g^{-1} for NaCl and Na$_3$Cit, respectively) and a slight increase in the total pore volume. The lower cellulose concentration plus the creation of bigger pores and cavities, led to an overall reduction of the available surface area and an increase of the total pore volume. MCB7-JC had a higher value of 439 m^2 g^{-1}, which could be related to its lower density and higher porosity. These, in conjugation with higher cellulose concentrations, contributed to a porous structure with more, smaller pores which maximized its specific surface area. This data can be complemented with **Figure 78**, where the pore size distribution is shown. The pore size distribution profile of MCB7-JC was sharp and composed mostly of mesopores in the range of 20 nm to 40 nm, while the majority of other sample profiles were broader and shifted to bigger pore dimensions. The relation between the profiles of MCB6-HLac-JC and MCB6-JC was similar but more pronounced to what was observed in **Chapter 4.3.2**, demonstrating that some of the trends observed at the laboratory scale remained during upscaling. Samples with a 5 wt.-% cellulose concentration had a significant fraction of pores over 70 nm, especially after adding salts. The average pore size was constant for most samples (from 25.30 nm to 27.36 nm), but it was higher for MCB5-2NaCl-JC and MCB5- 2Na$_3$Cit-JC (28.27 nm and 33.68 nm, respectively).
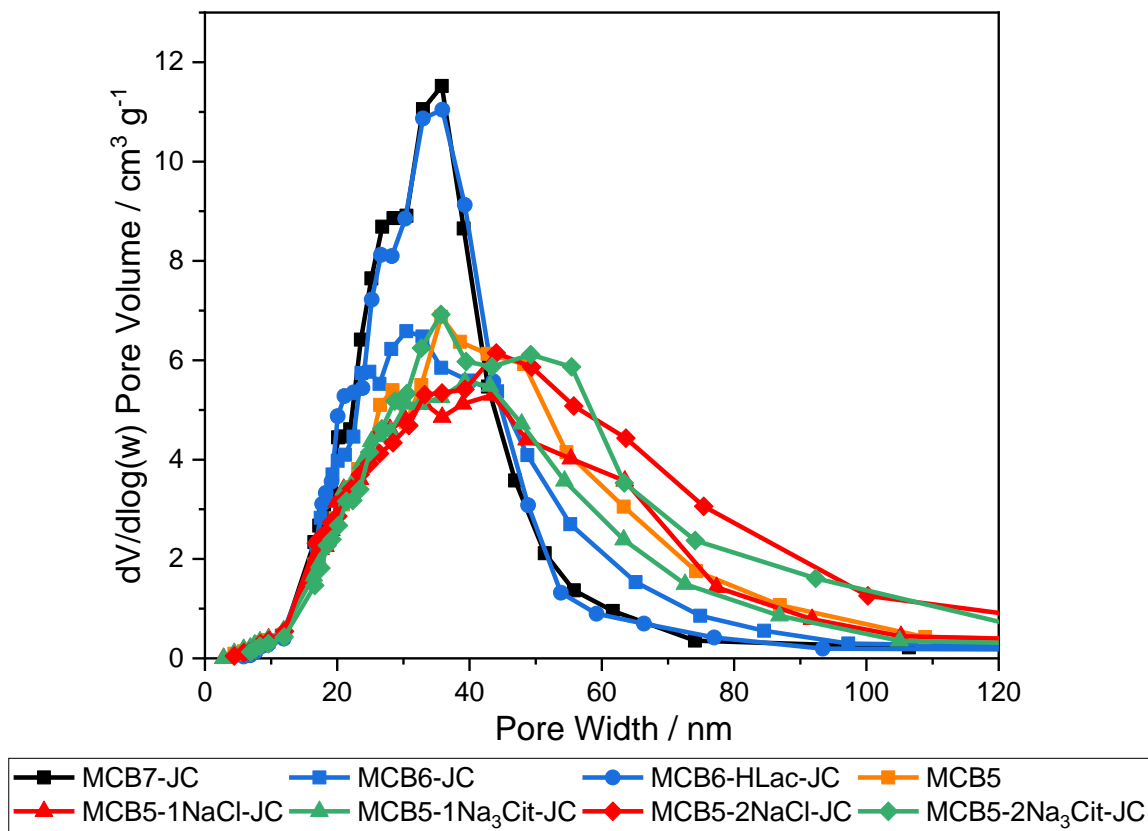
Figure 78 Pore size distribution of commercial cellulose aerogel beads produced at technical scale, using the JetCutter® (JC), from cellulose solutions of different concentrations without the addition of salt (black for 7 wt.-%; blue for 6 wt.-%, and orange for 5 wt.-%) and coagulated in different acids (square for acetic acid and circle for lactic acid). Some samples were synthesized from 5 wt.-% cellulose solutions to which salts were added (red for NaCl, and green for Na$_3$Cit) in different concentrations (triangle for 1 wt.-%, and rhombus for 2 wt.- %) before gelation.

The bigger presence of macropores for these two samples, which were linked to a lower cellulose content and the creation of bigger pores and cavities due to the scaffold effect of salts, was responsible for their higher average pore sizes. This agreed with their isotherms, as observed in the appendix (see **Figure 127**). As observed in **Figure 79**, the pore size distribution of the samples was not the main factor behind the different thermal conductivities observed. The samples with a cellulose concentration above or of 6 wt.-%, had thermal conductivities between 42.6 mW m^{-1} K^{-1} and 45.7 mW m^{-1} K^{-1}. MCB5-JC presented a thermal conductivity of 38.3 mW m^{-1} K^{-1} and this value slightly decreased when increasing concentrations of salt were added to the cellulose solution before gelation (a minimum of 37 mW m^{-1} K^{-1} was reached for MCB5-Na$_3$Cit-JC). The main factor behind this reduction in thermal conductivity was the

reduction of the solid conduction contribution due to the decrease of the cellulose content in the aerogels with lower cellulose concentration.[14] Adding salts promoted the creation of more pores and reduced the gas conduction factor of thermal conductivity. It meant that, while slight reductions in thermal conductivity were achieved, the presence of macropores over 70 nm in all samples hindered further reduction. Most of these macropores and cavities were non-detectable in the physisorption experiments but visible in SEM.[275, 276] The values presented here were slightly higher than others obtained in the literature for the same synthetic method, in the range of 30 mW m^{-1} K^{-1} to 32 mW m^{-1} K^{-1}.[57, 166, 170]
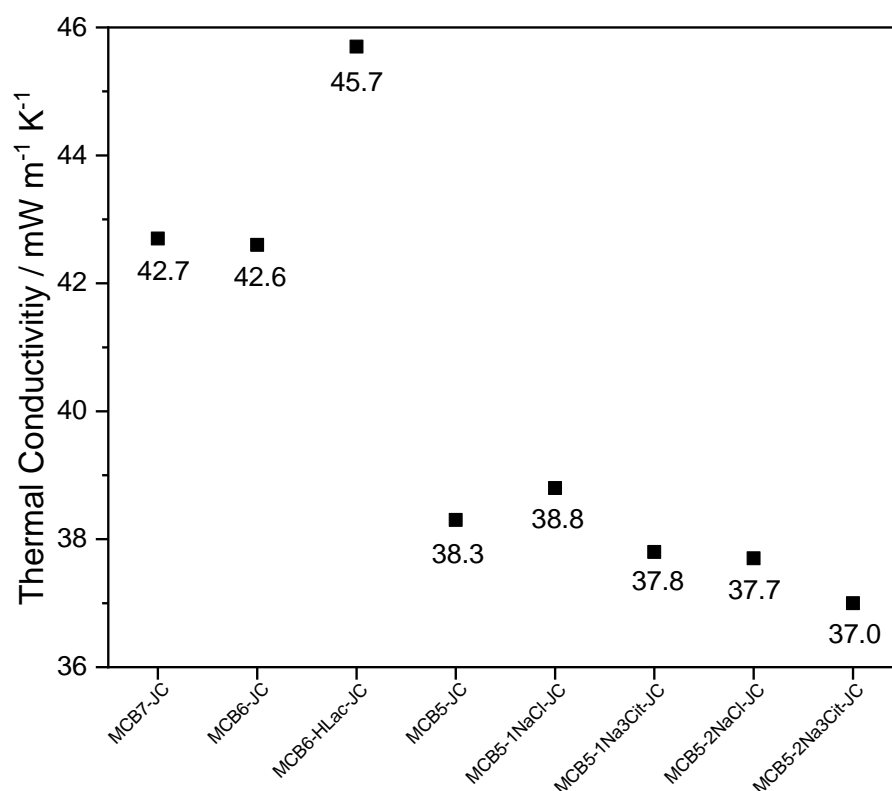
Figure 79 Thermal conductivity of commercial cellulose aerogel beads produced at technical scales, using the JetCutter$^{®}$ (JC), from cellulose solutions of different concentrations without the addition of salt (from 5 wt.-%, to 7 wt.-%) and coagulated in different acids (acetic acid and lactic acid). Some samples were synthesized from 5 wt.-% cellulose solutions to which salts were added (NaCl and Na$_3$Cit) in different concentrations (1 wt.-% and 2 wt.-%) before gelation.

Nonetheless, the conditions of the analysis influenced these results, such as the temperature, atmospheric pressure, altitude at which the measurement was performed, and moisture of the samples.[232] Besides, the different measurement methodologies used in multiple publications

hindered an accurate comparison between results, especially when some methods provide less accurate results, such as the use of Hot-Disk.[231, 233] Recently, Malfait et al. reinforced the need to analyze critically the thermal conductivity results presented in the literature. Regarding biobased aerogels, the authors affirmed that values obtained between 27 mW m^{-1} K^{-1} to 32 mW m^{-1} K^{-1} were unlikely considering that no commercial alternative was available with a thermal conductivity below 36 mW m^{-1} K^{-1}.[236]

Multiple recipes were conducted at technical scale, and the properties of the aerogels synthesized were similar. The thermal conductivity of the standard recipe (MCB7-JC, 42 mW m^{-1} K^{-1}) could be reduced to 37 mW m^{-1} K^{-1} through the reduction of the concentration of cellulose alongside the addition of salt to the cellulose solution before gelation. The addition of salt increased the surface tension of the droplets and preserved their spheroid shape when they entered into the coagulation bath. The induced changes in the pore size distribution of the aerogels were not enough to reduce the presence of macropores and further improve the thermal conductivity of the samples.

4.5 Manufacturing of Cellulose Aerogel Sheets

The 7 wt.-% MC solution had the appropriate viscosity for the upscaling in the CAProLi (0.30 Pa.s) as it was viscous enough to maintain its shape after the first flattening roll, but was not so viscous that it would stick to it. The viscosity was reduced with an increasing shear rate, especially at a higher cellulose concentration. The hemp-extracted cellulose used in this chapter has a higher DP compared with previous experiments. As the 3 wt.-% HC solution had a viscosity closer to the 7 wt.-% MC solution, was selected to be used in the CAProLi. **Table 14** shows the viscoelastic properties of the solutions chosen for upscaling.

Table 14 Viscoelastic properties of the cellulose solutions, from commercial (MC) and hemp-extracted celluloses (HC), selected for upscaling in the CAProLi.

Celluloses	Concentration / wt.-%	Viscosity / Pa·s	Gel point / s	Gel point after addition of 2 wt.-% NaCl / s	Storage modulus (140 s) after addition of 2 wt.-% NaCl / Pa
MC	7	0.30	483.3	0	47.2
HC	3	0.63	8.1	0	56.6

The MC solution reached the gel point after 483.3 s, which was too late for the solution to be used in the CAProLi. The time limit for the stable gel body creation was 140 s, as the conveyor belt could not run at a lower velocity. The hemp cellulose solution achieved the gel point after 8.1 s, a value within the 140 seconds range, but faster gelation was advisable. The addition of sodium salts was tested in **Chapter 4.3.1** and it was found that adding 2 wt.- % NaCl to an MC solution achieved an almost immediate gel point (0 s), faster than if other tested salts were added. These latter gel points were recorded after the cellulose solutions application in the rheometer/CAProLi. The liquid solutions could still be manipulated just after the dissolution of salts. As shown in **Table 14**, when 2 wt.-% NaCl was added to both solutions, and the gel point was reached before measurement. Therefore, after adding salt, all cellulose solutions showed suitable properties for upscaling. By comparing the storage modulus (G´) of the different gels after 140 s, both had a similar gel strength. A higher G´ resulted in a stronger gel body.[299] Monoliths were prepared from these solutions, and their shrinkage increased along the processing steps, especially during neutralization and drying, as shown in **Figure 80**.

Figure 80 Shrinkage of cellulose aerogels monoliths synthesized from a 7 wt.-% commercial cellulose solution (square for MCM7) and a 3 wt.-% hemp-extracted cellulose solution (circle for HCM3), without and after addition of 2 wt.-% NaCl (black for solutions without salt and red for solutions with salt).

Results and Discussion

The final shrinkage was 49% for MCM7 samples and 57% for HCM3 samples, with no influence from the salt's addition, as observed in previous chapters. The higher shrinkage for HCM3 samples was due to their lower cellulose concentration. The fibrillar network was less compacted, making it more prone to osmotic pressure during neutralization, solvent exchange, and drying.

The skeletal density of the aerogels remained stable at 1.52 g cm^{-3}, which was within the range of values found in the literature [68, 69]. **Table 15** shows the envelope densities of the different monolithic cellulose aerogels. HC samples had the lowest envelope density (0.11 g cm^{-3}) compared to the 0.16 g cm^{-3} to 0.17 g cm^{-3} found for the MC monoliths, with the addition of the salts playing no role in that property. This lower density was due to their lower cellulose concentration. The same trend had been observed for cellulose aerogels in other studies[298, 300]. The porosity range of the monolithic samples was between 88.96% and 93.79%, corresponding to the values found in the literature. [162].

Table 15 Properties of cellulose aerogel monoliths synthesized from a 7 wt.-% commercial cellulose solution (MCM7) and a 3 wt.-% hemp-extracted cellulose solution (HCM3), without and after addition of NaCl, at laboratory scale. The properties of the respective sheets (S) produced at technical scale, using the CAProLi are also found. Information on the specific surface area and total pore volume of the aerogels is presented later.

Samples	Volume Shrinkage / %	Envelope Density / g cm^{-3}	Porosity / %	Average Pore Size / nm
MCM7	49.40 ± 4.10	0.17	88.96	14.67
MCM7-2NaCl	48.82 ± 0.91	0.16	89.54	17.42
HCM3	57.20 ± 2.03	0.11	92.79	15.65
HCM3-2NaCl	56.74 ± 1.58	0.11	92.68	14.76
MCS7-2NaCl	-	-	-	21.51
HCS3-2NaCl	-	-	-	14.66

The samples synthesized with the CAProLi were investigated with SEM as their monolithic correspondents. **Figure 81** shows the MC and HC samples. All showed the typical randomly arranged 3D fibrillar network for cellulose aerogels.[35, 76] The MC monolithic sample presented bigger pores and cavities than its sheet correspondent. The hemp samples showed

fibrillar structures but with considerably longer fibrils compared to the MC sample´s fibers. This indicated a higher DP for HC. The differences between the sheet and monolith samples obtained from the same cellulose solution were due to the geometry of the gel body. A thinner sheet had a faster gelation in comparison with the monolith and, consequently, the cellulose fibers had different rates of reorganization as a fibrillar network. For hemp samples, as the cellulose concentration was low, the structures were similar, having large cavities and thin pore walls.
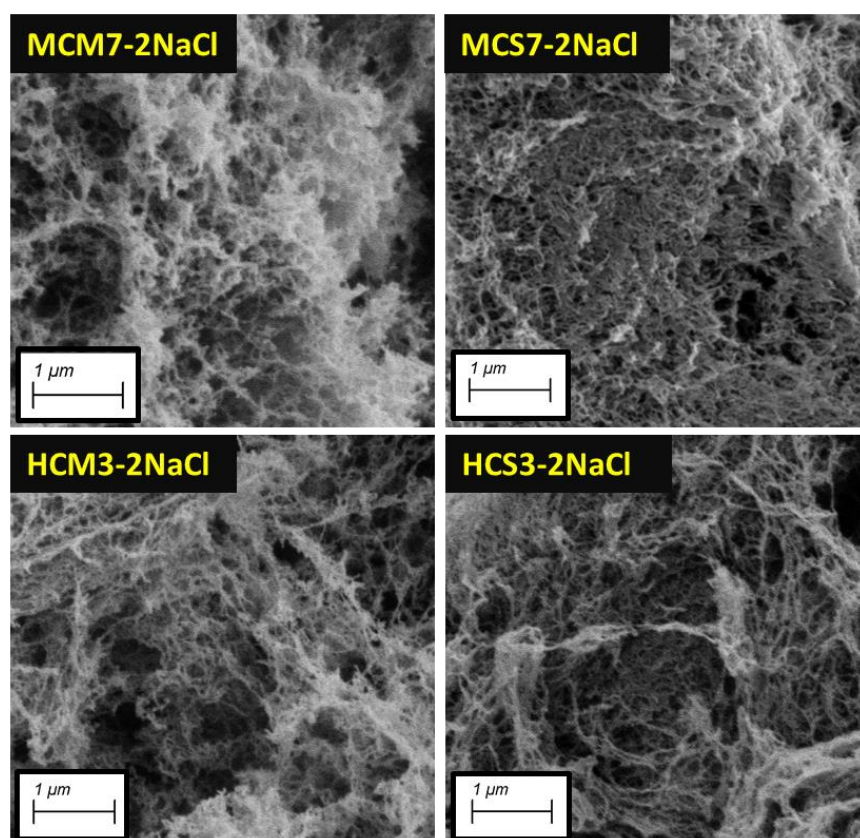
Figure 81 SEM pictures of the interior surface of cellulose aerogels produced from 7 wt.-% commercial cellulose solution (MCM7) and a 3 wt.-% hemp-extracted cellulose solution (HCM3) in the form of monoliths at laboratory scale and sheets (MCS7 and HCS3, respectively), produced at technical scale using the CAProLi. Before gelation, 2 wt.-% NaCl was added to their cellulose solutions.

The isotherms for these polysaccharide aerogels corresponded to a type IV shape, typical of mesoporous materials.[237] Regarding the specific surface area, present in **Figure 82**, MCM7 had 259 m^2 g^{-1} while HCM3 had a specific surface area of 204 m^2 g^{-1}. Looking at the influence of the 2 wt.-% NaCl, its addition increased the surface area of the MCM7 to 308 m^2 g^{-1}. The same effect was observed for the HCM3-2NaCl sample, whose specific surface area increased

to 216 m^2 g^{-1}. This had been observed previously in this work and the literature.[114] The comparison of the monolithic samples with the sheet samples shows a decrease in specific surface area from MCM7-2NaCl to MCS7-2NaCl while the opposite occurred for the hemp samples. Changes in the specific surface area between the monolith and sheet samples were explained by different geometry and gelation kinetics. In the CAProLi, a stronger acid was used to induce gelation, at a higher concentration (20 vol.-%). Combining these two factors, a faster gelation occurred which resulted in the formation of a different morphology. Additionally, inhomogeneities in the distribution of cellulose and salts contributed to the different results found between the sheet and monolith shapes for the same recipe.
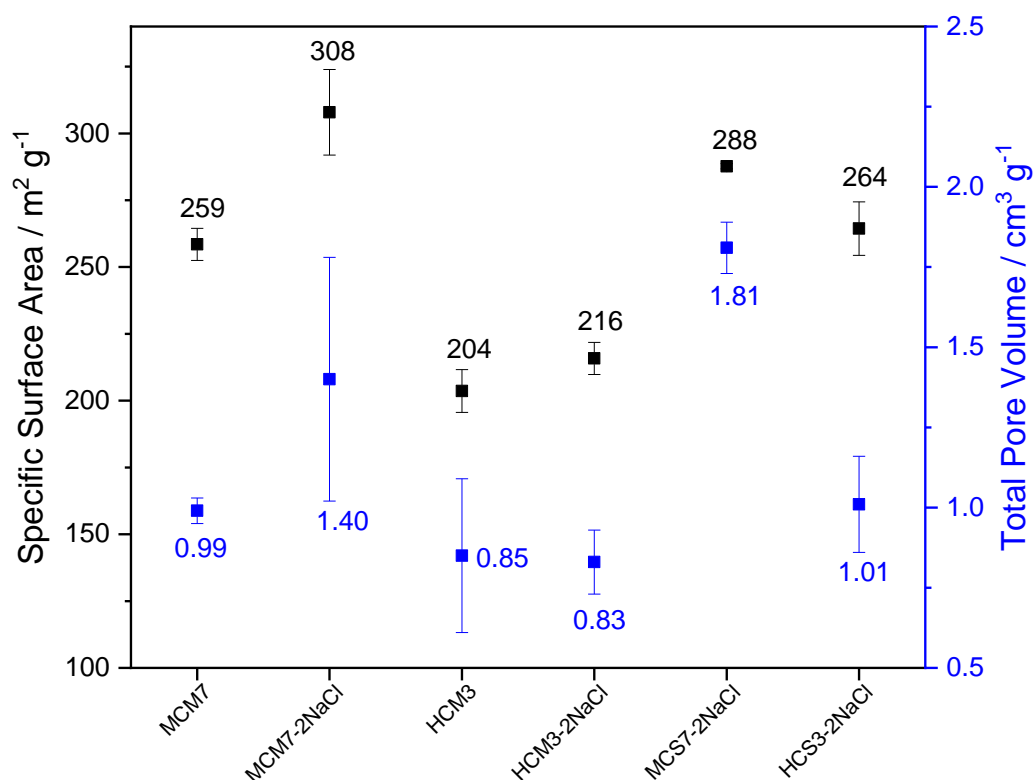
Figure 82 Specific surface area and total pore volume of cellulose aerogels synthesized from commercial (MC) and hemp-extracted cellulose (HC) solutions, without and after addition of 2 wt.-% NaCl, at different scales (monoliths synthesized in laboratory, M, and sheets synthesized at technical scale with the CAProLi, S).

In **Figure 83**, the pore size distribution of these samples is represented. Most pores were mesopores between 10 and 50 nm and macropores (especially for MCM7-2NaCl).
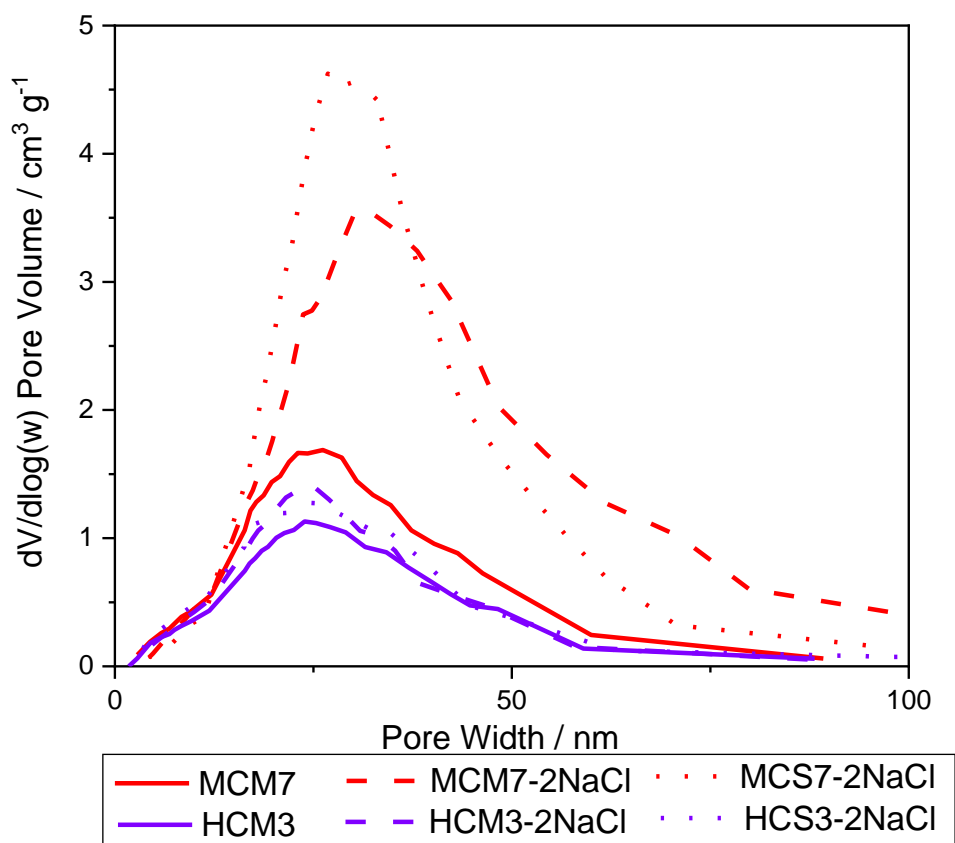
Figure 83 Pore size distribution of cellulose aerogels produced from different cellulose solutions (red for 7 wt.-% commercial cellulose, MC, solution, and violet for 3 wt.-% hemp-extracted cellulose, HC, solution), without (solid line) and after addition of 2 wt.-% NaCl, at different scales (dashed line for monoliths synthesized in laboratory, M, and dotted line for sheets synthesized at technical scale with the CAProLi, S).

The influence of the addition of 2 wt.-% NaCl to MCM7 had been discussed previously. Compared to the MCM7-2NaCl, MCS7-2NaCl showed a higher, sharper pore size distribution peak between 30 nm and 40 nm. This indicated an increase in the proportion of mesopores with medium size and a decrease in the presence of macropores. The pore size distribution of HCM3- 2NaCl and HCS3-2NaCl was similar, with a slight increase in pore volume for the latter at around 25 nm. The HCM3 sample had a smaller quantity of mesopores compared to HCM3- 2NaCl and HCS3-2NaCl. The addition of salt increased the proportion of mesopores in the aerogel. The upscaling of the HC recipe did not affect the pore size distribution of the synthesized aerogels while, for the MC recipe, the proportion of macropores was reduced. For the monolithic samples, the average pore width ranged from 14.67 nm to 17.42 nm, meaning there was no significant change when NaCl was added. For the sheets, the average pore width was higher for MCS7-2NaCl than for HCS3-2NaCl (21.51 nm vs. 14.66 nm, respectively), due

to higher shrinkage in the case of the hemp samples which had a lower cellulose content. Differences between sheet and monolith shapes were attributed to different gelation kinetics and inhomogeneities in cellulose and salt distribution.

Aerogel sheets of hemp cellulose were successfully produced using the CAProLi device. Despite being possible to continuously produce cellulose gel sheets, these had a thickness of < 0.3 mm, and therefore the recipes have to be optimized to achieve a faster gelation of the gel body with a higher thickness. Additionally, this would improve the strength of the gel, considering that the gel bodies obtained in this work presented some frailty. It was shown that the hemp cellulose had the highest porosity (93%). The specific surface area of the hemp cellulose aerogel sheets showed values comparable to the sheets obtained using MC. Total shrinkage for all cellulose aerogels was over 50%, which has to be considered in future dimension planning of the hemp cellulose sheets. Adding salt reduced the gelation time and increased the specific surface area. The gelation time reduction made it possible to use a lower cellulose concentration in the MC and the hemp cellulose, achieving stronger gel bodies in a shorter period. Coagulation kinetics were different depending on the geometry of the wet gels, causing differences in their aerogel structures. To improve the recipe for the usage in the CAProLi, a higher amount of hemp cellulose should be tried in combination with 2 wt.- % of NaCl. For operating with thicker solutions, it is recommended to use pressure and a slit die nozzle to pour the cellulose solution on the conveyor belt of the CAProLi. This work was a promising starting point for the technical continuous production of cellulose aerogel sheets and the introduction of the aerogel technology to a wider range of industry players. Additionally, the aerogels made of extracted hemp cellulose showed comparable properties to the aerogels made of commercial cellulose, indicating that agricultural wastes have the potential to be used as appropriate resources for aerogel production.

4.6 Manufacturing of Cellulose Aerogel Engineered Fibers

The cellulose aerogel fibers synthesized were white as shown in the representative **Figure 84**. The diameters of the fibers were not constant across their length due to the stick-slip effect inside the nozzle. Occasionally, while the fibers were drawn continuously, the fibers became thinner or thicker due to small mass fluctuations of cellulose in the solution. This variation in their diameter induced uncertainty in determining the average diameter and consequent density and porosity. For the porosity calculations, a value of 1.5228 g cm^{-3} was used as skeleton density.

4.6 Manufacturing of Cellulose Aerogel Engineered Fibers
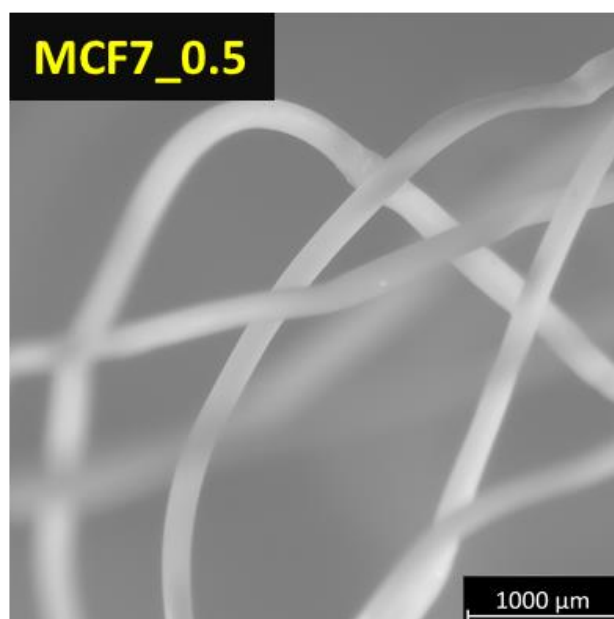
Figure 84 Optical microscope picture of a fragment of a 7 wt.-% commercial cellulose aerogel fiber (MCF7) synthesized using a 0.5 mm nozzle.

The envelope density ranged from 0.22 g cm^{-3} to 0.39 g cm^{-3}, as shown in **Table 16**. The values of porosity ranged from 74.10% to 85.40% and were slightly lower than the values found for other cellulose aerogels in the literature.[27, 36] An increase in cellulose concentration increased the fiber density for MCF samples, while the nozzle diameter was not a relevant factor. The increase in density led to a decrease in porosity.

Table 16 Properties of cellulose aerogel fibers synthesized from commercial (MCF) and hemp-extracted cellulose (HCF) at different cellulose concentrations (6 wt.-% to 7 wt.-%) and nozzle diameters (0.5 mm and 0.33 mm). Information on the specific surface area and total pore volume of the aerogels is presented later.

Sample	Fiber Diameter / mm	Diameter Shrinkage / %	Envelope Density / g cm^{-3}	Porosity / %	Average Pore Size / nm
MCF6_0.5	0.32±0.02	36.36	0.22	85.40	17.64
MCF7_0.5	0.40±0.01	19.57	0.39	74.10	19.09
MCF7_0.33	0.34±0.01	-3.59	0.35	77.04	17.38
HCF6_0.5	0.32±0.01	36.37	0.39	74.69	16.48
HCF7_0.5	0.34±0.01	32.36	0.31	79.36	16.67
HCF7_0.33	0.29±0.01	13.42	0.30	80.28	13.24

Results and Discussion

While the nozzle did not influence the porosity and density of the HCF7 samples, the increase in cellulose concentration decreased density. The reason for this discrepancy lies in the different molecular weights of the celluloses.

When the cellulose solution was introduced as a filament into the acidic bath, it coagulated into a stable gel. The speed of coagulation, the concentration and molecular weight of cellulose, as well as the dissolution media, determined the internal properties of the gel. During this process, shrinkage was observed, due to the osmose forces applied from the reactants outside and inside the filament. When the concentration of HC increased, these fibers interacted more with themselves and a network was more easily created than with MC´s smaller fibers. Due to the speed of coagulation, a stable less-organized structure with bigger pores was created, inducing a lower density and higher porosity. For MCF samples, the increase in cellulose concentration created a denser structure. These discrepancies originated from the measurement of the dimensions as well. As shown in **Figure 84**, the diameter of the fiber was not constant across its length. Drying separate straight segments of the fibers, and not of the entire coiled fiber sample, could provide more accurate results. For both celluloses, shrinkage was reduced when the nozzle´s diameter was lower as less osmose pressure was applied to the filament. Due to the small diameters of the nozzles, the reduction of shrinkage only slightly influenced the density and porosity of the cellulose aerogel fibers. A negative shrinkage was observed for MCF7_0.33, indicating swelling of the fiber. The organization of the pores in the aerogel fibers was studied using SEM and some representative pictures can be observed in **Figure 85**. The surface presented densely packed cellulose fibers, especially at a lower nozzle diameter. While at 0.5 mm, bigger macropores were observed in a reticulated surface, at 0.33 mm, the fibers were more packed on a smoother, more homogeneous surface with visible bigger pores. No significant influence was observed from the source of cellulose and cellulose concentration. As there existed polymer-rich and polymer-poor regions in the filament, different diffusion rates were present in the fiber gelation which explained different packaging on their surface.[43] When the fibers were thinner, coagulation was faster, a stable gel was more easily obtained and their surface densified while the fibers remained in the coagulation bath. For the same pumping speed, a thicker fiber would need more time to achieve a similar level of coagulation and sturdiness. The application of the same pumping speed to fibers whose diameters were not the same influenced their surface.
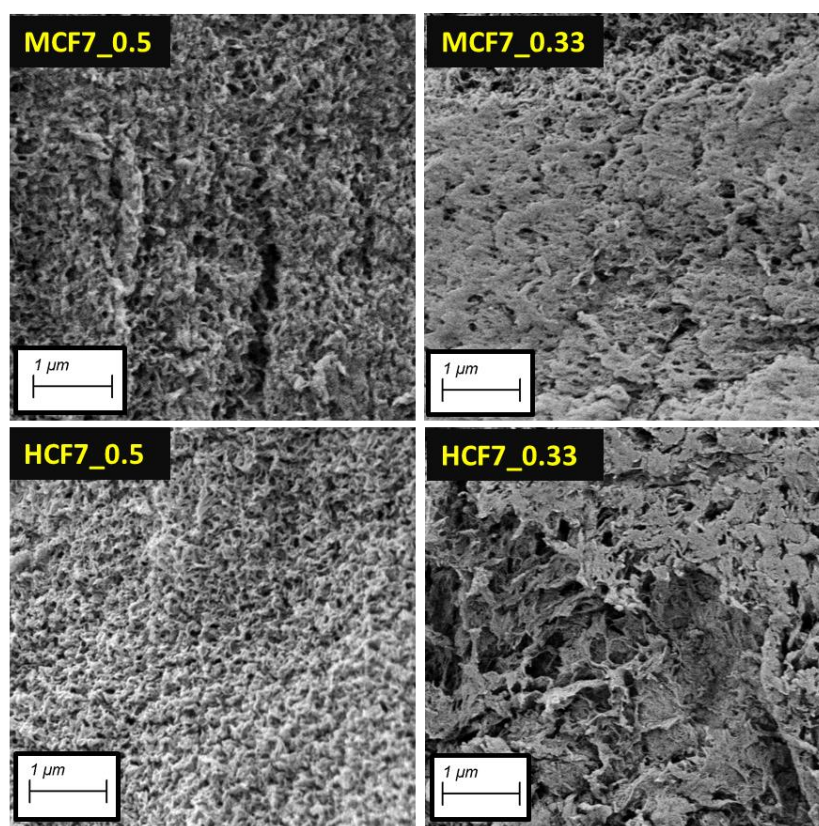
Figure 85 SEM pictures of the exterior surface of cellulose aerogel fibers synthesized from 7 wt.- % commercial (MCF7) and hemp-extracted cellulose (HCF7) solutions using different nozzle diameters (0.5 mm and 0.33 mm).

The structures in the interior, however, were less compact. It was visible a large variety of pores and cavities from the macroscale to the nanoscale, while the random fibrillar network was more dispersed into thinner walls. These can be observed in **Figure 86**. These differences between the surface and interior of the fibers were related to the coagulation speed. On the surface, the fast coagulation of cellulose fibers created a network whose fibrils continued to merge and aggregate after the first contact with acid. This aggregation into a mesh-like structure with fewer macropores was more notorious when the 0.33 mm nozzle was used.[107]A slower regeneration inside the fibers enabled a higher organization of the microfibrils into a dense 3D porous network, with smaller and more numerous pores. The cavities in the samples originated from the presence of bubbles in the cellulose solution and the stick-slip effect.[82] Another reason could be the very fast regeneration of cellulose fibers. As discussed in **Chapter 4.3.2**, bigger pores were observed for beads coagulated in HCl acid than in organic acid baths due to faster gelation. As the diameter of the aerogel fibers was lower than that of the beads (0.33 mm to 0.5 mm vs. 3 mm), the former had a faster gelation. Under these conditions, there was not enough time to achieve a higher compaction of cellulose and to create a porous network with

smaller, more numerous pores.[107]
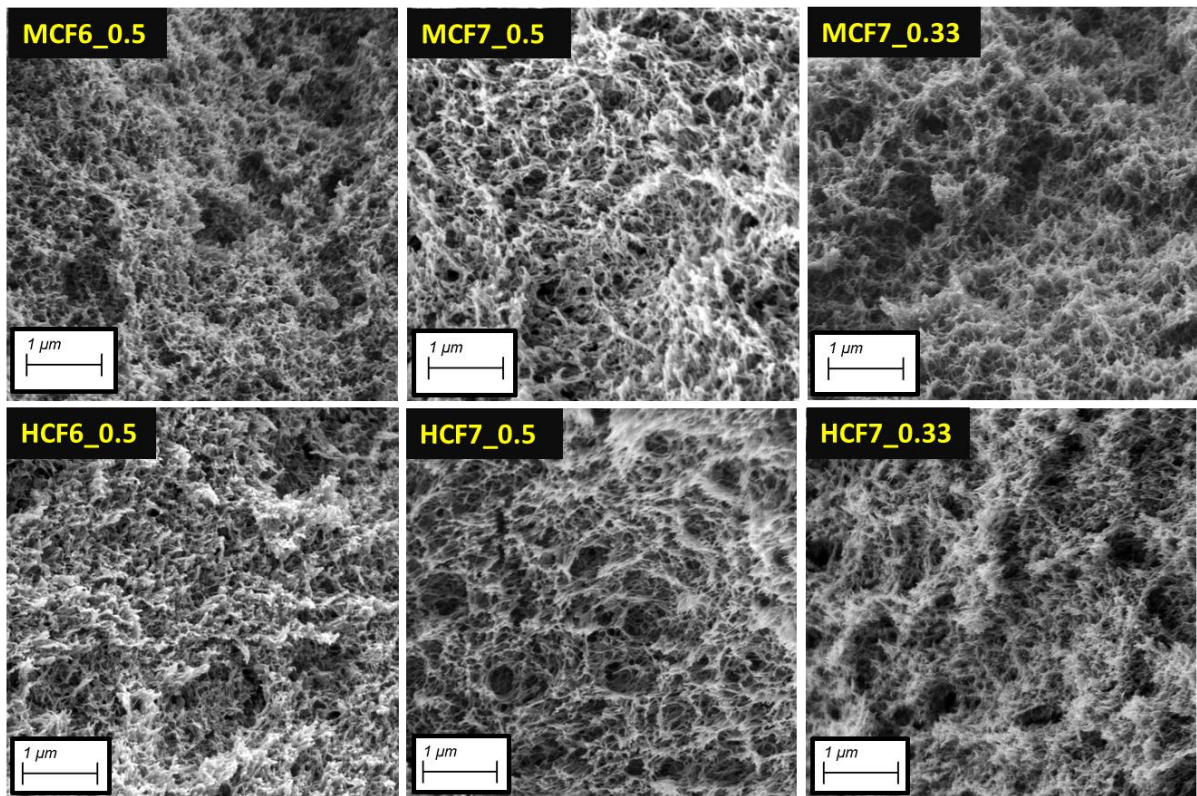
Figure 86 SEM pictures of the interior surface of cellulose aerogel fibers synthesized from commercial (MCF) and hemp-extracted cellulose (HCF) solutions of different cellulose concentrations (6 wt.- % and 7 wt.-%) using different nozzle diameters (0.5 mm and 0.33 mm).

This influenced the specific surface area and pore size distribution of the aerogel fibers. Each sample had different adsorption capacities but all were classified as type IV isotherms, as described by IUPAC (see in the appendix **Figure 128**).[44] The adsorption capacity of all samples was similar, except MCF7_0.5, whose capacity was higher. All hystereses could be considered H2(b) while some samples had sharp peaks before their desorption plateau. These could be related to the presence of non-filled macropores that were produced during spinning due to the presence of bubbles in the cellulose solution. **Figure 87** shows their influence on the specific surface area and total pore volume of the samples.
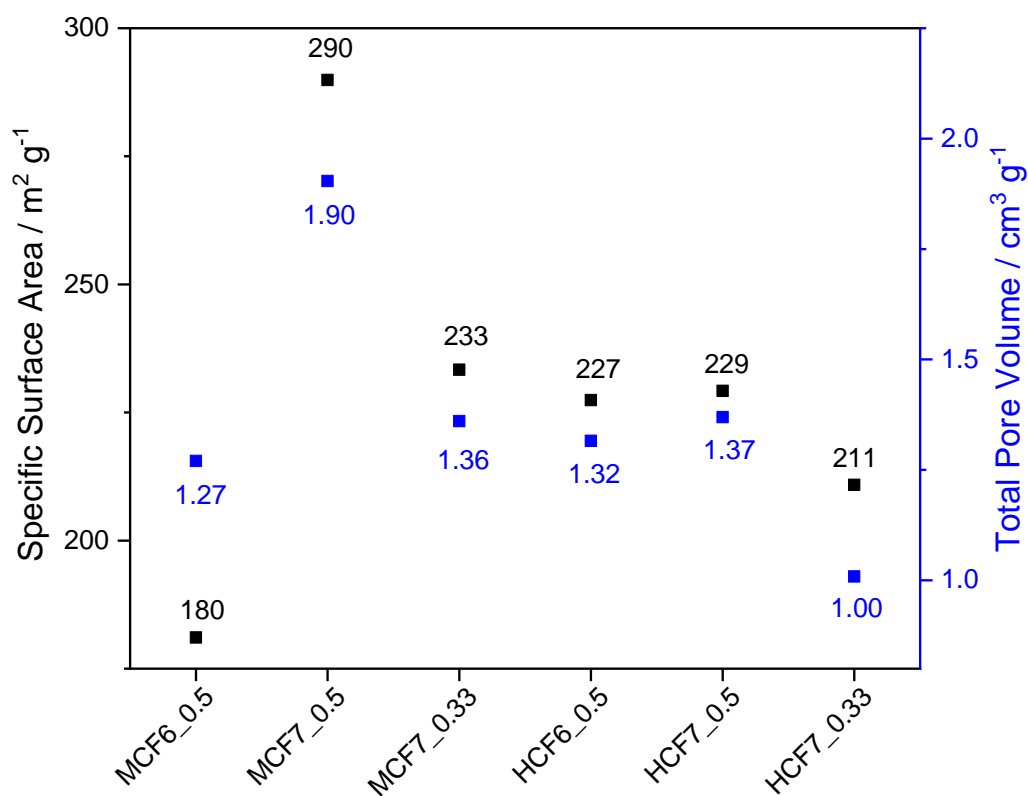
Figure 87 Specific surface area and total pore volume of cellulose aerogel fibers synthesized from commercial (MCF) and hemp-extracted cellulose (HCF) solutions of different concentrations (6 wt.- % and 7 wt.-%) using different nozzle diameters (0.5 mm and 0.33 mm).

There were no significant differences in the specific surface area and total pore volume between most aerogel fibers, independently of the cellulose used or other parameters. The surface areas ranged from 180 m^2 g^{-1} to 290 m^2 g^{-1} (slightly higher than the values recorded for cellulose aerogel fibers in literature)[191-193] while the total pore volumes were found between 1.00 cm^3 g^{-1} and 1.90 cm^3 g^{-1}. For both cellulose sources, a lower diameter led to decreases in specific surface area and total pore volume due to the promotion of faster coagulation.[107] When cellulose extracted from hemp was used, the increase in concentration did not affect the specific surface area. This was observed in previous studies on cellulose aerogels.[47] However, this was not the case for MCF6_0.5 and MCF7_0.5. MCF7_0.5 had a higher specific surface area and total pore volume than MCF6_0.5 due to its lower porosity. MCF6_0.5 had a higher porosity and lower density due to existing bigger pores. By increasing the cellulose content, MCF7_0.5 achieved a more packed, denser structure with smaller and more numerous pores, resulting in a higher specific surface area and pore volume. The low thickness of the gel

fiber could have led to a too-fast regeneration and the formation of a structure whose specific surface area was not maximized. This was observed when the HCl acid bath was used as a coagulation bath for bead production compared to when organic acids were used, in **Chapter 4.3.2**. Using smoother coagulation baths such as mixtures of ethanol, isopropanol, or acetone with water could create coagulants with Hansen parameters closer to the one from the cellulose solution and improve the fiber´s properties.[106, 195] These promote a slower regeneration but attention should be taken so it is fast enough to create a stable-shaped fiber prone to spinning. To better understand these trends, the pore size distribution of the samples is shown in **Figure 88**.

For all the samples, most pores were in the mesoporous region with a smaller fraction in the macroporous region. This agreed with the mesoporous character of cellulose aerogels found in other studies.[162, 191, 288] An increase in cellulose concentration, for both MC and HC, led to a sharpening of the pore size distribution curve due to creating a more intertwined cellulose network and increasing the proportion of smaller pores. A similar trend occurred when the diameter of the fiber was reduced from 0.5 mm to 0.33 mm. While a shoulder at 30 nm was visible for MCF7_0.33 and HCF7_0.33, the fraction of macropores was smaller which induced a smaller average pore size (from 19.09 nm to 17.38 nm for MCF7 and from 16.67 nm to 13.24 nm or HCF7). Depending on the processing parameters, it was possible to tune the pore size distribution of the samples. Besides, the hemp samples presented sharper distributions, with smaller pores, than their MC counterparts possibly due to the effect of different molecular weights and cellulose solution viscosities.
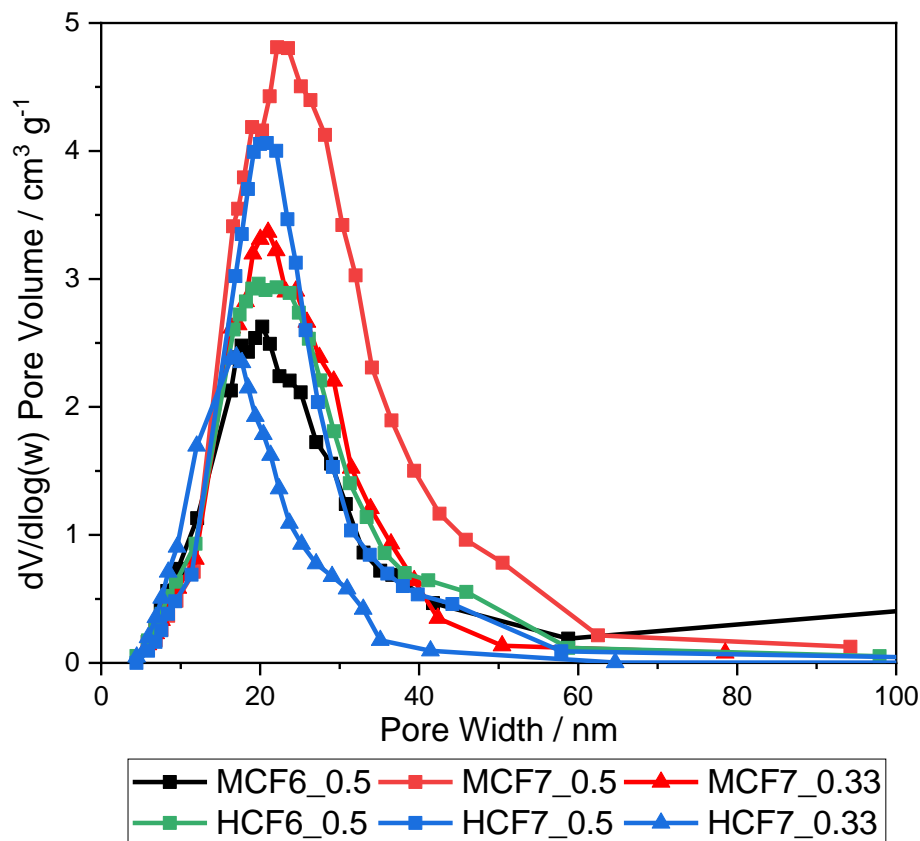
Figure 88 Pore size distribution of cellulose aerogel fibers produced from commercial (black for 6 wt.-%, MCF6, and red or 7 wt.-%, MCF7, cellulose concentration) and hemp-extracted cellulose (green for 6 wt.-%, HCF6, and blue for 7 wt.-%, HCF7, cellulose concentration) with different nozzle diameters (square for 0.5 mm and triangle for 0.33 mm).

Aerogel cellulose fibers were successfully synthesized and the same parameters could be applied to both HC and MC cellulose solutions. The produced fibers were highly porous and had low densities, with specific surface areas ranging from 180 m^2 g^{-1} to 290 m^2 g^{-1} and small average pore sizes (from 13 nm to 19 nm). Parameters such as pumping speed and fiber diameter did not affect the crystallinity or thermal profile of the aerogels while a higher cellulose concentration and smaller fiber diameter led to sharper pore size distributions, with higher content of smaller mesopores. Coagulation mechanisms and rates were essential in determining the aerogel's final properties. No significant differences were detected between the aerogel fibers produced from MC or HC, which indicated the suitability of using waste agriculture residues as a source of cellulose to produce aerogels. This further contributed to the promotion of a biobased circular economy and the industrial application of this technology.

4.7 Lignin Coating of Cellulose Aerogels

In the previous chapters, the aerogels synthesized, regardless of their shape, were highly porous and had high specific surface areas. However, cellulose aerogels are sensitive to moisture, which can destroy their porous structure due to hornification and negatively affect their thermal insulation properties in the long term.[23, 301] As discussed, lignin has been used as a hydrophobic additive.

4.7.1 Moisture Influence

Table 17 shows the changes in diameter and bulk density that occurred to a set of cellulose aerogel samples before (a) and after humidity exposure for 24 h, under an atmosphere with high humidity of 63% (b). These included 2 wt.-% flax-extracted cellulose beads (FCB2), 6 wt.-% hemp-extracted cellulose beads (HCB6) and 7 wt.-% commercial cellulose beads synthesized at laboratory and technical scale, using the JetCutter® (MCB7 and MCB7-JC respectively).

Table 17 Influence of moisture on the bulk density and diameter of representative cellulose aerogel beads before (a) and after exposure in a climate chamber (63% humidity, 24 h) on the bulk density and diameter of representative cellulose aerogel beads (b).

Samples	Bulk Density[a] / g cm^{-3}	Diameter[a] / mm	Bulk Density[b] / g cm^{-3}	Diameter[b] / mm
FCB2	0.06	2.35 ± 0.10	0.08	2.11 ±0.10
HCB6	0.12	3.08 ± 0.20	0.18	2.33 ± 0.40
MCB7	0.15	3.28 ± 0.10	0.22	2.52 ± 0.07
MCB7-JC	0.13	0.85 ± 0.09	0.23	0.69 ± 0.06

Under the tested conditions, water adsorbs on the exterior and interior surfaces of the beads primarily through surface diffusion.[302-304] Water molecules form hydrogen bonds with the OH functional groups available in the amorphous regions of the cellulose fibers, creating a monolayer after saturation of the interaction sites (non-freezing bound water).[305] Water can still be absorbed and create clusters in microvoids, that are trapped (freezing-bound water) inside the aerogel´s porous structure.[303, 306] Free water, under heating, is the first set of water molecules to evaporate, followed by freezing and non-freezing water (according to increasing enthalpies).[303, 307] Initially, water interacts with the cellulose network by

breaking the hydrogen bonds between cellulose fibers and swelling the beads. When water is removed by heating, these newly formed hydrogen bonds are broken, leading to an increase in the interaction between the cellulose fibers and a relaxation of the porous structure. This causes the densification of the pore walls, the shrinkage of the aerogel, and the consequent decrease of its share of mesopores and its specific surface area.[301, 308]

Densification and shrinkage were observed for the tested samples, especially those synthesized from hemp-extracted and commercial celluloses. This was due to their lower molecular weight compared with flax-extracted cellulose. Shorter fibers have fewer points of contact between them and resist worse against shrinkage, even at a higher concentration, compared to longer fibers.[240] Besides, flax beads could have absorbed less water due to their lower content in cellulose and lower number of OH groups available to interact with water molecules. The production scale did not influence these properties.

It was concluded that cellulose aerogels were prone to shrinkage under a humid atmosphere and coating was required to induce anti-moisture properties. Lignin was tested as a coating agent. Manich et al. noted that not only did the presence of lignin in hemp fibers reduce water primary absorption, but water adsorbed to lignin was also more easily removed than water bonded to cellulose.[309]

4.7.2 Chemical Interaction of Lignin with Wet Cellulose Gel

To effectively coat cellulose wet gel beads with lignin, it was essential to understand the chemistry behind the interaction between these two biopolymers. Two types of lignin were studied for this effect: Kraft lignin (Indulin AT, In) and soda lignin (P1000, P1), whose main properties are described in **Table 18**.

Results and Discussion

Table 18 Main chemical properties of Indulin AT (Ind) and P1000 (P1). Values with no references were obtained from the technical sheets of the products.

Lignin	Class of Lignin	Density / g cm^{-3}	Mw / g mol^{-1}	Particle Size Distribution / median, μm	OH$_{ph}$ / mmol g^{-1}	OH$_{al}$ / mmol g^{-1}	OH$_{ac}$ / mmol g^{-1}
Indulin AT (Ind)	kraft	0.4	3500-6096[140, 142, 310]	60[311]	2.1-4.1[140, 312]	2.27[313]	0.4[313]
P1000 (P1)	soda	0.3	2200-4000	65	2.7-3.1	1.8-2.1	0-1.2

The process used to obtain soda lignin was similar to the one used in this work for cellulose isolation from hemp and flax bast waste fibers, so it would be possible to extract soda lignin from those fibers. Kraft lignin is the most commonly available lignin in the market.[125, 141] **Figure 89** shows the amorphous structure of both Indulin AT and P1000 at the microscale.
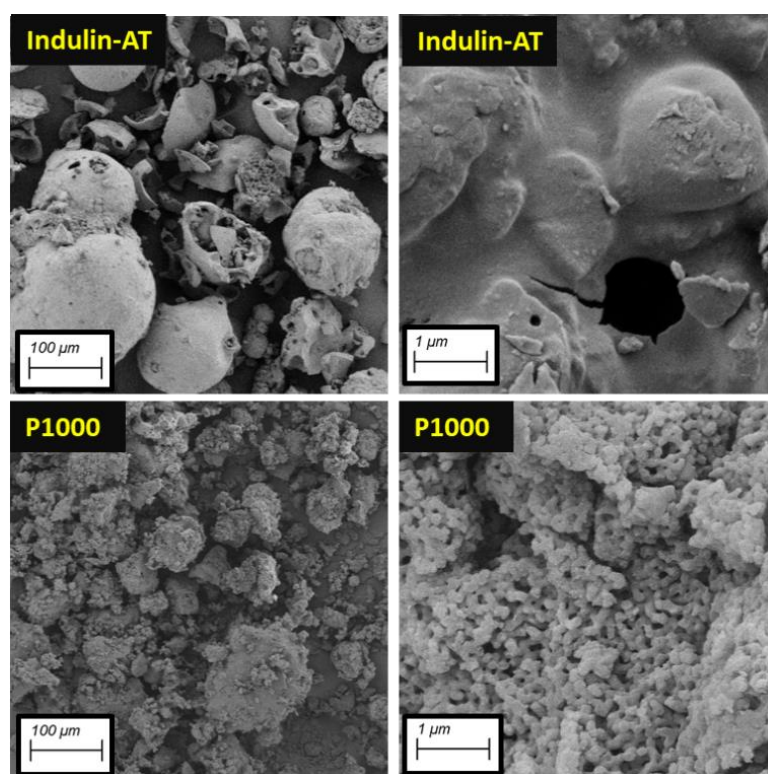
Figure 89 SEM pictures of Indulin AT and P1000 lignin at different magnifications.

Indulin-AT was composed of spheroid particles and fragments with smooth surfaces. At a higher magnification, the surface was a smooth mesh of lignin particles that were too small to be discerned. P1000 was composed of spheroid particles but with irregular surfaces. At 1 μm

scale, lignin globular aggregates were visible and created a rough and irregular surface. The chemical composition of each lignin influenced their aggregation behavior and subsequent morphology.

As shown in **Table 18**, the densities and particle size distribution of the used lignin were similar, but they presented more significant differences in their molecular weight and chemical composition. The M_w of Indulin AT was broader and higher than the one of P1000. While the concentration of OH_{ph} was higher than OH_{al} and OH_{ac} for both lignins, Indulin AT had a broader distribution of OH_{ph} and a higher concentration of OH_{ph} and OH_{al} than P1000. Only for OH_{ac}, P1000 had a higher variation in concentration and reached higher values than Indulin AT. These chemical differences were due to the different biomass sources and respective different chemical extraction processes required to obtain each class of lignin. These chemical compositions influenced how each lignin was dissolved in different media and interacted with the cellulose wet gels.

For the successful lignin adsorption on the cellulose wet gels, lignin should be well dissolved and interact more strongly with cellulose than with the solution media. Otherwise, it would be removed from the wet gel during the solvent-exchange steps. In the first set of experiments, lignin dissolution and adsorption were tested in ethanol:water mixtures. Other solvents could have been used[142] but most of them were not suitable for supercritical CO_2 drying. Goldmann et al. described excellent dissolution capacities of Indulin AT in ethanol:water mixtures, up to 80 wt.- %, (ratio 80:20 EtOH:H_2O, wt.- %).[140]

Important conclusions were drawn from the first set of experiments. When ethanol was selected as the final bath for drying and solvent exchange was performed, much of the lignin attached to the wet gel was leached to the bath. Visually, the beads that had become brownish due to contact with lignin returned to their white color after solvent exchange. It indicated that lignin´s adsorption was not strong enough to counterbalance its association with ethanol. Acetone was used as the final solvent for drying, as leaching was reduced due to the lower solubility of these lignins in acetone compared to the ethanol:water mixture[139, 140, 143]. When P1000 lignin was used, its dissolution in EtOH:H_2O at the tested ratios lignin:cellulose wet gel (L:C, wt.-%) was never complete and a suspension with small particles was observed. Increasing lignin concentration led to more concentrated suspensions and brownish aerogel beads, as shown in **Figure 90**. This showed increasing amounts of lignin adsorbed on the gel´s surface.

Figure 90 Picture of lignin coated 7 wt.-% commercial cellulose aerogel beads (MCB7), produced at technical scale using the JetCutter® (JC) and in a 2M lactic acid solution. Coating was performed with P1000 lignin (P1) after its dissolution in EtOH:H_2O (80:20, vol.-%) bath, at different lignin:cellulose wet gel (L:C, wt.-%) ratios (1:50 for MCB7-JC-P1-80:20-1:50 and 1:5 for MCB7-JC-P1-80:20-1:5).

For Indulin AT, an effective dissolution was observed, as reported by Goldmann et al.[140] When higher concentrations of Indulin AT were added to the EtOH:H_2O solution (L:C rate of 1:5), suspensions were formed and a layer of un-dissolved lignin stayed at the bottom of the baths, with a thickness proportional to the quantity of lignin added in excess.

After brushing the dried coated samples, no powder nor dust was released. This meant that the association by hydrogen bonds between cellulose and lignin, independently of its type, was strong enough to retain the lignin on the aerogel after mechanical stress. When the samples were put in a water bath, they quickly sank to the bottom, indicating that they were not hydrophobic regardless of the lignin used or the conditions applied.

In the second set of experiments, an alkali dissolution method was used. For both types of lignin, dissolution was complete and no particulates were found. For the same lignin concentration, increases in solution volume did not affect lignin adsorption on the wet gels. Some non-attached lignin fragments precipitated when the coated wet gel beads were introduced in acetone but could be removed from the bath.

The water absorption capacity was measured for all dried coated samples to understand the effectiveness of the coating method and the influence of the choice of lignin. The data is displayed in **Figure 91**. L:C ratios could not exceed 1:5, for the same bath volume, when lignin was dissolved in a basic medium. In the NaOH solution, lignin was dissolvable but its neutralization was required to interact and adsorb on the neutral cellulose wet gels. As lignin precipitation depends on the pH and salt concentration of the dissolution medium, an equilibrium was found between NaOH concentration and lignin concentration in the solution.

4.7 Lignin Coating of Cellulose Aerogels

At higher NaOH concentrations, more lignin could be dissolved but its precipitation occurred at higher pH, far from neutrality.[141, 144, 145]
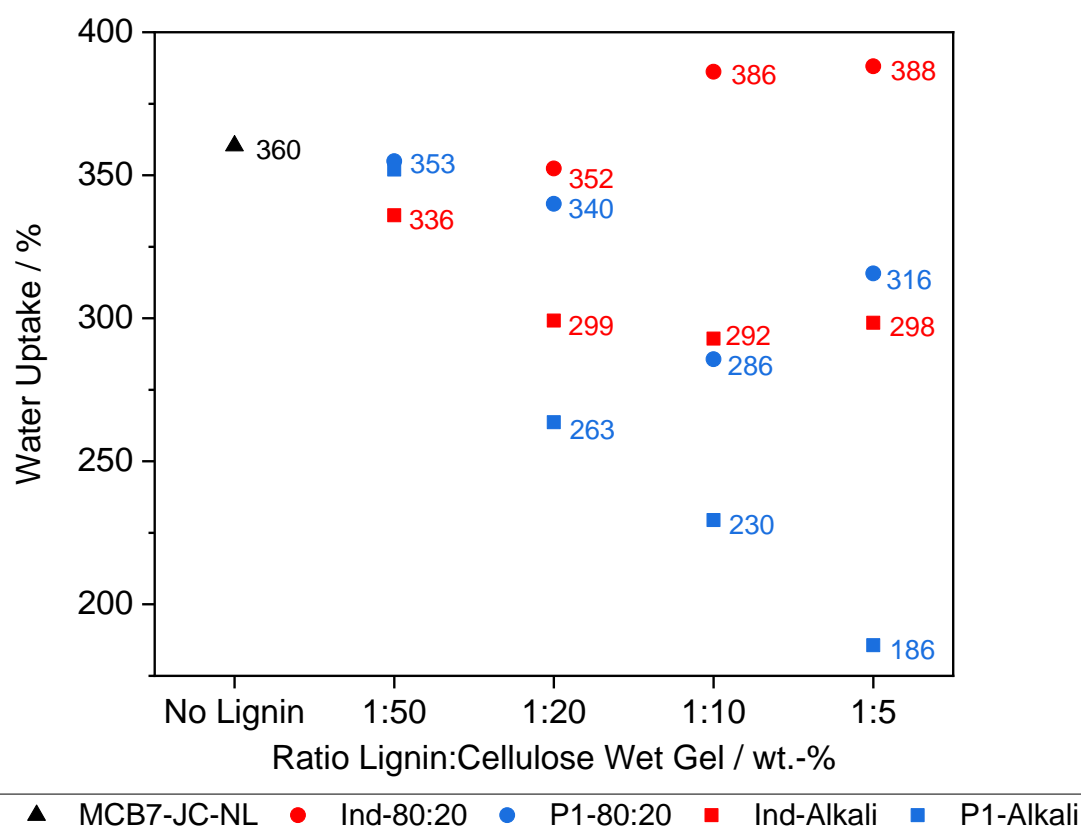
Figure 91 Water uptake of 7 wt.-% commercial cellulose aerogel beads (MCB7), produced at technical scale using the JetCutter® (JC) and in a 2M lactic acid solution, non-coated (black triangle for standard sample, MCB7-JC-NL), and coated with lignin (red for Indulin AT, In, and blue for P1000, P1) dissolved in different baths (circle for ethanol:water bath, 80:20, and square for NaOH bath, Alkali) at different lignin:cellulose wet gel ratios (from 1:50 to 1:5, L:C, wt.- %).

All samples absorbed significant quantities of water (from two to four times their original weight) indicating that some coating recipes promoted resistance to water absorption while not turning the aerogels hydrophobic.

For most series of tests, a minimum water uptake was reached at a certain lignin concentration and it increased for higher L:C ratios. For the 80:20 EtOH:H$_2$O dissolution system, different lignins yielded different water uptake trends. When Indulin AT was used, a minimum of 352% water uptake was reached (lower than the standard 360%) at 1:20, but it increased up to 388% at 1:5. For P1000, a lower water absorption minimum was reached at a higher L:C (286%, 1:10) and later increased to 316%.

This difference was related to the chemical structure of these two lignins and their interaction with the dissolution media. Indulin AT had higher molecular weight, higher OH content in phenolic and aliphatic groups, and a better dissolution than P1000 in EtOH:H_2O media. It was deduced that, as their dissolution mechanics were unequal, the fractions dissolved did not have the same molecular weight or chemical composition. Only the lighter fractions of P1000 were dissolved which, in conjugation with its lower molecular weight, coated more effectively the aerogel´s surface. For Indulin AT, a more uniform dissolution led to an accumulation of bigger particles on the surface of the wet gel without covering it effectively. These agglomerated particles, with more free OH moieties that did not interact with cellulose, easily adsorbed water and contributed to a higher water uptake with increasing lignin concentrations.[309]

Better results were obtained when dissolution occurred in basic media, for both lignins. While for Indulin AT water absorption stabilized after 1:20 and reached the minimum at 1:10 (293%), for P1000, the decrease was proportional to increasing concentrations of lignin. At 1:5, a minimum of 186% water uptake was obtained. Under these conditions, the dissolution was equally efficient for both lignins, so their chemical structure was the relevant factor. The sodium hydroxide water solution completely dissolved the lignin particles due to their charged nature, which remained dissolved after neutralization.[145] This disintegration of lignin microstructures enabled better adsorption on the cellulose wet gel bead surface. For Indulin AT, due to its higher molecular weight, there was a tendency to create agglomerates not homogeneously distributed on the surface of the aerogel. After reaching a minimum water uptake, more lignin and free OH groups adsorbed more water. Furthermore, highly cross-linked condensed units might have ionization resistance due to steric hindrance, as the OH_{ph} from uncondensed (terminal) units would be more easily accessible[312]. It should also be noted that while P1000 has no sulfur, Indulin AT had a 1.4% content in S moieties.[313] This could further hinder its ability to form hydrogen bonds with cellulose and its dissolution efficiency. In the case of P1000, a minimum water uptake was not reached meaning that increasing the lignin content in the bath without precipitation could have achieved better results.

4.7.3 Lignin coated Cellulose Aerogels

Due to achieving the lowest water uptake, only samples coated with the soda lignin P1000 were fully characterized. The aerogel beads became more brownish as more lignin was dissolved during the adsorption phase. For both dissolution approaches and regardless of the lignin content in the adsorption bath, the dimensions of the coated aerogels stayed stable from 700 μm to 800 μm. Representative coated samples are shown in **Figure 92**.

4.7 Lignin Coating of Cellulose Aerogels

For the same L:C ratios, the beads coated in EtOH:H_2O were more brownish than when coating occurred in a neutralized lignin water solution. As only the lighter fractions of lignin were dissolved in EtOH:H_2O, its adsorption and morphological appearance on the coated aerogel beads differed from when lignin of all molecular weights was available for coating.
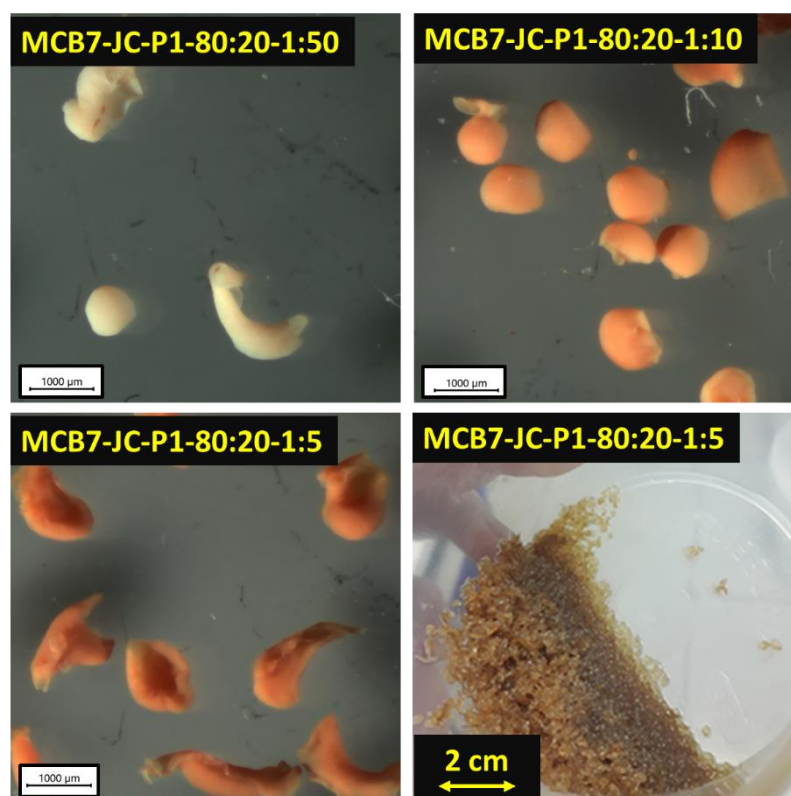
Figure 92 Pictures of lignin coated 7 wt.-% commercial cellulose aerogel beads (MCB7), produced at technical scale using the JetCutter® (JC) and in a 2M lactic acid solution. Coating was performed with P1000 lignin (P1) after its dissolution in EtOH:H_2O (80:20, vol.- %) bath, at different lignin:cellulose wet gel (L:C, wt.-%) ratios (from 1:50 to 1:5).

In the past chapters, the FTIR spectra of the cellulose aerogels have been consistent in presenting only the chemical signals of cellulose. **Figure 93** shows how their spectra changed after being coated with increasingly concentrated lignin solutions.
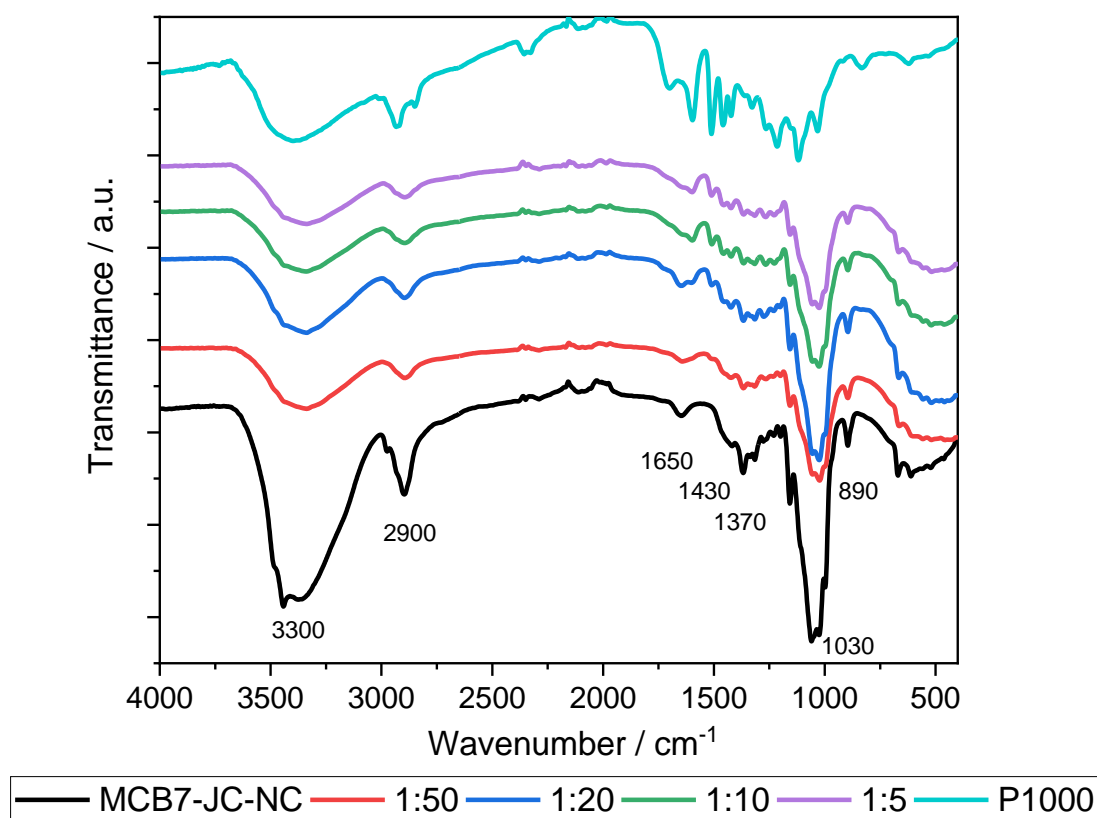
Figure 93 FTIR spectra of 7 wt.-% commercial cellulose aerogel beads (MCB7), produced at technical scale using the JetCutter® (JC) and in a 2M lactic acid solution, non-coated (black for standard sample, MCB7-JC-NC), and coated with P1000 lignin (P1) in EtOH:H$_2$O (80:20) bath at different lignin:cellulose wet gel ratios (red for 1:50; blue for 1:20; green for 1:10, and purple for 1:5). The spectrum of P1000 lignin is presented in light blue.

The peaks at 3300 cm^{-1} and 2900 cm^{-1}, corresponding to the O-H and C-H stretching vibrations of cellulose, became less intensive at higher L:C ratios. As more lignin covered the surface of the beads, the signals of the cellulose underneath were less pronounced in the FTIR spectra. At 2900 cm^{-1}, the peak became broader due to the signal at 2920 cm^{-1} and 2850 cm^{-1} from CH and CH$_2$ stretching from lignin.[254, 314] In **Figure 94**, the signals between 500 cm^{-1} and 1800 cm^{-1} are shown in detail.
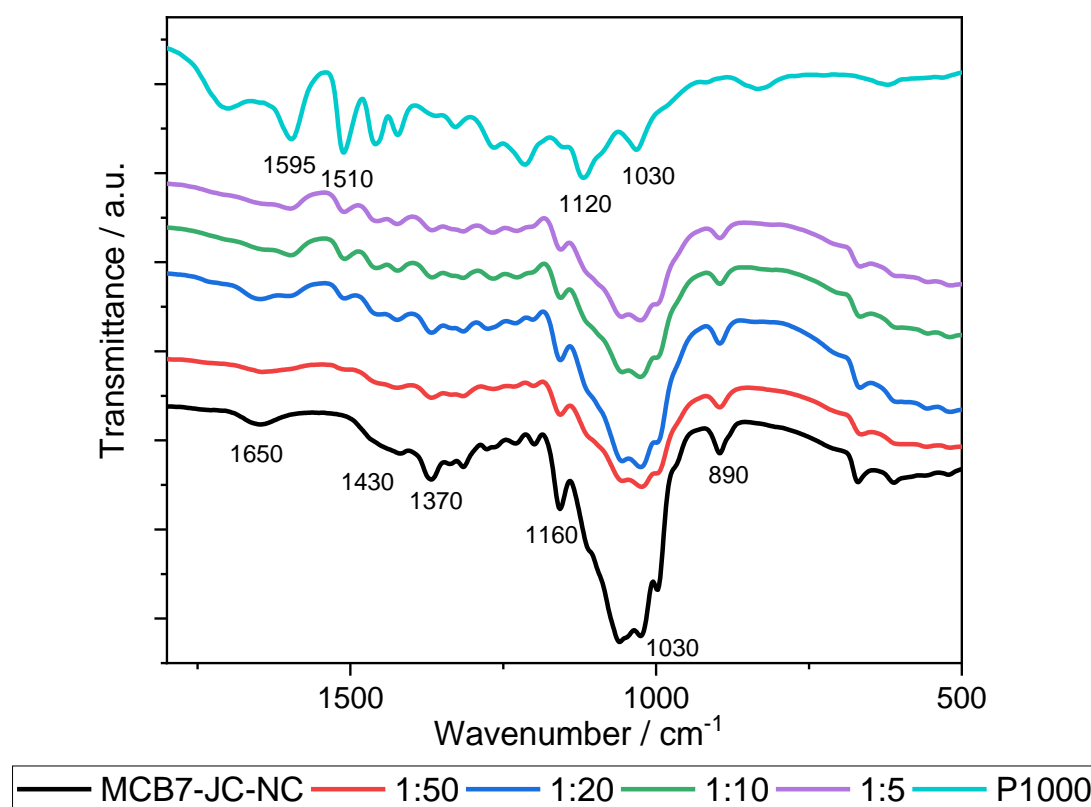
Figure 94 Detail of the FTIR spectra of 7 wt.-% commercial cellulose aerogel beads (MCB7), produced at technical scale using the JetCutter® (JC) and in a 2M lactic acid solution, non-coated (black for standard sample, MCB7-JC-NC), and coated with P1000 lignin (P1) in EtOH:H$_2$O (80:20) bath at different lignin:cellulose wet gel ratios (red for 1:50; blue for 1:20; green for 1:10, and purple for 1:5). The spectrum of P1000 lignin is presented in light blue.

The intensity of the peak associated with water adsorption on the surface of cellulose at 1650 cm^{-1} decreased and vanished over a 1:10 ratio. Peaks at 1595 cm^{-1} and 1510 cm^{-1}, associated with the C=C stretching vibrations from the aromatic rings of lignin, started appearing at 1:20.[254, 256, 314] The peaks at 1430 cm^{-1} and 1370 cm^{-1} were from cellulose´s CH$_2$ and CH bending. The latter became broader at higher L:C due to a signal of C-O stretching in lignin at 1360 cm^{-1}. The region between 1000 cm^{-1} and 1200 cm^{-1}, where the vibrations were related to the C-O-C and C-O stretching of cellulose, lost intensity and suffered shifts in its peaks due to signals originating from lignin. At 1120 cm^{-1} and 1030 cm^{-1}, deformation vibrations from C-H bonds in syringyl rings and from in-plane aromatic rings respectively from lignin contributed to the spectra of the aerogels.[256]

These spectra indicated that lignin was attached to the surface of the cellulose aerogel beads during the adsorption process. Lignin´s presence increased when higher quantities of lignin

were present in the coating solution. Nonetheless, the quantity of lignin attached to the aerogels did not significantly change the cellulose profile in their spectra.

In the appendix (see **Figure 114** and **Figure 115**), the FTIR spectra for the cellulose beads coated with increasing quantities of lignin dissolved in the basic medium are shown. The signals and trends found in the spectra were the same for the coated monoliths and similar but not so pronounced as what is shown in **Figure 93**. The signals of OH and CH stretching vibrations from cellulose were reduced for higher L:C ratios as other cellulose´s characteristic signs in the region between $500 \, cm^{-1}$ and $1800 \, cm^{-1}$. The signals of the C=C vibration from lignin ($1595 \, cm^{-1}$ and $1510 \, cm^{-1}$) were not as pronounced in **Figure 114** as in **Figure 93** due to the different lignin solubilities in both solvents. Smaller fragments of lignin, with lower condensation rates and fewer aromatic rings, were better dissolved in alkali media and were more accessible to adsorb onto the surface of the cellulose wet gels.[141] Heavier lignin particles were dissolved but could have been organized in bigger colloidal structures and remained in the bath after the coating period.[145] When in the presence of EtOH:H_2O (80:20), a smaller but more homogeneous fraction of lignin was available for coating which could have contributed to higher adsorption of bigger lignin agglomerates on the wet gel and a higher signal of C=C in FTIR of the coated aerogels.[140]

Through SEM, the attachment of lignin on the surface of the cellulose aerogel beads was visualized. In **Figure 95,** the lignin distribution on the aerogels after its dissolution in the EtOH:H_2O bath and adsorption is shown.
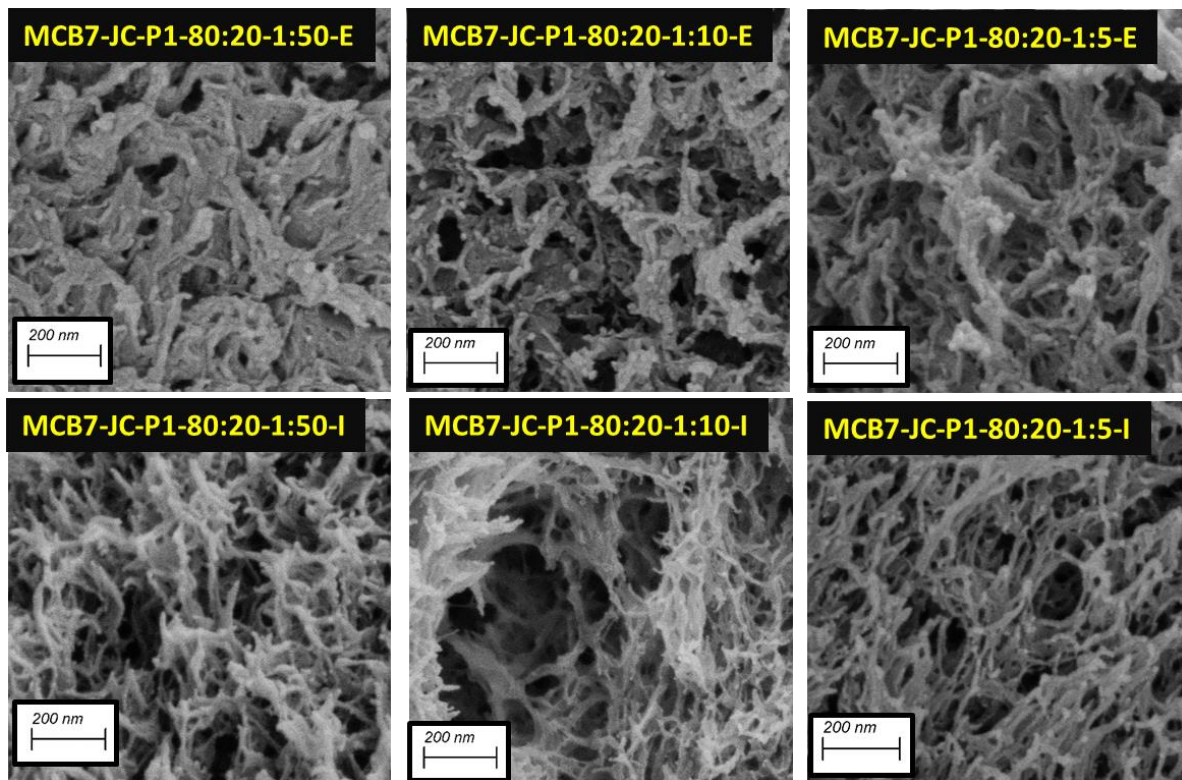
Figure 95 SEM pictures of the interior (I) and exterior (E) of lignin coated 7 wt.-% commercial cellulose aerogel beads (MCB7), produced at technical scale using the JetCutter® (JC) and in a 2M lactic acid solution. Coating was performed with P1000 lignin (P1) after its dissolution in EtOH:H$_2$O (80:20, vol.- %) bath, at different lignin:cellulose wet gel (L:C, wt.- %) ratios (from 1:50 to 1:5).

On the exterior surface of these samples, white spherical granules were visible, corresponding to lignin conglomerates. Those had a similar shape but smaller dimensions compared to what was observed in other studies focused on the influence of higher temperatures and pressure on lignin when integrating biomass.[315-317] While lignin was visible here, it was not when cellulose-lignin aerogel composites were created from a cellulose-lignin solution.[153, 154, 318] This could indicate that different dissolution, coating, and CO$_2$ supercritical drying conditions affected the agglomeration of lignin molecules and their corresponding shape and size. However, it could also mean that the coating protocol for preparing lignin-coated aerogels for SEM should be modified (using gold or iridium as coating agents) to improve resolution.[315, 316] These lignin agglomerates were unevenly distributed across the surface and were more numerous when a higher L:C ratio was applied. Despite this, the coated aerogels presented a porous structure similar to other samples discussed in this work. In the interior, a highly porous cellulose network was observed with no presence of lignin agglomerates except for L.C 1:5. This indicated that coating occurred only at the surface of the samples, in an

inhomogeneous way, and did not reach the interior of most samples. This agreed with the limited variation in water uptake observed for these samples independently of the L:C applied. In **Figure 96**, cellulose aerogel beads coated with neutralized dissolved lignin in water can be observed.
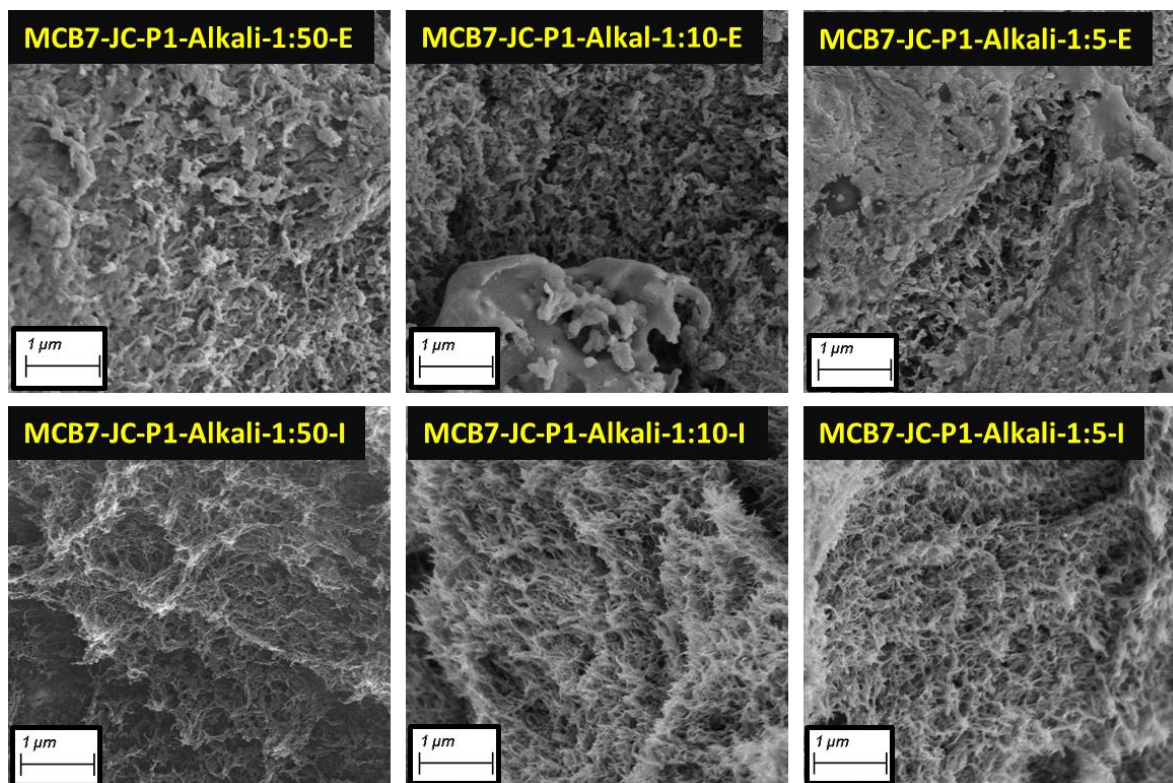
Figure 96 SEM pictures of the interior (I) and exterior (E) of lignin coated 7 wt.-% commercial cellulose aerogel beads (MCB7), produced at technical scale using the JetCutter® (JC) and in a 2M lactic acid solution. Coating was performed with P1000 lignin (P1), at different lignin:cellulose wet gel (L:C, wt.-%) ratios (from 1:50 to 1:5). This lignin was dissolved in alkali water solution and neutralized before coating.

Differences were noted between different ratios of L:C and lignin dissolution methods. Lignin was present as amorphous, non-porous, patches that increasingly covered the surface of the cellulose aerogel when increasing L:C ratios were used. Smaller aggregates as in **Figure 95** were still observed but at a lower number. NaCl crystals were detected, residues from the lignin´s neutralization that couldn´t be removed after coating due to lignin leaching in the presence of washing water. The surface coating was more homogeneous than when lignin was dissolved in EtOH:H$_2$O. In the interior porous network closer to the surface, small coated areas were observed as thicker cellulose fibrils united by lignin. Nonetheless, those structures were

unevenly distributed and were not observed in the core of the beads, whose structure was preserved. There, as in **Figure 95**, no lignin was observed.

Based on these results, it was found that when lignin was dissolved in an alkali medium and neutralized, it was more likely to interact with cellulose and each other, creating thin coating patches along the surface of the aerogel beads. This reduced the access of water to the interior of the beads and their water uptake.

The distribution of lignin on the surface of the aerogels affected the number of open pores and their adsorption capacity. The N_2 adsorbed by the samples varied with the lignin concentration on them, as shown in the appendix (see **Figure 129**). It shows type IV isotherms, with hystereses intermediates between H1 and H2(b), as described by IUPAC which are characteristic of mesoporous materials.[44] When the beads were coated with lignin dissolved in the ethanol:water bath, at a L:C 1:50 ratio, their adsorption capacity increased significantly from 1470 cm^3 g^{-1} to 2000 cm^3 g^{-1}. After reaching a maximum at 1:50, the adsorption capacity decreased at higher L:C ratios. However, there was no direct relation between the L:C ratio and the adsorption capacity of the coated samples. It was hypothesized that the increased adsorption of gas was due to the added contribution of lignin whose functional groups interacted with N_2. Nonetheless, as lignin was not homogeneously distributed, its contribution was not systematic. For the beads whose coating was performed in water, with neutralized lignin, the adsorption capacity decreased with higher L:C ratios, as shown in the appendix (see **Figure 130**). From the maximum adsorption at 1470 cm^3 g^{-1} for the blank sample, this value decreased proportionally as more lignin was present during coating, down to 748 cm^3 g^{-1} at 1:5. The classification of the isotherms is the same for the aerogel coated samples independently of the coating method. At low concentrations of lignin, the coating of the bead was neither homogeneous nor thick. As the content in lignin increased, lignin covered more of the surface area of the aerogel and created a more homogeneous, thicker film. In **Figure 95** this is observed. Besides, more salt residues from lignin´s neutralization were left on the surface of the beads when higher L:C ratios were used. This led to an increase of the sample´s mass that further decreased the values of adsorption obtained. The lack of efficient coating when it occurred in ethanol:water mixtures was supported by the values of specific surface area and total pore volume found for these samples, shown in **Figure 97**. Regarding the first property, it followed the same trend observed for the water uptake experiments. MCB7-JC-NC had 280 m^2 g^{-1}, while, in the coated samples, it ranged from 284 m^2 g^{-1} to 316 m^2 g^{-1}, with a minimum of 199 m^2 g^{-1} reached at 1:10. This indicated that the internal cellulose network remained mostly intact and accessible while lignin concentrated on the surface in a dispersed way.
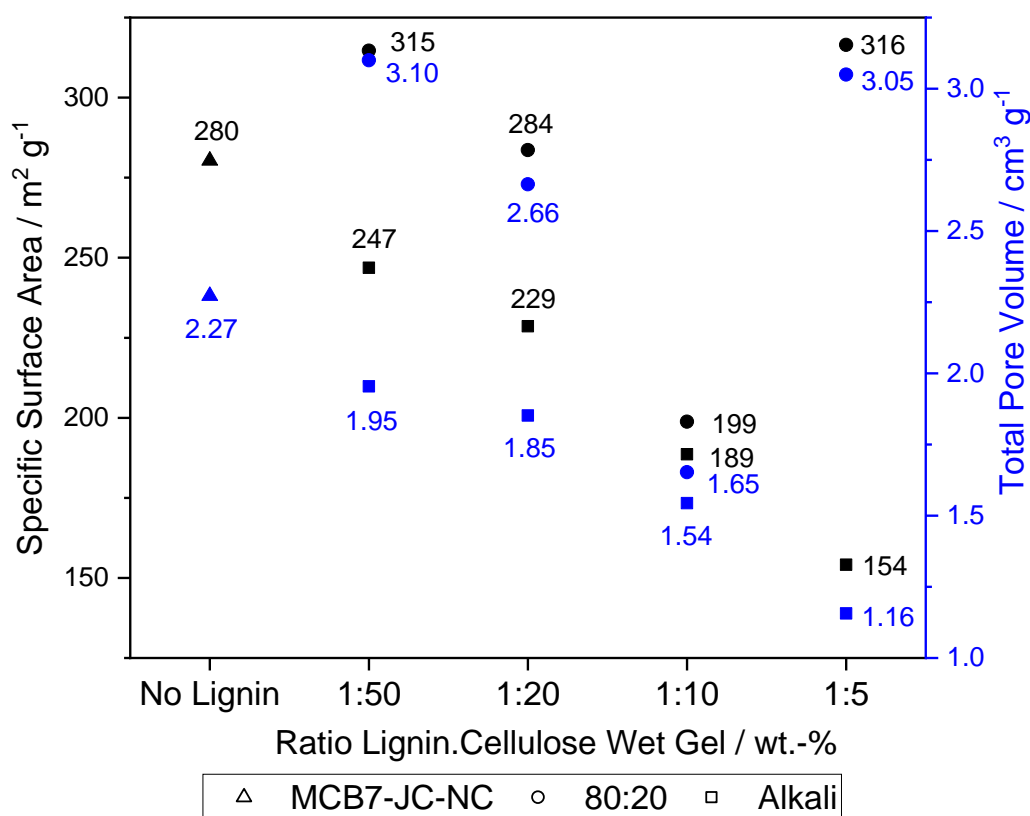
Figure 97 Specific surface area and total pore volume of 7 wt.-% commercial cellulose aerogel beads (MCB7), produced at technical scale using the JetCutter® (JC) and in a 2M lactic acid solution, non-coated (triangle for the standard sample, MCB7-JC-NL), and coated with P1000 lignin (P1) dissolved in different baths (circle for ethanol:water bath, 80:20, and square for NaOH bath, Alkali) at different lignin:cellulose wet gel ratios (from 1:50 to 1:5, L:C, wt.- %).

A more efficient surface covering could have occurred at 1:10, and, at 1:5, the extra lignin could have conglomerated but this was difficult to confirm based on the SEM pictures. The total pore volume increased, from 2.27 cm^3 g^{-1} for the blank sample to between 2.66 cm^3 g^{-1} and 3.10 cm^3 g^{-1} for the coated samples (exception at 1:10, with 1.65 cm^3 g^{-1}). This could be related to the inhomogeneous distribution of lignin conglomerates on the surface which created new empty micrometer-size spaces, influencing the total pore volume. When lignin dissolution occurred in the basic medium, a proportional reduction in both specific surface area and total pore volume was observed for increased concentrations of lignin during coating. From 280 m^2 g^{-1} found in the blank sample, the specific surface area steadily decreased to 154 m^2 g^{-1}, at a 1:5 L:C ratio. The same occurred to its total pore volume, which decreased from 2.27 cm^3 g^{-1} to 1.16 cm^3 g^{-1} when the presence of lignin was at its maximum. This was explained by the deposition of lignin on the exterior surface of the aerogels, which covered

patches of the surface pores, and the increasing presence of NaCl salt residues for higher LCs, which increased the sample´s mass. The pore size distribution of the samples coated in ethanol:water, shown in **Figure 98**, presented a mainly mesoporous porous structure, with a significant presence of macropores.
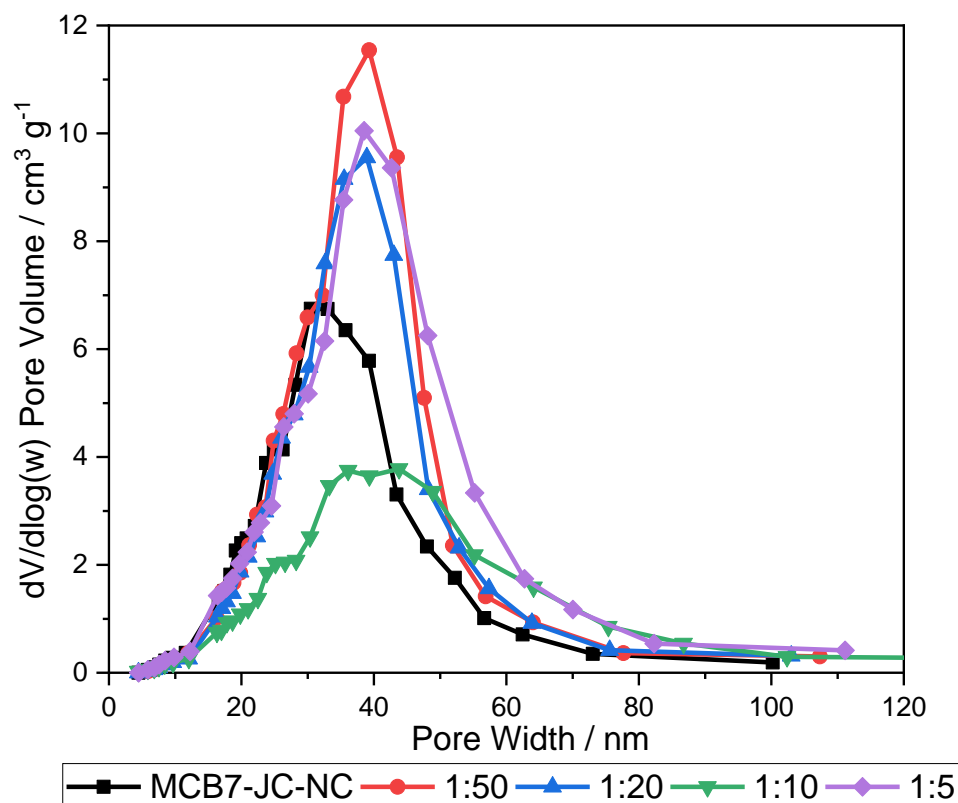
Figure 98 Pore size distribution of 7 wt.-% commercial cellulose aerogel beads (MCB7), produced at technical scale using the JetCutter® (JC) and in a 2M lactic acid solution, non-coated (black for standard sample, MCB7-JC-NC), and coated with P1000 lignin (P1) in EtOH:H$_2$O (80:20) bath at different lignin:cellulose wet gel ratios (red for 1:50; blue for 1:20; green for 1:10, and purple for 1:5).

The profiles of the aerogels became broader and shifted for bigger pore widths, especially bigger mesopores (the top of the distribution curves shifted from 30 nm to 40 nm) and macropores when coated. However, no significant differences existed between L.C ratios. This agrees with the inefficient and inhomogeneous coating observed in the SEM pictures. At 1:10, the fraction of mesopores < 30 nm compared to the macropores was the lowest of the samples. This explained the increase in average pore size from 25.3 nm of the standard to 29 nm for all coated samples.

Results and Discussion

When the samples were coated with lignin dissolved in a basic medium, as in **Figure 99**, there was a decrease in the pore volume for pores of all dimensions, particularly in the mesoporous range, with increasing lignin concentrations. At higher ratios (1:10 and 1:5), the profiles broadened further, with a lower proportion of mesopores below 30 nm and between 30 and 50 nm. The average pore size remained stable independently of the lignin:cellulose rate (25.3 nm for the blank sample and from 24.6 nm to 25.9 nm for the coated aerogel beads), indicating the homogeneity of the process.
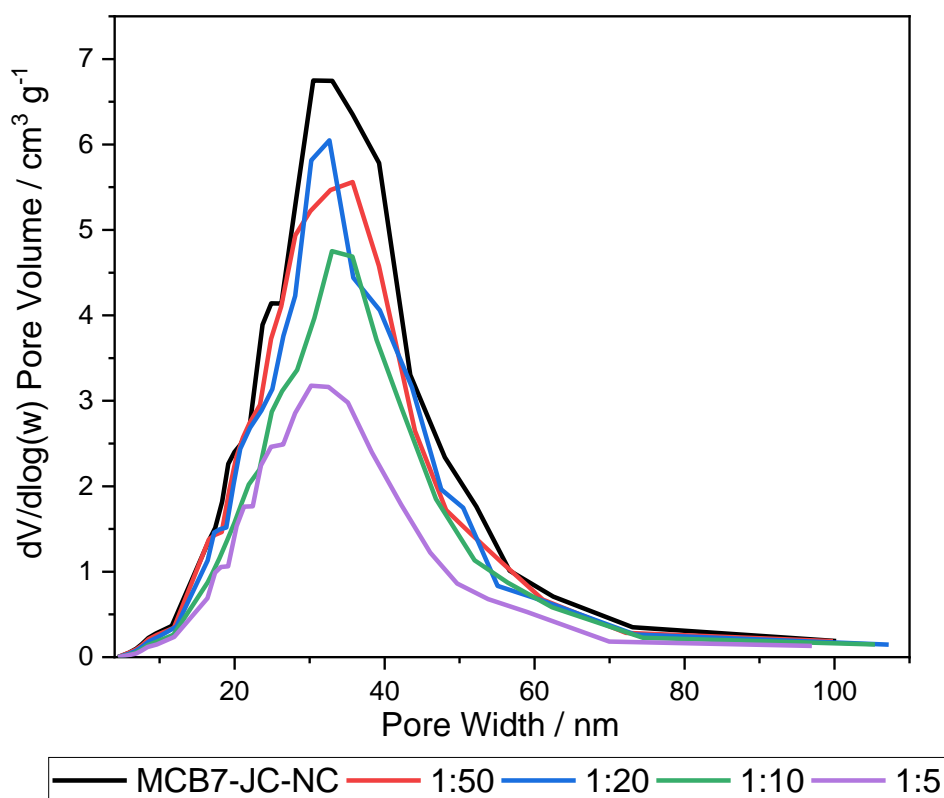
Figure 99 Pore size distribution of 7 wt.-% commercial cellulose aerogel beads (MCB7), produced at technical scale using the JetCutter® (JC) and in a 2M lactic acid solution, non-coated (black for standard sample, MCB7-JC-NC), and coated with P1000 lignin (P1) at different lignin:cellulose wet gel ratios (red for 1:50; blue for 1:20; green for 1:10, and purple for 1:5). This lignin was dissolved in alkali water solution and neutralized before coating.

The deposition of the lignin on the surface of the beads plus the presence of NaCl salt residues, reduced homogeneously the proportion of pores detected in the mesoporous and macroporous range. As fewer pores were available, water interacted less with these samples.

The thermogravimetric profile of cellulose aerogels showed a reduction in mass due to the evaporation of water at 100 °C. The mass loss at this temperature for cellulose aerogel beads in

the wet state, coated at a 1:5 L:C ratio with P1000 lignin dissolved in different media is shown in **Figure 100**. For the non-coated sample, MCB7-JC-NC, water composed up to 73% of the mass of the sample, and a plateau was reached at 165 °C, before the degradation of cellulose. When lignin was dissolved in an ethanol:water bath, MCB7-JC-P1-80:20-1:5, the water content was reduced to 50% and the stabilization occurred earlier, at 137 °C. Absorption was still significant due to the deficient coating of the beads´ surface. For the same LC ratio and when P1000 was dissolved in an alkali water solution, MCB7-JC-P1-Alkali-1:5, the water content was just 20% of the sample´s mass which started stabilization at 104 °C.
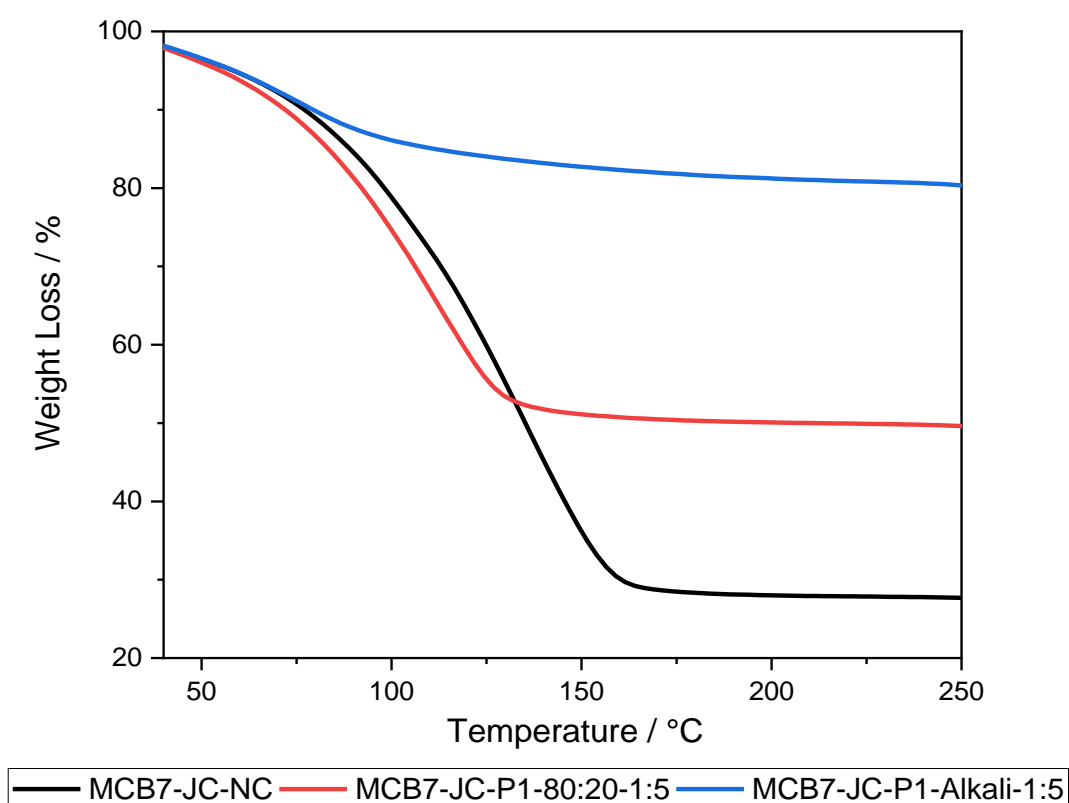
Figure 100 Thermal gravimetric profiles of 7 wt.-% commercial cellulose aerogel beads (MCB7), produced at technical scale using the JetCutter® (JC) and in a 2M lactic acid solution, non-coated (black for standard sample, MCB7-JC-NC), and coated at a 1:5 lignin:cellulose wet gel ratio with P1000 lignin (P1) dissolved in different media (red for ethanol:water bath, MCB7-JC-P1-80:20-1:5, and blue for NaOH bath, MCB7-JC-P1-Alkali-1:5).

In the DSC profiles, shown in **Figure 101**, a decrease in the energy consumption was observed when the beads absorbed less water. The decrease in the temperature at which the peaks were observed was related to the position of the water molecules in the porous structure of the aerogels.[307] When coating was less efficient, water adsorbed strongly on the surface and

interior of the beads, which required more energy to be evaporated. The addition of hydrophobic lignin to the cellulose surface and the decrease of the available pores induced a weaker, more superficial adsorption of water which required less energy to be removed.[309] This data indicated that the method developed with alkali dissolution of lignin, while not turning the cellulose aerogel hydrophobic, induced in the cellulose aerogel beads a great resistance to water absorption.
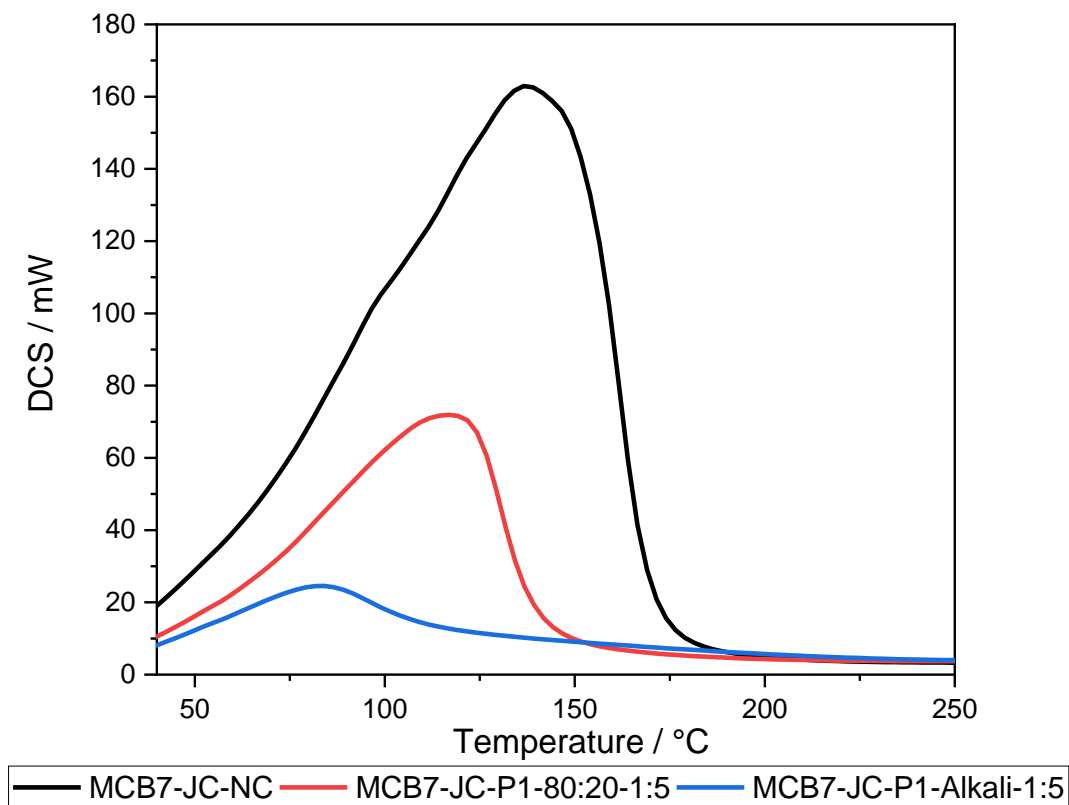
Figure 101 DSC profiles of 7 wt.-% commercial cellulose aerogel beads (MCB7), produced at technical scale using the JetCutter® (JC) and in a 2M lactic acid solution, non-coated (black for standard sample, MCB7-JC-NC), and coated at a 1:5 lignin:cellulose wet gel ratio with P1000 lignin (P1) dissolved in different media (red for ethanol:water bath, MCB7-JC-P1-80:20-1:5, and blue for NaOH bath, MCB7-JC-P1-Alkali-1:5).

In **Figure 102**, the thermogravimetric profile of the cellulose aerogel beads coated with lignin dissolved in alkali media can be observed. The fundamental behavior of these samples followed the typical profile of cellulose aerogels, as shown in previous chapters. The presence of a higher concentration of lignin in the coating bath led to its higher adsorption on the cellulose wet gels and consequent higher influence on the thermal behavior of the samples. Compared to the blank sample, the coated samples started their degradation at a lower temperature, achieved latter 50%

mass loss (from 321 °C to 310 °C), and, for higher L:C, had a higher residue content at 600 °C (12% to 21%). This was due to the larger temperature range at which lignin released volatiles (235 °C to 655 °C) compared to cellulose (250°C to 350 °C) and to the higher temperature at which lignin was mainly degraded (380°C to 500 °C), compared to 312°C to 350 °C of cellulose. As shown in the figure, the char residue of lignin was 41%. [228, 229, 242, 243]
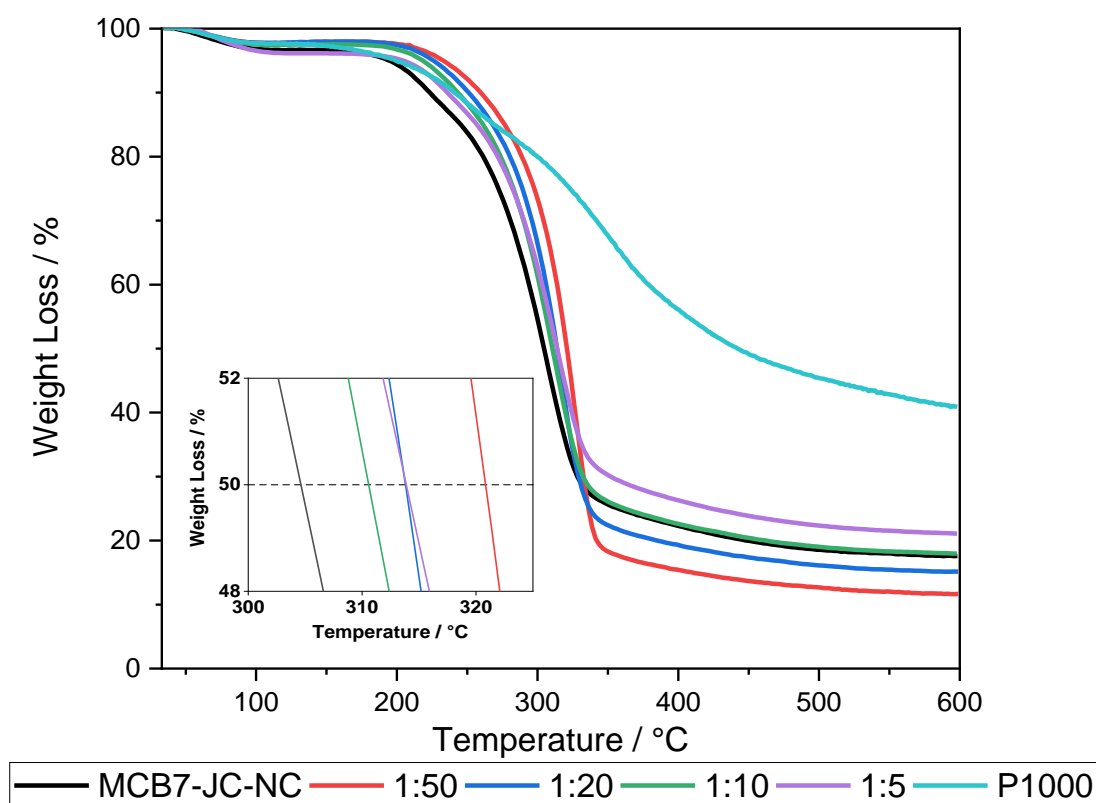
Figure 102 Thermal gravimetric profiles of 7 wt.-% commercial cellulose aerogel beads (MCB7), produced at technical scale using the JetCutter® (JC) and in a 2M lactic acid solution, non-coated (black for standard sample, MCB7-JC-NC), and coated with P1000 lignin (P1) at different lignin:cellulose wet gel ratios (red for 1:50; blue for 1:20; green for 1:10, and purple for 1:5). The profile of P1000 lignin is presented in light blue. This lignin was dissolved in alkali water solution and neutralized before coating.

The high molecular weight of lignin and the presence of branched crosslinked aromatic moieties contributed to a higher production of char compared to the release of volatiles.[319] The same trends were observed when lignin-cellulose aerogels were synthesized in literature and the monolith samples.[320] The differences between the profiles for each L:C ratio were small and no systematic trend was defined among themselves. This was due to the actual low concentration of lignin in the cellulose aerogels that was not enough to originate more striking

differences between L:C ratios. This low lignin concentration in the aerogel explained why the residue obtained for 1:50 and 1:20 was lower than for the standard monolith. At those low rates, where the coating was not concentrated enough, the lighter fractions of lignin adsorbed could more easily interact with cellulose through radical reactions than among themselves. This promoted the release of gases during pyrolysis and decreased the mass of residue compared with what was found for the non-coated sample. For higher L:C ratios, where more lignin interacted with himself and with heavier fractions, lignin carbonized and created non-volatile residues that remained as residue.

Due to the success of coating cellulose aerogel beads with P1000 lignin that had been dissolved in alkali medium, the same recipes were applied to 7 wt.-% commercial cellulose aerogel monoliths. The darker and clearer areas observed in each monolith in **Figure 103** indicated that their coating was not homogeneous.
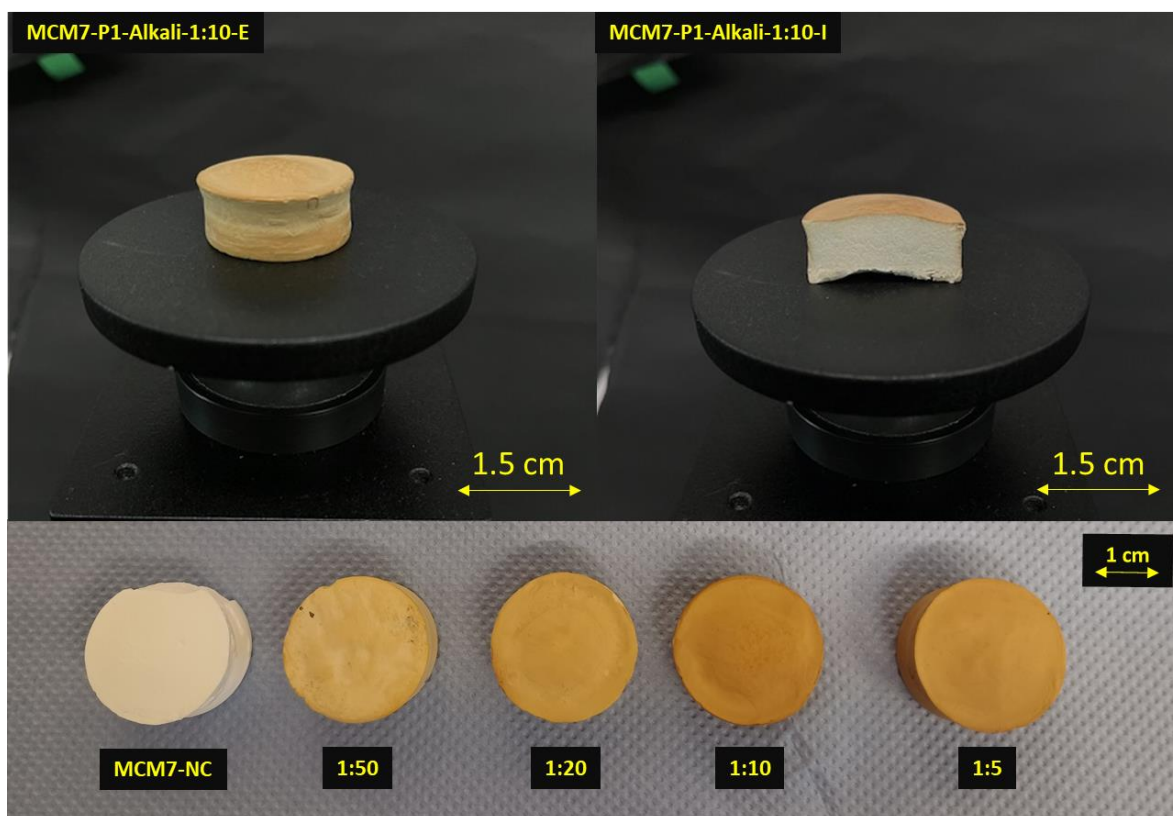
Figure 103 On top, pictures of the exterior (E) and interior (I) of a 7 wt.-% commercial cellulose aerogel monolith (MCM7) coated with P1000 lignin (P1) at a lignin:cellulose wet gel ratio of 1:5 (MCM7-P1-Alkali-1:5). At the bottom, the evolution of the surface color of the monoliths coated with P1000 lignin at different lignin:cellulose wet gel (L:C, wt.-%) ratios (from 1:50 to 1:5), starting with a non-coated sample (MCM7-NC). This lignin was dissolved in alkali water solution and neutralized before coating.

4.7 Lignin Coating of Cellulose Aerogels

As the monoliths were turned upside down during coating to ensure that all surfaces were in contact with the bath, these color differences could indicate different rates of adsorption for lignin. Depending on the molecular weight and ratio of different OH moieties of the lignin dissolved particles, optimum conditions for coating and its kinetics differed. Due to the heterogeneous character of lignin molecules, the coating conditions still needed to be optimized to ensure a more uniform distribution of lignin on bigger cellulose wet gel bodies.

The envelope density of the coated monoliths can be observed in **Table 19**.

Table 19 Properties of 7 wt.-% commercial cellulose aerogel monoliths non coated (MCM7-NC), and coated with P1000 lignin (P1) at different lignin:cellulose wet gel ratios (L:C, wt.- %). This lignin was dissolved in alkali water solution and neutralized before coating. Information on the specific surface area and total pore volume of the aerogels is presented later.

Samples	Volume Shrinkage / %	Envelope Density / g cm^{-3}	Porosity / %	Average Pore Size / nm
MCM7-NC	34.10	0.19	87.55	20.60
MCM7-P1-Alkali-1:50	34.00	0.19	87.69	9.76
MCM7-P1-Alkali-1:20	37.76	0.20	87.12	11.68
MCM7-P1-Alkali-1:10	39.57	0.22	85.71	8.77
MCM7-P1-Alkali-1:5	33.01	0.19	87.93	11.02

These samples presented low densities (from 0.19 g cm^{-3} to 0.22 g cm^{-3}), independently of the L:C ratio used. It showed that only a fraction of lignin remained on the aerogels compared to what was left in the dissolution bath. If all lignin dissolved in the bath was adsorbed on the gel, density would increase proportionally with higher L:C ratios. This was supported by the data obtained from the skeleton density of these samples and of pure cellulose and lignin. Cellulose had a skeleton density of 1.52 g cm^{-3} while P1000 lignin had a skeleton density of 1.38 g cm^{-3}. The skeleton density of the coated monoliths suffered little variation independently of the L:C ratio applied during coating (ranging from 1.54 g cm^{-3} to 1.58 g cm^{-3}). If a significant fraction of the solid backbone of the cellulose network was covered in lignin, it would have been expected a decrease in the skeleton density of the monoliths proportional to their content in lignin. The porosity of these aerogels remained constant, between 86% and 88%. The total volume shrinkage of the aerogels was not affected by the coating conditions, remaining stable

between 33% and 40%. The values of shrinkage observed were lower than the ones presented for other monoliths in previous chapters (40% to 55%). These values were not comparable because a different coagulation system (lactic acid ethanol bath) and drying solvent (acetone) were used for this study with lignin. These originated different regeneration kinetics during gelation and CO_2 supercritical drying, influencing differently the shrinkage of the synthesized cellulose aerogel monoliths.

Figure 104 shows the cellulose aerogel monoliths coated following the same procedure.
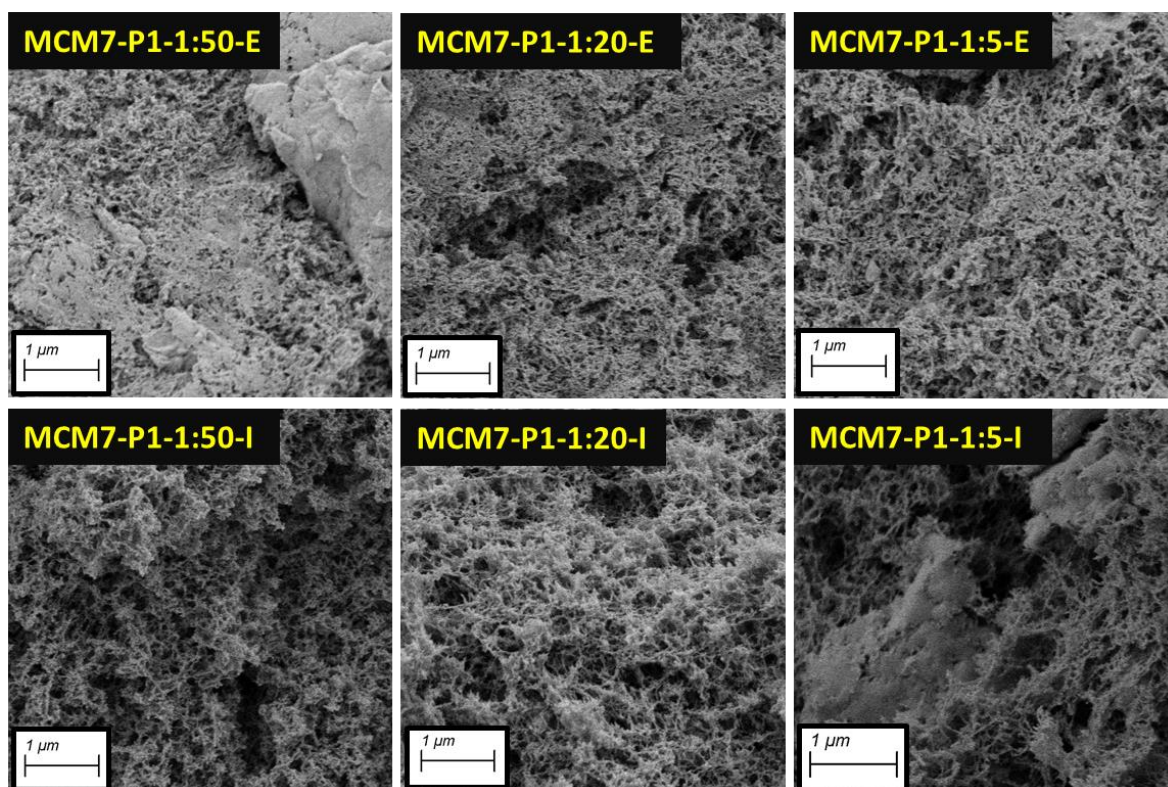
Figure 104 SEM pictures of the interior (I) and exterior (E) 7 wt.-% commercial cellulose aerogel monoliths coated with P1000 lignin (P1) at different lignin:cellulose wet gel ratios (L:C, wt.- %). This lignin was dissolved in alkali water solution and neutralized before coating.

The interior of the porous network of the aerogels was preserved while lignin was visible only on the surface of the monoliths. The coating was less homogeneous and instead of clear lignin-covered areas, as observed in **Figure 96**, the fibers were impregnated by lignin in some surface regions. The lower ratio of surface area to volume of the monoliths could have required more time or more volume of lignin solution during the coating phase to achieve a similar coating efficiency to the beads.

The isotherms for these polysaccharide-based aerogels corresponded to a type IV shape, typical of mesoporous materials.[237] When monoliths were coated with lignin dissolved in sodium

hydroxide solution, the specific surface area and the total pore volume decreased for higher ratios of L:C. These values can be studied in **Figure 105**. For the specific surface area, the non-coated monolith had 257 m^2 g^{-1} while this value was reduced to 151 m^2 g^{-1}, for 1:5. A smaller reduction rate was observed than in the correspondent beads. A significant reduction in the average pore size was found, ranging from 8.77 nm to 11.68 nm while for the non-coated monolith, this value was 20.60 nm. This data indicated that the coating of the cellulose body was not as efficient as for the correspondent beads due to the larger dimensions and lower area/volume ratio of the monoliths. Nonetheless, the coated area contributed to the blockage of the exterior pores.
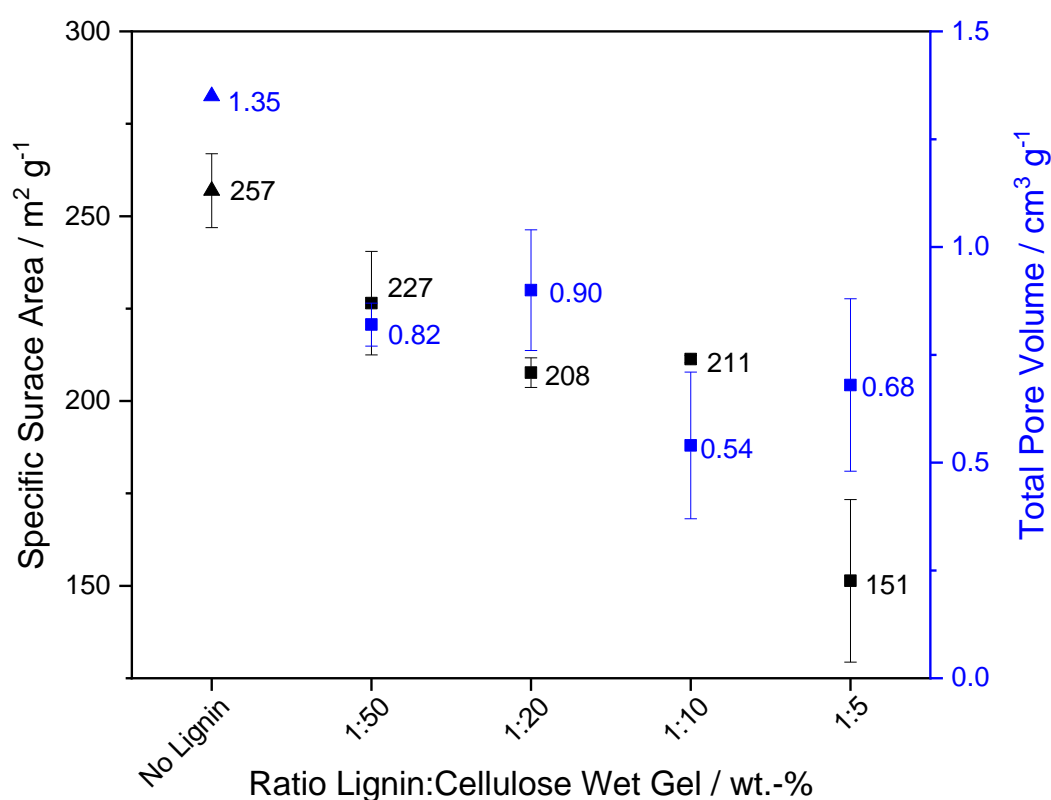
Figure 105 Specific surface area and total pore volume of 7 wt.-% commercial cellulose aerogel monoliths non-coated (triangle for the standard sample, MCM7-NC), and coated with P1000 lignin (P1) at different lignin:cellulose wet gel ratios (from 1:50 to 1:5, L:C, wt.- %). This lignin was dissolved in alkali water solution and neutralized before coating.

This data was compared to the pore size distribution of the monoliths, shown in **Figure 106**. The profiles presented lower adsorption of gas and a higher fraction of macropores compared to the ones in **Figure 99**. While some bigger mesopores and macropores were detected after coating, the creation of a lignin layer in some regions of the surface of the monoliths filled most

of the macropores, sharpening the pore size distribution and reducing the average pore size. As the coating was not homogeneous, the profile of the coated samples did not change significantly.
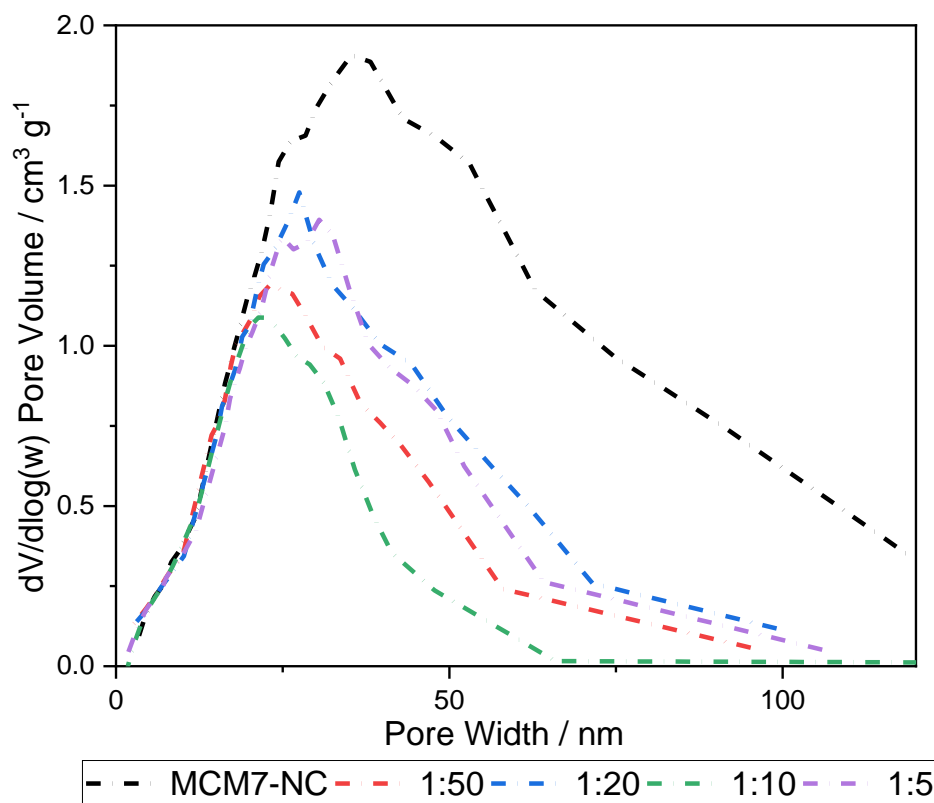
Figure 106 Pore size distribution of 7 wt.-% commercial cellulose aerogel monoliths non-coated (black for the standard sample, MCM7-NC), and coated with P1000 lignin (P1) at different lignin:cellulose wet gel ratios (red for 1:50; blue for 1:20; green for 1:10, and purple for 1:5). This lignin was dissolved in alkali water solution and neutralized before coating.

Based on the previous data, the water contact angle was tested on the surface of coated monoliths. In **Figure 107**, pictures of the monoliths after dropping water can be observed. After just three seconds, the water droplets were completely absorbed by the monolith which indicated that these were not hydrophobic and any improvement in their water resistance was feeble. This occurred for the standard sample and the coated samples up to 1:10. At 1:5, the droplet remained on the surface for up to one minute, which indicated an effective coating of the aerogel and a significant improvement in its resistance to water. This was in line with the data provided by other characterization techniques.
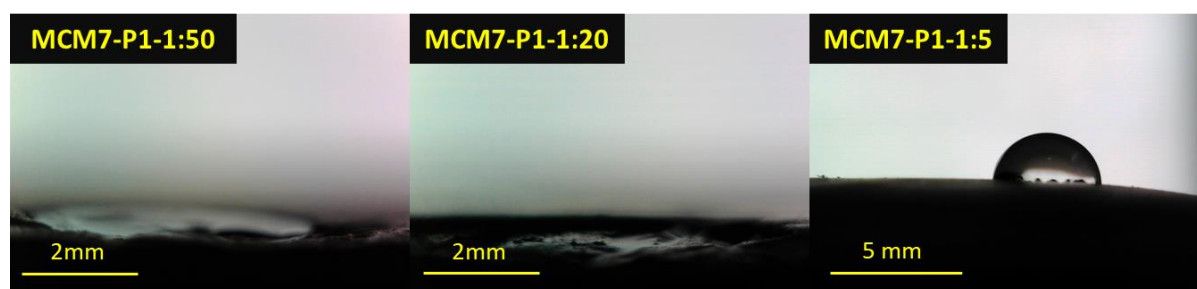
Figure 107 Surface of 7 wt.% commercial cellulose aerogel monoliths coated with P1000 lignin at different lignin:cellulose wet gel (L:C, wt.-%) ratios, three seconds after adding one water droplet on their surface. This lignin was dissolved in alkali water solution and neutralized before coating.

Different methods were developed to coat cellulose wet gels with lignin. This procedure had as its main goal, if not the hydrophobization of the aerogels, at least inducing in them moisture resistance. It was found that after dissolving soda lignin (P1000) in a NaOH water solution, neutralizing it, and using that bath as a coating agent, the wet gels were mostly covered by lignin. The dried aerogels maintained the lignin on their surface and had improved resistance against water absorption, while their internal structure was preserved. The coating was more effective for small beads than for monoliths. Chemical differences between the tested lignin and their mechanisms of dissolution and adsorption in different media proved to be determinants in the development of water-resistant materials. This study contributed to a better understanding of the interaction between cellulose and lignin and formulated a biobased alternative to protect aerogels from moisture.

4.8 Economic and Environmental Impact

As part of this work, important steps were taken to create a continuous production line for cellulose aerogels. This was made possible by close cooperation with KEEY Aerogels, the hosting industrial partner. Promising results were achieved by developing an optimized – faster and more efficient - continuous dissolution method of cellulose (see **Chapter 4.2**) and a cellulose extraction process from hemp and flax waste bast fibers which was proofed at pilot scale (see **Chapter 4.1**). Results of multiple recipes for the regeneration of cellulose in different shapes, such as beads, sheets, and fibers were developed and applied at a 2 L production scale, as described and discussed in **Chapters 4.4, 4.5, and 4.6.** Fast neutralization and solvent

exchange would be possible to perform continuously by passing through the wet gels a high flux of water and ethanol, respectively. The ethanol recovery unit would have a 98% recovery yield, while water could be purified from acids and salts. CO_2 could be recycled from the drying step and applied continuously to the wet gels, converting them into aerogels. One proposed primary process for industrial scale production involved dissolving cellulose, regenerating it into a wet gel, and continuously processing it through neutralization, solvent exchange, and CO_2 supercritical drying. A secondary process would entail recycling the synthesis and drying solvents, as shown in **Figure 108**.
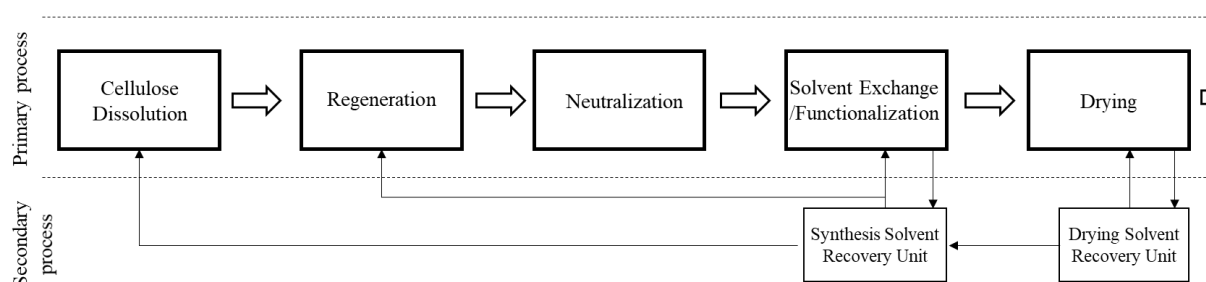
Figure 108 Process diagram of the continuous industrial synthesis of cellulose aerogels from dissolution and regeneration of cellulose to the formation of wet gels, their processing, and supercritical drying (primary process). The secondary process comprises the recycling of solvents.

Life cycle assessment (LCA) is a powerful tool for improving product synthesis and comparing parameters. However, the time, costs, and extensive database requirements often hinder its application for new processes and laboratory-to-technical scale comparisons.[321-325] Nonetheless, upscaling the process would bring environmental and economic advantages that would facilitate the industrial application of these materials. When analyzing the efficiency of the upscaling of the synthesis, the total mass used in the process, its robustness and controllability, and the rate of product synthesis (cycle time) should be considered. Besides, quality should be described based on whether the product satisfies the client's needs, as further purity or yield may lead to extra costs without adding value.[321]

Previous works have focused on the sustainability and costs of synthesizing aerogels, comparing silica with biobased alternatives at laboratory and technical scales.[326, 327] For all classes of aerogels, and even with a recycling rate of 95%, ethanol remains the biggest contributor to the global warming potential (GWP) of their synthesis (50%). It is the main driver for abiotic depletion (fossil), photochemical oxidation, and release of respiratory organic

4.8 Economic and Environmental Impact

compounds.[328] This is because ethanol is produced from the hydration of ethylene, which is an energy-intensive process, and whose ethylene is mostly obtained from fossil sources.[329] To mitigate these influences, shorter solvent-exchange cycles with lower volumes are recommended, as well as recycling and using ethanol produced from fermentation of biobased wastes.[323] Marco et al. when considering the recycling of 33% or 66% in ethanol, noted a significant reduction in emissions, especially in photochemical oxidation and volatile organic compounds.[328] The use of supercritical CO_2 in the drying process, even with 95% recycling rates, comprises 28% of the GWP for all classes of aerogels. Furthermore, it has a high carcinogenic influence.[326, 330] The water use has a significant influence, as distilled water should be used for the solvent exchange, and needs to be purified from solvents and reactants. This consumes more energy and waste disposal-associated costs.[321]

Regarding differences between silica and biobased aerogels, no consistent data has been collected. While Wang et al. concluded that biobased aerogels had from 75% to 92% lower GWP, energy consumption, and soil acidification potentials than silica-based aerogels, Antypa et al. found no difference between the silica and cellulose aerogels.[326, 327] However, it should be noticed that the thermal performance of silica aerogels is higher than that of cellulose aerogels, which plays an important role in the energy consumption of buildings or other facilities where they are applied. Disposal emissions can be ignored for biobased aerogels as they are degradable.[327]A further influence is reduced if the aerogels are produced from agricultural wastes that would be disposed of otherwise, as in the case of the aerogels synthesized in this work from hemp and flax waste bast fibers.[331, 332] Concerning the upscaling of the aerogel synthesis and processing, there was a substantial improvement in the environmental influence of the process.[333] The transition from laboratory to pilot scale resulted in an overall reduction of 40% in LCA influence, namely a reduction of 70% for human health, consumption of resources, and GWP. Influence reductions achieved 90% when the scale passed to the industrial scale. [325, 330, 334]This was due to the heat and solvent recovery that occurs at an industrial scale and to the lower waste production per kg of product. Besides, at an industrial scale, the reactors have better insulation and a lower surface-to-volume ratio, resulting in minimal heat loss compared to laboratory scale.[323] The infrastructure is not relevant as it comprises 1% of the influence, as well as transportation.[323, 335]

Based on this data, it can be assumed that upscaling the synthesis of cellulose aerogels to the industrial scale, especially those produced from renewable biobased wastes, would bring economic and environmental advantages compared to the current laboratory and technical scale developed methods. The higher efficiency of the synthetic process, associated with the

reduction of costs and larger production, would decrease the price of the aerogels and facilitate their large-scale introduction into the market. The upscaling of the synthesis of aerogels, in multiple shapes, studied in this work eases the development of a continuous industrial process for these materials´ synthesis.

4.8 Economic and Environmental Impact

5. Summary and Conclusions

In this work, various experiments and studies were performed. The first topic focused on the extraction and characterization of cellulose from hemp and flax waste bast fibers. The extraction process was performed at laboratory scale and then scaled up for technical use, producing chemically pure cellulose without compromising the efficiency of the process. Before converting the extracted cellulose to aerogels, systematic studies were carried out on the dissolution and regeneration conditions of cellulose, followed by analysis of the synthesized samples.

Cellulose dissolution was achieved at -10°C in 30 minutes for 100 mL solution when a cooling plate was used, which allowed for faster dissolution compared to the standard method used in this work.

For regeneration, a general trend was observed. For salts, adding NaCl and Na_2SO_4 favored faster cellulose gelation due to their affinity to water. Besides, it increased the specific surface area of the cellulose aerogels due to the pores created when these salts were removed during the neutralization and solvent exchange phases. The addition of trisodium citrate increased the gelation point of the cellulose solution and sharpened the pore size distribution of the aerogels. However, it did not increase their specific surface area as the other salts because of the bigger dimensions of the citrate anion and its organic character. The complex interaction between charged anions and cations with organic polymers in aqueous solutions still needs further understanding.

In the case of acids, the use of organic acids such as acetic, lactic, and citric acid as coagulants resulted in aerogels with higher specific surface areas and shifted their pore size distribution to smaller pores than the aerogels produced in HCl aqueous baths due to a promotion of slower gelation. The slower the regeneration of cellulose, the more time was available to create a filigree 3D cellulose network where the formation of smaller mesopores was maximized to the detriment of macropores. Both experiments provided tools to tailor the aerogels´ properties depending on the desired final application.

From these recipes, the synthesis of aerogels was tested from extracted cellulose in different shapes and scales. The synthesized cellulose aerogel beads, sheets, and fibers from extracted cellulose, especially hemp-extracted cellulose, had comparable properties to aerogels produced from commercial cellulose with the same recipes. The upscaling of their production using different equipment such as the JetCutter® and the CAProLi was successful while preserving their properties. These materials had high surface areas and low densities but were not considered superinsulators due to their high thermal conductivity (37 mW m^{-1} K^{-1} to

Summary and Conclusions

42 mW m^{-1} K^{-1}). Other applications where they could be used include filters and biomedical applications due to their high surface area and biocompatibility. The lignin coating of the aerogels induced resistance to water absorption but not hydrophobicity.

This work contributes to a better understanding of the relationship between the synthetic conditions of cellulose aerogels and their properties. Based on this knowledge, developing recipes for upscaling devices provides new opportunities for the industrial application and production of cellulose aerogels. Creating cellulose aerogels from agricultural wastes with comparable properties to current alternatives promotes the valorization of biomass waste resources and the development of a circular biobased economy, with economic, environmental, and social benefits for Humanity.

6. Outlook

This work covers a variety of topics, but some of them could not be investigated as thoroughly as desirable. This thesis has led to the formulation of new research questions. One of the main challenges with using biobased resources is the lack of uniformity in their properties, which are highly dependent on various factors, such as biomass species, plant growth conditions, and pre-treatment, among others. It would have been helpful to use different parts of hemp and flax, such as shives, but also hemp and flax waste bast fibers from other geographies and with different processing conditions to verify the reliability of the developed recipes and upscaling techniques. Regarding the systematic studies on cellulose regeneration and dissolution conditions, it would have been interesting to perform kinetic studies on stable gel body formation when different acids were used as coagulation baths. It would have been possible to quantify the coagulation speed associated with each acid and its influence on the aerogel´s properties. Using acidic solutions in organic media would also be a relevant field of study. Simulation work on the interaction of the different charged anions in the water:urea:NaOH system in the presence of cellulose would be useful to understand the physics and molecular interactions between these components in this heavily charged environment.

It would be worth studying the influence of cellulose dissolution conditions on aerogels by creating composites with cellulose I and II. Other studies have created those materials by adding fibers over the dissolution limit[172-175]. However, as done in this work, these composites can be synthesized by increasing the temperature at which dissolution occurs. The characterization of those composites and comparison of their properties with computer simulations would enrich the current knowledge on the mechanical and thermal conductivity properties of cellulose aerogel composites.

Cellulose aerogels were produced at technical scale in different shapes, but the optimization of their production conditions is still lacking. Conjugating that equipment with continuous systems for neutralization, solvent exchange, and CO_2 supercritical drying would be essential to improve the industrial production of cellulose aerogels and introduce them to the market.[23]

Regarding using lignin as a hydrophobic coating agent, it would be useful to analyze their particle size distribution in different dissolution media to better understand the adsorption behavior of these particles. With this information, it would be possible to, in combination with the pore size distribution of an aerogel, optimize the adsorption procedure and choose the most appropriate lignin and dissolution medium. The quantification of the lignin present in the coated material and further studies on the functionalization of the adsorbed lignin with phosphor to induce fire and additional moisture resistance would be helpful. These studies would increase

Outlook

the industrial interest in biobased aerogels and contribute to the elucidation of the fundamental chemical behavior of cellulose in coagulating agents and interaction with other biopolymers.

7. References

1.   United Nations, D.o.E.a.S.A., Population Division, *World Population Prospects 2019: Highlights*. 2019.
2.   Agency, E.E., *The European environment - state and outlook 2020. Knowledge for transition to a sustainable Europe*. 2019. p. 155-187.
3.   Comission, E., *Forging a climate-resilient Europe - the new EU Strategy on Adaptation to Climate Change*. 2021, European Commission.
4.   Energy, E.C.-D., *Energy efficiency in buildings*. 2020, European Commission - Department: Energy.
5.   Adamczyk, J. and R. Dylewski, *The impact of thermal insulation investments on sustainability in the construction sector.* Renewable and Sustainable Energy Reviews, 2017. **80**: p. 421-429.
6.   Magrini, A., et al., *From nearly zero energy buildings (NZEB) to positive energy buildings (PEB): The next challenge - The most recent European trends with some notes on the energy analysis of a forerunner PEB example.* Developments in the Built Environment, 2020. **3**.
7.   Martos, A., et al., *Towards successful environmental performance of sustainable cities: Intervening sectors. A review.* Renewable and Sustainable Energy Reviews, 2016. **57**: p. 479-495.
8.   Grove-Smith, J., et al., *Standards and policies for very high energy efficiency in the urban building sector towards reaching the 1.5°C target.* Current Opinion in Environmental Sustainability, 2018. **30**: p. 103-114.
9.   Kumar, D., et al., *Comparative analysis of building insulation material properties and performance.* Renewable and Sustainable Energy Reviews, 2020. **131**.
10.   Jelle, B.P., *Traditional, state-of-the-art and future thermal building insulation materials and solutions – Properties, requirements and possibilities.* Energy and Buildings, 2011. **43**(10): p. 2549-2563.
11.   Lopez Hurtado, P., et al., *A review on the properties of cellulose fibre insulation.* Building and Environment, 2016. **96**: p. 170-177.
12.   Abu-Jdayil, B., et al., *Traditional, state-of-the-art and renewable thermal building insulation materials: An overview.* Construction and Building Materials, 2019. **214**: p. 709-735.
13.   Rashidi, S., J.A. Esfahani, and N. Karimi, *Porous materials in building energy technologies—A review of the applications, modelling and experiments.* Renewable and Sustainable Energy Reviews, 2018. **91**: p. 229-247.
14.   Aegerter, M., A., Leventis, N., Koebel, M, M., Steiner III, S. A.,, *Springer Handbook of Aerogels*. 2023: Springer Nature Switzerland AG.
15.   Brandão, A.S., A. Gonçalves, and J.M.R.C.A. Santos, *Circular bioeconomy strategies: From scientific research to commercially viable products.* Journal of Cleaner Production, 2021. **295**.
16.   Attard, T.M., J.H. Clark, and C.R. McElroy, *Recent developments in key biorefinery areas.* Current Opinion in Green and Sustainable Chemistry, 2020. **21**: p. 64-74.
17.   Kircher, M., *Bioeconomy - present status and future needs of industrial value chains.* N Biotechnol, 2021. **60**: p. 96-104.
18.   Nita, L.E., et al., *New Trends in Bio-Based Aerogels.* Pharmaceutics, 2020. **12**(5).
19.   Thomas, S., Pothan, L, A., Mavelil-Sam, R.,, *Biobased Aerogels Polysaccharide and Protein-based Materials*. Green Chemistry, ed. J. Clark, H.,. 2018: Royal Society of Chemistry.
20.   Zhao, S., et al., *Biopolymer Aerogels and Foams: Chemistry, Properties, and Applications.* Angew Chem Int Ed Engl, 2018. **57**(26): p. 7580-7608.

References

21. Ganesan, K., et al., *Review on the Production of Polysaccharide Aerogel Particles.* Materials (Basel), 2018. **11**(11).

22. Takeshita, S., et al., *Chemistry of Chitosan Aerogels: Three-Dimensional Pore Control for Tailored Applications.* Angew Chem Int Ed Engl, 2021. **60**(18): p. 9828-9851.

23. Wang, Y., et al., *The advances of polysaccharide-based aerogels: Preparation and potential application.* Carbohydr Polym, 2019. **226**: p. 115242.

24. Budtova, T., et al., *Biorefinery Approach for Aerogels.* Polymers (Basel), 2020. **12**(12).

25. Gonçalves, B., *Upscaling of Cellulose Board Production Made From Hemp*, in *Department of Natural Sciences.* 2022, University of Applied Sciences Bonn-Rhein-Sieg.

26. Alemán, J.V., et al., *Definitions of terms relating to the structure and processing of sols, gels, networks, and inorganic-organic hybrid materials (IUPAC Recommendations 2007).* Pure and Applied Chemistry, 2007. **79**(10): p. 1801-1829.

27. Kistler, S.S., *Coherent Expanded Aerogels.* J. Phys. Chem, 1932. **36**(1): p. 52-64.

28. Hüsing, N. and U. Schubert, *Aerogels—Airy Materials: Chemistry, Structure, and Properties.* Angew. Chem. Int. Ed, 1998(37): p. 22-45.

29. Pierre, A.C. and G.M. Pajonk, *Chemistry of Aerogels and Their Applications.* Chem.Rev, 2002(102): p. 4243-4265.

30. Ziegler, C., et al., *Modern Inorganic Aerogels.* Angew Chem Int Ed Engl, 2017. **56**(43): p. 13200-13221.

31. Research, A.M. *Aerogel Market by Form (Blanket, Particle, Panel, Monolith), by Type (Silica, Polymers, Carbon, Others), by End Use Industry (Building and Construction, Oil and Gas, Automotive, Aerospace, Performance Coatings, Others): Global Opportunity Analysis and Industry Forecast, 2023-2032.* 2023 [cited 2023.

32. Budtova, T., et al., *Acoustic Properties of Aerogels: Current Status and Prospects.* Advanced Engineering Materials, 2022. **25**(6).

33. Kamal Mohamed, S.M., C. Heinrich, and B. Milow, *Effect of Process Conditions on the Properties of Resorcinol-Formaldehyde Aerogel Microparticles Produced via Emulsion-Gelation Method.* Polymers (Basel), 2021. **13**(15).

34. Romero-Montero, A., et al., *Biopolymeric Fibrous Aerogels: The Sustainable Alternative for Water Remediation.* Polymers (Basel), 2023. **15**(2).

35. Rose, A., et al., *Photocatalytic Activity and Electron Storage Capability of TiO2 Aerogels with an Adjustable Surface Area.* ACS Applied Energy Materials, 2022. **5**(12): p. 14966-14978.

36. Rashid, A.B., et al., *Silica Aerogel: Synthesis, Characterization, Applications, and Recent Advancements.* Particle & Particle Systems Characterization, 2023. **40**(6).

37. Sanchez, C., et al., *Applications of hybrid organic–inorganic nanocomposites.* Journal of Materials Chemistry, 2005. **15**(35-36).

38. Rolison, D.R. and B. Dunn, *Electrically conductive oxide aerogels: new materials in electrochemistry.* Journal of Materials Chemistry, 2001. **11**(4): p. 963-980.

39. Maleki, H., *Recent advances in aerogels for environmental remediation applications: A review.* Chemical Engineering Journal, 2016. **300**: p. 98-118.

40. Du, A., et al., *A Special Material or a New State of Matter: A Review and Reconsideration of the Aerogel.* Materials (Basel), 2013. **6**(3): p. 941-968.

41. Karamikamkar, S., H.E. Naguib, and C.B. Park, *Advances in precursor system for silica-based aerogel production toward improved mechanical properties, customized morphology, and multifunctionality: A review.* Adv Colloid Interface Sci, 2020. **276**: p. 102101.

42. Pekala, R.W., *Organic aerogels from the polycondensation of resorcinol with formaldehyde.* Journal of Materials Science, 1989. **24**: p. 3221-3227.

References

43. Feinle, A. and N. Hüsing, *Mixed metal oxide aerogels from tailor-made precursors.* The Journal of Supercritical Fluids, 2015. **106**: p. 2-8.

44. Nakanishi, Y., et al., *Colorless Transparent Melamine–Formaldehyde Aerogels for Thermal Insulation.* ACS Applied Nano Materials, 2020. **3**(1): p. 49-54.

45. He, F., et al., *Modified aging process for silica aerogel.* Journal of Materials Processing Technology, 2009. **209**(3): p. 1621-1626.

46. Subrahmanyam, R., et al., *On the Road to Biopolymer Aerogels-Dealing with the Solvent.* Gels, 2015. **1**(2): p. 291-313.

47. Gurikov, P., et al., *110th Anniversary: Solvent Exchange in the Processing of Biopolymer Aerogels: Current Status and Open Questions.* Industrial & Engineering Chemistry Research, 2019. **58**(40): p. 18590-18600.

48. Ubeyitogullari, A. and O.N. Ciftci, *Formation of nanoporous aerogels from wheat starch.* Carbohydrate Polymers, 2016. **147**: p. 125-132.

49. Soleimani Dorcheh, A. and M.H. Abbasi, *Silica aerogel; synthesis, properties and characterization.* Journal of Materials Processing Technology, 2008. **199**(1-3): p. 10-26.

50. Sahin, I., et al., *Kinetics of Supercritical Drying of Gels.* Gels, 2017. **4**(1).

51. Kim, C.E., J.S. Yoon, and H.J. Hwang, *Synthesis of nanoporous silica aerogel by ambient pressure drying.* Journal of Sol-Gel Science and Technology, 2008. **49**(1): p. 47-52.

52. Borisova, A., et al., *A sustainable freeze-drying route to porous polysaccharides with tailored hierarchical meso- and macroporosity.* Macromol Rapid Commun, 2015. **36**(8): p. 774-9.

53. Cheng, Q., C. Huang, and A.P. Tomsia, *Freeze Casting for Assembling Bioinspired Structural Materials.* Adv Mater, 2017. **29**(45).

54. Deville, S., *Ice-templating, freeze casting: Beyond materials processing.* Journal of Materials Research, 2013. **28**(17): p. 2202-2219.

55. Teagarden, D., L., and D. Baker, S., , *Practical aspects of lyophilization using non-aqueous co-solvent systems.* European Journal of Pharmaceutical Sciences, 2002(15): p. 115-133.

56. Basak, S. and R.S. Singhal, *The potential of supercritical drying as a "green" method for the production of food-grade bioaerogels: A comprehensive critical review.* Food Hydrocolloids, 2023. **141**.

57. Budtova, T., *Cellulose II aerogels: a review.* Cellulose, 2019. **26**(1): p. 81-121.

58. von Bommel, M.J. and A.B. de Haan, *Drying of silica gels with supercritical carbon dioxide.* Journal of Materials Science, 1994(29): p. 943-948.

59. O´Sullivan, A.C., *Cellulose: the structure slowly unravels.* Cellulose, 1997(4): p. 173-207.

60. Bessueille, L. and V. Bulone, *A survey of cellulose biosynthesis in higher plants.* Plant Biotechnology, 2008(25): p. 315–322.

61. Coseri, S., *Cellulose: To depolymerize... or not to ?* Biotechnology Advances, 2017(35): p. 251-266.

62. French, A.D., *Glucose, not cellobiose, is the repeating unit of cellulose and why that is important.* Cellulose, 2017. **24**(11): p. 4605-4609.

63. Medronho, B. and B. Lindman, *Competing forces during cellulose dissolution: From solvents to mechanisms.* Current Opinion in Colloid & Interface Science, 2014. **19**(1): p. 32-40.

64. Hindi, S.S.Z., *Differentiation and Synonyms Standardization of Amorphous andCrystalline Cellulosic Products.* Nanoscience and Nanotechnology Research, 2017. **4**(3): p. 73-85.

References

65.   Boufi, S., et al., *11 - Nanocellulose: Preparation methods and applications*, in *Cellulose-Reinforced Nanofibre Composites: Production, Properties and Applications*. 2017, Elsevier. p. 153-173.

66.   Fleming, K., D.G. Gray, and S. Matthews, *Cellulose crystallites.* Chemistry, 2001. **7**(9): p. 1831-5.

67.   Hallac, B.B. and A.J. Ragauskas, *Analyzing cellulose degree of polymerization and its relevancy to cellulosic ethanol.* Biofuels, Bioproducts and Biorefining, 2011. **5**(2): p. 215-225.

68.   Agarwal, U.P., et al., *Detection and quantitation of cellulose II by Raman spectroscopy.* Cellulose, 2021. **28**(14): p. 9069-9079.

69.   Geng, H., et al., *Characterisation of cellulose films regenerated from acetone/water coagulants.* Carbohydr Polym, 2014. **102**: p. 438-44.

70.   Östlund, Å., et al., *Modification of crystallinity and pore size distribution in coagulated cellulose films.* Cellulose, 2013. **20**(4): p. 1657-1667.

71.   Faria-Tischer, P.C., et al., *Preparation of cellulose II and IIII films by allomorphic conversion of bacterial cellulose I pellicles.* Mater Sci Eng C Mater Biol Appl, 2015. **51**: p. 167-73.

72.   Zhou, J., L. Zhang, and J. Cai, *Behavior of Cellulose in NaOH/Urea Aqueous Solution Characterized by Light Scattering and Viscometry.* Journal of Polymer Science: Part B: Polymer Physics, 2004. **42**(2): p. 347-353.

73.   Sjöholm, E., *Size Exclusion Chromatography of Cellulose and Cellulose Derivatives*, in *Handbook of Size Exclusion Chromatography and Related Techniques*, C. Wu, Editor. 2004, Marcel Dekker, Inc.

74.   Torres, F.G., J.J. Arroyo, and O.P. Troncoso, *Bacterial cellulose nanocomposites: An all-nano type of material.* Mater Sci Eng C Mater Biol Appl, 2019. **98**: p. 1277-1293.

75.   Thomas, B., et al., *Nanocellulose, a Versatile Green Platform: From Biosources to Materials and Their Applications.* Chem Rev, 2018. **118**(24): p. 11575-11625.

76.   Budtova, T. and P. Navard, *Cellulose in NaOH–water based solvents: a review.* Cellulose, 2015. **23**(1): p. 5-55.

77.   Wang, S., A. Lu, and L. Zhang, *Recent advances in regenerated cellulose materials.* Progress in Polymer Science, 2016. **53**: p. 169-206.

78.   Olsson, C. and G. Westm, *Direct Dissolution of Cellulose: Background, Means and Applications*, in *Cellulose - Fundamental Aspects*. 2013.

79.   Medronho, B. and B. Lindman, *Brief overview on cellulose dissolution/regeneration interactions and mechanisms.* Adv Colloid Interface Sci, 2015. **222**: p. 502-8.

80.   Kamide, K., K. Okajima, and K. Kowsaka, *Dissolution of Natural Cellulose into Aqueous Alkali Solution: Role of Super -Molecular Structure of Cellulose.* Polymer Journal, 1992. **24**(1): p. 71-86.

81.   Saalwächter, K., *Cellulose Solutions in Water Containing Metal Complexes.* Macromolecules 2000(33): p. 4094-4107.

82.   Schestakow, M., I. Karadagli, and L. Ratke, *Cellulose aerogels prepared from an aqueous zinc chloride salt hydrate melt.* Carbohydr Polym, 2016. **137**: p. 642-649.

83.   Sen, S., et al., *Ionic Liquid Character of Zinc Chloride Hydrates Define Solvent Characteristics that Afford the Solubility of Cellulose.* J Phys Chem B, 2016. **120**(6): p. 1134-41.

84.   Karadagli, I., et al. *Synthesis and characterization of highly porous cellulose aerogels for textiles applications.* in *CELLMAT 2012*. 2012. Desden, Germany: Fraunhofer Institute for Manufacturing Technology and Advanced Materials, IFAM.

85.   Zhang, C., et al., *Dissolution mechanism of cellulose in N,N-dimethylacetamide/lithium chloride: revisiting through molecular interactions.* J Phys Chem B, 2014. **118**(31): p. 9507-14.

References

86.   Heinze, T., et al., *Effective preparation of cellulose derivatives in a new simple cellulose solvent.* Macromol. Chem. Phys., 2000(201): p. 627-631.

87.   Uddin, A.J., et al., *Preparation and Physical Properties of Regenerated Cellulose Fibres from Sugarcane Bagasse.* Textile Research Journal, 2010. **80**(17): p. 1846-1858.

88.   Liebner, F., et al., *Cellulosic aerogels as ultra-lightweight materials. Part 2: Synthesis and properties 2nd ICC 2007, Tokyo, Japan, October 25–29, 2007.* Holzforschung, 2009. **63**(1).

89.   Lin, W.-H. and S.C. Jana, *Analysis of porous structures of cellulose aerogel monoliths and microparticles.* Microporous and Mesoporous Materials, 2021. **310**.

90.   Zeng, B., X. Wang, and N. Byrne, *Development of cellulose based aerogel utilizing waste denim-A Morphology study.* Carbohydr Polym, 2019. **205**: p. 1-7.

91.   Magali Egal, ‡ Tatiana Budtova,*,† and Patrick Navard, *Structure of Aqueous Solutions of Microcrystalline Cellulose/ Sodium Hydroxide below 0 °C and the Limit of Cellulose Dissolution.* Biomacromolecules, 2007(8): p. 2282-2287.

92.   Lu, A., et al., *Investigation on metastable solution of cellulose dissolved in NaOH/urea aqueous system at low temperature.* J Phys Chem B, 2011. **115**(44): p. 12801-8.

93.   Lue, A. and L. Zhang, *Rheological behaviors in the regimes from dilute to concentrated in cellulose solutions dissolved at low temperature.* Macromol Biosci, 2009. **9**(5): p. 488-96.

94.   Xiong, B., et al., *Dissolution of cellulose in aqueous NaOH/urea solution: role of urea.* Cellulose, 2014. **21**(3): p. 1183-1192.

95.   Pereira, A., et al., *Cellulose gelation in NaOH solutions is due to cellulose crystallization.* Cellulose, 2018. **25**(6): p. 3205-3210.

96.   Gunnarsson, M., et al., *The CO2 capturing ability of cellulose dissolved in NaOH(aq) at low temperature.* Green Chemistry, 2018. **20**(14): p. 3279-3286.

97.   Qi, H., et al., *The dissolution of cellulose in NaOH-based aqueous system by two-step process.* Cellulose, 2010. **18**(2): p. 237-245.

98.   Qi, H., C. Chang, and L. Zhang, *Effects of temperature and molecular weight on dissolution of cellulose in NaOH/urea aqueous solution.* Cellulose, 2008. **15**(6): p. 779-787.

99.   Song, J., et al., *Study on the interaction between urea and cellulose by combining solid-state 13C CP/MAS NMR and extended Hückel charges.* Cellulose, 2014. **21**(6): p. 4019-4027.

100.   Cai, L., Y. Liu, and H. Liang, *Impact of hydrogen bonding on inclusion layer of urea to cellulose: Study of molecular dynamics simulation.* Polymer, 2012. **53**(5): p. 1124-1130.

101.   Chen, Y., et al., *The thermodynamics of enhanced dope stability of cellulose solution in NaOh solution by urea.* Carbohydr Polym, 2023(311): p. 120744.

102.   Liu, G., et al., *Molecular dynamics studies on the aggregating behaviors of cellulose molecules in NaOH/urea aqueous solution.* Colloids and Surfaces A: Physicochemical and Engineering Aspects, 2020. **594**: p. 124663.

103.   Liu, G., et al., *A molecular dynamics study of cellulose inclusion complexes in NaOH/urea aqueous solution.* Carbohydrate Polymers, 2018. **185**: p. 12-18.

104.   Wernersson, E., B. Stenqvist, and M. Lund, *The mechanism of cellulose solubilization by urea studied by molecular simulation.* Cellulose, 2015. **22**(2): p. 991-1001.

105.   Huh, E., et al., *Thermodynamic analysis of cellulose complex in NaOH–urea solution using reference interaction site model.* Cellulose, 2020. **27**(12): p. 6767-6775.

106.   Gavillon, R.B., Tatiana, *Kinetics of Cellulose Regeneration from Cellulose-NaOH-Water Gels and Comparison with Cellulose-N Methylmorpholine-N-Oxide-Water Solutions.* Biomacromolecules, 2007(9): p. 424-432.

107.   Trygg, J., et al., *Physicochemical design of the morphology and ultrastructure of cellulose beads.* Carbohydr Polym, 2013. **93**(1): p. 291-9.

References

108. Shi, J., et al., *On preparation, structure and performance of high porosity bulk cellulose aerogel.* Plastics, Rubber and Composites, 2014. **44**(1): p. 26-32.

109. Zhang, L.M., Yuan; Zhou, Jinping; Cai, Jie, *Effects of Coagulation Conditions on the Properties of Regenerated Cellulose Films Prepared in NaOH/Urea Aqueous Solution.* Ind. Eng. Chem. Res, 2005(44): p. 522-529.

110. Isobe, N., et al., *Internal surface polarity of regenerated cellulose gel depends on the species used as coagulant.* J Colloid Interface Sci, 2011. **359**(1): p. 194-201.

111. Kawano, T., S. Iikubo, and Y. Andou, *The Relationship between Crystal Structure and Mechanical Performance for Fabrication of Regenerated Cellulose Film through Coagulation Conditions.* Polymers (Basel), 2021. **13**(24).

112. From, M., et al., *Tuning the properties of regenerated cellulose: Effects of polarity and water solubility of the coagulation medium.* Carbohydr Polym, 2020. **236**: p. 116068.

113. Parajuli, P., et al., *Cellulose-based monoliths with enhanced surface area and porosity.* Journal of Applied Polymer Science, 2020. **137**(34).

114. Parajuli, P., et al., *Tuning the morphological properties of cellulose aerogels: an investigation of salt-mediated preparation.* Cellulose, 2021. **28**(12): p. 7559-7577.

115. Gregory, K.P., et al., *Understanding specific ion effects and the Hofmeister series.* Phys Chem Chem Phys, 2022. **24**(21): p. 12682-12718.

116. Liu, L., Y. Wang, and A. Lu, *Effect of electrolyte on regenerated cellulose film as gold nanoparticle carrier.* Carbohydr Polym, 2019. **210**: p. 234-244.

117. Grignon, J. and A.M. Scallan, *Effect of pH and neutral salts upon the swelling of cellulose gels.* Journal of Applied Polymer Science, 1980. **25**(12): p. 2829-2843.

118. Zheng, Q., et al., *Fabrication and application of starch-based aerogel: Technical strategies.* Trends in Food Science & Technology, 2020. **99**: p. 608-620.

119. Chen, K. and H. Zhang, *Alginate/pectin aerogel microspheres for controlled release of proanthocyanidins.* Int J Biol Macromol, 2019. **136**: p. 936-943.

120. Alnaief, M., R. Obaidat, and H. Mashaqbeh, *Effect of processing parameters on preparation of carrageenan aerogel microparticles.* Carbohydr Polym, 2018. **180**: p. 264-275.

121. Wakerley, D.W., et al., *Solar-driven reforming of lignocellulose to H2 with a CdS/CdOx photocatalyst.* Nat Energy, 2017(2): p. 17021.

122. Mavelil-Sam, R., L.A. Pothan, and S. Thomas, *Chapter 1. Polysaccharide and Protein Based Aerogels: An Introductory Outlook*, in *Biobased Aerogels*. 2018. p. 1-8.

123. Rao, J., et al., *Hemicellulose: Structure, chemical modification, and application.* Progress in Polymer Science, 2023. **140**.

124. Salam, A., et al., *Crosslinked hemicellulose citrate–chitosan aerogel foams.* Carbohydrate Polymers, 2011. **84**(4): p. 1221-1229.

125. Chung, H. and N.R. Washburn, *Extraction and Types of Lignin*, in *Lignin in Polymer Composites*. 2016, Elsevier.

126. Grishechko, L.I., et al., *Lignin–phenol–formaldehyde aerogels and cryogels.* Microporous and Mesoporous Materials, 2013. **168**: p. 19-29.

127. Dang, Y.T., et al., *Green fabrication of bio-based aerogels from coconut fibers for wastewater treatment.* Journal of Porous Materials, 2022. **29**(4): p. 1265-1278.

128. Setyawan, H., et al., *Fabrication of Hydrophobic Cellulose Aerogels from Renewable Biomass Coir Fibers for Oil Spillage Clean-Up.* Journal of Polymers and the Environment, 2022. **30**(12): p. 5228-5238.

129. Yue, X., et al., *Superhydrophobic waste paper-based aerogel as a thermal insulating cooler for building.* Energy, 2022. **245**.

130. Jadhav, P.S., et al., *Biogenic Straw Aerogel Thermal Insulation Materials.* Advanced Engineering Materials, 2023. **25**(13).

References

131. Sun, J., et al., *Thermal-insulating, flame-retardant and mechanically resistant aerogel based on bio-inspired tubular cellulose.* Composites Part B: Engineering, 2021. **220**.

132. Azman Mohammad Taib, M.N., et al., *Recent progress in cellulose-based composites towards flame retardancy applications.* Polymer, 2022. **244**.

133. Liyanage, S., et al., *Production and Surface Modification of Cellulose Bioproducts.* Polymers (Basel), 2021. **13**(19).

134. Liang, X., et al., *Thermal Kinetics of a Lignin-Based Flame Retardant.* Polymers (Basel), 2020. **12**(9).

135. Hobbs, C.E., *Recent Advances in Bio-Based Flame Retardant Additives for Synthetic Polymeric Materials.* Polymers (Basel), 2019. **11**(2).

136. Solihat, N.N., et al., *Recent Developments in Flame-Retardant Lignin-Based Biocomposite: Manufacturing, and characterization.* Journal of Polymers and the Environment, 2022. **30**(11): p. 4517-4537.

137. Costes, L., et al., *Phosphorus and nitrogen derivatization as efficient route for improvement of lignin flame retardant action in PLA.* European Polymer Journal, 2016. **84**: p. 652-667.

138. Zhao, C., et al., *Revealing Structural Differences between Alkaline and Kraft Lignins by HSQC NMR.* Industrial & Engineering Chemistry Research, 2019. **58**(14): p. 5707-5714.

139. Fiţigău, I.F., F. Peter, and C.G. Boeriu, *Structural Analysis of Lignins from DifferentSources.* International Journal of Chemical, Molecular, Nuclear, Materials and Metallurgical Engineering, 2013. **7**(4).

140. Goldmann, W.M., et al., *Solubility and fractionation of Indulin AT kraft lignin in ethanol-water media.* Separation and Purification Technology, 2019. **209**: p. 826-832.

141. Melro, E., et al., *Dissolution of kraft lignin in alkaline solutions.* Int J Biol Macromol, 2020. **148**: p. 688-695.

142. Sameni, J., S. Krigstin, and M. Sain, *Solubility of Lignin and Acetylated Lignin in Organic Solvents.* BioResources, 2017. **12**(1): p. 1548-1565.

143. Norgren, M. and B. Lindström, *Dissociation of Phenolic Groups in Kraft Lignin at Elevated Temperatures.* Holzforschung, 2000. **54**(5): p. 519–527.

144. Lindström, T., *The colloidal behaviour of kraft lignin Part II. Coagulation of kraft lignin sols in the presence of simple and complex metal ions.* Colloid & Polymer Sci, 1980. **258**: p. 168-173.

145. Sewring, T., *Precipitation of Kraft Lignin from Aqueous Solutions*, in *Department of Chemistry and Chemical Engineering*. 2019, CHALMERS UNIVERSITY OF TECHNOLOGY.

146. Cayla, A., et al., *PLA with Intumescent System Containing Lignin and Ammonium Polyphosphate for Flame Retardant Textile.* Polymers (Basel), 2016. **8**(9).

147. Javed, A., et al., *Lignin-Containing Coatings for Packaging Materials-Pilot Trials.* Polymers (Basel), 2021. **13**(10).

148. Maximova, N., et al., *Lignin adsorption on cellulose fibre surfaces: Effect on surface chemistry, surface morphology and paper strength.* Cellulose, 2001. **8**: p. 113-125.

149. Koljonen, K., et al., *Precipitation of lignin and extractives on kraft pulp: effect on surface chemistry, surface morphology and paper strength.* Cellulose, 2004. **11**(2): p. 209-224.

150. Houtman, C.J. and R.H. Atalla, *CeIIuIose-Lignin Interactions (A Computational Study).* Plant Physiol, 1995. **107**(3): p. 977-984.

151. Costa, C., et al., *Lignin enhances cellulose dissolution in cold alkali.* Carbohydr Polym, 2021. **274**: p. 118661.

References

152. Sescousse, R., A. Smacchia, and T. Budtova, *Influence of lignin on cellulose-NaOH-water mixtures properties and on Aerocellulose morphology.* Cellulose, 2010. **17**(6): p. 1137-1146.

153. Gabov, K., et al., *Preparation, characterization and antimicrobial application of hybrid cellulose-lignin beads.* Cellulose, 2016. **24**(2): p. 641-658.

154. Ciolacu, D., et al., *MORPHOLOGICAL AND SURFACE ASPECTS OF CELLULOSE-LIGNIN HYDROGELS.* Cellulose Chem. Technol, 2013. **47**(5-6): p. 377-386.

155. Fernandes, I.A.A., et al., *Bacterial cellulose: From production optimization to new applications.* Int J Biol Macromol, 2020. **164**: p. 2598-2611.

156. Islam, M.U., et al., *Strategies for cost-effective and enhanced production of bacterial cellulose.* Int J Biol Macromol, 2017. **102**: p. 1166-1173.

157. Low, D.Y.S., et al., *Recent Developments in Nanocellulose-Reinforced Rubber Matrix Composites: A Review.* Polymers (Basel), 2021. **13**(4).

158. Chen, Y., et al., *Recent Progress on Nanocellulose Aerogels: Preparation, Modification, Composite Fabrication, Applications.* Adv Mater, 2021. **33**(11): p. e2005569.

159. Schestakow, M., *Nanostrukturierte Cellulose-Aerogel-Polyesterverbunde*, in *Fakultät für Georessourcen und Materialtechnik*. 2020, Rheinisch-Westfälischen Technischen Hochschule Aachen.

160. Klemm, D., et al., *Nanocelluloses: a new family of nature-based materials.* Angew Chem Int Ed Engl, 2011. **50**(24): p. 5438-66.

161. Mishra, S., P.S. Kharkar, and A.M. Pethe, *Biomass and waste materials as potential sources of nanocrystalline cellulose: Comparative review of preparation methods (2016 - Till date).* Carbohydr Polym, 2019. **207**: p. 418-427.

162. Long, L.Y., Y.X. Weng, and Y.Z. Wang, *Cellulose Aerogels: Synthesis, Applications, and Prospects.* Polymers (Basel), 2018. **10**(6).

163. Zaman, A., et al., *Preparation, Properties, and Applications of Natural Cellulosic Aerogels: A Review.* Energy and Built Environment, 2020. **1**(1): p. 60-76.

164. Sescousse, R., R. Gavillon, and T. Budtova, *Wet and dry highly porous cellulose beads from cellulose–NaOH–water solutions: influence of the preparation conditions on beads shape and encapsulation of inorganic particles.* Journal of Materials Science, 2010. **46**(3): p. 759-765.

165. Sescousse, R., R. Gavillon, and T. Budtova, *Aerocellulose from cellulose–ionic liquid solutions: Preparation, properties and comparison with cellulose–NaOH and cellulose–NMMO routes.* Carbohydrate Polymers, 2011. **83**(4): p. 1766-1774.

166. Rudaz, C., *Cellulose and Pectin Aerogels : Towards their nano-structuration.* 2013, Ecole Nationale Supérieure des Mines de Paris.

167. Cai, J., et al., *Cellulose aerogels from aqueous alkali hydroxide-urea solution.* ChemSusChem, 2008. **1**(1-2): p. 149-54.

168. Buchtová, N. and T. Budtova, *Cellulose aero-, cryo- and xerogels: towards understanding of morphology control.* Cellulose, 2016. **23**(4): p. 2585-2595.

169. Gavillon, R. and T. Budtova, *Aerocellulose: New Highly Porous Cellulose Prepared from Cellulose-NaOH Aqueous Solutions.* Biomacromolecules, 2008. **9**(1): p. 269-277.

170. Nguyen, S.T., et al., *Advanced thermal insulation and absorption properties of recycled cellulose aerogels.* Colloids and Surfaces A: Physicochemical and Engineering Aspects, 2014. **445**: p. 128-134.

171. Kaya, M. and A. Tabak, *Recycling of an Agricultural Bio-waste as a Novel Cellulose Aerogel: A Green Chemistry Study.* Journal of Polymers and the Environment, 2019. **28**(1): p. 323-330.

References

172. Duchemin, B.J.C., A.P. Mathew, and K. Oksman, *All-cellulose composites by partial dissolution in the ionic liquid 1-butyl-3-methylimidazolium chloride.* Composites Part A: Applied Science and Manufacturing, 2009. **40**(12): p. 2031-2037.

173. Duchemin, B.J.C., et al., *Aerocellulose based on all-cellulose composites.* Journal of Applied Polymer Science, 2010. **115**(1): p. 216-221.

174. Gindl, W. and J. Keckes, *All-cellulose nanocomposite.* Polymer, 2005. **46**(23): p. 10221-10225.

175. Korhonen, O. and T. Budtova, *Gelation of cellulose-NaOH solutions in the presence of cellulose fibers.* Carbohydr Polym, 2019. **224**: p. 115152.

176. Bian, H., et al., *Preparation of Diameter-Controlled Cellulose Aerogel Spheres via Atomization Method and Their Load Performance.* Macromolecular Materials and Engineering, 2020. **305**(11).

177. Coombs Obrien, J., et al., *Continuous Production of Cellulose Microbeads via Membrane Emulsification.* ACS Sustainable Chemistry & Engineering, 2017. **5**(7): p. 5931-5939.

178. Druel, L., et al., *Cellulose Aerogel Microparticles via Emulsion-Coagulation Technique.* Biomacromolecules, 2020. **21**(5): p. 1824-1831.

179. Gericke, M., J. Trygg, and P. Fardim, *Functional cellulose beads: preparation, characterization, and applications.* Chem Rev, 2013. **113**(7): p. 4812-36.

180. Preibisch, I., et al., *Polysaccharide-Based Aerogel Bead Production via Jet Cutting Method.* Materials (Basel), 2018. **11**(8).

181. Chan, E.S., et al., *Prediction models for shape and size of ca-alginate macrobeads produced through extrusion-dripping method.* J Colloid Interface Sci, 2009. **338**(1): p. 63-72.

182. Lee, B.B., P. Ravindra, and E.S. Chan, *Size and Shape of Calcium Alginate Beads Produced by Extrusion Dripping.* Chemical Engineering & Technology, 2013: p. n/a-n/a.

183. Schroeter, B., et al., *Cellulose aerogel particles: control of particle and textural properties in jet cutting process.* Cellulose, 2020. **28**(1): p. 223-239.

184. Sheng, Z., et al., *The Rising Aerogel Fibers: Status, Challenges, and Opportunities.* Adv Sci (Weinh), 2023. **10**(9): p. e2205762.

185. Schulz, B., *Cellulose-Aerogelfasern*, in *Fakultät für Georessourcen und Materialtechnik*. 2016, Rheinisch-Westfälischen Technischen Hochschule Aachen.

186. Asaadi, S., et al., *Renewable High-Performance Fibers from the Chemical Recycling of Cotton Waste Utilizing an Ionic Liquid.* ChemSusChem, 2016. **9**(22): p. 3250-3258.

187. Shen, H., T. Sun, and J. Zhou, *Recent Progress in Regenerated Cellulose Fibers by Wet Spinning.* Macromolecular Materials and Engineering, 2023.

188. Cai, J., Zhang, L., Jinping, Z., Hao, L., Chen, H., Jin, H, *Novel Fibers Prepared from Cellulose in NaOH/Urea Aqueous Solution.* Macromolecular Rapid Communications, 2004. **25**: p. 1558-1562.

189. Wan, C. and J. Li, *Cellulose aerogels based on a green NaOH/PEG solution: Preparation, characterization and influence of molecular weight of PEG.* Fibers and Polymers, 2015. **16**(6): p. 1230-1236.

190. Yang, Y., et al., *Structure and properties of regenerated cellulose fibers from aqueous NaOH/thiourea/urea solution.* Cellulose, 2017. **24**(10): p. 4123-4137.

191. Karadagli, I., et al., *Production of porous cellulose aerogel fibers by an extrusion process.* The Journal of Supercritical Fluids, 2015. **106**: p. 105-114.

192. Rostamitabar, M., et al., *Effect of Cellulose Characteristics on the Properties of the Wet-Spun Aerogel Fibers.* Applied Sciences, 2021. **11**(4).

193. Rostamitabar, M., et al., *Cellulose aerogel micro fibers for drug delivery applications.* Mater Sci Eng C Mater Biol Appl, 2021. **127**: p. 112196.

References

194. Mroszczok, J., et al., *Cellulose Aerogel Fibres for Thermal Encapsulation of Diesel Hybrid Engines for Fuel Savings in Cars.* Materials Today: Proceedings, 2017. **4**: p. S244-S248.

195. Meifang, Z., et al., *Continuous cellulose aerogel fiber and preparation method thereof* E.P. Office, Editor. 2016, NAT UNIV DONG HWA.

196. Meifang, Z., et al., *Preparation method of continuous cellulose/TiO2 aerogel fiber with photocatalytic performance* E.P. Office, Editor. 2016, NAT UNIV DONG HWA.

197. Manaia, J.P., A.T. Manaia, and L. Rodriges, *Industrial Hemp Fibers: An Overview.* Fibers, 2019. **7**(12).

198. Zuk, M., et al., *Linseed, the multipurpose plant.* Industrial Crops and Products, 2015. **75**: p. 165-177.

199. Daria, M., L. Krzysztof, and M. Jakub, *Characteristics of biodegradable textiles used in environmental engineering: A comprehensive review.* Journal of Cleaner Production, 2020. **268**.

200. Stanzilla, *Flax field in Morsan (Eure, France).* 2015: Wikimedia Commons.

201. Aleks, *Cultivation of industrial hemp for fiber and for grain in france.* 2000: Wikimedia Commons.

202. Schluttenhofer, C. and L. Yuan, *Challenges towards Revitalizing Hemp: A Multifaceted Crop.* Trends Plant Sci, 2017. **22**(11): p. 917-929.

203. Amaducci, S., et al., *Key cultivation techniques for hemp in Europe and China.* Industrial Crops and Products, 2015. **68**: p. 2-16.

204. Kotecka-Majchrzak, K., et al., *Oilseed proteins – Properties and application as a food ingredient.* Trends in Food Science & Technology, 2020. **106**: p. 160-170.

205. Parvez, A.M., J.D. Lewis, and M.T. Afzal, *Potential of industrial hemp (Cannabis sativa L.) for bioenergy production in Canada: Status, challenges and outlook.* Renewable and Sustainable Energy Reviews, 2021. **141**.

206. Zhao, J., et al., *Bioconversion of industrial hemp biomass for bioethanol production: A review.* Fuel, 2020. **281**.

207. Ingrao, C., et al., *Energy and environmental assessment of industrial hemp for building applications: A review.* Renewable and Sustainable Energy Reviews, 2015. **51**: p. 29-42.

208. Musio, S., J. Mussig, and S. Amaducci, *Optimizing Hemp Fiber Production for High Performance Composite Applications.* Front Plant Sci, 2018. **9**: p. 1702.

209. Shim, Y.Y., et al., *Flaxseed (Linum usitatissimum L.) oil processing and selected products.* Trends in Food Science & Technology, 2015. **43**(2): p. 162-177.

210. Bekhit, A.E.-D.A., et al., *Flaxseed: Composition, detoxification, utilization, and opportunities.* Biocatalysis and Agricultural Biotechnology, 2018. **13**: p. 129-152.

211. Goyal, A., et al., *Flax and flaxseed oil: an ancient medicine & modern functional food.* J Food Sci Technol, 2014. **51**(9): p. 1633-53.

212. Ramesh, M., *Flax (Linum usitatissimum L.) fibre reinforced polymer composite materials: A review on preparation, properties and prospects.* Progress in Materials Science, 2019. **102**: p. 109-166.

213. Melelli, A., et al., *Evolution of the ultrastructure and polysaccharide composition of flax fibres over time: When history meets science.* Carbohydr Polym, 2022. **291**: p. 119584.

214. Manian, A.P., M. Cordin, and T. Pham, *Extraction of cellulose fibers from flax and hemp: a review.* Cellulose, 2021. **28**(13): p. 8275-8294.

215. Saleem, M.H., et al., *Flax (Linum usitatissimum L.): A Potential Candidate for Phytoremediation? Biological and Economical Points of View.* Plants (Basel), 2020. **9**(4).

References

216. Amaducci, S. and H. Gusovius, *Hemp - Cultivation, Extraction and Processing*, in *Industrial Applications of Natural Fibres: Structure, Properties and Technical Applications*, J. Müssig, Editor. 2010, John Wiley & Sons, Ltd.

217. Akin, D.E., *Flax – Structure, Chemistry, Retting and Processing*, in *Industrial Applications of Natural Fibres: Structure, Properties and Technical Applications*, J. Müssig, Editor. 2010, John Wiley & Sons.

218. Ebskamp, M.J.M., *Engineering flax and hemp for an alternative to cotton.* Trends in Biotechnology, 2002. **20**(6): p. 229-230.

219. Kopania, E., J. Wietecha, and D. Ciechańska, *Studies on Isolation of Cellulose Fibres from Waste Plant Biomass.* Fibers and Textiles in Eastern Europe, 2012. **20**(96): p. 167-172.

220. Virtanen, T., et al., *A physico-chemical characterisation of new raw materials for microcrystalline cellulose manufacturing.* Cellulose, 2011. **19**(1): p. 219-235.

221. Petrova, S.N., I.Y. Volkova, and A.G. Zakharov, *Oxidative Delignification of Flax Fiber.* Russian Journal of Applied Chemistry, 2003. **76**(8): p. 1344-1347.

222. Modenbach, A.A. and S.E. Nokes, *Effects of Sodium Hydroxide Pretreatment on Structural Components of Biomass.* Transactions of the ASABE, 2014: p. 1187-1198.

223. Oriez, V., J. Peydecastaing, and P.-Y. Pontalier, *Lignocellulosic Biomass Mild Alkaline Fractionation and Resulting Extract Purification Processes: Conditions, Yields, and Purities.* Clean Technologies, 2020. **2**(1): p. 91-115.

224. Buranov, A.U. and G. Mazza, *Lignin in straw of herbaceous crops.* Industrial Crops and Products, 2008. **28**(3): p. 237-259.

225. More, A., T. Elder, and Z. Jiang, *A review of lignin hydrogen peroxide oxidation chemistry with emphasis on aromatic aldehydes and acids.* Holzforschung, 2021. **75**(9): p. 806-823.

226. Nguyen, H.S.H., et al., *Understanding the effects of cellulose fibers from various pre-treated barley straw on properties of aerogels.* Fuel Processing Technology, 2022. **236**.

227. Freitas, P.A.V., C. Gonzalez-Martinez, and A. Chiralt, *Influence of the cellulose purification process on the properties of aerogels obtained from rice straw.* Carbohydr Polym, 2023. **312**: p. 120805.

228. Ratke, L., Gurikov, P, *The Chemistry and Physics of Aerogels_ Synthesis, Processing, and Properties*. 2021: Cambridge University Press.

229. Swimm, K., et al., *Impact of thermal coupling effects on the effective thermal conductivity of aerogels.* Journal of Sol-Gel Science and Technology, 2017. **84**(3): p. 466-474.

230. Jennings, S.G., *The Mean Free Path In Air.* J. Aerosol Sci., 1988. **19**(2): p. 159-166.

231. Reichenauer, G., U. Heinemann, and H.P. Ebert, *Relationship between pore size and the gas pressure dependence of the gaseous thermal conductivity.* Colloids and Surfaces A: Physicochemical and Engineering Aspects, 2007. **300**(1-2): p. 204-210.

232. Ebert, H.-P., et al., *Intercomparison of Thermal Conductivity Measurements on a Nanoporous Organic Aerogel.* International Journal of Thermophysics, 2021. **42**(2).

233. Baldinelli, G., et al., *Thermal conductivity measurement of insulating innovative building materials by hot plate and heat flow meter devices: A Round Robin Test.* International Journal of Thermal Sciences, 2019. **139**: p. 25-35.

234. Gurikov, P., et al., *A novel approach to alginate aerogels: carbon dioxide induced gelation.* RSC Advances, 2015. **5**(11): p. 7812-7818.

235. Groult, S. and T. Budtova, *Tuning structure and properties of pectin aerogels.* European Polymer Journal, 2018. **108**: p. 250-261.

236. Malfait, W.J., et al., *The poor reliability of thermal conductivity data in the aerogel literature: a call to action!* J Solgel Sci Technol, 2024. **109**(2): p. 569-579.

References

237. Aegerter, M.A., N. Leventis, and M.M. Koebel, *Aerogels Handbook*. 2011: Springer New York.

238. Askari, R., S. Taheri, and S.H. Hejazi, *Thermal conductivity of granular porous media: A pore scale modeling approach.* AIP Advances, 2015. **5**(9).

239. Masamune, S. and J.M. Smith, *THERMAL CONDUCTIVITY OF BEDS OF SPHERICAL PARTICLES.* Ind. Eng. Chem. Fundamen., 1963. **2**(2): p. 136-142.

240. Duffy, J., ;, *Measuring the rheology of polymer solutions*. 2015.

241. Prüße, U., Jahnz, U., Wittlich, P., Breford, J & Vorlop, K.,, *Bead production with JetCutting and rotating disc/nozzle technologies.* Landbauforschung Völkenrode, 2002. **241**: p. 1-10.

242. Trilokesh, C. and K.B. Uppuluri, *Isolation and characterization of cellulose nanocrystals from jackfruit peel.* Sci Rep, 2019. **9**(1): p. 16709.

243. Poletto, M., H.L. Ornaghi, and A.J. Zattera, *Native Cellulose: Structure, Characterization and Thermal Properties.* Materials (Basel), 2014. **7**(9): p. 6105-6119.

244. Segal, L., Creely, J., J., Martin, A., E., Jr.,and Conrad, C., M., *An Empirical Method for Estimating the Degree of Crystallinity of Native Cellulose Using the X-Ray Diffractometer.* Textile Research Journal, 1959. **29**(10): p. 786-794

245. Park, S., Baker, J.O., Himmel, M.E. et al., *Research Cellulose crystallinity index: measurement techniques and their impact on interpreting cellulase performance.* Biotechnology for Biofuels, 2010. **3**(10): p. 1-10.

246. Nam, S., et al., *Segal crystallinity index revisited by the simulation of X-ray diffraction patterns of cotton cellulose Ibeta and cellulose II.* Carbohydr Polym, 2016. **135**: p. 1-9.

247. Lstiburek, J., *Relative Humidity*. 2002.

248. Block, S.S., *Humidity Requirements for Mold Growth.* Applied and Environmental Microbiology, 1953. **1**(6): p. 287-293.

249. Beuchat, L.R., et al., *Low-Water Activity Foods: Increased Concern as Vehicles of Foodborne Pathogens.* Journal of Food Protection, 2013. **76**(1): p. 150-172.

250. Costa, D., B. Milow, and K. Ganesan, *Impact of Weak Organic Acids as Coagulants on Tailoring the Properties of Cellulose Aerogel Beads.* Chemistry, 2024: p. e202401794.

251. Beluns, S., et al., *From Wood and Hemp Biomass Wastes to Sustainable Nanocellulose Foams.* Industrial Crops and Products, 2021. **170**.

252. Pircher, N., et al., *Impact of selected solvent systems on the pore and solid structure of cellulose aerogels.* Cellulose (Lond), 2016. **23**: p. 1949-1966.

253. Zhao, H., et al., *Interactions between cellulose and N-methylmorpholine-N-oxide.* Carbohydrate Polymers, 2007. **67**(1): p. 97-103.

254. Goliszek, M., et al., *The Influence of Lignin Diversity on the Structural and Thermal Properties of Polymeric Microspheres Derived from Lignin, Styrene, and/or Divinylbenzene.* Materials (Basel), 2019. **12**(18).

255. Yuan, Z., N.S. Kapu, and D.M. Martinez, *An eco-friendly scheme to eliminate silica problems during bamboo biomass fractionation.* Nordic Pulp & Paper Research Journal, 2017. **32**(1): p. 4-13.

256. Chaudhary, R. and P.L. Dhepe, *Solid base catalyzed depolymerization of lignin into low molecular weight products.* Green Chemistry, 2017. **19**(3): p. 778-788.

257. Mohamed, S.E., et al., *Removal of Lignin from Pulp Waste Water's Black Liquor via By-Pass Cement Dust.* Eurasian Chemico-Technological Journal, 2009. **11**: p. 51-59.

258. Astruc, J., et al., *Isolation of cellulose-II nanospheres from flax stems and their physical and morphological properties.* Carbohydr Polym, 2017. **178**: p. 352-359.

259. Apaydın Varol, E. and Ü. Mutlu, *TGA-FTIR Analysis of Biomass Samples Based on the Thermal Decomposition Behavior of Hemicellulose, Cellulose, and Lignin.* Energies, 2023. **16**(9).

References

260. Le Moigne, N., K. Jardeby, and P. Navard, *Structural changes and alkaline solubility of wood cellulose fibers after enzymatic peeling treatment.* Carbohydrate Polymers, 2010. **79**(2): p. 325-332.

261. Cai, J. and L. Zhang, *Unique Gelation Behavior of Cellulose in NaOH/Urea Aqueous Solution.* Biomacromolecules, 2006. **7**(1): p. 183-189.

262. Remmler, T., ; , *How to measure the shear viscosity properly?* 2016: International Expo for Materials Testing.

263. Bastos-González, D., et al., *Ions at interfaces: the central role of hydration and hydrophobicity.* Current Opinion in Colloid & Interface Science, 2016. **23**: p. 19-28.

264. Kang, B., et al., *Hofmeister Series: Insights of Ion Specificity from Amphiphilic Assembly and Interface Property.* ACS Omega, 2020. **5**(12): p. 6229-6239.

265. Nebot, V.J., et al., *Rational design of heat-set and specific-ion-responsive supramolecular hydrogels based on the Hofmeister effect.* Chemistry, 2014. **20**(44): p. 14465-72.

266. Moghaddam, S.Z. and E. Thormann, *The Hofmeister series: Specific ion effects in aqueous polymer solutions.* J Colloid Interface Sci, 2019. **555**: p. 615-635.

267. Swann, J.M., et al., *Effect of the Hofmeister anions upon the swelling of a self-assembled pH-responsive hydrogel.* Langmuir, 2010. **26**(12): p. 10191-7.

268. Lo Nostro, P. and B.W. Ninham, *Hofmeister phenomena: an update on ion specificity in biology.* Chem Rev, 2012. **112**(4): p. 2286-322.

269. Lu, F., et al., *Extensional rheology of cellulose/NaOH/urea/H2O solutions.* Cellulose, 2016. **23**(5): p. 2877-2885.

270. Akpek, A., *Detailed Analysis of the Effects of Viscosity Measurement Errors Caused by Heat Transfer during Continuous Viscosity Measurements under Various Temperature Changes and the Proposed Solution of a Non-Dimensional Parameter Called the Akpek Number.* Applied Sciences, 2023. **13**(19).

271. Yue, Y., *A Comparative Study of Cellulose I and II Fibers and Nanocrystals*, in *Agricultural and Mechanical College*. 2011, Louisiana State University

272. Yang, Y.P.Z., Y.; Lang, Y. X. and Yu, M, H., *Structural ATR-IR analysis of cellulose fibers prepared from a NaOH complex aqueous solution.* IOP Conference Series: Materials Science and Engineering, 2017. **213**.

273. Kljun, A., et al., *Comparative analysis of crystallinity changes in cellulose I polymers using ATR-FTIR, X-ray diffraction, and carbohydrate-binding module probes.* Biomacromolecules, 2011. **12**(11): p. 4121-6.

274. Baldovino-Medrano, V.G., V. Niño-Celis, and R. Isaacs Giraldo, *Systematic Analysis of the Nitrogen Adsorption–Desorption Isotherms Recorded for a Series of Materials Based on Microporous–Mesoporous Amorphous Aluminosilicates Using Classical Methods.* Journal of Chemical & Engineering Data, 2023. **68**(9): p. 2512-2528.

275. Thommes, M. and C. Schlumberger, *Characterization of Nanoporous Materials.* Annu Rev Chem Biomol Eng, 2021. **12**: p. 137-162.

276. Thommes, M., et al., *Physisorption of gases, with special reference to the evaluation of surface area and pore size distribution (IUPAC Technical Report).* Pure and Applied Chemistry, 2015. **87**(9-10): p. 1051-1069.

277. Poletto, M., et al., *Materials produced from plant biomass: part II: evaluation of crystallinity and degradation kinetics of cellulose.* Materials Research, 2012. **15**(3): p. 421-427.

278. Qin, Y., et al., *Sodium sulfate–diatomite composite materials for high temperature thermal energy storage.* Powder Technology, 2015. **282**: p. 37-42.

279. Jenks, W.P., Westheimer, F.H. . *pKa Data Compiled by R. Williams*. 2022 [cited 2022 9.3]; Available from:

References

https://organicchemistrydata.org/hansreich/resources/pka/pka_data/pka-compilation-williams.pdf.

280. Cao, B., C. Wang, and Z. Zhou, *Insights into the interactions between cellulose and biological molecules.* Carbohydrate Research, 2023. **523**: p. 108738.

281. Berga, L., et al., *Cellulose dissolution and regeneration using a non-aqueous, non-stoichiometric protic ionic liquid system.* Cellulose, 2020. **27**(16): p. 9593-9603.

282. Parviainen, A., et al., *Predicting cellulose solvating capabilities of acid-base conjugate ionic liquids.* ChemSusChem, 2013. **6**(11): p. 2161-9.

283. Ganesan, K., et al., *Design of aerogels, cryogels and xerogels of cellulose with hierarchical porous structures.* Materials & Design, 2016. **92**: p. 345-355.

284. Zainul Armir, N.A., et al., *Regenerated Cellulose Products for Agricultural and Their Potential: A Review.* Polymers (Basel), 2021. **13**(20).

285. Jin, H., Nishiyama, Y., Wada, M. & Kuga, S., *Nanofibrillar cellulose aerogels.* Colloids and Surfaces A: Physicochemical and Engineering Aspects, 2004. **240**: p. 63-67.

286. Grosman, A. and C. Ortega, *Capillary Condensation in Porous Materials. Hysteresis and Interaction Mechanism without Pore Blocking/Percolation Process.* Langmuir, 2008. **24**: p. 3977-3986.

287. Park, I., *Adsorption Hysteresis Dynamics*, in *Seventh International Conference on Fundamental of Adsorption* 2001: Nagasak, Japan.

288. Sen, S., et al., *Recent developments in biomass derived cellulose aerogel materials for thermal insulation application: a review.* Cellulose, 2022. **29**(9): p. 4805-4833.

289. Yan, C.-F., H.-Y. Yu, and J.-M. Yao, *One-step extraction and functionalization of cellulose nanospheres from lyocell fibers with cellulose II crystal structure.* Cellulose, 2015. **22**(6): p. 3773-3788.

290. Hoepfner, S.L., R, *Open porous cellulose aerogel fibers.* 2008.

291. Ramiah, M.V., *Thermogravimetric and differential thermal analysis of cellulose, hemicellulose, and lignin.* Journal of Applied Polymer Science, 1970. **14**(5): p. 1323-1337.

292. Kwan, V. and S. Consta, *Effect of droplet size and counterions on the spatial distribution of ions - Inferring microscopic properties from nanoscale simulations of charged droplets*, T.U.o.W.O. Department of Chemistry, London, Ontario, Canada, Editor. 2020.

293. Liu, L., et al., *The development history and prospects of biomass-based insulation materials for buildings.* Renewable and Sustainable Energy Reviews, 2017. **69**: p. 912-932.

294. Kumar, A., et al., *Integrated Valorization of Desalination Brine through NaOH Recovery: Opportunities and Challenges.* Angew Chem Int Ed Engl, 2019. **58**(20): p. 6502-6511.

295. Urbańczyk, E., M. Sowa, and W. Simka, *Urea removal from aqueous solutions—a review.* Journal of Applied Electrochemistry, 2016. **46**(10): p. 1011-1029.

296. Pegram, L.M. and M.T. Record Jr, *Hofmeister Salt Effects on Surface Tension Arise from Partitioning of Anions and Cations between Bulk Water and the Air-Water Interface.* J. Phys. Chem. B, 2007. **111**: p. 5411-5417.

297. Dong, K.J., et al., *Role of interparticle forces in the formation of random loose packing.* Phys Rev Lett, 2006. **96**(14): p. 145505.

298. Hoepfner, S., L. Ratke, and B. Milow, *Synthesis and characterisation of nanofibrillar cellulose aerogels.* Cellulose, 2008. **15**(1): p. 121-129.

299. Zoveidavianpoor, M., *Current Topics in the Utilization of Clay in Industrial and Medical Applications.* 2018: IntechOpen.

300. Arcari, M., et al., *Structure–property relationships of cellulose nanofibril hydro- and aerogels and their building blocks.* Nanoscale, 2020. **12**(21): p. 11638-11646.

References

301. Li, C.G., et al., *Study of the microstructure of chitosan aerogel beads prepared by supercritical CO(2) drying and the effect of long-term storage.* RSC Adv, 2022. **12**(33): p. 21041-21049.

302. Bedane, A.H., et al., *Theoretical modeling of water vapor transport in cellulose-based materials.* Cellulose, 2016. **23**(3): p. 1537-1552.

303. Nakamura, K., T. Hatakeyama, and H. Hatakeyama, *Studies on Bound Water of Cellulose by Differential Scanning Calorimetry.* Textile Research Journal, 1981. **51**: p. 607-613.

304. Mihranyan, A., et al., *Moisture sorption by cellulose powders of varying crystallinity.* Int J Pharm, 2004. **269**(2): p. 433-42.

305. Carles, J.E. and A.M. Scallan, *The determination of the amount of bound water within cellulosic gels by NMR spectroscopy.* Journal of Applied Polymer Science, 1973. **17**(6): p. 1855-1865.

306. Popineau, S., et al., *Free/bound water absorption in an epoxy adhesive.* Polymer, 2005. **46**(24): p. 10733-10740.

307. Gezici-Koç, Ö., et al., *Bound and free water distribution in wood during water uptake and drying as measured by 1D magnetic resonance imaging.* Cellulose, 2016. **24**(2): p. 535-553.

308. Celino, A., et al., *The hygroscopic behavior of plant fibers: a review.* Front Chem, 2013. **1**: p. 43.

309. Manich, A.M., et al., *Influence of alkaline delignification on moisture uptake behavior and bonding enthalpies of hemp.* Journal of Applied Polymer Science, 2021. **138**(39).

310. Lu, Y., et al., *Characterisation of mass distributions of solvent-fractionated lignins using analytical ultracentrifugation and size exclusion chromatography methods.* Sci Rep, 2021. **11**(1): p. 13937.

311. Yang, H., *Biobased Aromatic Chemicals by Lignin Depolymerization and Defunctionalization.* 2022, University of Groningen.

312. Goldmann, W.M., et al., *Determination of Phenolic Hydroxyl Groups in Technical Lignins by Ionization Difference Ultraviolet Spectrophotometry (Δε-IDUS method).* Periodica Polytechnica Chemical Engineering, 2016.

313. Rohde, V., et al., *Fractionation of three different lignins by thermal separation techniques—A comparative study.* GCB Bioenergy, 2018. **11**(1): p. 206-217.

314. Geminiani, L., et al., *Differentiating between Natural and Modified Cellulosic Fibres Using ATR-FTIR Spectroscopy.* Heritage, 2022. **5**(4): p. 4114-4139.

315. Lv, H., et al., *Influence of Supercritical CO2 Pretreatment of Corn Stover with Ethanol-Water as Co-Solvent on Lignin Degradation.* Chemical Engineering & Technology, 2013. **36**(11): p. 1899-1906.

316. Donohoe, B.S., et al., *Visualizing lignin coalescence and migration through maize cell walls following thermochemical pretreatment.* Biotechnol Bioeng, 2008. **101**(5): p. 913-25.

317. Lu, Q., et al., *Comparative antioxidant activity of nanoscale lignin prepared by a supercritical antisolvent (SAS) process with non-nanoscale lignin.* Food Chemistry, 2012. **135**(1): p. 63-67.

318. Guo, X., et al., *Effect of lignin and released acid on the gelation and aerogel fabrication of whole biomass in the lithium bromide molten salt hydrate system.* Cellulose, 2023. **30**(10): p. 6233-6246.

319. Yang, W., et al., *Investigation of holocellulose-lignin interactions during pyrolysis of wood meal by TGA-FTIR.* Biomass Conversion and Biorefinery, 2021.

320. Tan, Z., et al., *Lignin: Excellent hydrogel swelling promoter used in cellulose aerogel for efficient oil/water separation.* J Colloid Interface Sci, 2023. **629**(Pt A): p. 422-433.

References

321. Lapkin, A., Constable, D. J.C.,, *Green Chemistry Metrics: Measuring and Monitoring Sstainable Processes* 2009: Blackwell Publishing Ltd.

322. Tufvesson, L.M., et al., *Life cycle assessment in green chemistry: overview of key parameters and methodological concerns.* The International Journal of Life Cycle Assessment, 2012. **18**(2): p. 431-444.

323. Piccinno, F., et al., *Predicting the environmental impact of a future nanocellulose production at industrial scale: Application of the life cycle assessment scale-up framework.* Journal of Cleaner Production, 2018. **174**: p. 283-295.

324. Khoo, H.H., V. Isoni, and P.N. Sharratt, *LCI data selection criteria for a multidisciplinary research team: LCA applied to solvents and chemicals.* Sustainable Production and Consumption, 2018. **16**: p. 68-87.

325. Hein, H. and J. Schwarte, *Innovative insulation materials - specific issues performing LCA in early development phases.* Advanced Materials Proceedings, 2018. **3**(9): p. 531-535.

326. Albrecht, S., et al., *Life cycle assessment of advanced building materials towards NZEBs.* E3S Web of Conferences, 2022. **349**.

327. Wang, Y., et al., *Life cycle assessment of a novel biomass-based aerogel material for building insulation.* Journal of Building Engineering, 2021. **44**.

328. De Marco, I., S. Riemma, and R. Iannone, *Life cycle assessment of supercritical impregnation: Starch aerogel + α-tocopherol tablets.* The Journal of Supercritical Fluids, 2019. **143**: p. 305-312.

329. Sutter, J., *Life Cycle Inventories of Petrochemical Solvents*. 2007.

330. De Marco, I., et al., *An environmental study on starch aerogel for drug delivery applications: effect of plant scale-up.* The International Journal of Life Cycle Assessment, 2018. **23**(6): p. 1228-1239.

331. Piccinno, F., et al., *Life Cycle Assessment of a New Technology To Extract, Functionalize and Orient Cellulose Nanofibers from Food Waste.* ACS Sustainable Chemistry & Engineering, 2015. **3**(6): p. 1047-1055.

332. Foroughi, F., et al., *A Review on the Life Cycle Assessment of Cellulose: From Properties to the Potential of Making It a Low Carbon Material.* Materials (Basel), 2021. **14**(4).

333. Pinto, I., et al., *Environmental impact of the subcritical production of silica aerogels.* Journal of Cleaner Production, 2020. **252**.

334. Kara, I.T., et al., *Life Cycle Assessment of Aerogels: A Critical Review.* J Sol-Gel Sci Technol, 2024. **111**: p. 618-649.

335. Karatum, O., et al., *Life Cycle Assessment of Aerogel Manufacture on Small and Large Scales: Weighing the Use of Advanced Materials in Oil Spill Remediation.* Journal of Industrial Ecology, 2018. **22**(6): p. 1365-1377.

8. Appendix

8.1 FTIR
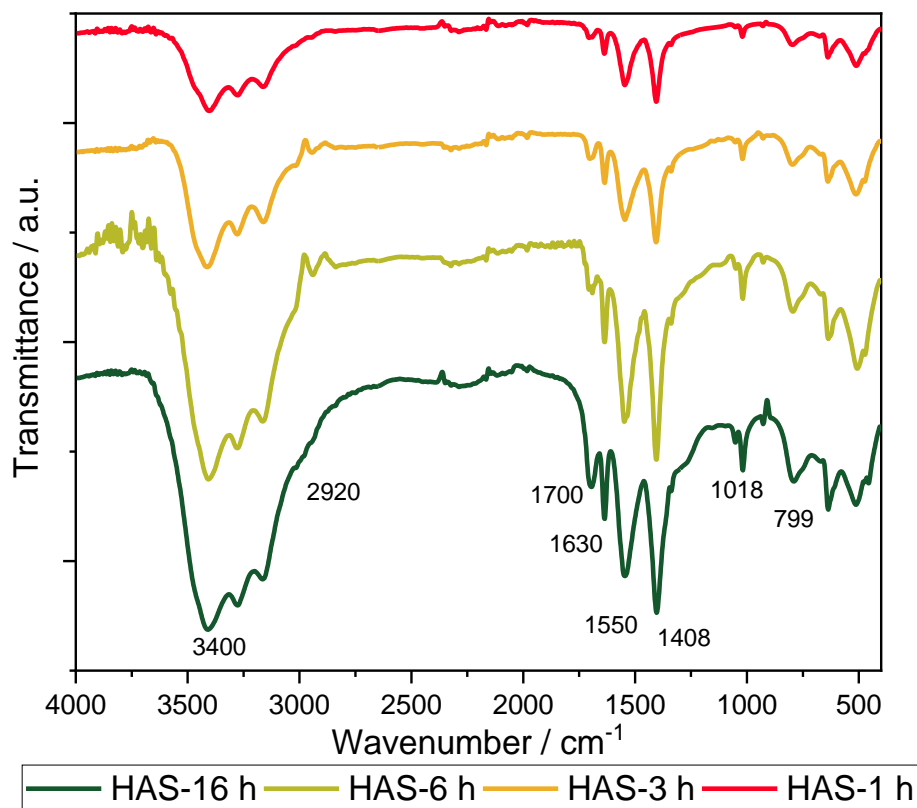
Figure 109 FTIR spectra of the first supernatant of the alkali treatment of hemp (HAS), according to residence time (dark green for 16 h, light green for 6 h, orange for 3 h and red for 1 h) before the heating phase. The hemp fibers were milled to > 1 mm before the alkali treatment.

8.1 FTIR
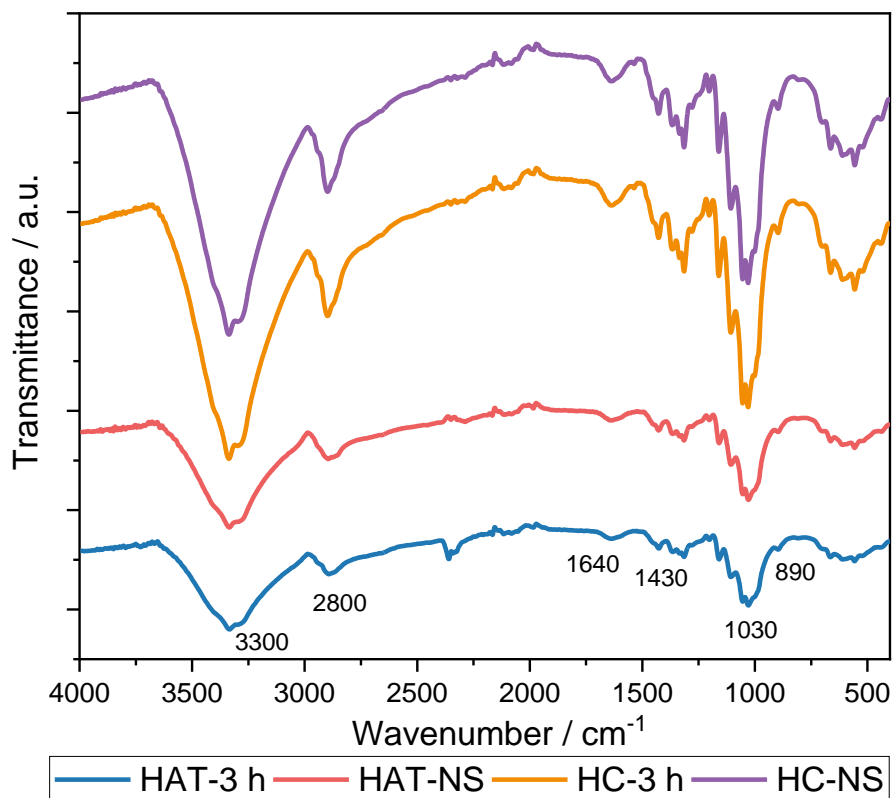
Figure 110 FTIR spectra of hemp alkali-treated intermediates (HAT) and hemp-extracted cellulose samples (HC) obtained with and without stirring (NS) (blue for HAT-3 h, red for HAT- NS, orange for HC-3 h, and purple for HC-NS). The hemp fibers were milled to > 1 mm before the alkali treatment. The room temperature residence time used for the alkali treatment and bleaching was three hours.
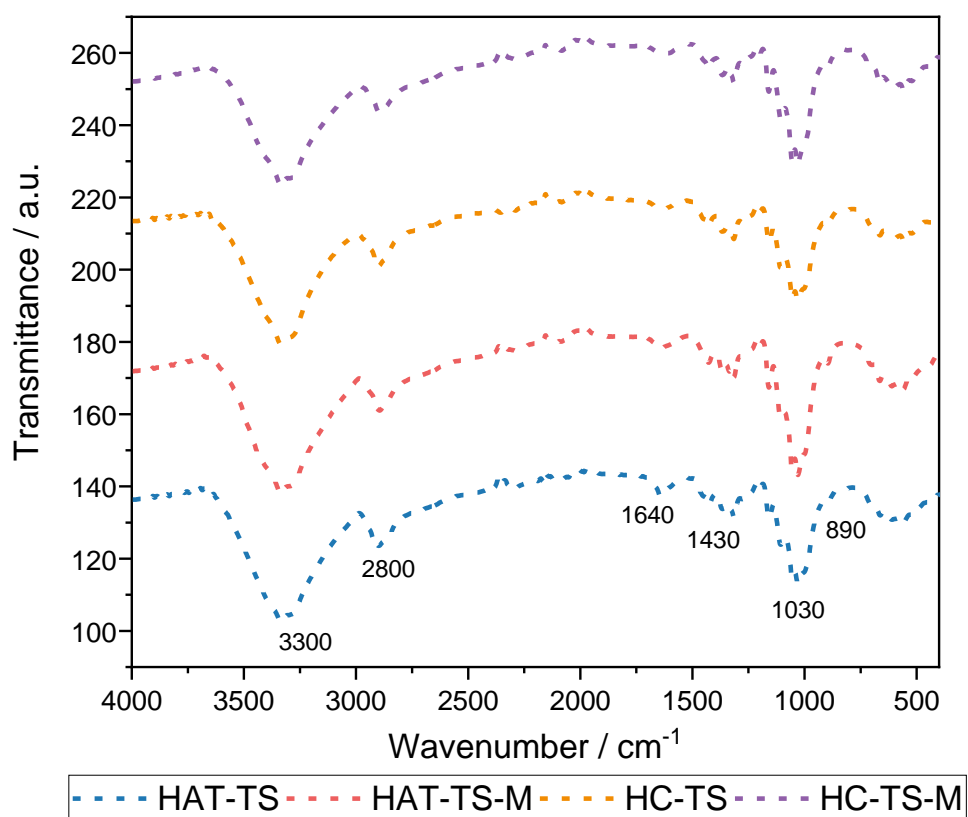
Figure 111 FTIR spectra of hemp alkali-treated intermediates (HAT) and hemp-extracted cellulose samples (HC) obtained at technical scale (TS) from milled and finely milled (M) hemp bast fibers (blue for HAT-TS, red for HAT-TS-M, orange for HC-TS, and purple for HC- TS- M). The hemp fibers were milled to > 1 mm or < 0.2 mm (finely milled, M) before the alkali treatment. The room temperature residence time used for the alkali treatment and bleaching was three hours.
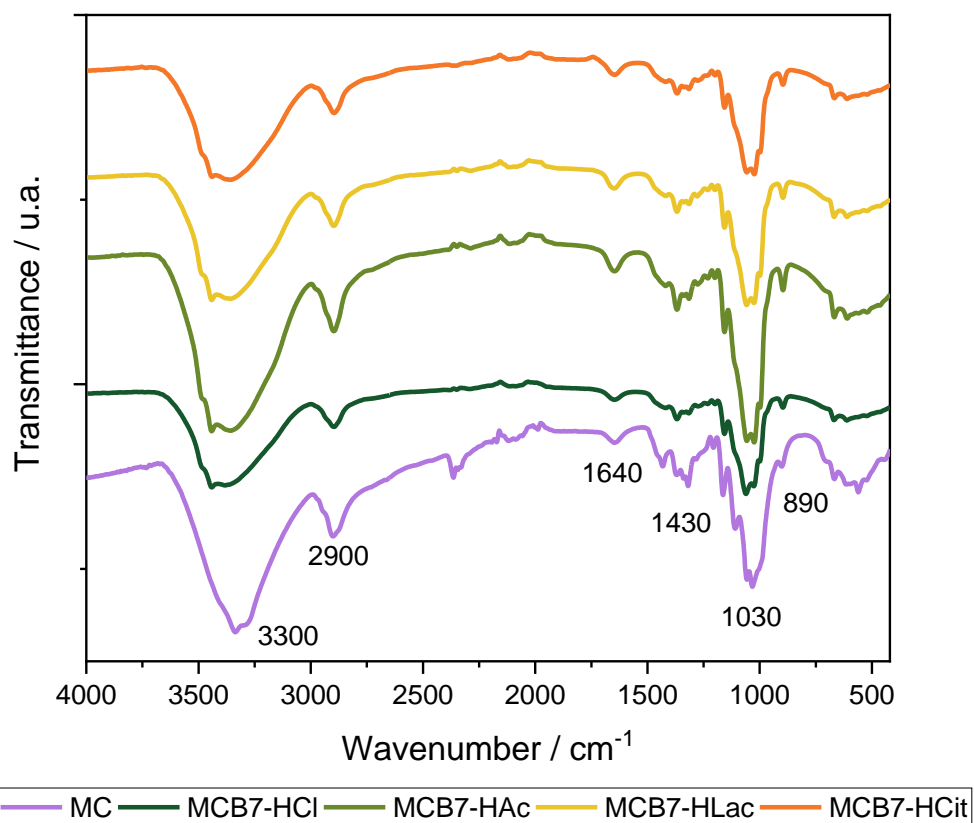
Figure 112 FTIR spectra of 7 wt.-% commercial cellulose aerogel beads (MCB7) gelled in different regeneration bathes (dark green for HCl; light green for HAc; golden for HLac, and orange for HCit). Commercial cellulose (MC) appears in purple.[250] (CC BY-NC, https://creativecommons.org/licenses/by-nc/4.0/)
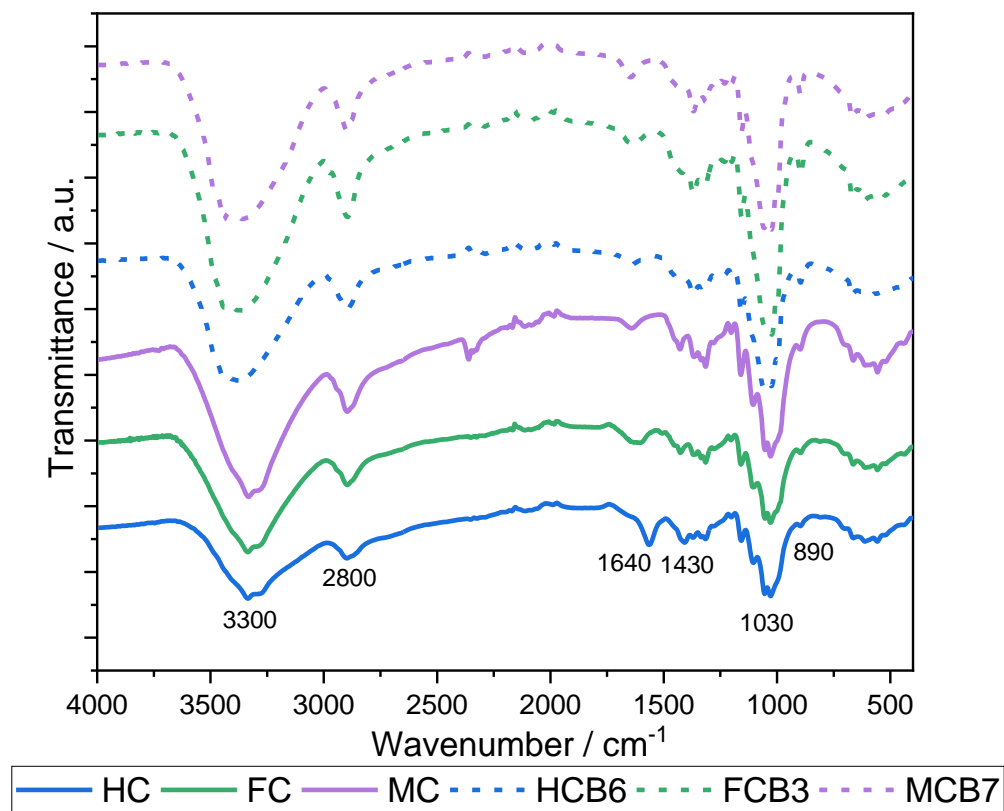
Figure 113 FTIR spectra of used celluloses (blue for HC, green for FC, and purple for MC) and respective representative aerogel beads (blue short dashed line for HB6, green short dashed line for FB3, and purple short dashed line for MCB7).
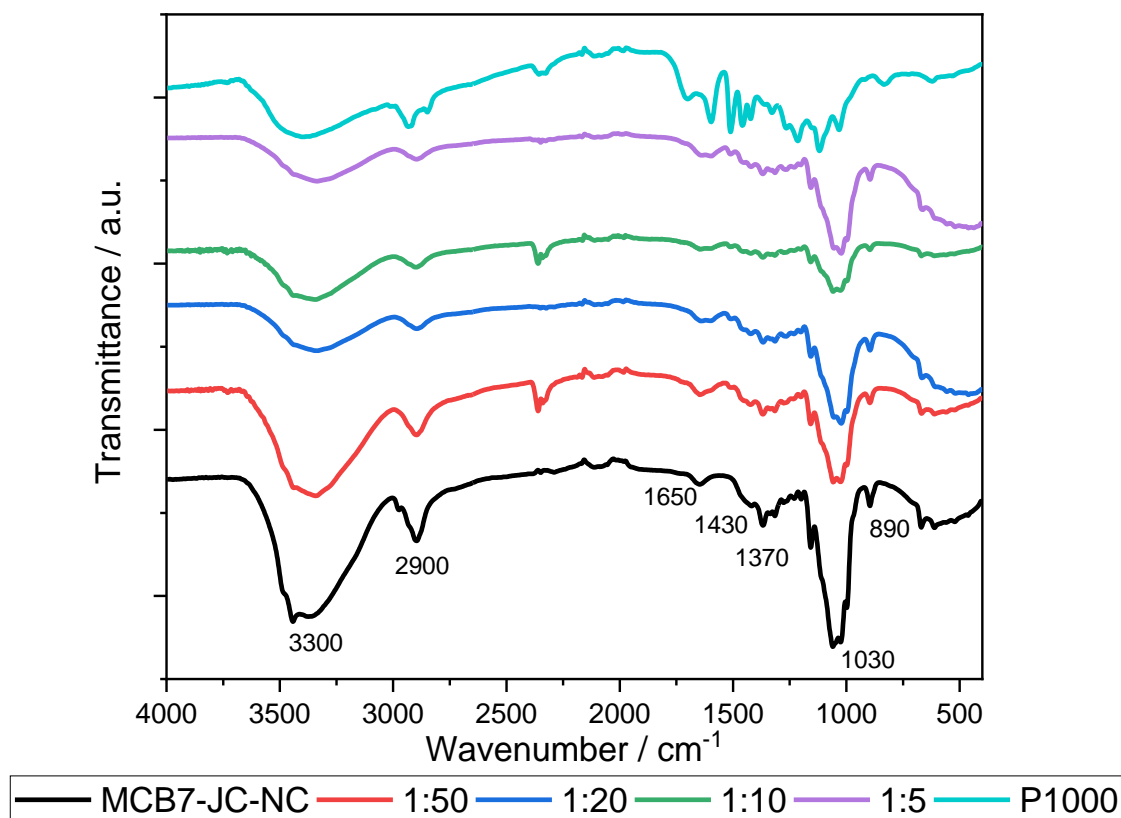
Figure 114 FTIR spectra of 7 wt.-% commercial cellulose aerogel beads (MCB7), produced at technical scale using the JetCutter® (JC) and in a 2M lactic acid solution, non-coated (black for standard sample, MCB7-JC-NC), and coated with P1000 lignin (P1) at different lignin:cellulose wet gel ratios (red for 1:50; blue for 1:20; green for 1:10, and purple for 1:5). The spectrum of P1000 lignin is presented in light blue. This lignin was dissolved in alkali water solution and neutralized before coating.
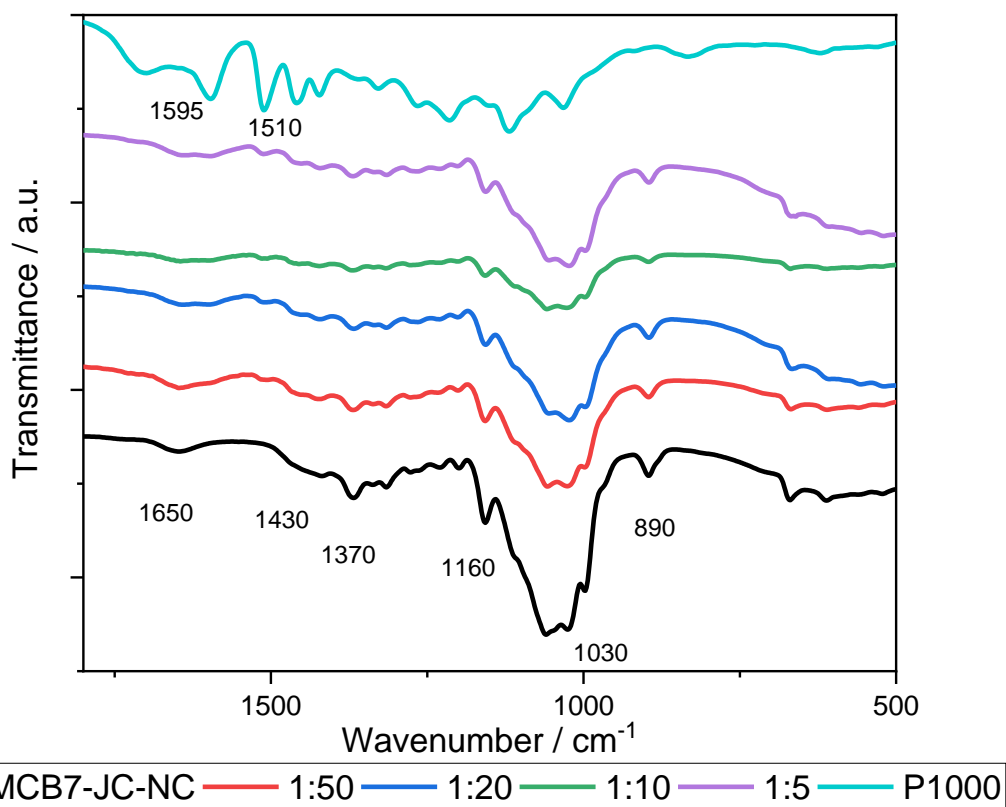
Figure 115 Detail of the FTIR spectra of 7 wt.-% commercial cellulose aerogel beads (MCB7), produced at technical scale using the JetCutter® (JC) and in a 2M lactic acid solution, non-coated (black for standard sample, MCB7-JC-NC), and coated with P1000 lignin (P1) in basic medium at different lignin:cellulose wet gel ratios (red for 1:50; blue for 1:20; green for 1:10, and purple for 1:5). The spectrum of P1000 lignin is presented in light blue. This lignin was dissolved in alkali water solution and neutralized before coating.

8.2 XRD Reference Reflection Positions and Spectra

Table 20 Native cellulose I reflections positions, d-spacing and Miller indices (hkl), PDF number 00-003-0289, CuKα = 1,54060 Å, from the International Center for Diffraction Data.

2θ / °	d spacing / Å	Intensity	*h*	*k*	*l*
14.0908	6.28	20	1	0	1
14.9018	5.94	80			
16.4941	5.37	70	-1	1	1
17.3396	5.11	20	1	0	1
20.6387	4.3	60	0	2	1
22.8419	3.89	100	0	0	2
28.2171	3.16	40	1	3	0
29.0622	3.07	40	-1	2	2
30.3775	2.94	40			
31.2486	2.86	40	1	3	1
34.0612	2.63	60	3	1	0
34.6037	2.59	40	-2	3	1
34.8816	2.57	80	0	4	0
38.6095	2.33	40	-2	3	2
41.5829	2.17	60	2	4	0
42.6109	2.12	20	1	2	3
44.3687	2.04	20	3	0	2
46.5339	1.95	40	-4	1	2

Appendix

Table 21 Cellulose II reflections positions, d-spacing and Miller indices (hkl), PDF number 00-056-1717, CuKα = 1,54060 Å, from the International Center for Diffraction Data.

2θ / °	d spacing / Å	Intensity	h	k	l
10.9973	8.03862	13	0	1	0
12.1866	7.25669	280	-1	1	0
12.2646	7.21072	16	1	0	0
14.9485	5.92155	18m	-1	1	1
14.9485	5.92155	m	1	0	1
17.1871	5.155	20	0	0	2
19.7754	4.48573	5	-1	2	0
19.9214	4.4532	999	1	1	0
20.4494	4.33939	17	0	1	2
21.1316	4.20081	31m	-1	1	2
21.1316	4.20081	m	1	0	2
21.5867	4.11327	18	-1	2	1
21.7209	4.08815	20	1	1	1
22.0976	4.01931	82	0	2	0
23.5824	3.76949	17	-2	1	1
23.7402	3.7448	25	0	2	1
24.6725	3.60536	17	2	0	0
26.0125	3.42259	10	-2	2	1
26.1628	3.40327	11	2	0	1
26.3149	3.38394	83	-1	2	2
27.9944	3.18463	17	-2	1	2
28.2171	3.16	12	0	1	3
28.7475	3.10289	58m	-1	1	3
28.7475	3.10289	m	1	0	3
29.955	2.9805	5	1	2	0
30.0937	2.96708	42	-2	2	2
31.0525	2.87762	10	-1	3	1
31.2123	2.86325	14	1	2	1
32.6611	2.73947	12	2	1	1
32.8928	2.7207	11	1	1	3
33.4128	2.67954	14	0	3	0
33.6759	2.6592	7	-3	1	0
34.1903	2.62036	34	-2	1	3
34.3027	2.61203	7	0	2	3
34.5932	2.59076	8	-1	3	2
34.7852	2.5769	89	-3	1	1
35.9995	2.49271	41m	-2	2	3
35.9995	2.49271	m	2	1	2
36.5809	2.45442	41	0	1	4
37.9641	2.36811	9	-3	2	2
38.1845	2.35495	58	-3	3	1
38.4241	2.34081	5	3	0	1

40.3505	2.23339	28m	-1	2	4
40.3505	2.23339	m	1	1	4
40.8919	2.20506	84	1	3	0
40.9857	2.20023	41	-2	3	3
41.1542	2.19161	13	-2	4	1
41.4634	2.17598	27m	2	2	1
41.4634	2.17598	m	-2	1	4
42.756	2.11314	7	0	3	3
42.9376	2.10462	46	-3	1	3
43.9909	2.05664	7	-2	4	2
44.488	2.03481	17m	-3	4	1
44.488	2.03481	m	-1	4	2
44.7165	2.02494	6	-4	2	0
45.6869	1.98416	25	-1	1	5
46.0245	1.97039	39m	0	4	1
46.0245	1.97039	m	3	0	3
46.544	1.9496	6	1	2	4
46.9825	1.93242	9	-4	3	1
47.1618	1.92549	15m	-3	4	2
47.1618	1.92549	m	-4	1	1
47.5908	1.90913	15	2	1	4
48.2455	1.88474	11	-4	2	2
48.4226	1.87826	11	-2	4	3
48.5527	1.87353	9	-1	2	5
49.5541	1.83799	8	-4	3	2
49.7274	1.83199	11	-4	1	2
50.2495	1.81417	5	-4	4	0
51.9771	1.75786	9	3	0	4
54.5814	1.67998	12m	0	1	6
54.5814	1.67998	m	-1	4	4
54.9739	1.66891	6	2	1	5
55.2061	1.66244	6	-3	5	2
55.6608	1.64993	5	1	4	2
56.2458	1.63415	6	0	3	5
62.7578	1.47933	7m	-3	6	1
62.7578	1.47933	m	-2	5	4
64.4942	1.44363	5	3	2	4

Figure 116 XRD diffractograms and respective crystallinity indexes (IC_S) of hemp alkali-treated intermediates (HAT) and hemp-extracted cellulose samples (HC) obtained with and without stirring (NS) (blue for HAT-3 h, red for HAT-NS, orange for HC-3 h, and purple for HC-NS). The hemp fibers were milled to > 1 mm before the alkali treatment. The room temperature residence time used for the alkali treatment and bleaching was three hours.
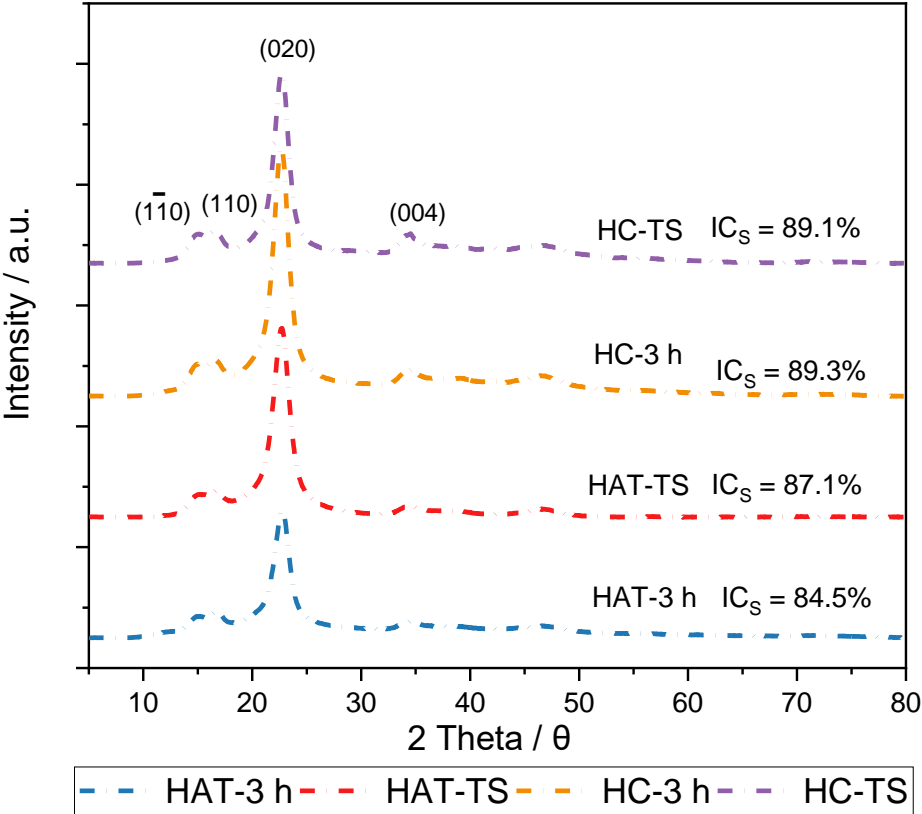
Figure 117 XRD diffractograms and respective crystallinity indexes (IC_S) of hemp alkali-treated intermediates (HAT) and hemp-extracted cellulose samples (HC) obtained at laboratory and technical scale (TS) (blue for HAT-3 h, red for HAT- TS, orange for HC-3 h, and purple for HC-TS). The hemp fibers were milled to > 1 mm before the alkali treatment. The room temperature residence time used for the alkali treatment and bleaching was three hours.
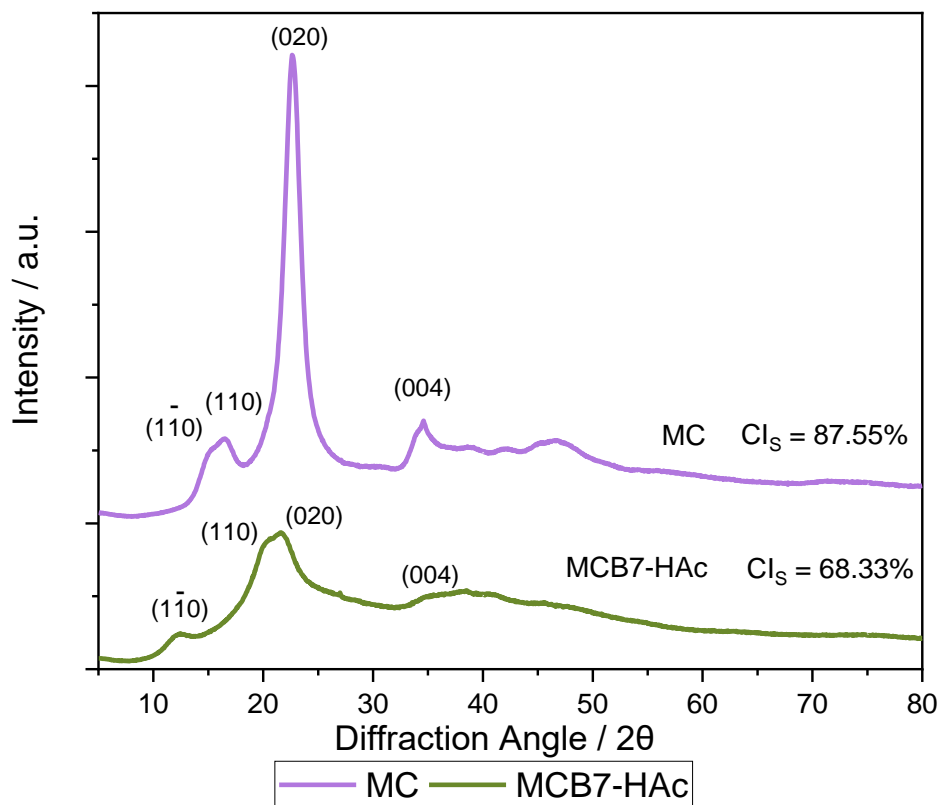
Figure 118 XRD diffractograms and respective crystallinity indexes (IC_S) of 7 wt.-% commercial cellulose aerogel beads (MCB7) regenerated in an acetic acid aqueous bath (light green for MCB7-HAc) and commercial cellulose (purple for MC).[250] (CC BY-NC, https://creativecommons.org/licenses/by-nc/4.0/)
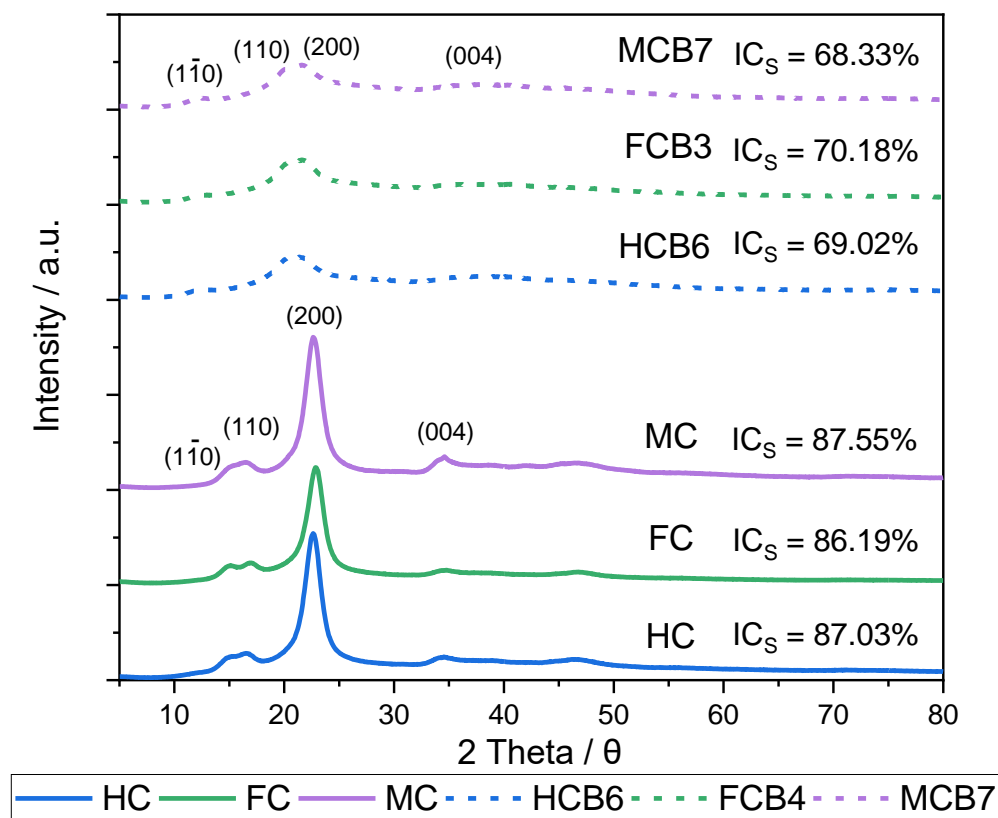
Figure 119 XRD diffractograms and respective crystallinity indexes (IC_S) of used celluloses (blue for HC, green for FC, and purple for MC) and respective representative aerogel samples (blue short dashed line for HCB6, green short dashed line for FCB3, and purple short dashed line for MCB7).

8.3 TGA
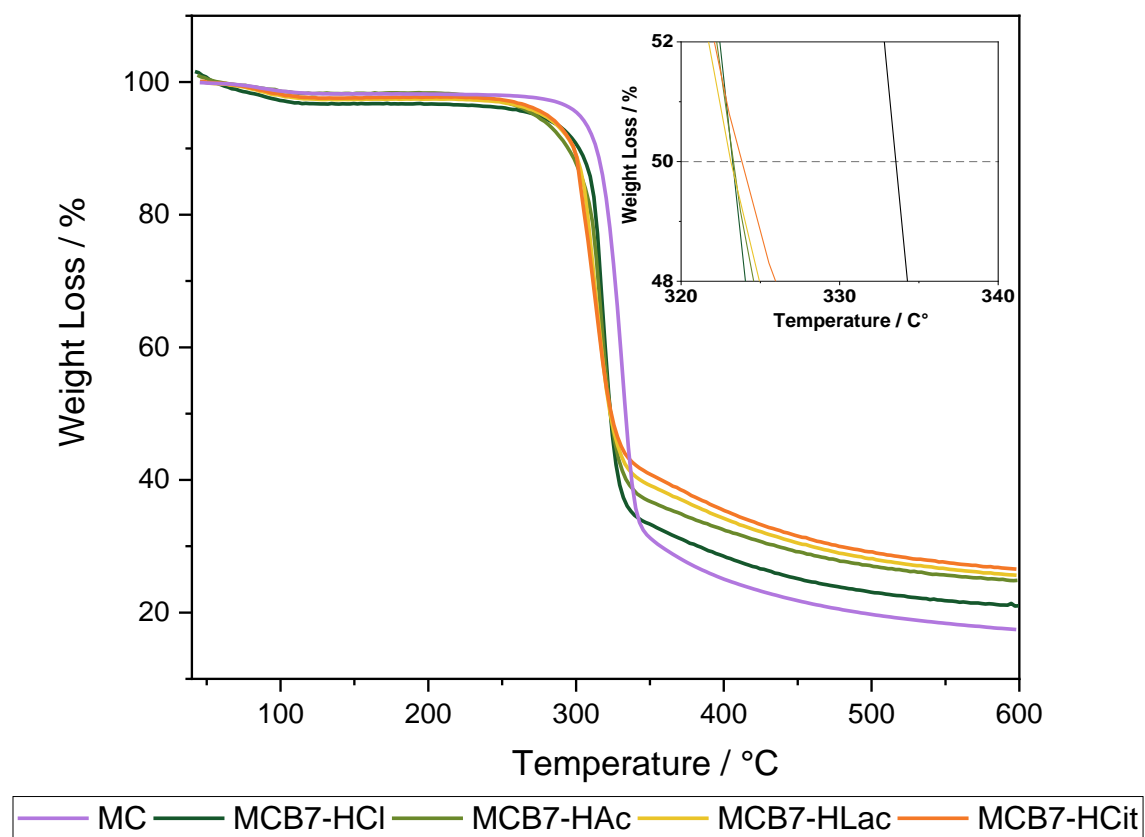
Figure 120 Thermal gravimetric profile of 7 wt.-% commercial cellulose aerogel beads (MCB7) gelled in different regeneration bathes (dark green for HCl, light green for HAc, golden for HLac and orange for HCit) and commercial cellulose (purple for MC).
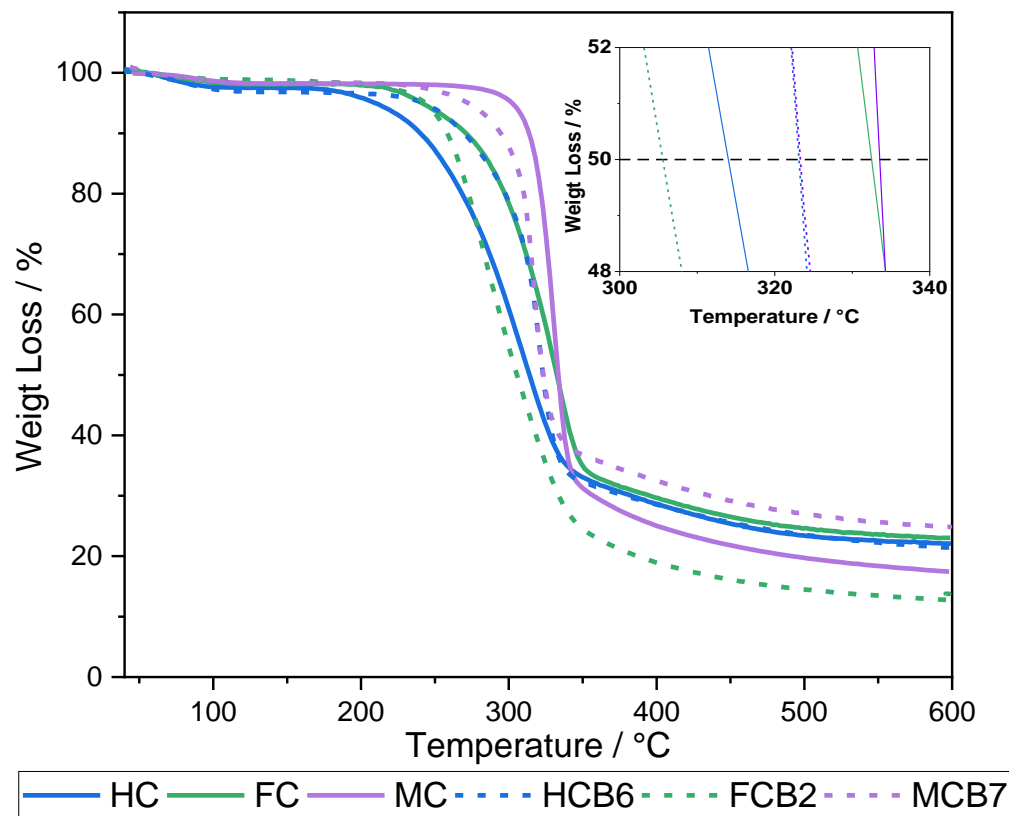
Figure 121 Thermal gravimetric profiles of used celluloses (blue for HC, green for FC, and purple for MC) and respective representative aerogel samples (blue short dashed line for HCB6, green short dashed line for FCB2, and purple short dashed line for MCB7).

8.4 Rheology
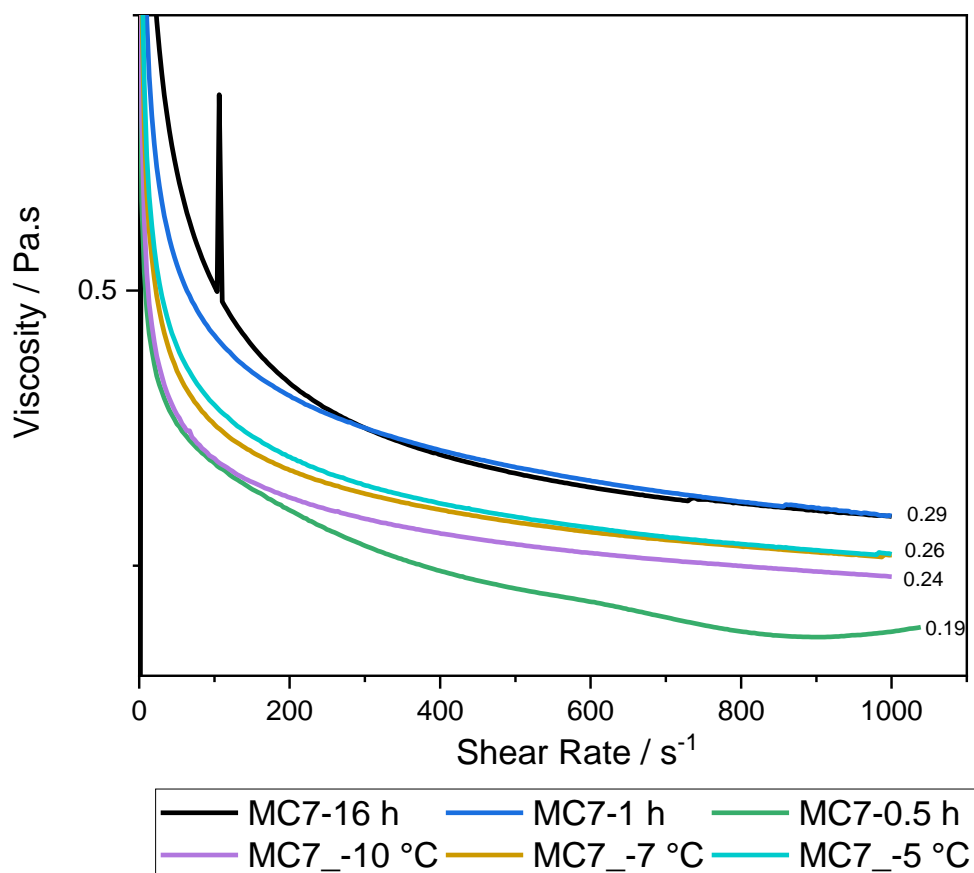
Figure 122 Dynamic viscosity of a 7 wt.-% commercial cellulose solution (MC7) after different residence times at -20 °C (black for sixteen hours, blue for one hour, and green for 30 minutes), and when dissolution occurred continuously at different temperatures (purple for - 10°C, gold for -7 °C and cyan for – 5 °C).
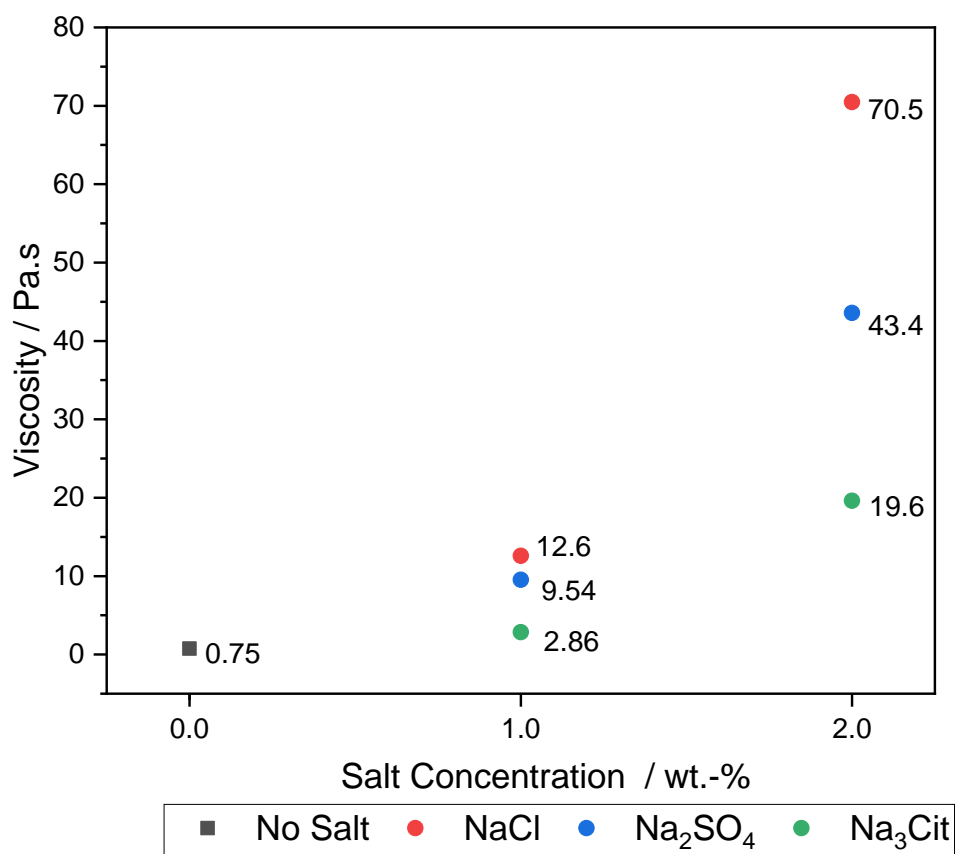
Figure 123 Static viscosity of 7 wt.-% commercial cellulose solution without (black for "No Salt"), and after addition of sodium salts at different concentrations (red circle for NaCl; blue circle for Na_2SO_4, and green circle for Na_3Cit). Cellulose was dissolved and the solutions were prepared after storage at -20 °C for 16 hours.

8.5 Physisorption Isotherm Curves
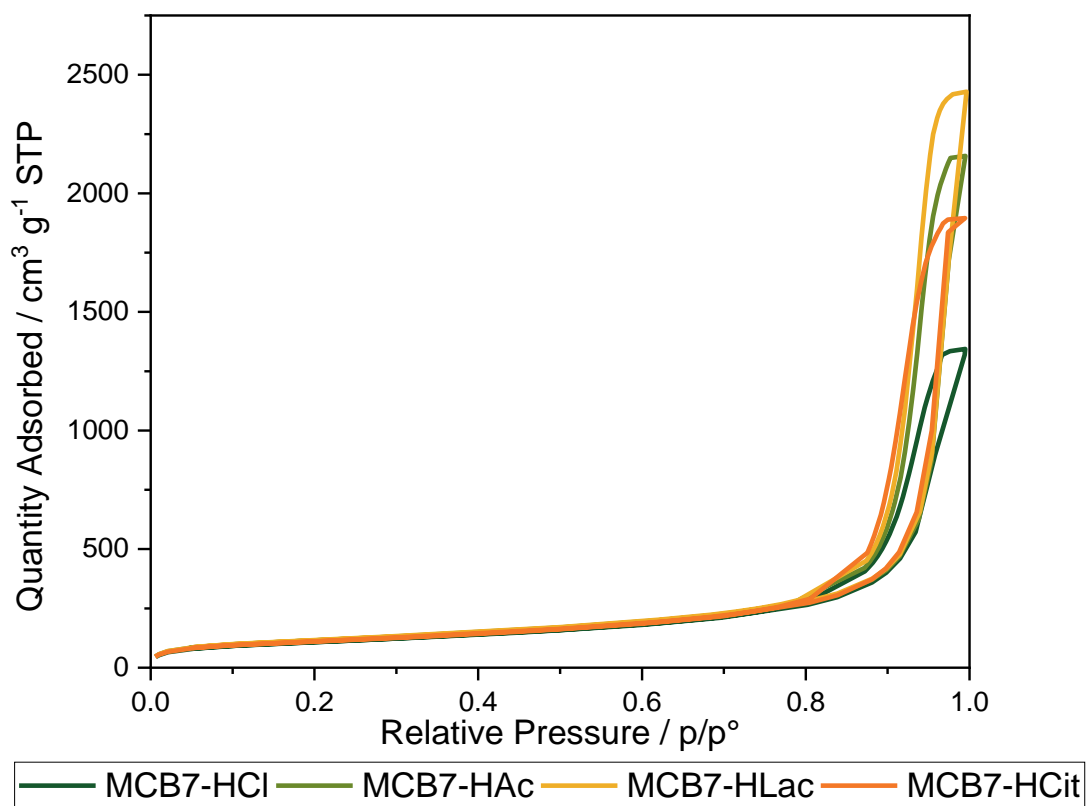
Figure 124 N_2 adsorption-desorption isotherms of commercial cellulose aerogel beads (MCB7) gelled in different regeneration bathes (dark green for HCl, light green for HAc, golden for HLac and orange for HCit).
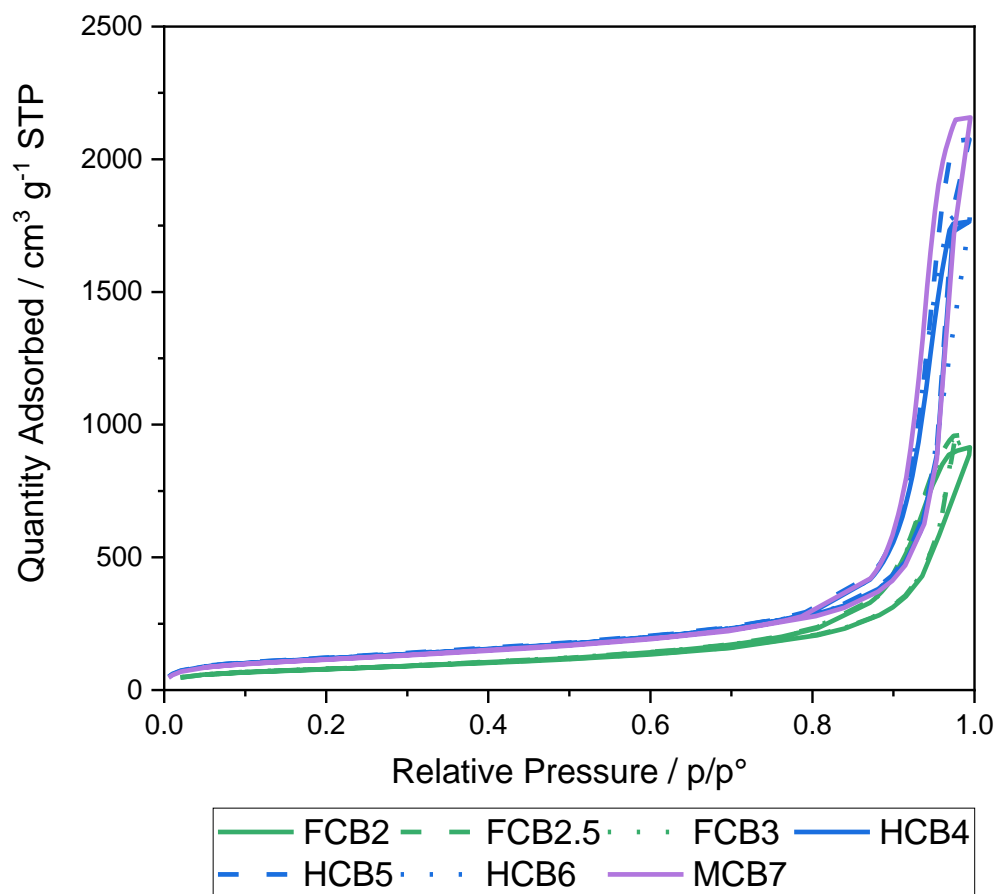
Figure 125 N$_2$ adsorption-desorption isotherms of aerogel samples produced from flax-extracted (green for FCB), hemp-extracted (blue for HCB), and commercial cellulose (purple for MCB) at different cellulose concentration (green solid line for 2 wt.%, green dashed line for 2.5 wt.- %, green dotted line for 3 wt.-%, blue solid line for 4 wt.-%, blue dashed line for 5 wt.- %, blue dotted line for 6 wt.-%, and purple solid line for 7 wt.-%).
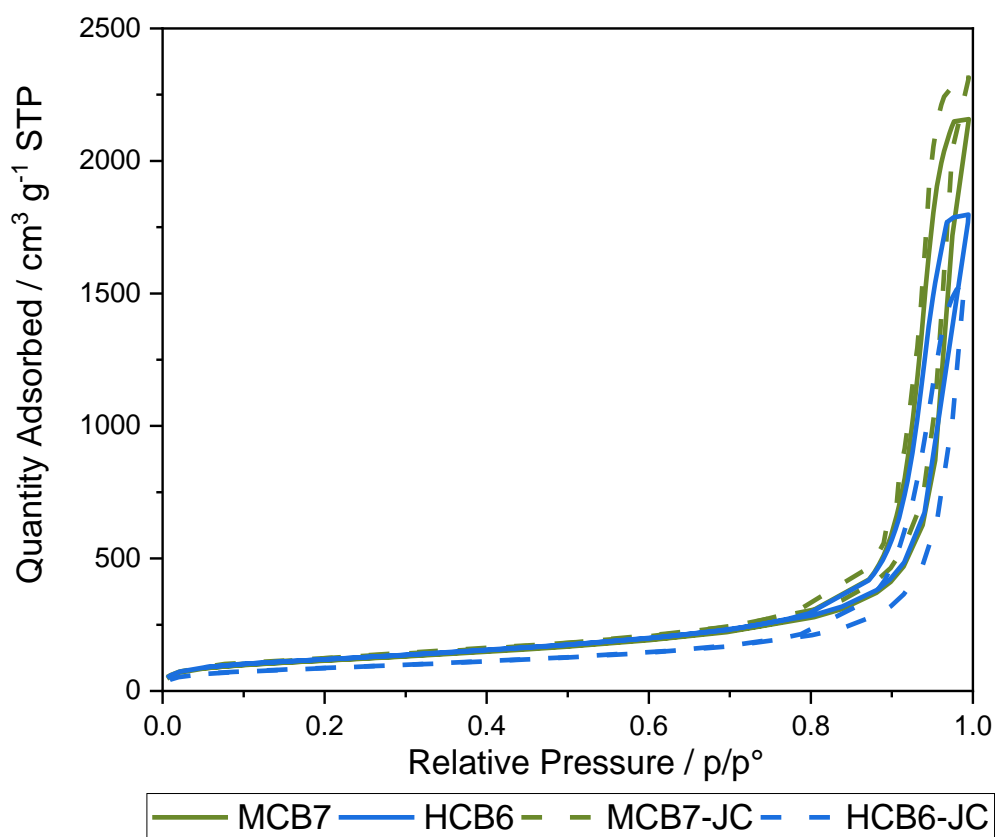
Figure 126 N_2 adsorption-desorption isotherms of cellulose aerogel beads synthesized from a 7 wt.-% commercial cellulose solution (green for MCB7) and a 6 wt.-% hemp-extracted cellulose solution (blue for HCB6), at different scales (solid line for laboratory scale and dash line for technical scale, using the JetCutter®, JC).

Figure 127 N$_2$ adsorption-desorption isotherms of commercial cellulose aerogel beads produced at technical scale, using the JetCutter®, from cellulose solutions of different concentrations without the addition of salt (black for 7 wt.-%, blue for 6 wt.-% and orange for 5 wt.-%) and coagulated in different acids (square for acetic acid and circle for lactic acid). Some samples were synthesized from 5 wt.-% cellulose solutions to which salts were added (red for NaCl and green for Na$_3$Cit) in different concentrations (triangle for 1 wt.-% and rhombus for 2 wt.-%) before gelation.
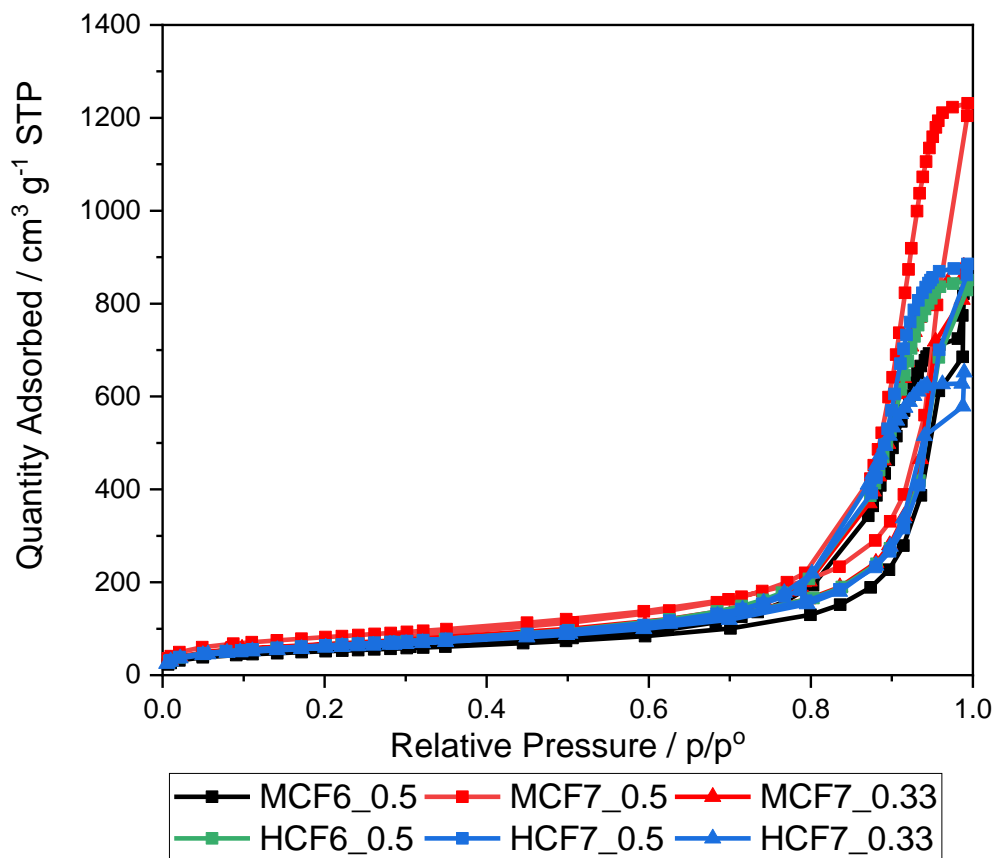
Figure 128 N_2 adsorption-desorption isotherms of cellulose aerogel fibers produced from commercial (black for 6 wt.-%, MCF6, and red for 7 wt.-%, MCF7, cellulose concentration) and hemp-extracted cellulose (green for 6 wt.-%, HCF6, and blue for 7 wt.-%, HCF7, cellulose concentration) with different nozzle diameters (square for 0.5 mm and triangle for 0.33 mm).
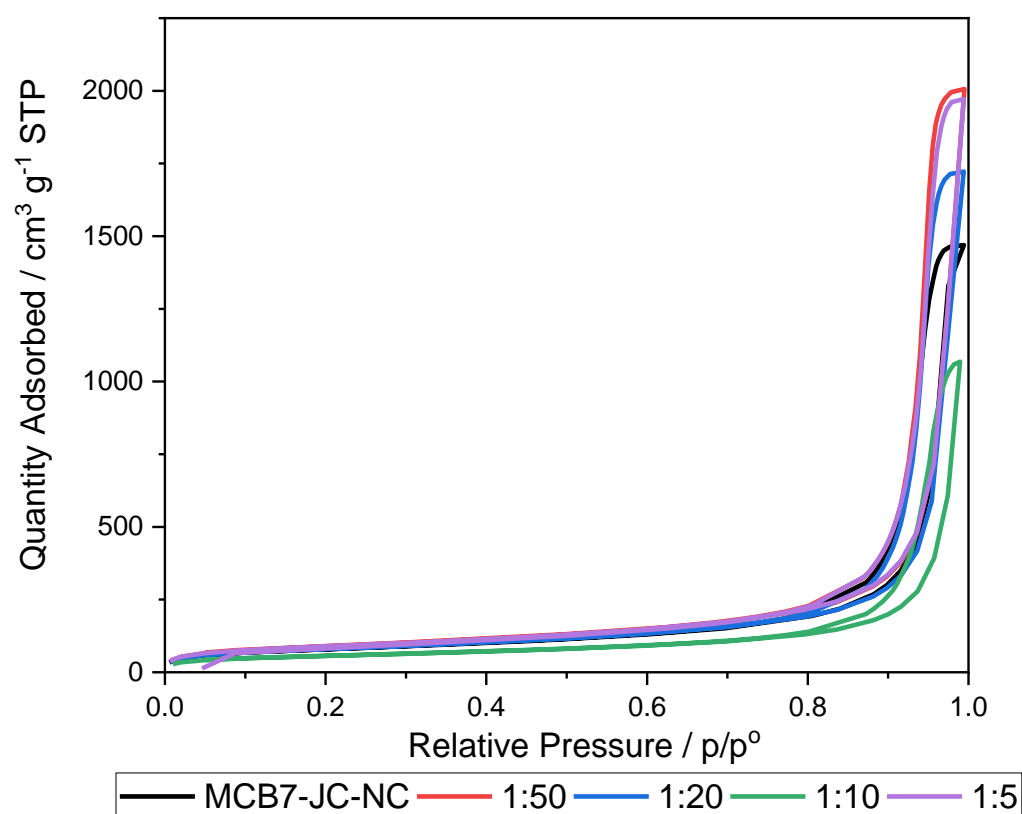
Figure 129 N_2 adsorption-desorption isotherms of 7 wt.-% commercial cellulose aerogel beads (MCB7), produced at technical scale using the JetCutter® (JC) and in a 2M lactic acid solution, non-coated (black for standard sample, MCB7-JC-NC), and coated with P1000 lignin (P1) in EtOH:H_2O (80:20) bath at different lignin:cellulose wet gel ratios (red for 1:50; blue for 1:20; green for 1:10, and purple for 1:5).

Figure 130 N_2 adsorption-desorption isotherms of 7 wt.-% commercial cellulose aerogel beads (MCB7), produced at technical scale using the JetCutter® (JC) and in a 2M lactic acid solution, non-coated (black for standard sample, MCB7-JC-NC), and coated with P1000 lignin (P1) at different lignin:cellulose wet gel ratios (red for 1:50; blue for 1:20; green for 1:10, and purple for 1:5). This lignin was dissolved in alkali water solution and neutralized before coating.

8.6 List of Figures

Appendix

8.7 List of Tables

8.8 Eidesstattliche Erklärung

Hiermit versichere ich an Eides statt, dass ich die vorliegende Dissertation selbstständig und ohne die Benutzung anderer als der angegebenen Hilfsmittel und Literatur angefertigt habe. Alle Stellen, die wörtlich oder sinngemäß aus veröffentlichten und nicht veröffentlichten Werken dem Wortlaut oder dem Sinn nach entnommen wurden, sind als solche kenntlich gemacht. Ich versichere an Eides statt, dass diese Dissertation noch keiner anderen Fakultät oder Universität zur Prüfung vorgelegen hat; dass sie - abgesehen von unten angegebenen Teilpublikationen und eingebundenen Artikeln und Manuskripten - noch nicht veröffentlicht worden ist sowie, dass ich eine Veröffentlichung der Dissertation vor Abschluss der Promotion nicht ohne Genehmigung des Promotionsausschusses vornehmen werde. Die Bestimmungen dieser Ordnung sind mir bekannt. Darüber hinaus erkläre ich hiermit, dass ich die Ordnung zur Sicherung guter wissenschaftlicher Praxis und zum Umgang mit wissenschaftlichem Fehlverhalten der Universität zu Köln gelesen und sie bei der Durchführung der Dissertation zugrundeliegenden Arbeiten und der schriftlich verfassten Dissertation beachtet habe und verpflichte mich hiermit, die dort genannten Vorgaben bei allen wissenschaftlichen Tätigkeiten zu beachten und umzusetzen. Ich versichere, dass die eingereichte elektronische Fassung der eingereichten Druckfassung vollständig entspricht.

Teilpublikation: D. Costa, B. Milow, K. Ganesan, *Chem. Eur. J.* 2024, 30, e202401794.

_____

Diogo Manuel Amaral Santos Costa

Almada, 25.09.2024

8.9 Publications and Conferences

Publications

D. Costa, B. Milow, K. Ganesan, *Chem. Eur. J*. 2024, 30, e202401794.

Costa, Diogo (2022) European researchers probing hemp cellulose for use in high-tech gels. Hemp Today.

Conferences

Costa, Diogo and Ganesan, Kathirvel and Sahraeian, Razmehr and Deyholos, Michael and Pakpour, Sepideh and Milow, Barbara (2021) Highly Porous Materials of Cellulose from Agricultural Residues. Oral presentation. In: 7th International Polysaccharide Conference - Book of Abstracts, p. 75. EPNOE. 7th International Polysaccharide Conference, 2021-10-11 - 2021-10-15, Nantes, France.

Costa, Diogo and Ganesan, Kathirvel and Milow, Barbara (2022) Synthesis of cellulose aerogel beads from agricultural residues. Pitch. In: 5th International EPNOE Junior Scientist Meeting 2022. 5th International EPNOE Junior Scientist Meeting 2022, 2022-09-08 - 2022-09-09, Aveiro.

Costa, Diogo and Goncalves, Bruno and Ganesan, Kathirvel and Milow, Barbara (2022) Impact of the anions in the production of monolithic cellulose aerogels. Poster/Poster pitch. In: 6th International Seminar on Aerogels. 6th International Seminar on Aerogels, 2022-09-28 - 2022-09-30, Hamburg, Germany.

Costa, Diogo and Schick, Simon and Seide, Gunnar and Milow, Barbara (2023) Synthesis of Cellulose Aerogel Fibers from Agricultural Residues and Considerations on its Continuous Production. Oral presentation. In: 31st European Biomass Conference and Exhibition, p. 17. ETA Florence. 31st European Biomass Conference and Exhibition, 2023-06-05 - 2023-06-08, Bologna, Italy.

Costa, Diogo and Philippe, Kanda and Milow, Barbara (2023) Upscaling of Cellulose Extraction from Hemp Bast Fibers and Production of Cellulose Aerogel Beads: An Industrial Case. Oral presentation. In: 3rd International Conference on Aerogels for Biomedical and Environmental Applications, pp. 73-74. University of Maribor, University Press. 3rd International Conference on Aerogels for Biomedical and Environmental Applications, 2023-07-05 - 2023-07-07, Maribor, Slovenia. doi: 10.18690/um.fkkt.2.2023. ISBN 978-961-286-762-1.

Patents

Continuous Neutralization and Solvent-exchange of Wet-gel Cellulose Fibers. D. Costa, S. Schick, G. Seider, B. Milow, Application -Nr. 10 2024 115 066.1 submitted on the 5. June 2024

Coating of Cellulose Wet Gels with Lignin. D. Costa, B. Milow, Application -Nr. 10 2024 112 076.2 submitted on the 30. April 2024

8.10 Zugänglichkeit von Daten und Materialien

Die Dissertation beinhaltet die Gewinnung von Primärdaten oder die Analyse solcher Daten oder die Reproduzierbarkeit der in der Dissertation dargestellten Ergebnisse setzt die Verfügbarkeit von Datenanalysen, Versuchsprotokollen oder Probenmaterial voraus. Die Daten sind auf dem internen Laufwerk des Instituts für Werkstoff-Forschung (DLR Köln) gesichert (inklusive Backups), sowie die hergestellten Proben archiviert, und den Personen der Abteilung WF-AEG zugänglich (entsprechend den Vorgaben der Erstbetreuerin).

8.11 Curriculum Vitae

Diogo Manuel Costa

+351 963 622 140 | diogomascosta@gmail.com | www.linkedin.com/in/diogo-manuel-costa/

EDUCATION

Faculty of Mathematics and Natural Sciences, Cologne University   **Cologne, Germany**

Doctoral Program in Chemistry   Apr 2021 – Present

   Enrolled in Marie Curie European Industrial Doctorate: Biobased Value Circle
   Research project: Biobased Aerogels: From Lab to Technical Scale

Instituto Superior Técnico, Lisbon University   **Lisbon, Portugal**

Master's Program in Chemistry   Sep 2018 – Nov 2020

   GPA: 19/20

   Master thesis developed at ICPEES, Strasbourg University, on the topic: Valorisation of biochars as catalysts for methane steam reforming. GPA: 19/20

Nova School of Science and Technology, Nova Lisbon University   **Almada, Portugal**

Bachelor's Program in Applied Chemistry   Sep 2015 – Jun 2018

   GPA: 18/20

   Bachelor thesis: Pyrolysis of used cooking oils using low-cost carbonated catalysts. GPA: 19/20

   Best freshman student at the program (2016); Best graduate student from all scientific programs (2018).

WORK EXPERIENCE

KEEY Aerogels   **Habsheim, France**

PhD Researcher   Oct 2022 – Apr 2024

   Developed technical scale recipes for the synthesis of cellulose aerogels and their post-modification using other biopolymers such as lignin

   Wrote dissemination articles for specialized industry magazines and patent applications

German Aerospace Center   **Cologne, Germany**

PhD Researcher   Apr 2021 – Apr 2024

   Developed experimental procedures to synthetise cellulose aerogels (beads, films; fibers) from hemp and flax waste fibers and optimize their properties as thermal insulators

   Characterized biomass samples (FTIR, XRD, TGA/DSC), cellulose solutions (rheology; tensiometry) and nano-porous materials (physisorption, densities, SEM and microscopy)

   Analysed data and presented scientific results in international conferences (poster, oral) and scientific publications

   Supervised master thesis students and co-organized international summer school and conferences

SKILLS

   Languages: Portuguese (Native), English (Proficient – Cambridge C2), French (Proficient), German (intermediate)

   Technical: Microsoft Office Tools (Advanced), Python (Basic), Origin (Advanced)